ECONOMIC MINERALISATION OF THE LOCH MAREE GROUP AND TECTONIC CORRELATION OF THE LEWISIANOID INLIERS OF SCARDROY AND ORRIN

Euan McIntosh

Submitted in fulfilment of the requirements of the

Degree of Master of Science (Research)

School of Geographical and Earth Sciences, College of Science and Engineering

University of Glasgow

Abstract

This project has twin aims: examining sulphide mineralisation within the Lewisian hosted Loch Maree Group (LMG) whilst testing correlation of the Gruinard Belt and Flowerdale inliers with the LMG, and dating along strike poorly studied Lewisianoid inliers within the Moine. This will provide a better understanding of the continuity – or not – of basement structures, and hence potential mineralisation, across the Moine Thrust. Whole rock multi-element assay, major and trace element analysis, and U-Pb dating of zircon were conducted across four main field areas of both economic and tectonic interest. These were: 1) the Gairloch Schist Belt of the LMG and Flowerdale inliers; 2) the Gruinard Belt; 3) the Scardroy inliers; 4) the Orrin inlier.

Exploration of the Gairloch Schist Belt reveals, in addition to the Kerry Road deposit, widespread but dominantly very low-grade sulphide mineralisation. An inlier of exhalative lithologies at Flowerdale is very likely correlatable with the main exposure of the Belt and records potentially economic grades of Au worthy of further investigation. A second inlier of highly altered ultra-mafic rocks remains enigmatic in both origin and position relative to the LMG or basement Lewisian. The Gruinard Belt records a late-Laxfordian age c. 1780 – 1670 Ma and hence cannot be correlated with the LMG as proposed by previous studies. It instead is considered to represent a separate association of supra-crustal material tectonically introduced into the basement gneisses c. 200 Ma after the accretion of the LMG. A well-defined Caledonian aged Pb-loss event and related zircon growth requires further study but may be related to fluid flow and heating during Caledonian nappe stacking.

Gneisses from the Scardory and Orrin inliers record dominantly Archean U-Pb protolith ages (c. 2.7 – 2.85 Ga) with Laxfordian and Renlandian metamorphic signatures while one sample presents a c. 1.7 Ga protolith age, suggesting Laxfordian magmatism within the inlier. This history, along with geochemical analysis of associated mafic and intermediate rocks, supports correlation with the Lewisian of the foreland and any Baltican heritage for the basement to the Northern Highlands is not expressed in this area. The shared basement between Hebridean and Northwest Highland terranes, as evidenced by correlation of Lewisianoid inliers with the foreland, allows for the LMG, associated mineralisation, and late-Laxfordian supracrustal rocks to exist east of the Moine Thrust. Although exactly along strike there is no evidence of LMG like rocks at Scardroy, likely due to lateral displacement across Moine thrust, however the belt may exist at depth below overlying Moinian cover.

Acknowledgments

This thesis would not have been possible without considerable help from a great many people. My Glasgow supervisors Dr. Iain Neill and Dr. John MacDonald have been truly amazing in the help and guidance they have given me throughout. I'm not sure Iain realised how often I'd be popping into his office and latterly WhatsApp, but I hope he managed to get some work done in-between. Gavin Berkenheger and GreenOre Gold PLC offered their time and money very generously and I would like to thank him for some excellent days in the field.

The project was primarily funded by GreenOre and two grants: from The Edinburgh Geological Society and the Geological Society of London. All three are thanked for their backing along with the University of Glasgow for absorbing various costs and Professor Rob Strachan and Professor Jamie Toney for supporting statements. Robert McDonald and Mark Wildman provided invaluable assistance with all matters technical and were exceedingly generous with their time and expertise. Dr. Eddie Dempsey, Dr. Anna Bird and Kit Hardman at Hull conducted the LA ICP MS analysis and were very helpful in its interpretation. Dr. John Faithfull and Dr George Guice are thanked for enlightening conversation about the Lewisian, a Sisyphean topic if ever there was one. Strathconon Estate are thanked for access and conciliatory comments about the weather.

Twitter has played a massive role in my engagement with geology and although there are far too many people to mention, the community as a whole is amazing and has made rocks almost as interesting as Brexit… almost. General shoutouts for help and motivation in no particular order to; Charlie, Macca, Moxie, Ruf Dug, Bikes, Hammocks, and Falafel.

My parents and family have offered me nothing but unwavering support in everything and I certainly wouldn't be here without them, so thanks to Iain, Rona, Katie, and Stewart. Finally, I would like to thank all my friends for putting up with maybe one or two too many rock stories. Alex, Lachlan, Louise, and Mary would have made it up quite a few hills a lot faster if I didn't stop to look at every interesting exposure, while Frank and Rach put up with the rapidly accumulating rocks in the flat with excellent grace. Finally, really this time, Iain really must be thanked again for going above and beyond as a supervisor, consistently cheerful, constructive and supportive, patient, always managing to guide me towards the right idea without rancour at the three wrong ways I insisted on doing it first, thank you.

I nod and nod to my own shadow and thrust
A mountain down and down.
Between my feet a loch shines in the brown,
It's silver paper crinkled and edged with rust.
My lungs say No;
But down and down this treadmill hill must go.

Parishes dwindle. But my parish is
This stone, that tuft, this stone
And the cramped quarters of my flesh and bone.
I claw that tall horizon down to this;
And suddenly
My shadow jumps huge miles away from me.

Climbing Suilven - Norman MacCaig

Table of Contents

Authors Declaration

I declare that, except where explicit reference is made to the contribution of others, that this dissertation is the result of my own work and has not been submitted for any other degree at the University of Glasgow or any other institution.

Name: **Euan McIntosh** Signature:

All data is presented in appendices at the end of this dissertation or is available in electronic form on request from the author.

List of Figures

List of Tables

Chapter 1: Introduction

The Highlands of Scotland have played a pivotal role in the development of modern geology (Peach et al., 1907). The region has been shaped by geologic events over a period of three billion years; containing some of the oldest rocks in Europe, classic examples of thrusting, poly-metamorphism, and orogenic systems (Trewin, 2002). It has spent much of this time at the margins of continents, and so at the junction of many global events leading to a complicated and hotly debated geology (Burton, 2016; Dewey et al., 2016, 2015). One of the major arguments revolves around the amalgamation of Scotland through the Archean, Proterozoic, and Palaeozoic from a series of lithospheric blocks or tectonostratigraphic terranes, "blocks" henceforth, and the extent to which these were truly separate.

First developed through work in the cordillera of western North America (Coney et al., 1980; Freeland and Dietz, 1973; Irwin, 1972), the concept of the terrane has since been extensively applied around the world. The terrane is defined as a tectonically bounded package of rocks that displays an internally consistent stratigraphy and shared history (Irwin, 1972), with correlation across bounding lineaments only possible post amalgamation with another crustal block. A terrane can vary in size from many hundreds of kilometres in length, to small fragments only a few kilometres in area. They can form in a diverse range of environments and as such can contain a wide variety of internal histories. As the docking of terranes to a larger crustal block is usually associated with compressive or transpressive tectonic events, oblique collisions or post collisional strike slip movement can disrupt terranes and translate them thousands of kilometres along margins. Partial subduction or obduction of the terrane as well as the major internal disruption associated with a collisional event can complicate internal and external correlation of the terrane. Determining the origin of these terranes can be complicated by their variable size, lack of suitable geochronological or paleomagnetic data, deformation or metamorphism associated with accretion and post accretional movements. As such significant difficulties can arise in determining truly allochthonous terranes from more locally derived and disrupted autochthonous blocks. It is also commonplace for lithospheric blocks to rift apart, only to later re-amalgamate, with the rifted block being para-autochthonous with respect to its original and current neighbours. Such a concept may also be referred to as 'accordion tectonics' (Aitchison and Buckman, 2012)

An extensive body of work (Dewey et al., 2015 and references within) applies the terrane model to Scottish geology. At a large scale the geology of Scotland is comprised of a series of distinct blocks bounded by large faults. The commonly accepted divisions, or major terranes, and their bounding faults are shown in Figure 1.1. Debate exists around the relative allochthonous nature of each with respect to its neighbours. All display a Laurentian or Peri-Laurentian affinity in lithology and fauna from the Palaeozoic until their final amalgamation (Fletcher and Rushton, 2007; Stubblefield, 1956). The displacement along bounding faults is often unclear or contested but there is a general lack of evidence for thousands of kilometres of movement that would allow truly exotic blocks to be juxtaposed (Dewey and Strachan, 2003; Smith and Watson, 1983). Furthermore an increasing body of work has begun to correlate a shared history and in some cases shared lithologies between these proposed terranes. This includes recent work corelating the uppermost Torridonian and the Morar group across the Moine Thrust (Bonsor et al., 2012; Krabbendam et al., 2014) and

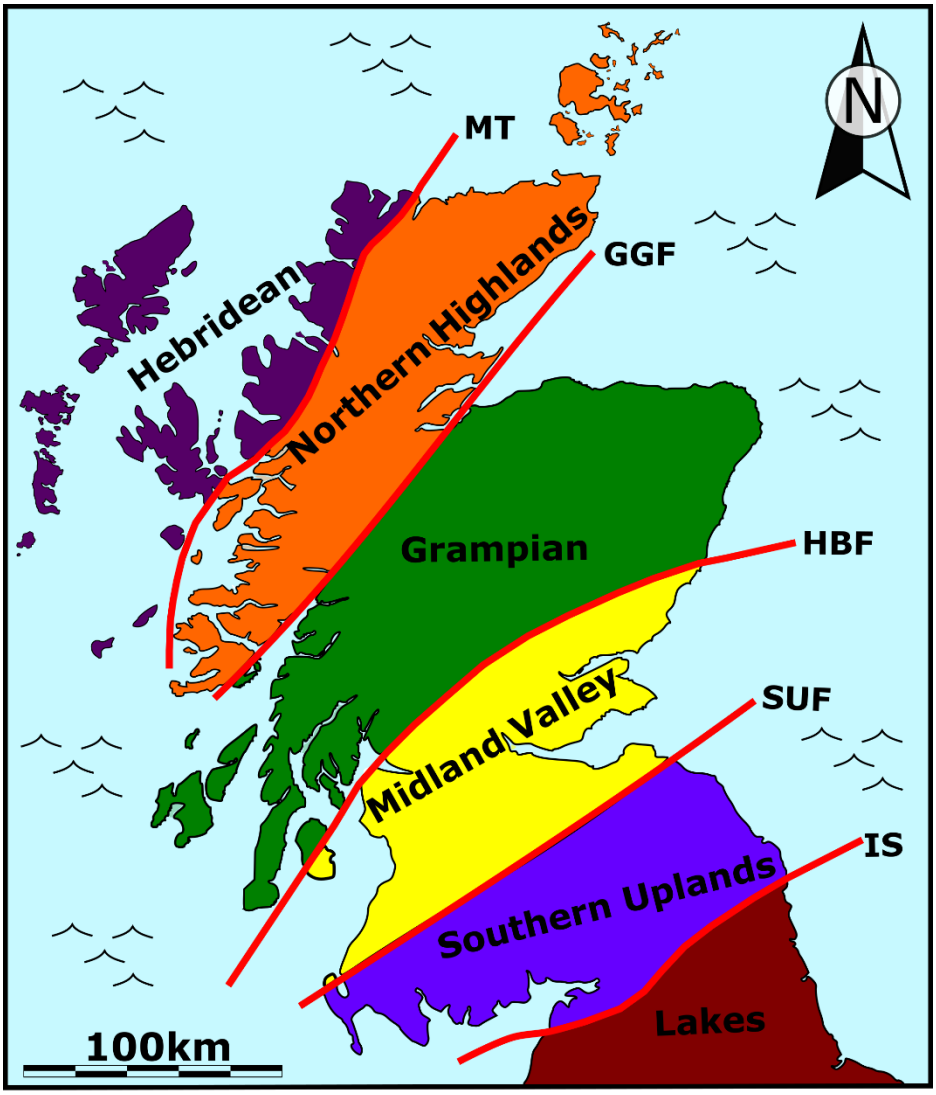

Figure 1.1. Generalised map showing commonly accepted terranes of Scotland and bounding faults or lineaments. **MT** – Moine Thrust, **GGF** – Great Glen Fault, **HBF** – Highland Boundary Fault, **SUF** – Southern Uplands Fault, **IS** – Iapetus Suture

that showing that Moine-like rocks form the sub-Dalradian basement south of the Great Glen fault (Noble et al., 1996). The scale of movement present within Scotland may then be on the order of local shuffling of crustal blocks rather than truly exotic terranes.

Underlying the dominantly mid to upper crustal rocks of these "terranes" are variably exposed basement rocks. Best exposed in the Hebridean Terrane, and occasionally occurring as tectonic slivers within the Northern-Highlands Terrane, are quartzo-feldspathic gneisses of amphibolite and granulite facies with minor mafic/ultramafic intrusions collectively known as the Lewisian or Lewisian Gneiss Complex (LGC). These gneisses have been subjected to multiple phases of deformation and metamorphism during the Late Archean and Proterozoic and represent a small fragment of a larger region of Archean and Paleoproterozoic crust that forms the Laurentian shield of North America and Greenland (Park, 1995). This basement and the extent to which it underlies the rest of Scotland provides an important line of evidence for correlation across the major terranes and in constraining their assembly. The first order large blocks brought together in the Paleozoic (Fig 1.1) are not the only area of Scottish geology where the terrane has been invoked. The basement rocks themselves have become the more recent focus of intensive study with regards to their possible assembly from multiple terranes in the Archean and Proterozoic. Here the normal complications of defining a terrane are multiplied by the sparse and often ambiguous evidence found in these lower crustal rocks (Kinny et al., 2005; Park et al., 2005).

Despite its key role in the history of geology as a science and the continuous study of its rocks over a century Scotland has been largely overlooked in terms of its economic geology (Fig. 1.2). Small-scale historic mineral extraction has occurred for many thousands of years, however large-scale commercial exploration largely ignored the area until the second half of the 20th Century (Colman et al., 2000). After significant discoveries in geologically similar regions of Canada and Ireland to those that form the Scottish Highlands, it was realised that important reserves of many economic elements could exist. The discovery of the Gairloch Kerry Road Cu-Zn-Au deposit in the 1970's (Jones et al., 1987) was "one of the highlights of minerals exploration in Scotland" (Coats et al., 1997). This deposit proved that Proterozoic belts in the primarily Archean basement rocks were a promising target for exploration. As much of Scotland is potentially formed of, or underlain by such basement, this significantly increased the potential for economic mineralisation. As such the understanding of the structure of this basement moved from a purely academic question towards one with an economic impetus behind it.

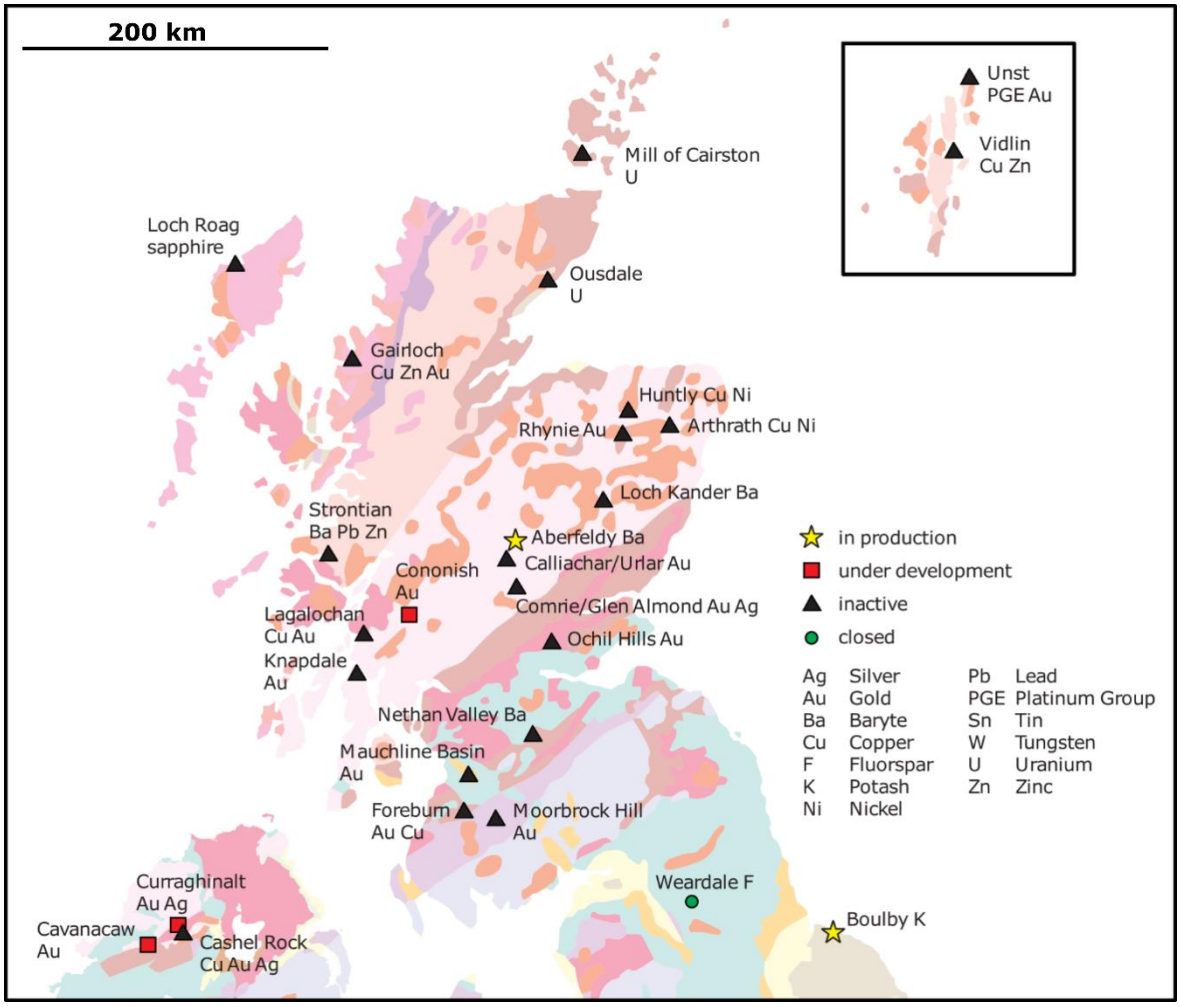

Figure 1.2. Map from Colman et al., (2000) showing mineral prospects discovered or developed since 1965.

The work presented here seeks to address how improvements in the tectonic correlation of this basement can be used to inform the search for economic mineralisation. Detailed study of mineralisation hosted within the same belt as the Kerry Road deposit will help to define the extent to which the ore-body may be part of a larger zone with the potential for additional economic discoveries to be made beneath shallow cover or drift. The structure of the Proterozoic belts and hence the areas of potential economic importance are intimately tied to the tectonics of their formation along sutures and major boundaries within the basement. The application of terrane tectonics is a key factor in determining the constraints on the structure and areas of likely mineralisation. Geochronological and geochemical analysis will help to constrain the age, environment of formation, and overall structure of key areas in relationship to the LGC as a whole. Finally, the potential for mineralisation to continue east of the Moine Thrust is assessed by examination of the along strike inliers at Scardroy and Orrin and the determination of their provenance with respect to the LGC (Fig. 2.1).

Chapter 2: Regional Geology

The large geographical spread of the project along with its composite tectonic and economic aims requires a sound basis in much of the Archean and Proterozoic geology of northern Scotland. As the focus of comparison and required background for much of the work presented here, it is particularly crucial to have a strong base knowledge of the Lewisian Gneiss Complex. This helps to place the analysis of the Loch Maree Group and Gruinard Belt of the Hebridean Terrane (HT) as well as the basement inliers of the Northern Highlands terrane presented here in a proper regional context.

2.1 - Hebridean Terrane

2.1.1 - Lewisian Gneiss Complex

The basement of the HT is formed of dominantly felsic, tonalite-trondhjemite-granodiorite (TTG), orthogneisses. These Lewisian gneisses were originally treated as one monolithic unit affected in their whole by several metamorphic events (Peach et al., 1907; Sutton and Watson, 1950). The advent of modern isotopic dating and mineral separation techniques has demonstrated that this is not the case and that it is better described as the Lewisian Gneiss Complex (LGC).

Primary magmatic zircon has given a range of protolith crystallisation ages that are often distinct across major lineaments (Friend and Kinny, 2001; Kinny et al., 2005; Kinny and Friend, 1997; Love et al., 2010). Along with the recognition of differential metamorphic grade and events not shared across the complex as a whole, this has led to the suggestion that it is in fact comprised of disparate terranes assembled into their current configuration by the end of the last major event to affect the complex, the late-Laxfordian, at c. 1600 Ma. A great deal of debate exists around this assembly, particularly the application of a terrane model to the complex, with many authors rejecting piecemeal assembly in favour of simpler models involving only two plates, or breakup and reassembly of the same crust (Fischer et al., 2021; Kelly et al., 2008; Mason, 2016, 2012; Park, 2005). Although the number of blocks, and their relative exoticness is controversial, internal heterogeneities and sutures do exist within the Lewisian (Goodenough et al., 2013, 2010). Much of the debate therefore hinges on the difficulty of applying an essentially upper crustal theory of terrane accretion to lower

crustal rocks that lack much of the traditional paleomagnetic, stratigraphic, and palaeontological evidence commonly used to define an upper crustal terrane (Holdsworth et

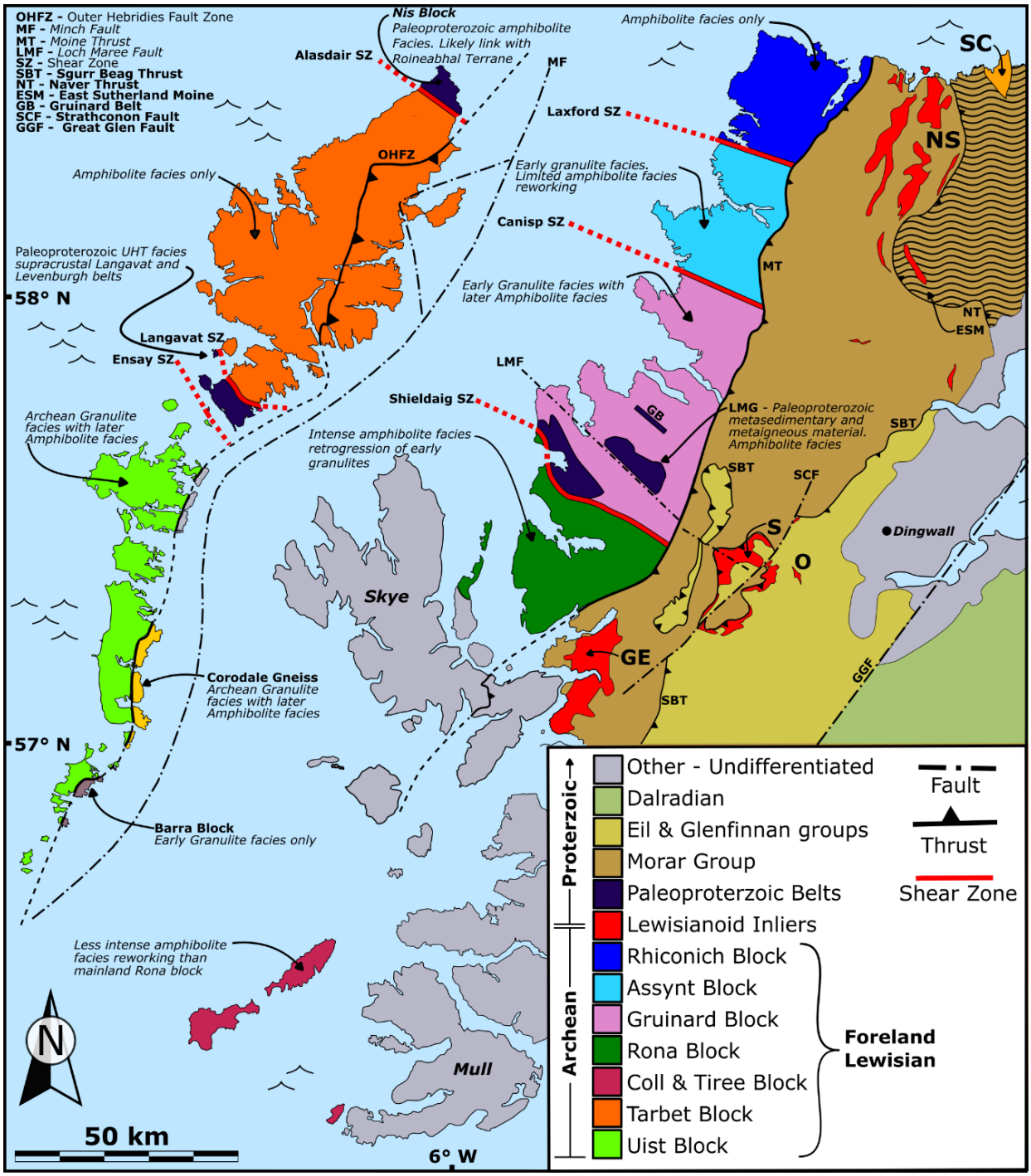

Figure 2.1. Simplified geologic map showing areas of interest to this study. Lewisian blocks are not in stratigraphic order. Lewisian division into blocks from Kinny et al., (2005) with general comments from (Kinny and Friend, 1997; Friend and Kinny, 2001; Kinny et al., 2005). The exact boundaries and differentiation between blocks is a subject of debate and delineation here is for descriptive purposes and does not imply support for any given model. Post Lewisian cover omitted from Hebridean Terrane. Inliers; **NS** – North Sutherland, **GE** – Glenelg, **O** – Orrin inlier, **S** – Scardroy, **SC** – Strathy Complex.

al., 2019).

SHRIMP U-Pb dating of zircon has determined the age of the protolithic melts throughout the complex to be c. 3000 – 2700 Ma (Friend and Kinny, 2001; Kinny et al., 2005; Kinny and Friend, 1997) with older ages of up to c. 3150 Ma interpreted as inherited cores. Variation of protolith ages between blocks provides a central line of evidence for distinct terranes within the complex. For example, Kinny and Friend, (1997) find the Assynt region records an emplacement age of 2960 – 3030 Ma, while the adjacent Rhiconich block to the north of the Laxford Shear Zone gives a younger age of 2800 – 2840 Ma. Other discontinuities in protolith ages across major lineaments are present in published ages from throughout the complex and a detailed discussion of every 'terrane' and the evidence for it is beyond the scope of this work. However this dating is often reliant on only a few samples from any one area and the degree of heterogeneity within any single block is often unclear (Fischer et al., 2021).

In the c. 3000 Ma since its emplacement, the LGC has been affected by a series of tectono-thermal events variably expressed across the complex. The earliest is a c. 2950 Ma anatectic event recorded within a portion of the Rona block (Love et al., 2010), whilst the earliest reasonably widespread event is the 'Badcallian'. This term has been broadly and variably applied to any early high-grade event across the complex variously assigned to either c. 2500 Ma or c. 2700 Ma. It has been suggested to only apply to the granulite facies metamorphic event at c. 2480 Ma in the Assynt block (Friend and Kinney, 1995; Kinny et al., 2005; Kinny and Friend, 1997; Love et al., 2004). However a prominent metamorphic event is present within the Gruinard block at c. 2730 (Love et al., 2010) and some authors report the c. 2700 event from within the Assynt block (Zirkler et al., 2012). Early high-grade events are found in several other blocks of the LGC however they are often very poorly dated, undated, or difficult to interpret due to ambiguous U-Pb zircon data tending to smear along concordia. As such the term will here retain its original meaning: early high-grade metamorphism, with the important caveat that in different blocks these events may be temporally and spatially unrelated and as such events shall be primarily be referred to by age where possible. Where present, the Badcallian is generally followed on the mainland by a retrogressive amphibolite facies event associated with the formation of shear zones and fluid infiltration known as the Inverian (Evans, 1965). Most prominent at the boundaries between the Assynt, Gruinard, and Rhiconich blocks, this event may be related to movement along these bounding shear zones as these blocks were juxtaposed (Goodenough et al., 2013, 2010; Kinny et al., 2005). Early events across the complex are commonly difficult to interpret due to partial resetting of U-Pb systems. Taylor et al., (2020) propose that a near continuous spread of metamorphic

zircon ages from 2700 Ma to 2500 Ma represent one continuous metamorphic event where the LGC was held at high temperatures near the base of the crust for c. 200 Ma. High heat flow may have been provided by the intrusion of significant volumes of mafic magma, now disrupted and represented by mafic pods and larger complexes within the Lewisian.

These ultramafic, mafic, and associated or distinct metasedimentary lithologies form a volumetrically very minor part of the LGC compared to the dominant felsic orthogneisses, varying in size from metre scale highly sheared pods, to the 7 km^2 Ben Strome complex (Guice, 2019). In general, these minor components of the complex are comparatively poorly understood and almost universally undated. It has been argued that these assemblages represent the disrupted remnants of sagducted greenstone belts (Johnson et al., 2016). Whilst a second interpretation has suggested an intrusive origin for most of these bodies with emplacement into the TTG gneisses at an early - pre-Badcallian - date (Guice, 2019; Guice et al., 2018; 2020).

The Ben Strome complex is the largest and best studied of these bodies with both pre-TTG (Johnson et al., 2016; Park, 2002; Rollinson and Windley, 1980) and post-TGG (Guice, 2019; Guice et al., 2020, 2018) emplacement ages assigned to it. The complex is composed of modally layered mafic and ultramafic rocks. Mafic lithologies include metagabbros, garnet amphibolite, and amphibolite in variable proportions. Ultramafic lithologies consist of dominant metapyroxinite with minor metaperidotite. Layering is commonly observed in the ultramafic portion but is less discernible in mafic layers, perhaps due to their greater susceptibility to metamorphism. The complex displays Badcallion and Inverian folding and is cross cut by Scourie Dukes and Laxfordian shear zones (Guice, 2019).

Other rare occurrences show evidence of predating the TTG gneisses suggesting these small bodies may represent fragments of Archean mantle into which voluminous magmas were emplaced (Guice et al., 2020). The Loch an Daimh Mor complex is one such occurrence that potentially pre-dates the LGC. This body has platinum group element (PGE) patterns comparable with mantle portions of ophiolites and falls within the abyssal peridotite field in terms of its geochemistry. As such it is the most likely candidate within the LGC for Archean mantle material and suggests not all mafic/ultramafic bodies in the LGC are related to one style or period of formation (Guice et al., 2020).

Mafic dykes are found throughout the Lewisian associated with a period, or periods, of crustal extension. These form important markers and can be used for relative dating of events

and features throughout the complex. Their occurrence throughout most, but not all, of the LGC indicates that during their emplacement many of the blocks that form the LGC were closely associated. There is however debate about the relation between dykes of the Outer Hebrides, the central mainland, and the southern parts of the complex, with chemical and perhaps temporal differences between them (Davies and Heaman, 2014; Mason et al., 2004). U-Pb baddeleyite dating of two mainland dykes by Heaman and Tarney (1989) gave ages of 2418 ± 7, and 1992 ± 3 Ma, suggesting at least two unrelated swarms are present. Baker et al., (2018) date dykes from the Rona terrane at 1989 ± 4 Ma and term this later c. 1990 Ma set of dykes as the Strathan swarm. Davies and Heaman (2014) suggest the majority of dykes were emplaced over a prolonged period c. 40 Ma between c. 2418 and 2375 Ma, and that this earlier swarm are the Scourie Dykes *stricto sensu*. Prolonged and intermittent extension during the pre-Laxfordian Paleoproterozoic is further supported by a set of extensional quartz-pyrite veins with the Assynt block dated at 2249 ± 77 Ma, after the emplacement of the last of the Scourie dykes, but prior to the intrusion of the c. 1990 Ma suite (Vernon et al., 2014).

The Laxfordian event postdates the intrusion of all dyke suites and variably affects the entirety of the LGC. The Laxfordian can be divided into two cycles, an early event c. 1.91 to 1.85 Ga and a later event at c. 1.75 to 1.65 Ga (Mason, 2012; Mason, 2016). The early event is associated with the formation of an active margin and accretion of a series of supracrustal belts; the Outer Hebridean Langavat and Leverburgh belts, and the mainland Loch Maree Group. These are dominated by rocks of oceanic to volcanic-arc affinities and may lie along a Paleoproterozoic suture marking their accretion to the Lewisian gneisses (Park, 2001: 2002; Mason, 2016). A c. 100 Ma hiatus in metamorphism is then followed by the late-Laxfordian, an event likely triggered by the accretion of the Malin block, juvenile Paleoproterozoic crust to the SW of the Lewisian, at c. 1.75 to 1.65 Ga (Park, 2005). The later event is associated with peak amphibolite facies metamorphism linked to significant crustal thickening throughout the complex and dominates the preserved field evidence of the Laxfordian. Many different structures have been assigned a “Laxfordian” age based primarily on their relationships to pre-Laxfordian structures. Absolute dates for these Laxfordian structures are rare and as such it has become a catch all term for any post-Scourie Dyke events within the complex. New work (Holdsworth et al., 2020) has assigned an age of c. 1.55 Ga to the last of these structures, a set of regional scale brittle faults. This age is incompatible with the previous estimates of the late-Laxfordian and implies a distinct event; termed the Assyntian.

The final tectonic event evident in the LGC is the Grenvillian. This is a major orogenic event of the late Mesoproterzoic (1.2 – 1.0 Ga) associated with the formation of Rodinia from the amalgamation of Laurentia, Baltica, and Amazonia. Evidence for it is best preserved along the former eastern margin of Laurentia; present day North America, Ireland, Scotland, and Scandinavia (Rivers, 1997; Sanders et al., 1987). The Grenville Orogeny is poorly studied in Scotland with the most definitive evidence for it found in the Lewisianoid Glenelg inliers east of the Moine Thrust (Storey, 2008; Strachan et al., 2020). In the foreland the only evidence for the event is pseudotachylite associated with brittle crush belts within the Lewisian dated at c. 980 – 1020 Ma (Sherlock et al., 2008).

2.1.2 - The Loch Maree Group

The Loch Maree Group (LMG) is a suite of supracrustal metasedimentary and metavolcanic rocks exposed in two belts, the Gairloch Schist Belt (GSB), and Loch Maree Schist Belt (LMSB) (Fig 2.2). The LMG is distinct from the surrounding Lewisian gneisses in its diversity of lithology, metamorphic grade, age, and environment of formation (Park, 2002). The group has been commonly interpreted as a subduction-accretionary-arc complex accreted to the Lewisian in the early-Laxfordian (Mason, 2012; Park et al., 2001; Whitehouse et al., 1997). The contact between the LMG and the Lewisian basement is disputed with some assigning all boundaries a tectonic nature (Coats et al., 1997; Johnson et al., 1987; Park, 2010; Park et al., 2001), and others suggesting a basal unconformity exists (Kerr et al., 2015).

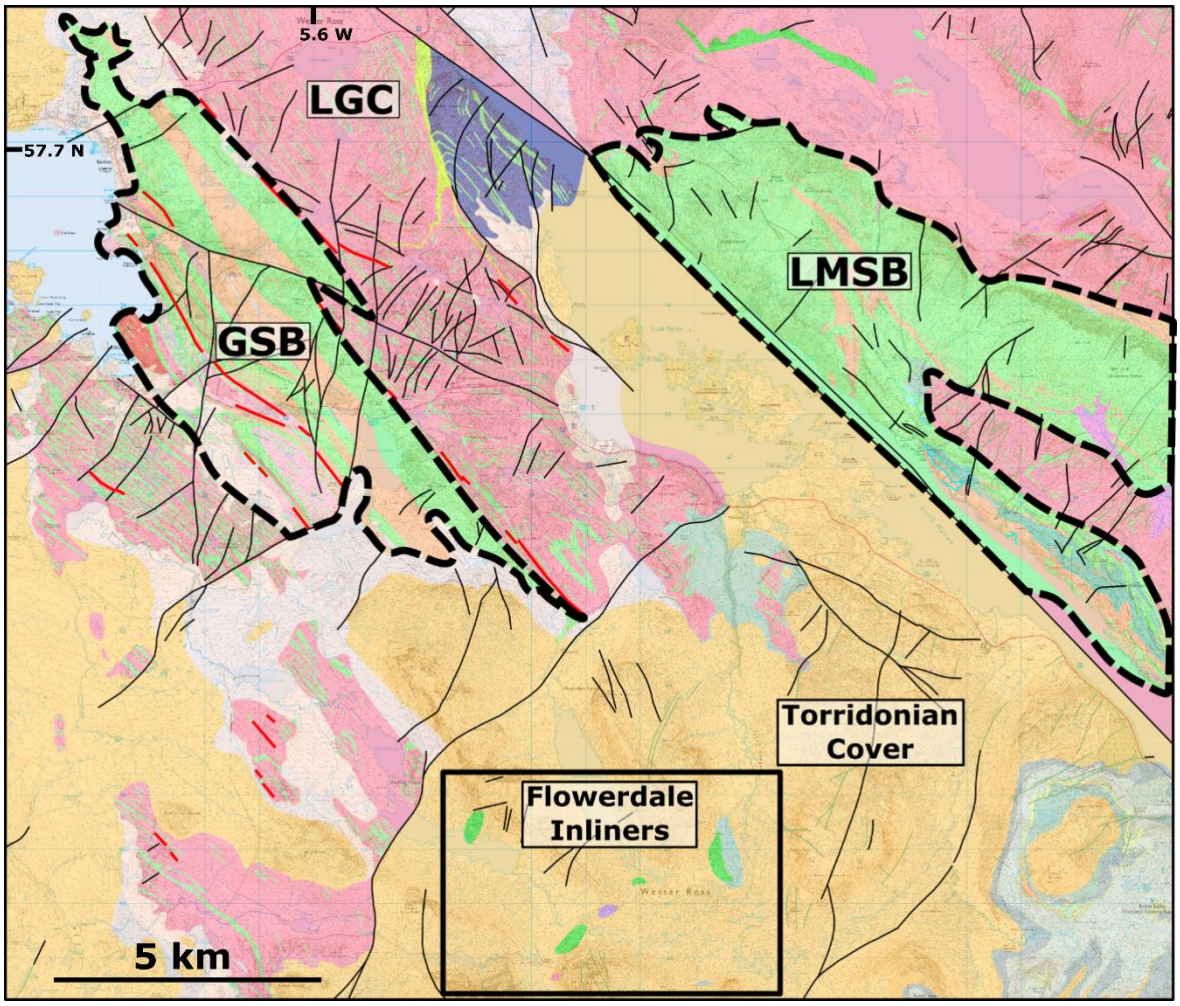

Figure 2.2. Area map showing the exposure of the Gairloch Schist Belt (GSB) and Loch Maree Schist Belt (LMSB) within the basement Lewisian Gneiss Complex (LGC) and overlying Torridonian sedimentary cover. Flowerdale inliers are shown lying along strike from the GSB. BGS mapping from Digimap (2020).

The internal structure of both belts is dominated by sheared and faulted contacts between units with the entire exposure of the GSB lying within the Gairloch shear zone (GSZ), a major late-Laxfordian structure that dips steeply to the north east. The GSZ overprints earlier Laxfordian fabrics and is estimated to have a minimum displacement of c. 9.5 km of dextral shear and a NE up component of c. 5.5 km (Park, 2010). The LMSB is synformal in shape with the Letterewe Gneiss exposed at the core as part of the structurally overlying gneisses. The LMSB is poorly studied compared to the GSB due to remoteness and former access restrictions. The British Geological Survey (Coats et al., 1997) undertook the most detailed work on the area to date. The rocks of the LMSB are bounded to the south by the Loch Maree fault and folded around the core of the Letterewe synform. They are tectonically bound on basal and upper surfaces by Lewisian gneisses and contain several internal thrusts. Despite this significant disruption of original stratigraphy, a tentative correlation between units of the LMSB and GSB was made and the general stratigraphy of the two belts is similar.

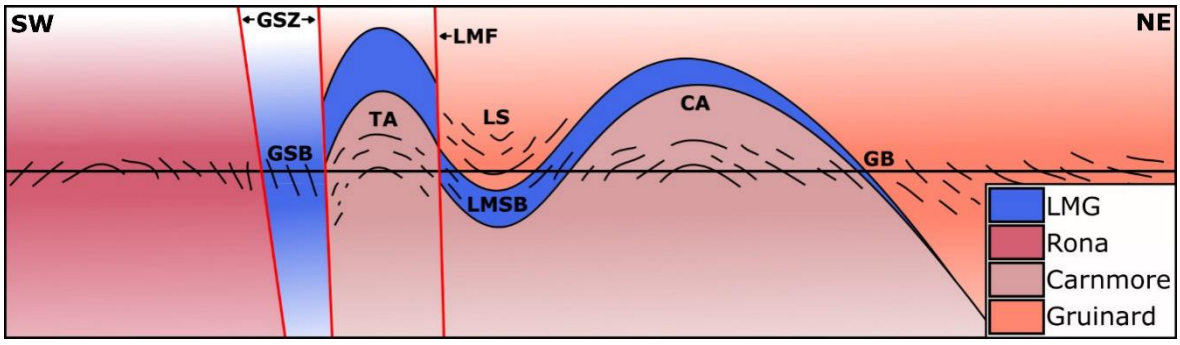

Figure 2.3. Generalised cross section showing possible structural relationships between outcrops of the LMG at Gairloch and Loch Maree with potential linkage of rocks exposed in the Gruinard Belt (**GB**) with the LMG. **GSZ –** Gairloch Shear Zone, **TA –** Tollie Antiform, **LMF –** Loch Maree Fault, **LS –** Letterewe Synform, **CA –** Carnmore Antiform. Modified from Park et al., (2001)

Three major schist units are exposed within the GSB; the Flowerdale, Kerrysdale, and Charlestown schists (Fig 2.4). These are semipelitic to psammitic in composition and typically display an amphibolite facies assemblage of biotite-quartz-plagioclase ± hornblende (Floyd et al., 1989). The schists are chemically distinguished as a series of greywackes and lithic sandstones with material sourced from two dominant sources, felsic continental crust, and tholeiitic basalts. Detrital zircon ages from the Flowerdale Schist (Whitehouse et al., 1997) give two distinct ages for source material. One is an Archean component (3.0 – 2.5 Ga) likely sourced from Lewisian gneisses, while a second Paleoproterozoic (2.2 – 2.0 Ga) component constrains the maximum age of deposition. This younger group indicates a juvenile evolved source that is no longer exposed within the Hebridean Terrane.

The amphibolites of the LMG occur as large sheets separated by metasedimentary units. They are generally foliated and dominated by hornblende and plagioclase with minor quartz, biotite, garnet, and chlorite (Park, 2002). Geochemically they can be separated into two distinct groups, termed A and B, with both plotting in the tholeiitic field (Johnson et al., 1987). Group A amphibolites show flat rare-earth-element (REE) profiles, while group B shows LREE enrichment. Park (2002) interprets group A as representing oceanic basaltic material and based on their Ti-enrichment assigns them to an ocean plateau environment. Group B amphibolites are interpreted as sills emplaced directly into their surrounding metasediments. He suggested their enriched LREE profiles are due to crustal contamination in a more evolved arc like environment and that they may significantly postdate group A in age.

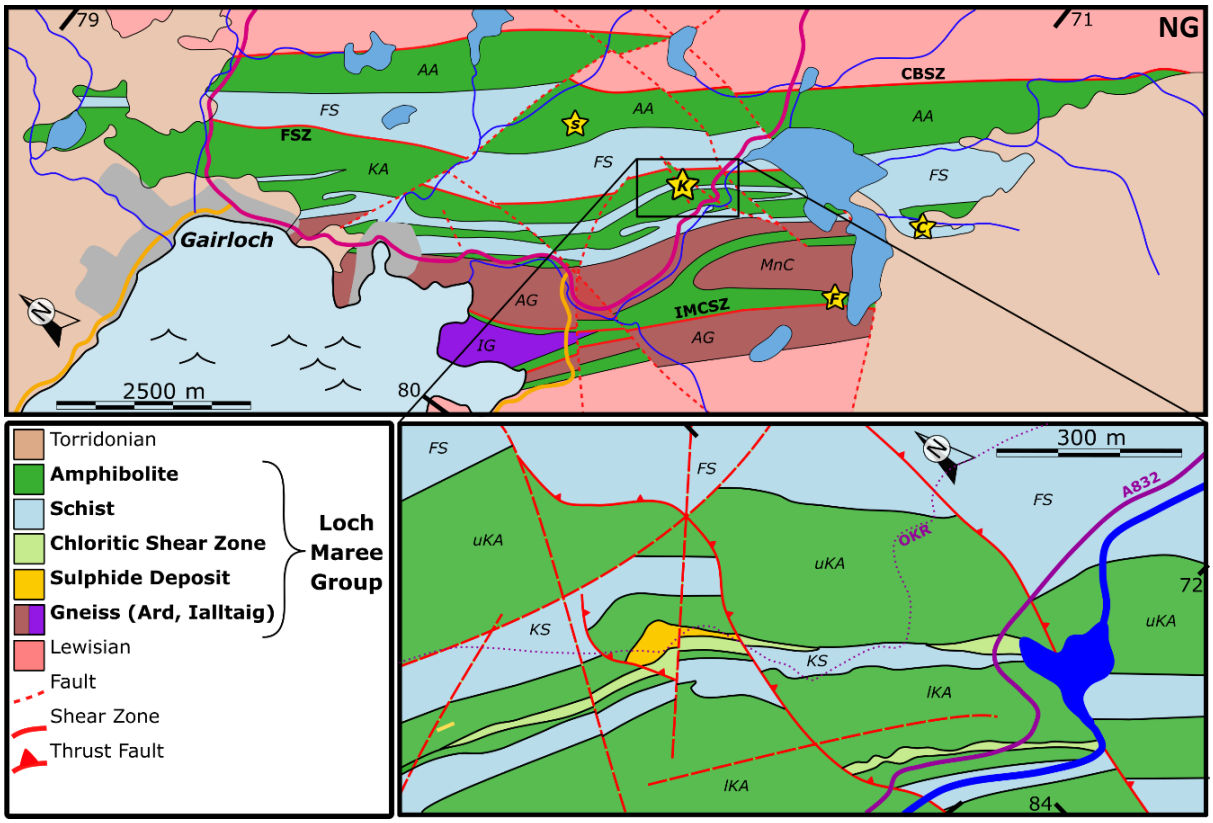

Figure 2.4. Generalised map of the Gairloch Schist Belt showing large scale outcrop of amphibolites, gneiss and schist (generalised after Park, 2002). Mineralised localities indicated by stars, with an inset map of the Kerry Road locality in the lower box (modified from Jones et al., 1987). **K** - Kerry Road, **S** - Sidhean Mor, **F** - Druim na Fearna, **C** - Allt na Cosaig. **AA** – Aundrary Amphibolite, **FS** – Flowerdale Schist, **KA** – Kerrysdale Amphibolite (**u**-upper, **l**-lower), **KS** - Kerrysdale Schist- **AG** – Ard Gneiss, **IG** – Ialltaig Gneiss **MnC** - Mill Na Claise Gneiss, **CBSZ** - Creag Bhan shear zone **FSZ** - Flowerdale shear zone, **IMCSZ** - Ialltaig-Mill na Claise shear zone.

Along the southern edge of the GSB a series of gneisses occur intercalated with schists and amphibolites. The Ard and Mill na Claise gneisses are granodioritic to tonalitic in composition. Park et al., (2001) date their emplacement at 1903 ± 3 Ma, therefore postdating the depositional age of the metasedimentary units. This age is assigned to the D1/2 events of the early-Laxfordian and suggest the gneisses may have been generated by melting of the underplating oceanic plateau during accretion of the LMG to the Lewisian.

Within the GSB a small shear bounded zone of granulite facies gneiss termed the Ialltaig Gneiss is found. U-Pb zircon dating gives a protolith age of c. 2000 Ma with high grade metamorphism at c. 1870 Ma (Love et al., 2004). The fact that the rest of the GSB does not record any evidence of granulite facies metamorphism and the shear bounded nature of the block led Kinny et al., (2005) to suggest it deserved its own terrane status. Park, (2005) however has suggested that it may bear relation to granulite rocks found in the chronologically and lithologically similar Leverburgh and Langavat Belts of South-Harris. Significant thrusting and strike slip faulting associated with their accretion may have juxtaposed lower and higher grade rocks within these belts (Park, 2010). This is supported by a number of anorthosite xenoliths found within amphibolites of the LMSB (Cattell and Williams, 1988) similar to those found in the Outer Hebrides Igneous Complex. Laxfordian metamorphism has been better constrained within these Hebridean belts and Mason (2010) suggests that correlation of the LMG with the South-Harris Belts implies the early-Laxfordian age of peak metamorphism proposed by Park (2001) for the LMG is incorrect. Instead it is suggested that accretion may have taken place early in the Laxfordian, but burial and peak metamorphism did not occur until the late-Laxfordian. Peak metamorphic conditions in the LMG during the Laxfordian reached amphibolite facies at 530 ± 20°C and 6.5 ± 1.5 kbar under geothermal gradients of c. 20 – 30°C km^{-1} (Droop et al., 1999). This requires burial to c. 20 km and substantial crustal thickening. Greenschist facies retrogression occurred throughout the belt, along with significant brittle deformation and faulting linked to the Grenvillian at c. 1000 Ma (Campbell et al., 2019; Sherlock et al., 2008)

2.1.2.1 - Sulphide Mineralisation in the LMG

The interpretation of the LMG as a subduction-accretion-arc complex suggests the area may be a target for economic mineral exploration. Volcanogenic massive sulphide (VMS) deposits are found in many arc, back arc, and oceanic plateau environments around the world similar to the proposed tectonic models for the LMG (Barrie and Hannington, 1999).

VMS deposits (Fig 2.5) are sulphide bearing formations formed by precipitation from hydrothermal fluids at, or near the seafloor associated with spreading ridges, back-arc basins, and volcanic arcs. Classification is by host rock composition, ranging from mafic to felsic volcanic rocks and varying degrees of intercalated sedimentary material. Mafic-siliciclastic deposits such as that found at in the LMG are dominated by sub-equal proportions of mafic and siliciclastic rocks (Barrie and Hannington, 1999). Sulphide mineral formation can occur either as primary precipitation directly from mineralised fluids, or as replacement of existing sub-sea lithologies. As such they are commonly strata-bound, either as a benthic exhalative horizon or focused along specific layers in the shallow seafloor.

The structure of a VMS deposit will vary depending on the host rock and size of the deposit but will generally contain several distinct zones (Dubé et al., 2007; Lydon, 1984). Below the seafloor a stockwork ore of fractured host rock forms as rising fluids boil due to decreasing pressure. Proximal to the main feeder zone, hydrothermal alteration of host rocks occurs through: advanced argillic, argillic, and propylitic stages with increasing distance from the main conduit. Once fluids reach the ocean floor interaction with cold sea water causes precipitation of massive sulphide ores that settle out of the water column. Slumping and reworking of primary sulphides as deposits grow and collapse is common. Periods of burial and quiescence can lead to the formation of multiple sulphide lenses contained in host rocks and complicated crosscutting relationships between feeder zones and ores (Galley et al., 2007)

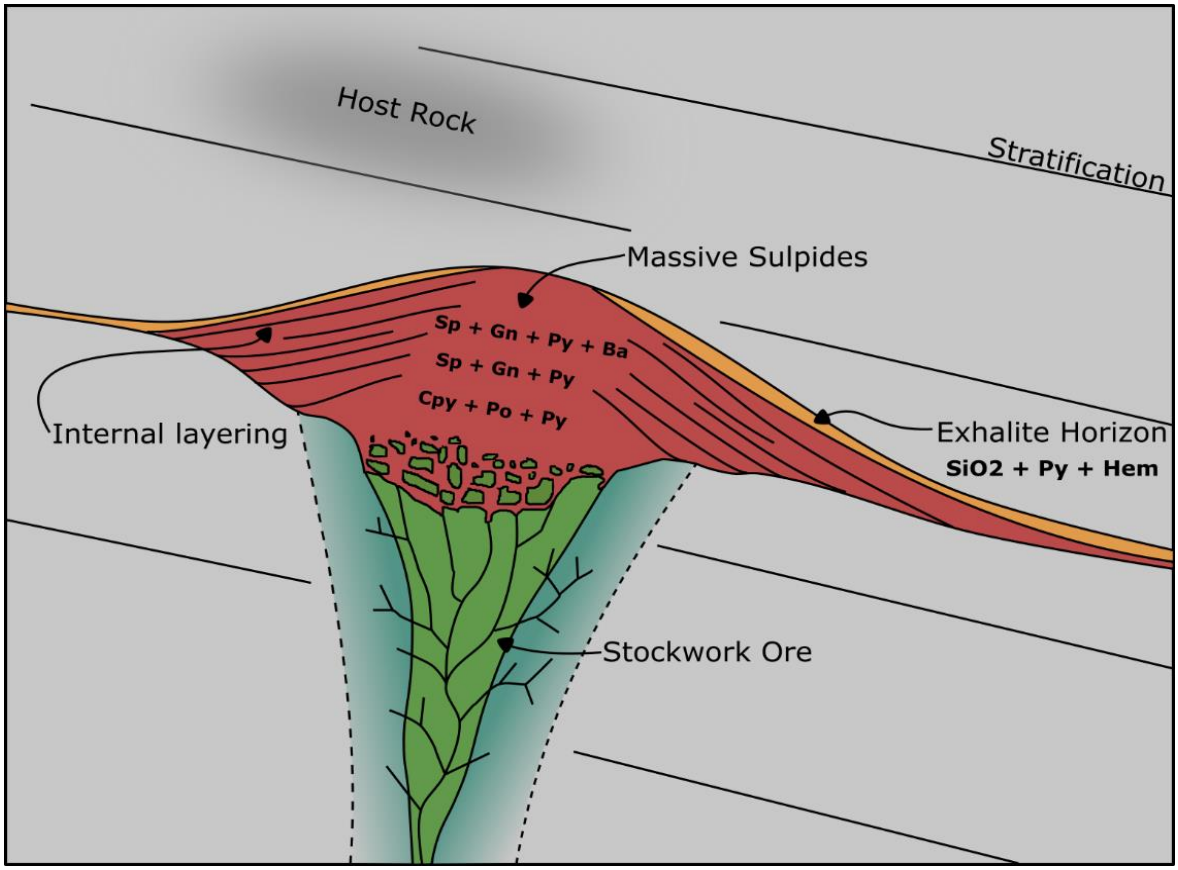

Figure 2.5. Idealised model of a VMS deposit after Lydon (1984). The stockwork zone is formed of fractured and hydrothermally altered host rock and is discordant with host rock stratification. The massive sulphide lenses are massive to internally stratified and feature zonation in mineral content that relates to the decreasing temperature of the rising fluids. The exhalative horizon is formed of metal rich muds and can extend over a large area.

Sulphide mineralisation is present at several locations throughout both the Gairloch and Loch Maree schist belts. Exploration has focused primarily on the GSB due to proximity to the road and former access restrictions within the LSMB with the the major discovery of this exploration being the Kerry Road deposit. This significant base and precious metal deposit is the only known VMS deposit from Scotland (Coleman et al., 2000). The Kerry Road deposit was first identified as a copper bearing limestone by Peach and Horne (1907) and then extensively prospected by Consolidated Gold Fields (CGF) (Jones et al., 1987). The deposit takes the form of a stratiform volcanogenic massive sulphide of the Besshi type, due to the sub-equal proportion of mafic volcanic and siliciclastic host rocks. Sulphides form c. 20% of the deposit and are found as lenses, schistose parallel bands, disseminations, and stringer ore. The sulphide mineralogy is dominated by pyrite and pyrrhotite, with minor chalcopyrite, sphalerite, marcasite, and very rare galena and native gold. Over 9000 m of core across 87 drill holes was used to define the size of the orebody, which at the time – the 1980's, was below economic grade for the size of the deposit: 0.5 Mt at 1 g/t Au, 1% Cu and

0.5% Zn (Greenore Gold, unpublished). Gold values for 1 m intercepts are up to 5 g/t. The ore body is fault bounded by a northwards trending thrust that dips to the east and as such mineralisation occurs below increasing depth of overburden in this direction (Jones et al.,

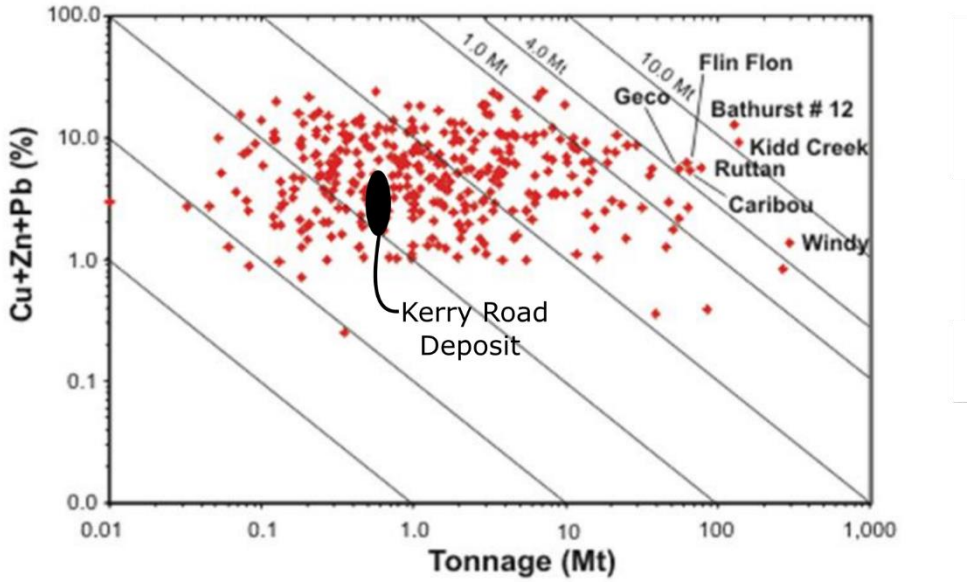

Figure 2.6 Kerry Road deposit showing estimates of reserve potential overlayed on a figure showing global VMS deposits from Meinert (2007)

1987)

As part of exploration within the GSB several other mineralised occurrences were located, although none were deemed to reach the economic potential of the main orebody. Northwest of Kerry Road, c. 400 m, a narrow gossan occurs at Teangadh Bhuidhe Mhor in a series of banded hornblende and chloritic schists. Assay by CGF found similar metal values, 1.4 % Cu, 700 ppm Zn, and 0.9 ppm Au, to the main Kerry Road deposit. Sulphides: pyrrhotite, pyrite, chalcopyrite, sphalerite, are present as deformed bands and disseminations and display similar textures to Kerry Road. This along with its similar stratigraphic position and proximity to the main orebody suggest they are related to one another. Continuous mineralisation between the two is unlikely due to the presence of several faults in the ground between (Jones et al., 1987) and geophysical evidence for a podiform shape to the smaller gossan, however they may be temporally related to the same mineralising event.

Several other occurrences of sulphide mineralisation (Fig. 2.4) occur throughout the GSB that are not directly related to the Kerry Road deposit (Jones et al., 1987). A band of sulphides can be traced intermittently through the Aundrary Amphibolite, at the contact between coarse-massive and fine-banded schists, for almost 6 km. The most continuous exposure occurs near the summit of Sidhean Mor where it outcrops as a gossan reaching c.

20 m in width. The unit consists of strongly deformed and intermixed hornblende and siliceous schists that grade into surrounding amphibolites. The schists are composed of quartz, mica, amphibole, and calcite, while the sulphides disseminated and banded throughout are predominantly pyrite and pyrrhotite. As part of the exploration undertaken by CGF two cores of 110 m and 70 m were drilled near the summit of Sidhean Mor which confirmed the continuation of the unit to depth. The unit is dominated by iron sulphides with base-metal values found to be low, 300 ppm Cu, 600 ppm Zn, and precious metals below the limits of detection along the entire strike of the gossan (Jones et al., 1987). The Allt na Cossaig was investigated after discovery of sulphide bearing cobbles in the basal Torridonian conglomerate and a coincident geophysical anomaly. Two scout holes encountered quartz-mica schists with pyrite and graphitic banding, but only minor metal enrichment. Near the southern boundary of the GSB a massive amphibolite intercalated in a series of gneisses, marbles, and amphibolites was found to be slightly enriched in copper - 0.26 %.

With the exception of the narrow gossan at Teangadh Bhuidhe Mhor, other mineralisation throughout the GSB differs significantly in style, base, and precious metal content from the Kerry Road deposit. This combined with the wide stratigraphic spread of the mineralised areas suggests that they are likely not directly related and significant age differences may exist between mineralising episodes. As significant structural breaks occur throughout the GSB and many boundaries are tectonic rather than stratigraphic this is to be expected. Mineralised zones within different units may have formed distally and been brought together through later faulting.

To the south-east of the Allt na Cossaig the GSB and Lewisian gneisses are concealed below both the Torridonian and glacial deposits. Several inliers of Lewisian and likely LMG rocks occur in the Flowerdale Forest, a remote area to the south of Beinn an Eoin (Fig. 2.7). These consist of six small inliers along a 5 km length of glen floor. From west to east they are found at Loch a’ Bhealaich, Suileagan a’ Bhealaich, two at Loch na Cabhaig, Gorm-loch na Beinne, and An Lungard.

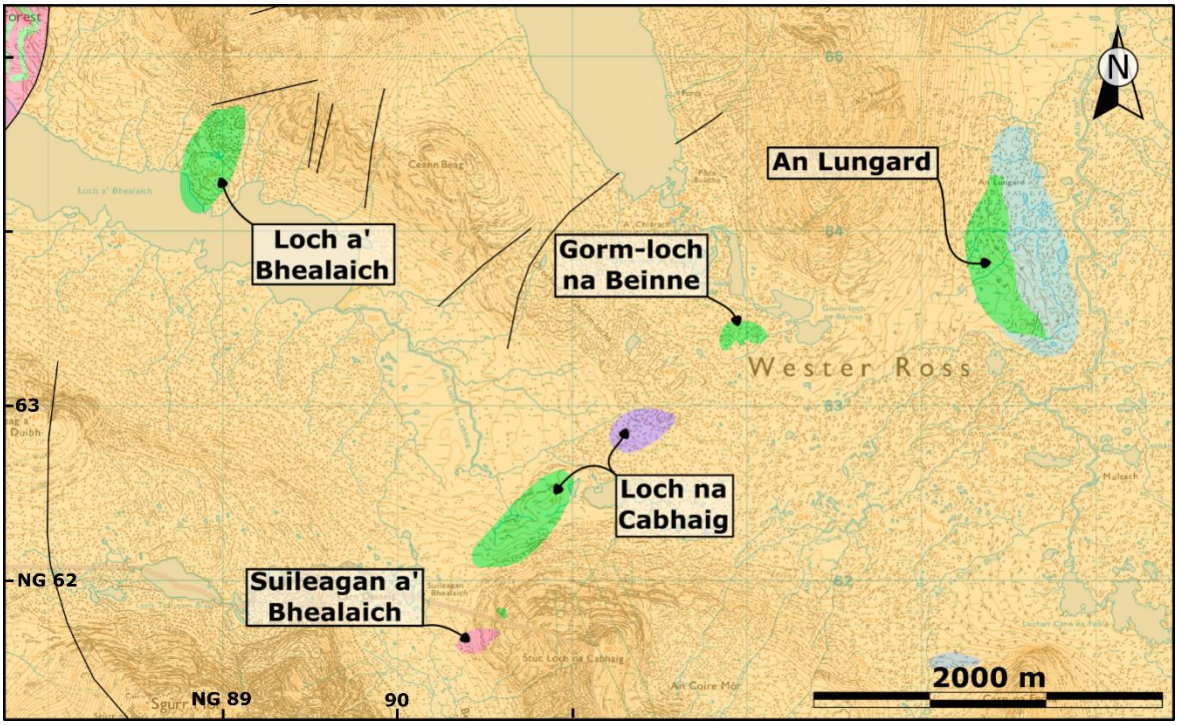

Figure 2.7. Location and simplified geological map showing large areas of Torridonian cover and the named Flowerdale inliers. Digimap (2020)

The largest inlier occurs at An Lungard where a massive amphibolite outcrops on the western side of Strath Lungard. The amphibolites here have been corelated with the Aundrary amphibolite of the GSB based on similar appearance, mineralogy, and stratigraphic position along strike (Coats et al., 1997). The Loch a' Bhealaich inlier is composed of layered mafic/ultramafic schists and may represent part of a layered intrusion (Coats et al., 1997). At Suileagan a' Bhealaich a small ridge of felsic gneiss is exposed below the basal Torridonian unconformity. The exposure is 100 m long and is dominated by coarse feldspar and quartz with minor amphiboles and biotite. This gneiss closely resembles the Lewisian gneisses that dominate the foreland. The Loch Na Cabhaig inliers are exposed in ground several hundred metres north-east and south west of the loch. The inlier to the south west is comprised of strongly banded fine-grained amphibolite. At the second inlier 800 m to the north-east a suite of coarse mafic and ultramafic rocks are present. The rocks of the inlier are only very weakly foliated to massive and are heavily altered. The British Geological Survey (BGS) Mineral Report Programme made a brief examination of the inlier (Coats et al., 1997) confirming its mafic/ultramafic composition and geophysical surveying showing a westward continuation beneath Torridonian cover.

The inlier at Gorm-loch na Beinne occurs 8 km along strike to the south east from the Allt na Cosaig exposure, and 800 m to the north-east of the Loch Na Cabhaig inlier. A small hillock to the west of the loch is formed of interbanded hornblende-felsic schist similar to the Kerrysdale amphibolite. A diverse range of lithologies occur as float, subcrop, and potential outcrop in an area of poorly exposed peatbog between the hillock and the loch (Fig. 2.8). These include mica schists, exhalative facies oxides and sulphides, amphibolites, gneisses, and mylonitic material. Metasedimentary lithologies are all slightly elevated in Au, Cu, and As, while exhalative lithologies contain Au levels as high as 4 ppm and enrichment in Zn, Cu, and As (Coats et al., 1997). Coats et al., (1997) suggest that the area can be correlated with the Kerry Road deposit on the basis of similar stratigraphic position and mineralisation style.

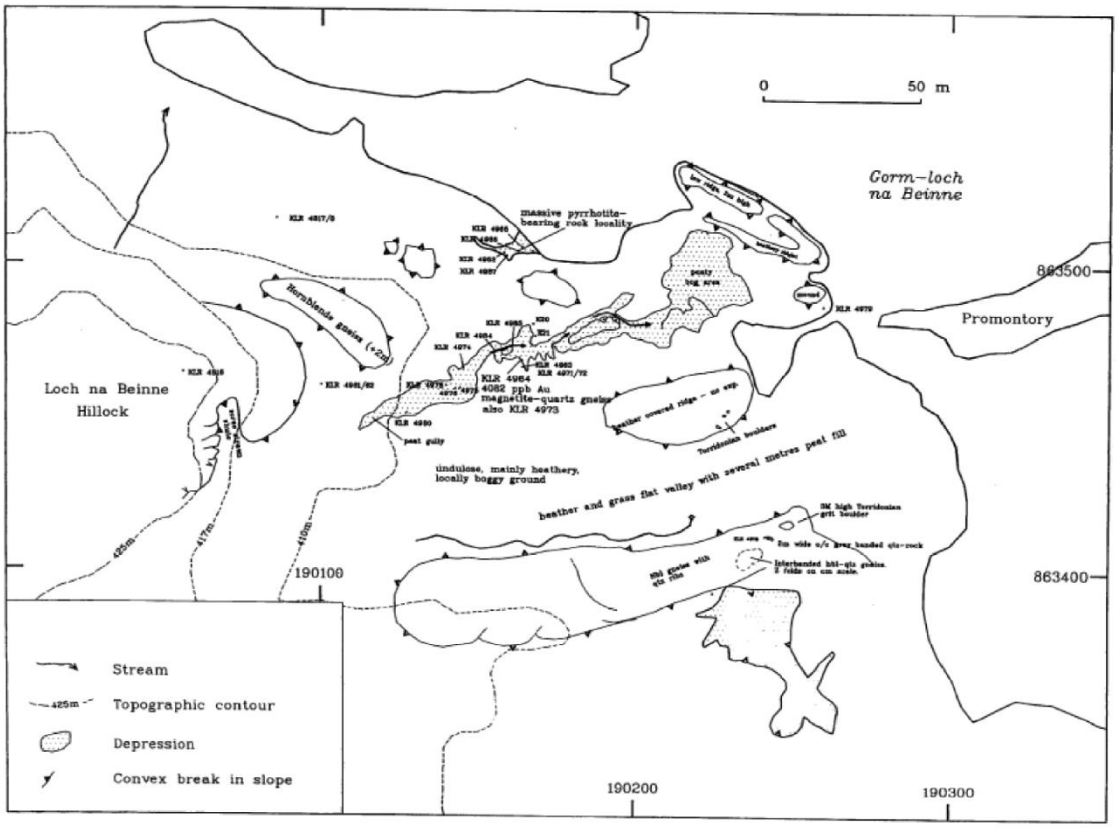

Figure 2.8. Map from Coats et al., (1997) showing the location of samples collected by the BGS from the Gorm-loch na Beinne inlier. Grades are recorded for some samples including an Au value of 4082 ppb from the central peat gully.

Sulphide mineralisation within the LMSB occurs in several units and includes stratiform pyrite ores, exhalative units, and schists. Some units can be matched with those in the GSB, such as a pyrite and pyrrhotite rich band within the Ben Lair hornblende schist that is a likely corelate of the Sidhean Mor gossan. Base and precious metals levels are generally low, with the highest Au level measured at 790 ppm. This coupled with the generally high levels of

exposure throughout the belt suggests there is not a comparatively sized metalliferous deposit to the Kerry Road site at a near surface position. Carbonate veins hosting sulphide minerals occur throughout the LMSB. These are generally fault related, trend north-easterly, and contain brecciated host rock as well as coarse pyrite. No metal enrichment was detected, suggesting that they had not scavenged and upgraded any metal deposits from other primary sources (Coats et al., 1997).

The potential for development of the Kerry Road site in light of improved economic prospects for a deposit of its size has led to renewed interest in the study of these satellite sites and the possible occurrence of others beneath shallow glacial or Torridonian cover.

2.1.4 - Gruinard Belt

The Gruinard Belt outcrops c. 10 km to the north of the LMSB, east of Gruinard Bay (Fig. 2.1). It comprises a thin band of mica schists, quartzites, and amphibolites trending NW – SE. The belt lies along the diffuse and highly strained boundary between amphibolite facies gneisses to the south, and granulite facies gneisses to the north (Love et al., 2010), and as such has been invoked at a potential terrane boundary of uncertain age (Love et al., 2010). It has been assigned both Archean (Crane, 1972; Park, 2002) and Proterozoic ages (Park et al., 2005; 2001) but no direct dating of the rocks has so far been undertaken. Contacts between metasedimentary units and the gneisses have been highly tectonised and no original contact relationships are discernible (Crane, 1972). Mapping shows lensoidal exposures of mica schists and quartzites are wrapped by garnet amphibolites trending NW – SE in a c. 300 m wide zone bounded on either side by higher grade Lewisian gneisses. Crane (1972) suggest Scourie dykes crosscut the belt and hence assigned it a pre-dyke age. He further assigned it a post-Badcallian age based on the lack of an early fabric and associated high grade metamorphism. Based on this interpretation he suggests the belt represents an unconformable cover sequence upon the Badcallian gneisses.

However the recently suggested Proterozoic ages (Love et al., 2010; Park et al., 2001, Park, 2005) allows for potential correlation with the Loch Maree Group, as in Figure 2.9, with the belt representing a continuation of the LMG on the north side of the Carnmore antiform (Love et al., 2010). This model is favoured by Park, (2005) where he proposes a two plate collisional model for the LGC as an alternative to the piecemeal terrane assembly model (Friend and Kinny, 2001; Kinny et al., 2005). The collision between an upper plate of peak granulite facies rocks variably retrogressed during the event, and a lower plate of late-Laxfordian peak amphibolite facies gneisses explains much of the current differences in metamorphic grade found across the complex (Crowley et al., 2015). The dominantly amphibolite facies gneisses of the Outer Hebrides would lie at a lower structural level than the mainland where a mixture of upper and lower plate gneisses and their bounding shear zones are exposed (Mason, 2016). In this model the LMG and Gruinard belts as well as the Outer Hebridean Langavat, Levenburgh, and Ness Paleoproterozoic belts lie along the suture zone between the two plates (Fig. 2.9).

The proposed Proterozoic ages for the belt and the potential for correlation with the LMG across the Carnmore antiform is a testable hypothesis. The spatial association of amphibolites and metasedimentary rocks withing the Gruinard Belt bears an at least passing

resemblance to the LMG, although within the LMG true quartzites are rare and the metasediments are dominated by schistose semipelites to psammites. The detrital zircon record of LMG metasediments (Whitehouse et al., 1997) displays two distinct peaks; a Late-Archaean peak, 3.06 - 2.48 Ga, potentially sourced from Lewisian gneisses and a Paleoproterozoic peak at 2.2 - 2.0 Ga that constrains the depositional age. The detrital zircon record of metasediments from the Gruinard belt could provide an important means of correlation, either positive or negative with the LMG. If Paleoproterozoic zircon exists within these rocks then a pre-dyke, for 2.4 Ga Scourie Dykes *sensu stricto*, age of deposition as argued by Crane (1972) would not be possible. Absence of this peak could suggest an Archean age for the belt and provide evidence against the models of Park et., (2001, 2005) and Love et al., (2010).

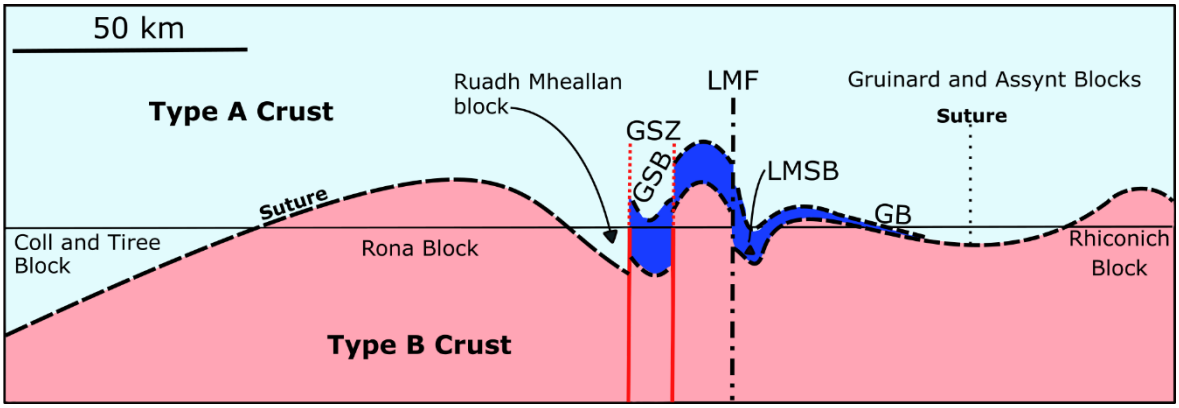

Figure 2.9. Simplified model of the mainland LGC modified from Park, (2005) with the complex split into blocks of three types based on their Laxford ian metamorphic features. **Type A Crust** – Upper-plate partially retrogressed granulites. **Type B Crust** – Lower-plate peak amphibolite facies metamorphosis. Paleoproterozoic complexes including oceanic and volcanic arc material including the mainland LMG and the Outer Hebridean Langavat and Levenburgh belts. **GB –** Gruinard Belt, **GSB –** Gairloch Schist Belt, **GSZ –** Gairloch Shear Zone, **LMSB –** Loch Maree Schist Belt, **LMF –** Loch Maree Fault.

2.2 – Basement to the Northern Highlands

The Sub-Moine basement to the NHT is exposed in a series of inliers of dominantly felsic orthogneisses that range in size from tens of kilometres to small c. 500 m slivers of material within the Moine metasediments (Tanner et al., 1970). Inliers are poorly studied compared to the LGC of the foreland, and in many cases the work is outdated and predates a modern theory of plate tectonics and terranes (Moorbath and Taylor, 1974; Sutton and Watson, 1952; Tanner and Geoffrey, 1970). The metamorphic histories of these rocks are especially poorly constrained. Events recorded in the foreland Lewisian may be present and may allow for correlation of inliers with individual foreland terranes based on protolith ages and metamorphic histories (Friend et al., 2008). Additionally a series of Proterozoic and Palaeozoic orogenic events may be recorded, including the Grenvillian, Renlandian, Knoydartian, and Caledonian (Bird, 2011; Storey, 2008). These inliers play a central role in addressing the extent to which the Moine and associated basement is allochthonous in regard to the foreland west of the Moine Thrust. On initial inspection their lithological similarity suggests correlation with the LGC, but the possibility of them forming part of a terrane accreted to the Laurentian margin either during or prior to the Caledonian is one worthy of examination.

Three main groups of inliers occur (Fig. 2.1); those found in northern Sutherland below the Naver Thrust, ones in the Scardory – Fannich area near or immediately above the Sgurr Beag Thrust, and finally those immediately above the Moine Thrust in Glenelg and Skye. Many inliers are fault bounded within the Moine, however in some cases original depositional unconformities exist between the inliers and the overlying Moine (Krabbendam et al., 2018) with some preserving way-up evidence that shows rocks younging away from the inliers. These conformable relationships mean that the current basement inliers are in many cases the original depositional basement to the Moine sedimentary rocks and allow some inferences into depositional controls upon the Moine to be drawn. Tanner et al., (1970) suggests that inliers found along the trace of the Sgurr Beag Thrust and above the Morar Group may be slices of a “basement high” within the original depositional basins of the Moine that potentially separated the Morar, and Glenfinnan – Loch Eil groups.

The correlation of Lewisianoid inliers with the foreland and the related potential continuation of mineralisation is influenced by the displacement across the Moine Thrust. Of particular relevance is the depth of detachment and deformation and the degree of

basement involvement and lateral movement that may have displaced rather than simply shortened structures within the basement. Correlation of major features across the Moine Thrust is complicated by the limited basement exposure within the NHT and the comparatively poor study of the basement inliers in comparison with the foreland. The best candidate for matching between the Hebridean and Northern Highland terranes is the Loch Shin Line, a geophysical lineament and associated exploitative granitic and appinitic intrusions into the overlying Moine. Holdsworth et al., (2015) propose this represents the continuation of the parallel and along strike Laxford Shear Zone below the Moine Nappes. In the foreland this separates the Rhiconich and Assynt blocks and if correlation with the Loch Shin Line is correct suggests a similar separation may be evident within inliers north and south of the line, if they represent simple slivers of Lewisian basement.

2.2.1 – Glenelg

The two Glenelg inliers, east and west, are the best studied of the Lewisianoid inliers within the Moine (Alderman, 1936), displaying a diverse range of lithologies and metamorphic histories (Fig. 2.10). The western Glenelg gneisses are dominated by Archean, c. 2.6 - 2.8 Ga (Kinny et al., 2008) orthogneiss with granulite metamorphism at c. 2.7 Ga and high-pressure eclogite faceis metamorphism at c. 1.75 Ga. This c. 1.75 Ga event may be a higher pressure expression of the amphibolite facies Laxfordian event recorded in the foreland (Storey, 2008: Storey et al., 2005). Amphibolite sheets cut gneissose layering and may be correlatable with Scourie dykes of the Lewisian (Ramsay, 1957). On the bases of these dates and lithologies is is generally considered that the western inlier is correlatable with the LGC.

The eastern gneisses contain in addition to c. 2.7 Ga orthogneiss; pelitic gneisses, graphitic pelites, marbles, and a range of semipelitic to psammitic gneissose rocks of generally Paleoproterozoic age. Small eclogite boudins and layers occur throughout the eastern inlier and may represent mafic intrusions or volcaniclastic sedimentary material (Krabbendam et al., 2018). The Eastern Glenelg gneisses display evidence of metamorphism at c. 1440 to 1490 Ma (Storey, 2002) concurrent with the Hallandian event in Scandinavia. Eclogite facies metamorphism in the eastern inlier is dated at c. 1.1 Ga and linked to the Grenvillian. As such the eastern gneisses do not record any of the events common within the LGC and only share a similar protolith age.

Although eclogites are found within both the eastern and western inliers, the ages for each are markedly different. As such the inliers record two separate high-pressure metamorphic events within a compact area and a suture must exist between them. The eastern and western gneisses therefore likely straddle the Grenville metamorphic front and were brought together during the collapse and exhumation of this orogen at c. 1000 Ma (Storey, 2002). This interpretation suggests that to the east of the eastern Glenelg inlier Grenvillian rocks may dominate the sub-Moine basement.

2.2.2 – Sutherland

Kinny et al. (2008) use U-Pb Zircon protolith ages to tentatively correlate the Borgie and Farr inliers with the Assynt block and the Ribigill inlier with the Rhiconich block. As all three inliers lie north of the proposed trace of the Loch Shin Line this suggests that either significant shuffling of inliers due to Caledonian deformation has occurred, or that simple matching between foreland and inliers may not be possible for other reasons. This is not altogether unexpected due to the variation within the foreland itself and the c. 100 km of shortening along the Moine Thrust (Elliott and Johnson 1980; Soper & Barber 1982; Butler & Coward 1984). These correlations are reliant on similar protolith ages and evidence of a roughly Laxfordian aged Pb loss event, while none of the inliers display evidence for the 2730 Ma or 2490 Ma metamorphic events expressed throughout the Gruinard and Assynt blocks respectively. This may suggest that these events are not expressed to the east of the current foreland, or that these inliers derive from an entirely separate crustal block that shares a similar protolith age to the Lewisian.

This discordance with the LGC is also evident within other northerly inliers. Strachan et al., (2020) present evidence of magmatism at 1770 – 1650 Ma along with metasedimentary units with a maximum depositional age of 1802 ± 51 Ma from the Loch Shin inlier. These features are not presently recognised within the Lewisian of the foreland and postdate the youngest phase of juvenile magmatism and sedimentation within the LGC, the LMG, by at least 100 Ma. Strachan et al., (2020) argue this, along with evidence for a 1100 – 1000 Ma Grenvillian suture and high-pressure metamorphism at Glenelg, provides evidence that the basement to the NHT may not be correlatable with the LGC and instead is Baltican in origin. They propose that during the c. 1100 – 1000 Ma collision of Baltica and Laurentia, prior to the final assembly of Rodinia, the suture zone ran through the present day NHT. The Moine thrust is proposed to have reworked this Grenvillian age structure (Strachan et al., 2020) and

mark the approximate boundary between Laurentian and Baltic basement. Direct evidence of this suture is present in the form of the Glenelg eclogites (Krabbendam et al., 2018; Storey et al., 2005), with a Baltican provenance for NHT inliers providing indirect evidence.

Not all inliers within the Moine are Precambrian in age. The Strathy Complex outcrops on the north coast of Sutherland (Fig. 2.1) and is comprised of silicic grey gneisses and amphibolites with minor marbles and ultramafic lithologies. It lies structurally below the overlying Moine and the boundary between the two is tectonic (Bird, 2011). Burns et al., (2004) assigned the complex a Grenvillian age based on $^{147}Sm/^{144}Nd$ isotopes, and suggested it formed related to subduction within the Rodinian ocean. However U-Pb zircon analyses from a trondhjemetic gneiss gives a crystallisation age of 503 ± 2 Ma (Dunk et al., 2019). As such the Strathy complex may date from the late Cambrian and was tectonically juxtaposed with the Moine during the Caledonian orogeny. Dunk et al., (2019) propose that a continental fragment was rifted from the Laurentian margin at c. 600 Ma carrying with it both the Northern Highland and Grampian terranes. Subduction zones and associated magmatic arcs formed on both sides of this microcontinent in the Late Cambrian, the Strathy Arc to the north, and the Midland Valley Arc to the south. During the Caledonian orogeny the microcontinent was accreted back to the Laurentian margin during the closure of the Iapetus ocean and associated back arc. The Strathy arc was imbricated within Moinian rocks, and the Midland Valley arc collided with the Grampian terrane to the south. Although the events proposed significantly post-date those of major importance to the NHT basement, they reinforce the likelihood of successive rifting and amalgamation of terranes along the Larurentian margin over repeated cycles of continental assembly and breakup.

2.2.3 – Strathconon

The Strathconon inliers (Fig. 2.10), the main focus of the work from the NHT presented in this study, are the largest collection of inliers within the Moine and yet the least studied. The group is volumetrically dominated by the large, c. 60 km^2, Scardroy inlier. This is comprised of grey gneiss with minor amounts of mafic and ultramafic material, marbles, and clastic metasedimentary rocks (Sutton and Watson, 1952). It is exposed above the Sgurr Beag Thrust (SBT) (William and Tanner, 1970) intercalated within the Moine above the Morar Group and below the Glenfinnan Group. Moorbath and Taylor (1974) obtain a whole rock Rb-Sr age of 2,810 ± 120 Ma, 2741 ± 120 Ma when adjusted for a more modern ^{87}Rb decay constant (Bird, 2011), and K-Ar ages from hornblende and biotite indicative of Caledonian

age resetting of these systems. Moorbath and Taylor (1974) use these data to correlate the inlier with the foreland Lewisian with additional and significant Caledonian reworking. Immediately to the east of the Strathconon Fault lies an undated inlier termed by this study the 'Loch Airigh' or 'Airigh' inlier. Its relationship with the main Scardoy mass is unclear due to the intervening Strathconon Fault. The Strathconon Fault runs subparallel to the Great Glen Fault and likely records motion subordinate to this larger fault. The only empirical study of the fault shows a period of sinistral motion at c. 430 – 425 Ma synchronous with the emplacement of the Ratagain granite (Stewart et al., 2001). Approximately 5 km to the east of the Airigh inlier is the Orrin inlier. This small area of gneisses lies entirely within the Glenfinnan Group and is exposed over an area of c. 2.7 km^2 in the core of an anticline (Fleuty, 1961). No dating has so far been carried out on the Orrin inlier.

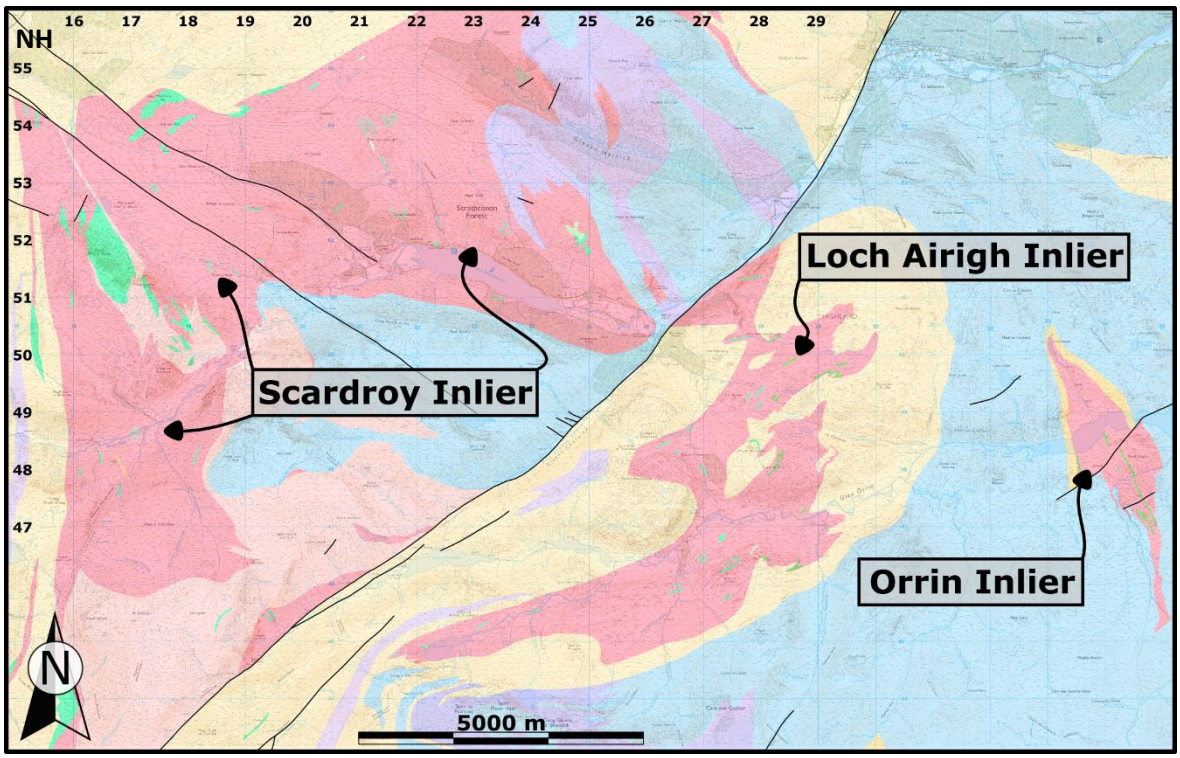

Figure 1.10. Generalised geologic map of the Strathconon inliers. The westerly Scardroy inlier is volumetrically dominant. The central 'Loch Airigh' inlier, as named by this study, lies east of the NE-SW trending Strathconon Fault. The small Orrin inlier is the most easterly. BGS mapping from Digimap (2020).

Reassessment of these central inliers in light of the potential exotic, non-Laurentian, origins within other inliers is considered a priority. All of the recent work on the NHT basement has focused on the Glenelg and Northern-Sutherland inliers, with no recent published work from Scardroy and the surrounding area. This leaves a considerable geographic hole in present data and is a problem for any attempted unifying model of these inliers. Geochronology and whole rock geochemical data presented within this study attempts to fill this gap and add

these inliers to within the ongoing discussion around the origin of the NHT basement. The origin of the sub-Moine basement has importance to any possible along strike continuation of mineralisation associated with the Lewisian supracrustal belts. The potential for this continuation was considered high enough for the BGS to examine the Scardroy inlier as part of the Special Mineral Report Programme (Coats et al., 1993).

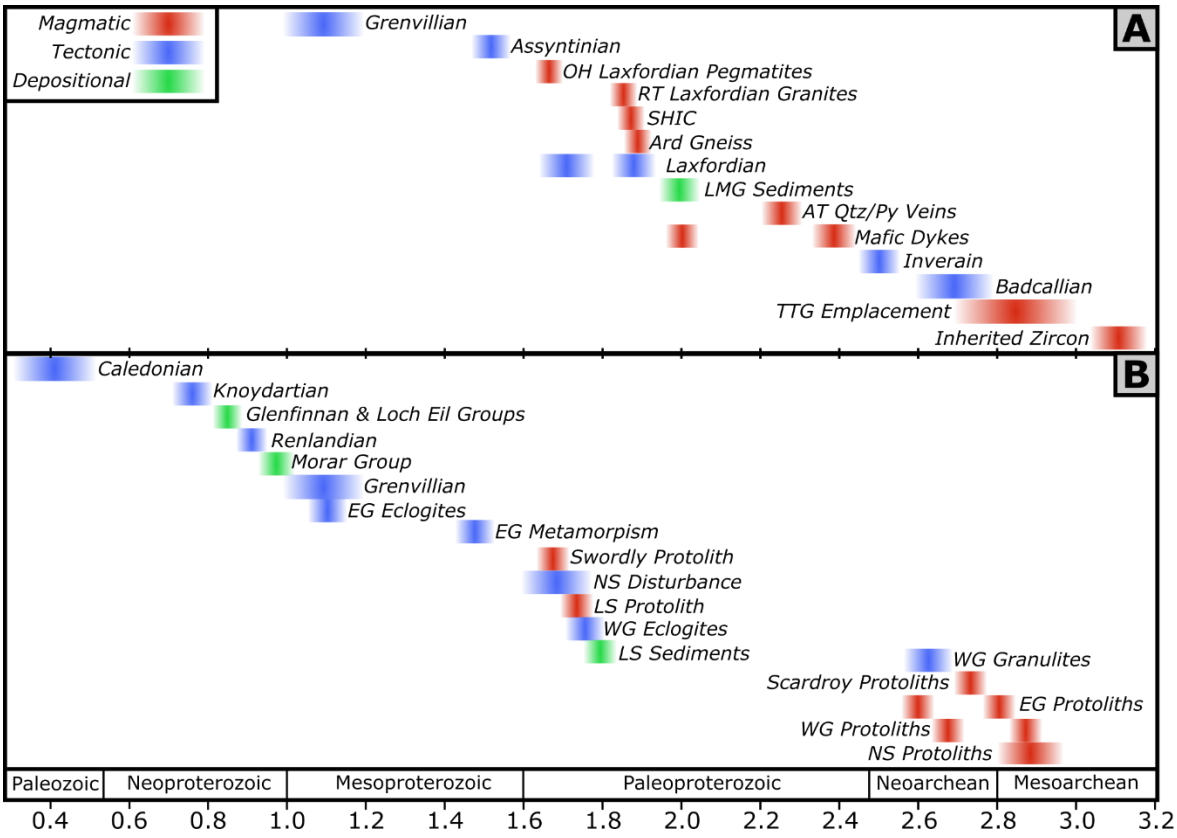

Figure 2.11. Generalised timeline of tectonic, magmatic, and depositional events to have affected the Hebridean **(A)** and Northern Highland **(B)** terranes with an emphasis on the basement rocks. Ages are generalised and may be subject to debate. Inclusion of events does not imply they occur across the region as a whole and evidence may be localised to a single block. **AT** – Assynt Terrane, **OH** – Outer Hebridean, **EG** – Easter Glenelg inlier, **WG** – Western Glenelg inlier, **NS** – North Sutherland inliers, **LS** – Loch Shin inlier. References for dates discussed in text.

Chapter 3: Methods

3.1 Field Work

Field work and sample collection was conducted over three trips. The first focused exclusively on the mineralisation of the LMG in conjunction with GreenOre Gold PLC (GreenOre) and was conducted over the 3rd and 4th of October 2019. A second visit on the 30th October to the 1st November facilitated the collection of additional samples from the LMG with GreenOre, and sites of tectonic interest to this study at the Gruinard Belt and Flowerdale inliers. Sample collection at the Scardory and Orrin inliers took place on the 23rd and 24th of January 2020. All sample locations, accompanying field photos and descriptions are detailed in Chapter 4. A longer field season had initially been planned to add detailed mapping of parts of the Scardroy and Orrin inliers and place collected samples in a better geologic context, however due to travel restrictions related to SARS-CoV-2 this was not possible.

3.2 Optical Microscopy

All thin sections and polished blocks were produced by the author at the University of Glasgow following standard procedures. Optical petrography in both transmitted and reflected light was conducted using an Olympus BX41 binocular microscope with attached Olympus DP25 camera.

3.3 Metallurgical Assay

Samples K25251 – K25274 inclusive were sent to ALS Global, Loughrea, Co. Galway for analysis. Here the samples were crushed to 70% < 2 mm (ALS code - CRU-31) and then riffle split (SPL-21). 1000 g of each sample was pulverised to 85% < 75 µm (PUL-32) before analysis. Gold content was analysed for 30 g samples using fire assay and atomic absorption spectrometry (Au-AA25). Upper and lower detection limits were 0.01 ppm and 100 ppm. All other elements were analysed via four-acid digestion and analysis via inductively coupled plasma atomic emission spectroscopy on a 0.4 g sample (ME-ICP61a). Duplicates, blanks, and standards were run for quality control and are presented in the appendix.

Analytes with upper and lower detection limits for each are presented in the table below. Due to the commercial nature of the laboratories used, uncertainties were not reported for each value in either data tables or associated figures. All certification is available on request from ALS Global, or viewable on their website.

Table 1. Upper and lower detection limits for elements analysed in addition to Au by ALS for samples K25251 – K25274

Analyte	Range (ppm)						
Ag	1 - 200	Cr	10 – 100,000	Na	0.05% - 30%	Ti	0.05% - 30%
Al	0.05% - 30%	Cu	10 – 100,000	Ni	10 – 100,000	Tl	50 – 50,000
As	50 – 100,000	Fe	0.05% - 50%	P	50 – 100,000	U	50 – 50,000
Ba	50 – 50,000	Ga	50 – 50,000	Pb	20 – 100,000	V	10 – 100,000
Be	10 – 10,000	K	0.1% - 30%	S	0.05% - 10%	W	50 – 50,000
Bi	20 – 50,000	La	50 – 50,000	Sb	50 – 50,000	Zn	20 – 100,000
Ca	0.05% - 50%	Mg	0.05% - 50%	Sc	10 – 50,000		
Cd	10 – 10,000	Mn	10 – 100,000	Sr	10 – 100,000		
Co	10 – 50,000	Mo	10 – 50,000	Th	50 – 50,000		

3.4 Rock Crushing

Samples for whole-rock geochemistry and mineral extraction were crushed at the University of Glasgow. Weathered surfaces were removed with a diamond-bladed rock saw and larger specimens were reduced to an appropriate size with a rock splitter. The sample was then run through the jaw crusher at decreasing jaw separation to reduce the sample to an appropriate size. Between each sample the jaws and collection tray were throuroughly cleaned of dust and rock fragments. For samples requiring mineral separation, aproximately 1.5 kg of sample was crushed. For samples undergoing whole-rock geochemistry approximately 100 g of sample was crushed and then a representative c. 10g of sample bagged and dispatched for analysis.

3.5 Whole Rock Geochemistry

Trace element analyis was performed at Activation Laboratories Ltd, Ancaster, Ontario, Canada. This was made possible by the financial support of a grant from the Edinburgh Geologic Society. The number of samples was limited by this funding and as such only selected samples were analysed. Aproximately 10 g of rough pulp sample was sent to

ActLabs; once there these were pulverized to 95% <105 µm using a mild steel mill (prep code – RX4). Analysis was then conducted using lithium metaborate/tetraborate fusion, nitric acid digestion, and inductively coupled plasma mass spectrometry (ICP-MS) (prep code – 4Litho). Analytes and lower detection limits are presented in the table below. Due to the commercial nature of the laboratories used, uncertainties were not reported for each value in either data tables or associated figures. Instead, general uncertainties are reported by the lab as: Major oxides >100x detection limit - +/- 5%, Minor/Trace element >100x detection limit - +/- 10%. Additionally all certification is available on request from Activation Laboratories Ltd, or viewable on their website.

Table 2. Analytes and lower detection limits for whole rock geochemistry

Analyte	**Limit (% / ppm)**						
Al_2O_3	0.01%	Be	1	Rb	22	La	0.1
CaO	0.01%	Bi	0.4	Sb	0.5	Ce	0.1
Fe_2O_3	0.01%	Co	1	Sc	1	Pr	0.05
K_2O	0.01%	Cr	20	Sn	1	Nd	0.1
MgO	0.01%	Cs	0.5	Sr	2	Sm	0.1
MnO	0.001%	Cu	10	Ta	0.1	Eu	0.05
Na_2O	0.01%	Ga	1	Th	0.1	Gd	0.1
P_2O_5	0.01%	Ge	1	Tl	0.1	Tb	0.1
SiO_2	0.01%	Hf	0.2	U	0.1	Dy	0.1
TiO_2	0.001%	In	0.2	V	5	Ho	0.1
LOI	0.01%	Mo	2	W	1	Er	0.1
Ag	0.5	Nb	1	Y	1	Tm	0.05
As	5	Ni	20	Zn	30	Yb	0.1
Ba	2	Pb	5	Zr	2	Lu	0.01

3.6 XRD

X-ray powder diffraction (XRD) was conducted at at the University of Glasgow, Joseph Black Building, with the assistance of the School of Chemistry. Several grams of each sample were finely powdered using a mortar and pestle. Measurements were obtained between a start position of 5 °2Th and an end position 90 °2Th. Scan type was continuous, with a scan step time of 30 seconds. Generator settings were 40 mA at 40 kV.

3.7 Mineral Separation

After the sample had been crushed, the fraction 90 – 500 µm was separated by sieving and then washed to remove fines and clays. Once dry the sample was vertically magnetically separated to remove strongly magnetic minerals. The non-magnetic component was then separated using lithium heteropolytungstate (LST) with a density of 2.8 g/mL. The component with a density greater than 2.8 g/mL was washed and dried. It was then magnetically separated at an angle of 20°. Magnetic fractions were separated at 0.4 A, 0.8 A, and 1.2 A. The non-magnetic fraction was separated using diiodomethane (DIM) with a density of 3.32 g/mL following the correct safety procedures. The fraction with a density > 3.32 g/mL was washed and examined under a binocular microscope. Grains identified as zircon were handpicked and arranged into a grid. This was transferred to double sided tape and then placed inside a 25 mm round mould into which resin was poured. Once cured the samples were removed from the moulds and sanded to an initial flatness at c. half zircon thickness with 800 grit paper. Rough polishing was achieved with 1200 and 4000 grit papers. Polishing was completed using a suspension of 1 µm aluminium oxide powder on a cloth mat until the sample resin and zircon grains appeared highly polished under reflected light.

3.8 Geochronology

This analysis was supported by a grant from the Geological Society of London. Analysis was conducted at the University of Hull on an Applied Spectra, Resolution-SE 193nm laser ablation system. LA spot size was 20/16 µm with a beam fluoresce of 2.5 J sm-2, a pulse width of 5 ns, a repetition rate of 10 Hz and an ablation duration of 30 s. ICP-MS analysis was carried out for masses 204, 206, 207, 208, 232, 235, and 238 on an Agilent 8800. NIST-612 glass and the Plešovice standard were used as primary reference materials with the 91500 zircon standard used as a secondary reference material. Data were processed at the University of Hull using Iolite v.3, Data Reduction Scheme - X_U_Pb_Geochron4 of Paton et al., (2011). Data processing and classification of core and rim spots were done by Kit Harman and Dr Eddie Dempsey. All processed data are presented in Appendix 3 - 7. Analysis of processed data was conducted using IsoplotR (Vermeesch, 2018).

Chapter 4: Results

4.1 - Loch Maree Group

The work conducted into mineralisation of the LMG was part funded and supported by GreenOre Gold PLC (GreenOre). GreenOre is a "junior exploration company focused on identifying high potential gold prospects in Scotland". They acquired the Gairloch licence in mid-2018. This licence covers the main Kerry Road deposit as well as the surrounding area from the Rubha Reidh peninsula in the north, to the Flowerdale forest in the south. The original project at the Kerry Road site was abandoned due to it being below economic grade at the time, though recent increases in metal prices have led to its revaluation. As part of its initial reassessment of the deposit in 2019 GreenOre drilled a 55 m deep borehole stepped back from the main outcrop, Fig 4.1. This test hole confirmed the grades as originally reported by Jones et al., (1987) at 1 g/t Au, 0.9% Cu and 0.6% Zn over 17m (including 8 m at 1.8 g/t Au, 1.4% Cu and 0.7% Zn). At the time of discovery the deposit was not tested for Cobalt, with GreenOre's initial drilling returned Co values of up to 370 ppm. This is a value below the standalone economic grade, but one which adds diversity to the potential mine output.

The sampling strategy, formed in conjunction with GreenOre, was designed to follow up on reports from Jones et al., (1987) and Coats et al., (1997) and investigate additional mineralisation potential throughout the GSB. The VMS model for the Kerry Road orebody supports the possibility of additional mineralised localities as VMS deposits are commonly found in belts containing multiple pods of mineralisation (Galley et al., 2007). The work described in Jones et al., (1987) had focused primarily on the main ore deposit at Kerry Road, however several other sites had been identified as of potential interest. As part of this study each of these locations was visited and resampled. Additionally, a general exploration of the area led to the collection of additional float and outcrop samples based on distinctive weathering patterns. Coats et al., (1997) had identified the Flowderdale area, and specifically the Gorm-loch na Beinne inlier, as of interest due to the occurrence of sulphide bearing float within peat. Exploratory sampling and geophysical surveys confirmed the existence of potentially economic mineralisation in the area with gold values of up to 4 ppm. This study resampled the Gorm-loch na Beinn inlier and the nearby inliers at Loch na Cabhaig. In all 33 samples were collected from the GSB or potential GSB outcrops. Of these 24, K25251 –

K25274, were of economic interest and were assayed for a wide range of elements at ALS Minerals, Loughrea, Ireland (ALS). In addition, selected samples were analysed at the University of Glasgow using reflected and transmitted light microscopy. The 9 samples collected from the Loch na Cabhaig inliers, M1 – M9, were of interest due to the occurrence of ultramafic rocks near to, or potentially within the LMG. These samples were analysed at the University of Glasgow using XRD, transmitted light microscopy, and whole rock trace element analysis at Activation Laboratories Ltd, Ancaster, Canada. Locations of all samples are plotted on Fig. 4.2 and are additionally presented in Appendix 1 along with the field descriptions for each sample.

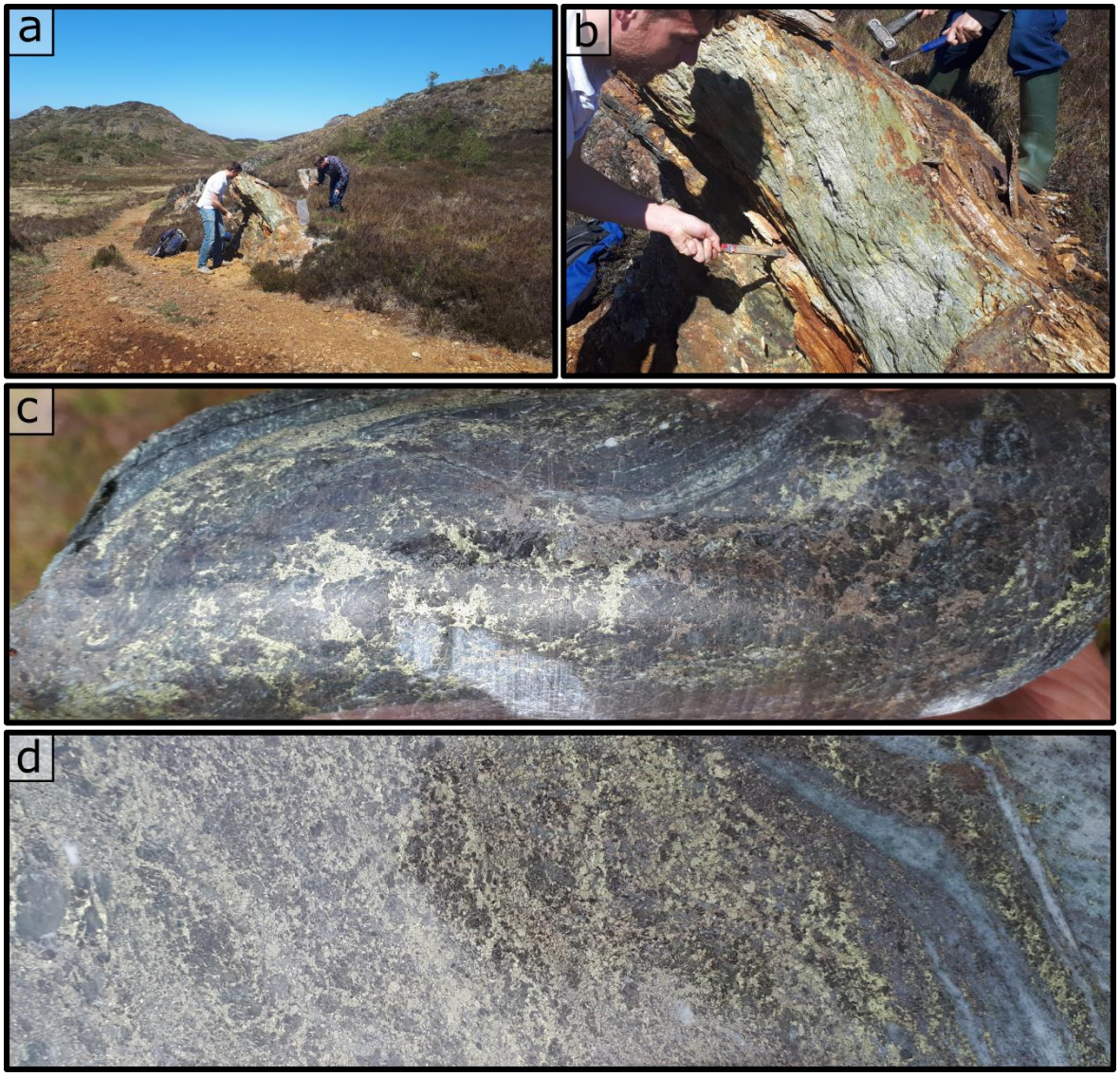

Figure 4.1 Kerry Road ore-body**. a)** The Kerry Road site showing orange weathered regolith and outcrop of the main orebody. **b)** Closeup of sampling the Kerry Road site showing the malachite stained and foliated outcrop dipping to the NE **c)** Pictures of core obtained from the GreenOre confirmatory drilling showing highly tectonised sulphides and host rock. **d)** A second image of core from the GreenOre sampling showing high ratio of sulphides to host rock and a well-defined durchbewegung fabric incorporating host rock fragments in a sulphide matrix of pyrite, chalcopyrite, and pyrrhotite.

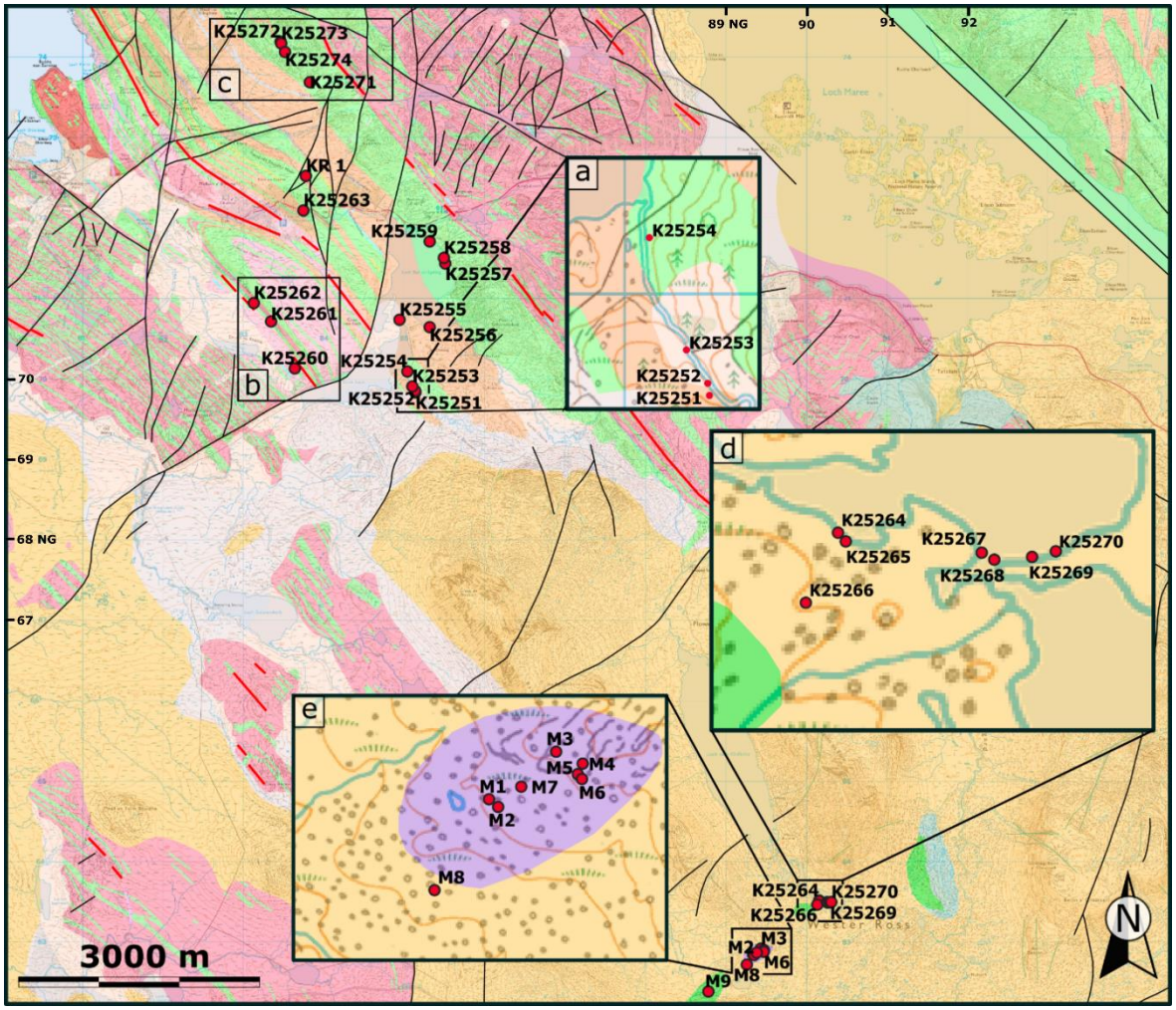

Figure 4.2. Map showing the location of samples collected from the GSB and surrounding areas. Kerry Road locality marked by sample KR1. Sites from Jones et al., (1987); **a)** Allt na Cosaig, **b)** Druim na Fearna, **c)** Sidhean Mor. Sites from Coats et al., (1997); **d)** Gorm-loch na Beinn **e)** Loch na Cabhaig. BGS 1:50,000 geologic mapping and Ordnance Survey 1:50,000 basemap from Digimap (2020)

4.1.1 - Field Observations and Petrography

4.1.1.1 - Allt na Cosaig

The Allt na Cosaig flows NW into the Dubh Loch at the south end of Loch Bad an Sgalaig (Fig 4.2). The area contains the most south-easterly exposure of the stratigraphically lower schist units of the GSB before they are concealed below Torridonian cover. The site occupies a similar stratigraphic position within the belt as the Kerry Road deposit, lying directly below the Flowerdale Schist. Jones et al., (1987) describe the exploration undertaken after discovery of sulphide bearing pebbles in the overlying Torridonian basal conglomerate. Initial magnetic and resistivity (VLF-EM) geophysical surveys produced a coincident anomaly under the Allt na Cosaig. Sampling of an exposed quartz-mica schist revealed elevated levels of Zn (0.33 wt%) as well as Pb and Cu. An amphibolite schist in contact with the quartz-mica schists contained abundant magnetite bands. Two drill holes encountered 9 m thickness of quartz-mica-carbonate schists with elevated Cr levels (0.3 wt%) but only trace amounts of sulphide mineralisation. They assign the geophysical anomalies to abundant graphitic and pyritic bands within the quartz-mica schist, but these did not display any geochemical anomalies worthy of further investigation at the time.

In conjunction with GreenOre, the author returned to the site and collected samples for assay and analysis. Two samples (K25251 – 2) were collected from an oxidised outcrop of fine grained foliated and folded amphibolite forming the southern side of the deeply incised burn. The north bank of the stream is formed of highly shattered pale schists that display a pronounced foliation parallel to that recorded in the amphibolite. The two outcrops sampled are separated by c. 20m with the upstream outcrop striking 340° and dipping at 70° and the downstream outcrop striking 310° and dipping 80°. This strike is consistent with the overall NE trend of the GSB with variation attributable to small scale folding and faulting. An additional sample (K25253) was collected from the stream bed c. 100 m downstream to the NW where low water levels revealed a series of calcite veins containing large brassy and euhedral pyrite crystals. Veins varied in width from c. 10 mm to c. 100 mm with pyrite up to c. 30 mm. The veins appeared to be near vertical and ran 320° – 140°, parallel to the course of the Allt na Cosaig. The presence of these veins along with the boundary between amphibolite and pale schists may indicate the presence of a fault exploited by the watercourse.

On return from the site, along the east side of Dubh Loch and Loch Bad an Sgalaig, a series of samples of heavily oxidised sulphide bearing float were collected from the shore-line (K25254, 55, 57, 58). In hand specimen all float samples displayed a high specific gravity and obvious naked eye sulphide contents of c. 50% or more with host rock occurring as dark rounded clasts within this sulphide matrix. In addition two outcrop samples from the east

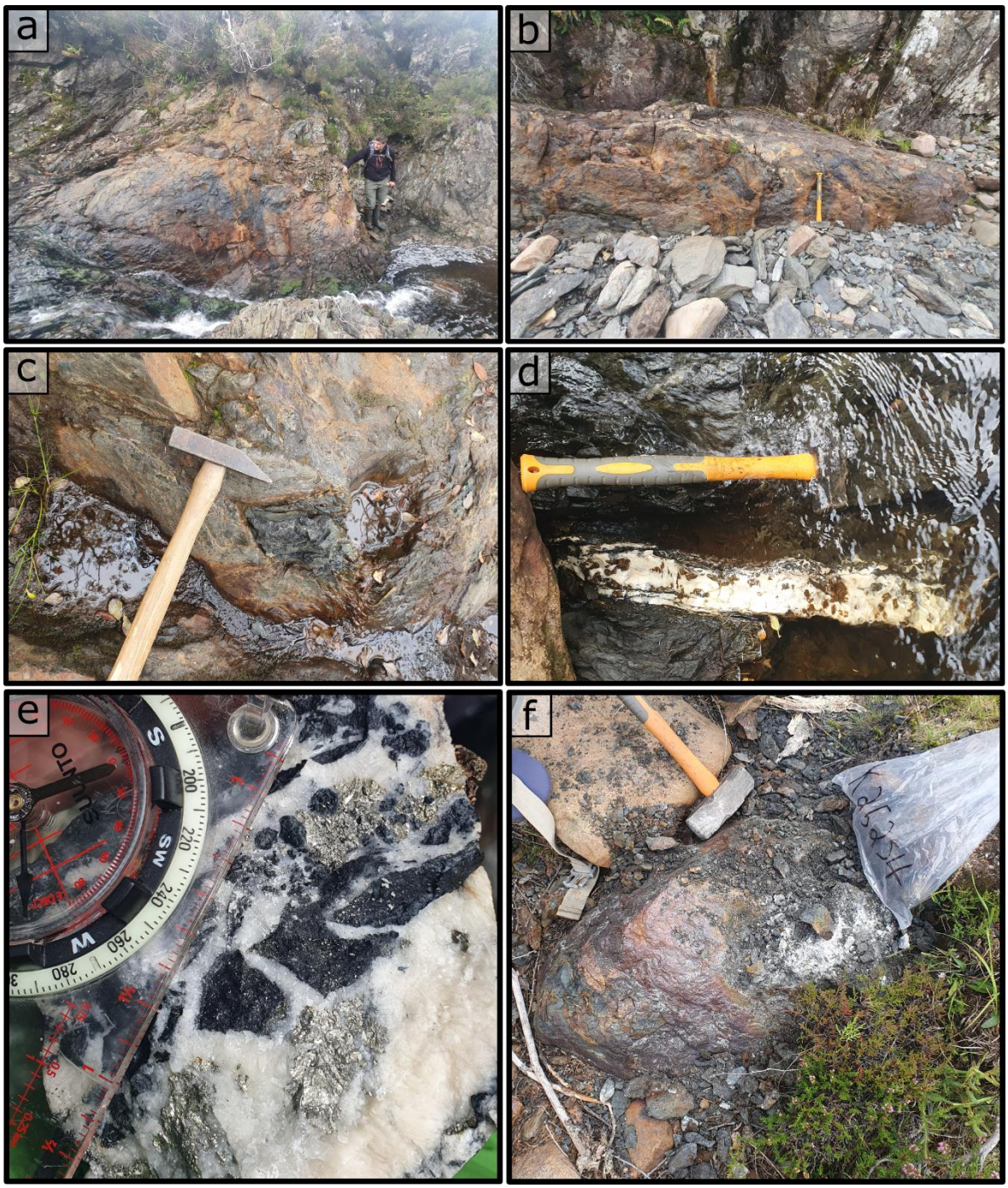

Figure 4.3. a) Outcrop of sample K25251 showing oxidised unit on south bank of Allt na Cosaig. **b)** Sample K25252 c. 20 m downstream from a) showing likely continuation of the same unit. **c)** Shear indicator in K25252. **d)** Calcite vein in the Allt na Cosaig with large oxidised pyrite, K25253. **e)** Fresh sample of calcite vein K25253 showing large brassy pyrite and brecciated texture of wall rock incorporated into vein. **f)** K25254 float sample at mouth of Allt na Cosaig showing distinctive weathering.

side of the loch were collected due to distinct oxide weathering. K25256 was an orange coloured and strongly cleaved schist poorly exposed near the loch shore. K25259 occurred as a narrow, c. 30 cm, band of orange oxidised rock within an amphibolite. In addition, several occurrences of iron seeps and associated mineral precipitation occurred along the loch shore where water exited the peat cover.

In thin section, Fig. 4.4, K25251 and K25252 display a fine, 0.05 – 0.1 mm, matrix dominated by pleochroic amphibole and quartz. Large garnets up to 3 mm are present as metamorphic porphyroblasts that overgrow the existing foliation with occasional strain wrapping of the foliation. Small garnets 0.5 mm are found along foliated coarser quartz veins. Disseminated opaques are found throughout the matrix with concentration in fractures and make up c. 5 % of the rock. Float sample K25255 displays a tightly folded amphibole and quartz dominated host rock present as rounded clasts ranging in size from c. 40 mm to single 0.25 mm grains in a sulphide matrix. Small clasts are sub-angular to rounded suggesting a degree of rotation within the matrix. Sulphides are dominated by Pyrite (Py), with Sphalerite (Sp), and minor Chalcopyrite (Ccp), and Galena (Gn). This durchbewegung texture indicates that sulphide phases pre-date at least one major deformational phase.

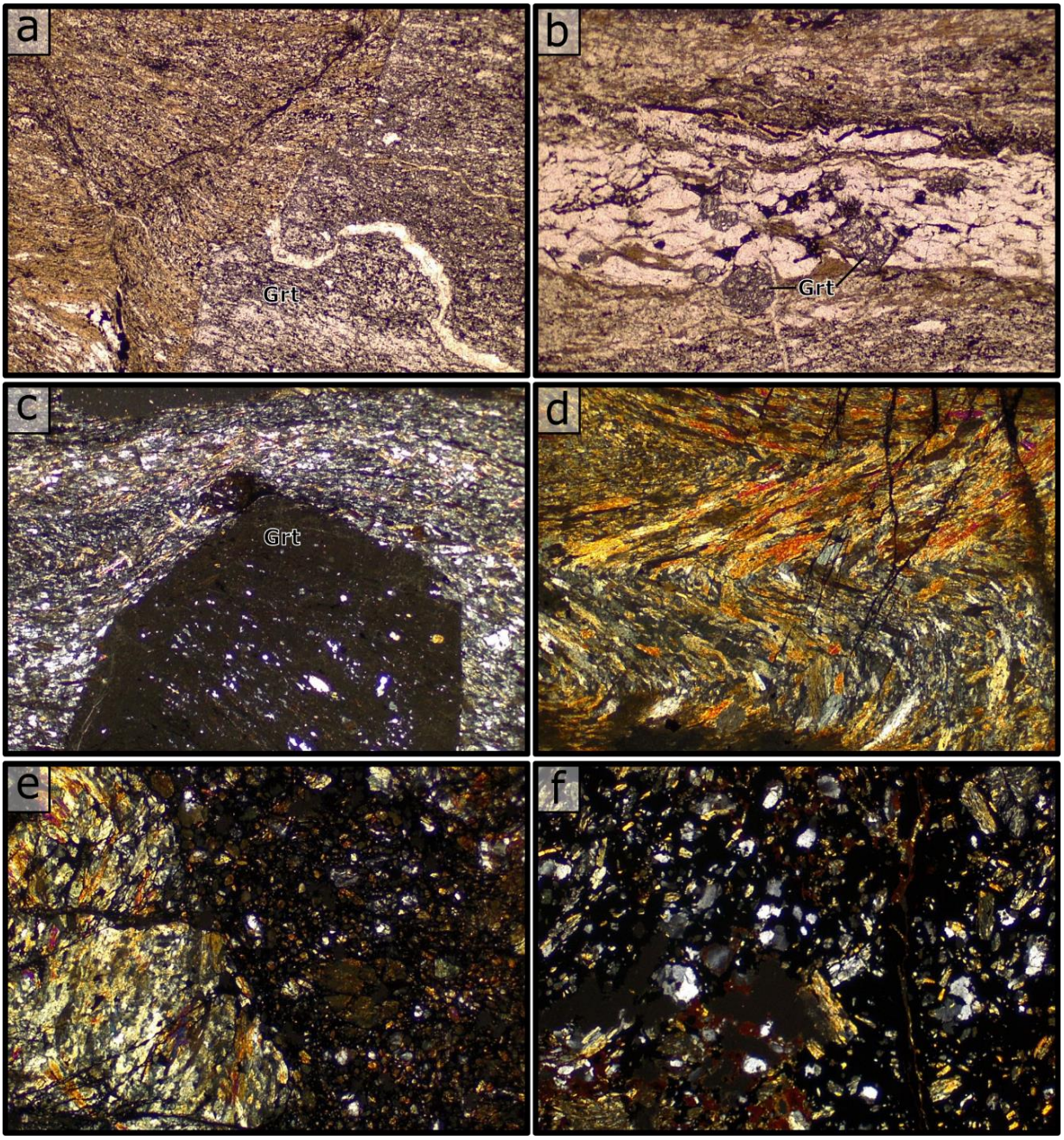

Figure 4.4. FOV in all photomicrographs – 4mm **a)** K25251 – ppl - Large garnet in fine grained amphibole rich matrix. Folded quartz vein overgrown by garnet. Fine grained sulphides visible as dark areas of matrix. **b)** K25251 – ppl – Deformed coarse quartz vein with small, 0.25 - 0.5 mm garnets. **c)** K25251 - xpl – Garnet showing foliation in internal inclusion and strain wrapping. **d)** K25254 – xpl – Tight folding in amphibole and quartz host rock. **e)** K25254 – xpl – Large fractured host rock fragment (left) and durchbewegung textured sulphide/host rock (right) **f)** K25254 – xpl – Durchbewegung textured sulphides and host rock.

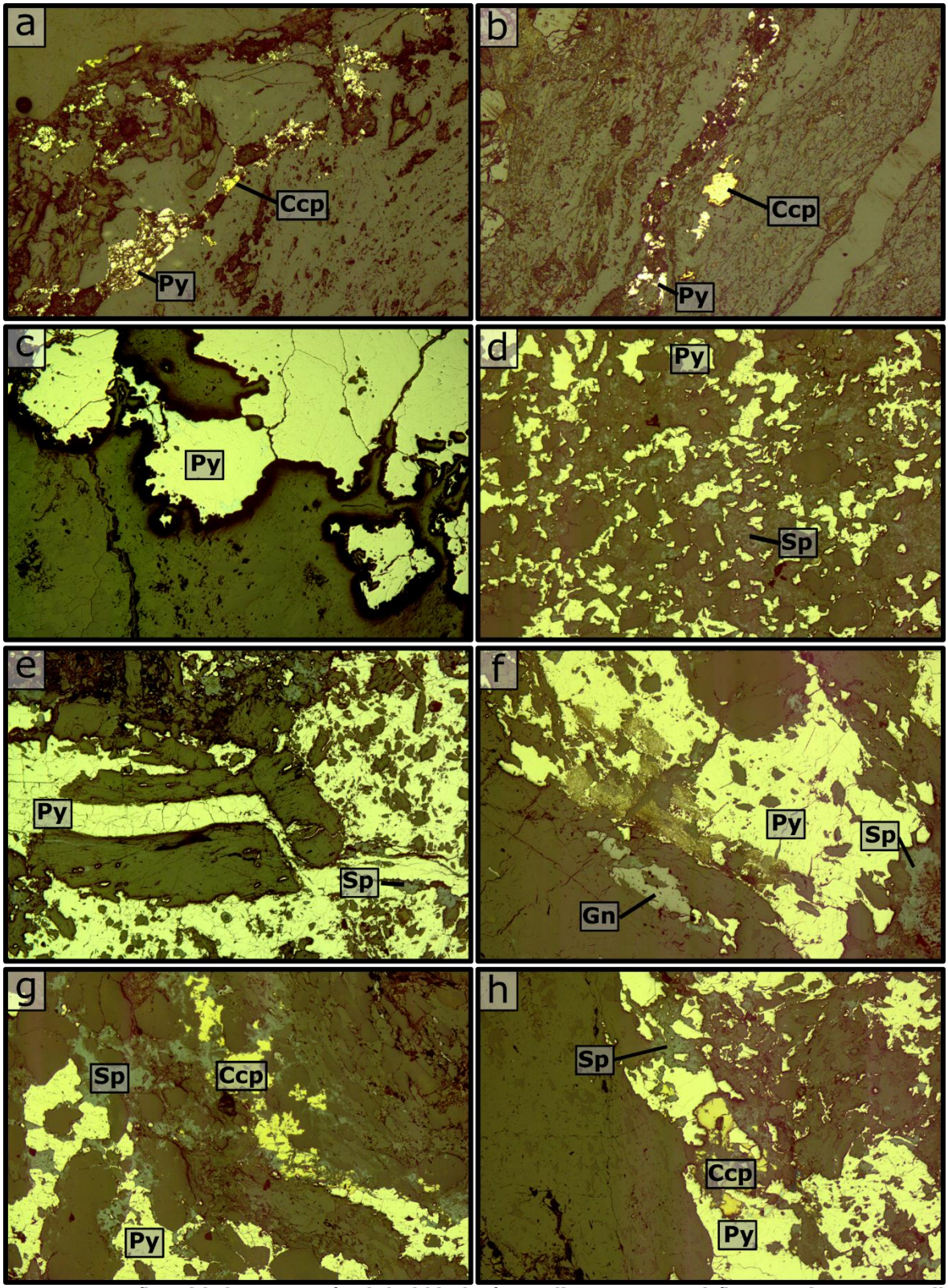

Figure 4.5. Reflected light images of polished blocks from Allt na Cosaig and float samples. FOV in all photomicrographs – 4mm **a)** Fine pyrite and chalcopyrite in sample K25251 **b)** Minor veined pyrite and chalcopyrite parallel to foliation in K25251 **c)** Coarse pyrite in course calcite vein - K25253 **d)** Durchbewegung textured pyrite, sphalerite, and host rock - K25255 **e)** Durchbewegung textured pyrite cut by later pyrite vein - K25255 **f)** Coarse pyrite with minor sphalerite and galena - K25255 **g)** Coarse and euhedral pyrite with sphalerite and chalcopyrite - K25255 **h)** Coarse to durchbewegung textured pyrite with minor sphalerite and chalcopyrite - K25255

4.1.1.2 - Druim na Fearna

The Drium na Fearna area lies at the southern boundary of the GSB. Here Lewisian gneisses are tectonically intercalated with amphibolites, marbles, and schists of the GSB. Anomalous Cu values, 0.26 wt%, were recorded from a massive amphibolite containing disseminated chalcopyrite, bornite, malachite, chalcocite, pyrite and pyrrhotite. Intermittent occurrences of chalcopyrite were found for over 4 km along the southern edge of the GSB, but mineral potential was considered to be low (Jones et al., 1987).

The amphibolite described by Jones et al., (1987) was re-sampled (K25260). This displayed abundant cross-cutting sets of quartz veins with minor oxidation weathering at the surface of the outcrop. Two samples (K25261 – 62) were collected from the upper section of the Allt na Claise a few hundred metres to the NW. Both samples consisted of strongly banded amphibolite with minor pyrite visible in hand specimen. These two samples lie close to the trend of the Mill na Claise crush belt and were collected due to the potential for fluids within this zone to upgrade any disseminated mineralisation.

In thin section all three samples (K25260 – 62) are comprised of subequal proportions of green pleochroic amphibole (0.25 – 1 mm), sericitisised plagioclase, and quartz. The strong banding observed at hand specimen scale is defined by segregation of amphibole, and plagioclase/quartz into 1 – 3 mm wide zones with amphibole aligned parallel to this banding. Sulphides are found disseminated throughout the section at no more than c. 5 % and are c. 0.25 – 0.05 mm in size.

4.1.1.3 - Sidhean Mor

A near continuous gossan of orange weathered sulphide rich rock can be traced through the Aundrary Amphibolite for nearly 6 km (Jones et al., 1987). This is the stratigraphically highest unit within the GSB and outcrops along the northern boundary of the belt with the LGC. At Sidean Mor this gossan is hosted in a zone of mixed schists and amphibolites within the Aundrary Amphibolite. The band of schists and sulphides occurs along the boundary between coarse grained massive amphibolite, and fine grained banded amphibolites (Fig. 4.6).

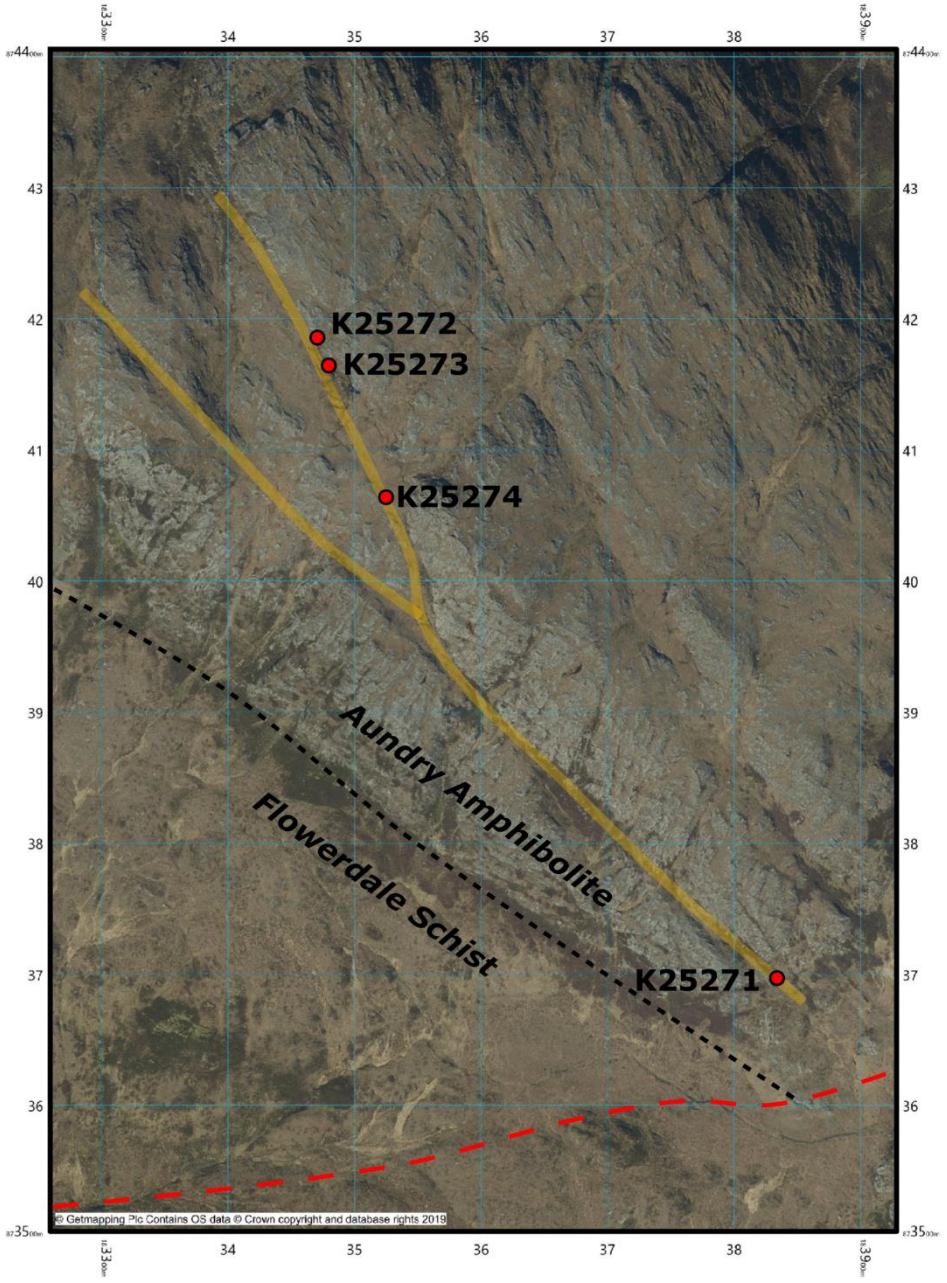

Figure 4.6 Aerial imagery showing the surface trace of the Sidhean Mor gossan as a prominent weathered gully between resistant amphibolites. Digimap (2020)

The gossan was traced from its first occurrence at the base of Sidhean Mor, near a minor fault, in a westerly direction to near the summit of Sidhean Mor. Sample K25271 was collected from the easternmost exposure of this gossan where is it is c. 5 m wide (Fig. 4.7a) and in direct contact with amphibolite on both sides. The trace of the unit occupies a prominent gully running across the topography and visible on aerial imagery (Fig. 4.6). South of the summit the gossan bifurcates with samples K25272 – 74 collected from the northern branch at its widest observed point in an area of flat ground c. 100 m to the west of the summit. This is the location described in Jones et al., (1987) where two test holes were drilled that returned only iron sulphides in the form of Py and Po of up to 30 % in siliceous schists. Here the gossan reaches c. 20 m in width and is moderately well exposed. The unit is heavily oxidised and prominent convolute folding is present at outcrop scale (Fig. 4.7b,c). In thin section the samples show banding formed of coarse (0.25 – 1 mm) quartz rich zones and fine grained (0.05 – 0.25 mm) mica and actinolite rich zones. This banding is commonly pinched out and disrupted, suggesting a high degree of deformation. Sulphides vary in concentration between samples from c. 5 % to c. 20 % and are concentrated in but disseminated throughout the finer grained amphibole rich layers.

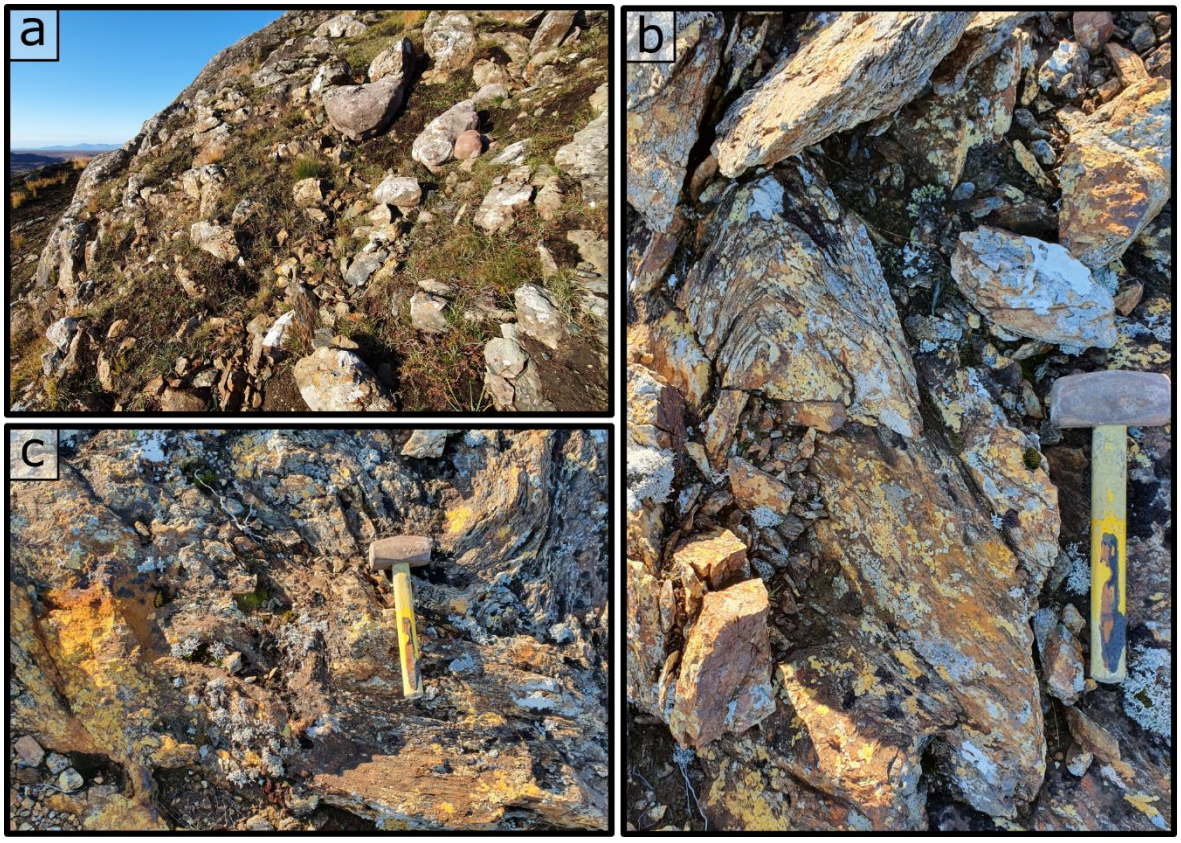

Figure 4.7. Field photos showing outcrop of the Sidhean Mor gossan. **a)** K25271 – 5 m wide exposure of oxidised sulphide bearing unit at the eastern base of Sidhean Mor. **b) and c)**. K25272/3 – Heavily folded and oxidised outcrop of gossanous unit to the west of the summit.

4.1.1.4 - Gorm-loch na Beinne

GreenOre had a particular interest in the Gorm-loch na Beinne inlier due to reports in Coats et al., (1997) of Au values of up to 4 ppm. In addition to litho-geochemical sampling, magnetic and VLF geophysical surveys were conducted across the inlier by the BGS. Two large magnetic deviations occur, the first occurs over the hillock (Fig. 4.8c) and is a positive anomaly of 5000 nT. A second anomaly occurs close to the shore of the loch and has a positive amplitude of 2000 nT adjacent to a 5000 nT negative anomaly. A strong VLF-M anomaly occurs adjacent to the second magnetic anomaly and is comparable to the geophysical responses over the main Kerry Road mineralised horizon. These strong geophysical anomalies in conjunction with the precious metal anomalies justify economic interest in the inlier. The sampling undertaken and reported here was limited by two main factors. Firstly, the area is remote and requires a 10 km walk in and out on stalking paths and then trackless bog. Secondly, exposure is very poor, with the majority of samples reported by Coats et al., (1997) being float recovered from the peat cover, sometimes with significant manual digging. This sampling appears to have been fairly extensive and may be the reason little material was available at the surface for sampling by this study.

The best exposure in the inlier occurs where amphibolite is exposed on the hillock to the west of the loch (Fig. 4.8) and in several smaller outcrops to the north and south of the main peat gully. This amphibolite was deemed by Coats et al., (1997) to resemble the Kerrysdale amphibolite on textural and geochemical grounds. This was not sampled as part of this study as all sampling was focused on the mineralised lithologies. Samples from the central peat gully were collected based on evidence of mineralisation at hand specimen scale due to either the presence of visible sulphide minerals, oxidation products, or high specific gravity. Two samples (K25264 - 65) were collected in a shallow embayment into the peat cover at the location described as containing massive pyrrhotite bearing rock by Coats et al., (1997). These samples were shallowly protruding from the peat, and it is unclear as to whether they represent large float or possible outcrop, as such they have been deemed subcrop (Fig. 4.8a). Despite their proximity, c. 50 cm, the two samples were separated due to differences in lithology with K25265 containing appreciable hematite with sulphides in comparison to only sulphides in K25264.

Exposure in the main peat gully was very poor with no evidence of the multiple float samples collected by Coats et al., (1997). At one location at the south edge of the main peat gully the bank appeared to have recently collapsed and exposed several blocks. Here sample K25266

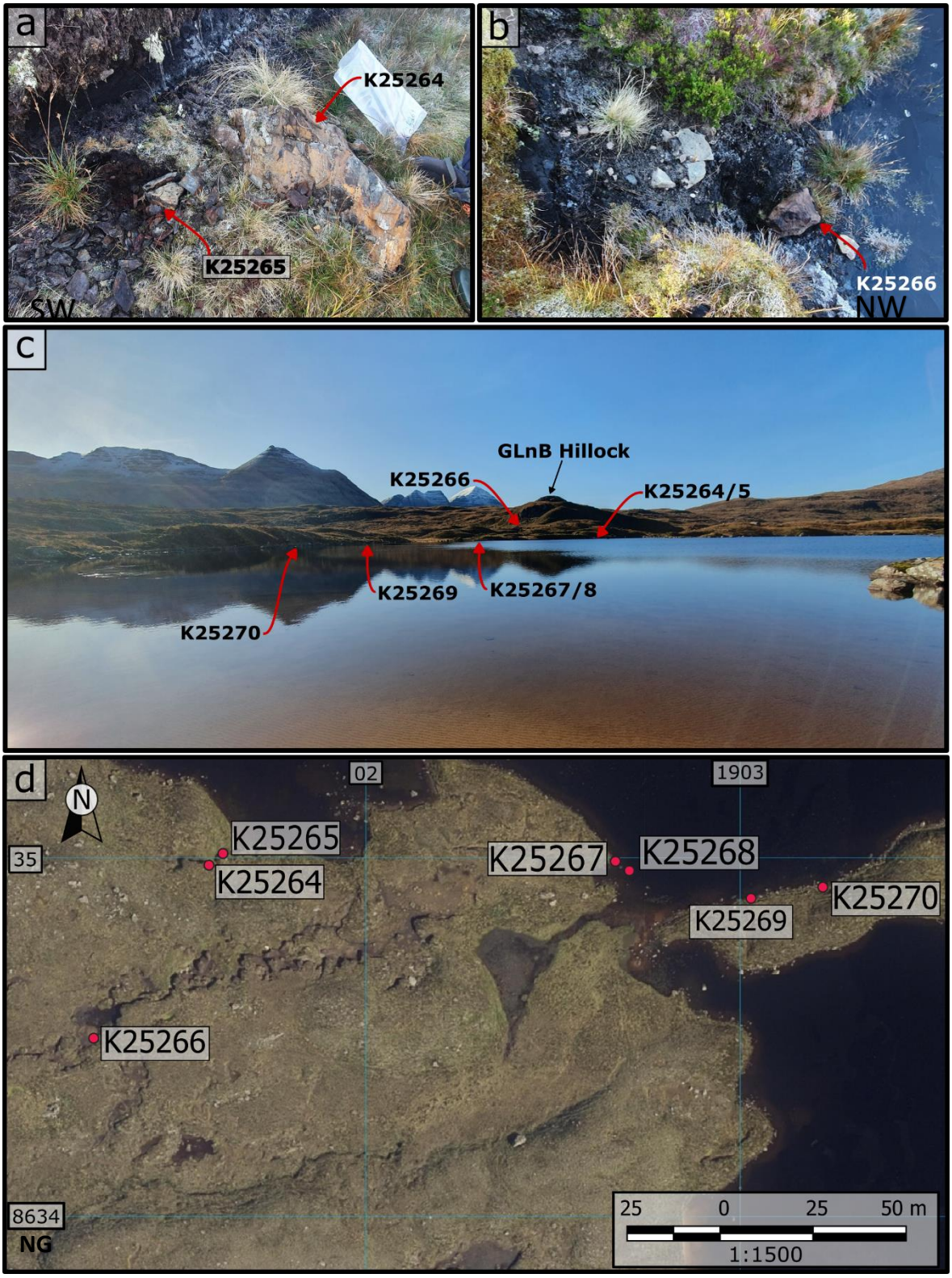

Figure 4.8. a) Samples K25264/5 showing large block protruding from peat cover. Darker red colour of K25265 due to hematite. The difficulty of assessing the in-situ nature of the blocks led to their classification as Subcrop. Sample bag 30cm. **b)** Sample K25266 (40 cm) in central peat gully. Pale rock to the left of the sample is quartz rich and resembles the quartz mylonite (KLR 4975) of Coats et al., (1997) **c)** View from the east side of the loch showing the distribution of samples in low lying ground below the hillock **d)** Arial photo with sample locations showing poor exposure and large central peat gully. Digimap (2020)

was collected from a large block located in the peat bank (Fig. 4.8b). In addition to the mineralised sample collected from this locality, a white quartzite was observed in the bank but was not collected. This location was the closest located sample to KLR 4964; collected by Coats et al., (1997) that returned an assay value of 4 ppm. Samples K25267 – 68 were collected from shallow water on the west side of the loch near the promontory. It was observed while collecting these samples that the loch-bed was orange/yellow in colour, possibly reflecting an oxidised component to the sediments. Coats et al., (1997) suggested that sulphide facies exhalates may underlie much of the loch based on the geophysical anomalies and a tentative proposed stratigraphy from float mapping. Samples K25269 – 70 were collected from the northern side of the promontory bisecting the loch with K25270 large enough to be classed as a likely in situ outcrop. In polished section the samples show a range of sulphide minerals and associated textures (Fig. 4.9). K25266 shows small amounts of disseminated/minor veining of pyrite and chalcopyrite. K25268 shows larger altered anhedral pyrite with exsolution and rimming textures. K25269 shows massive pyrrotite and pyrite forming up to c. 40% of the sample in a heavily disrupted host rock.

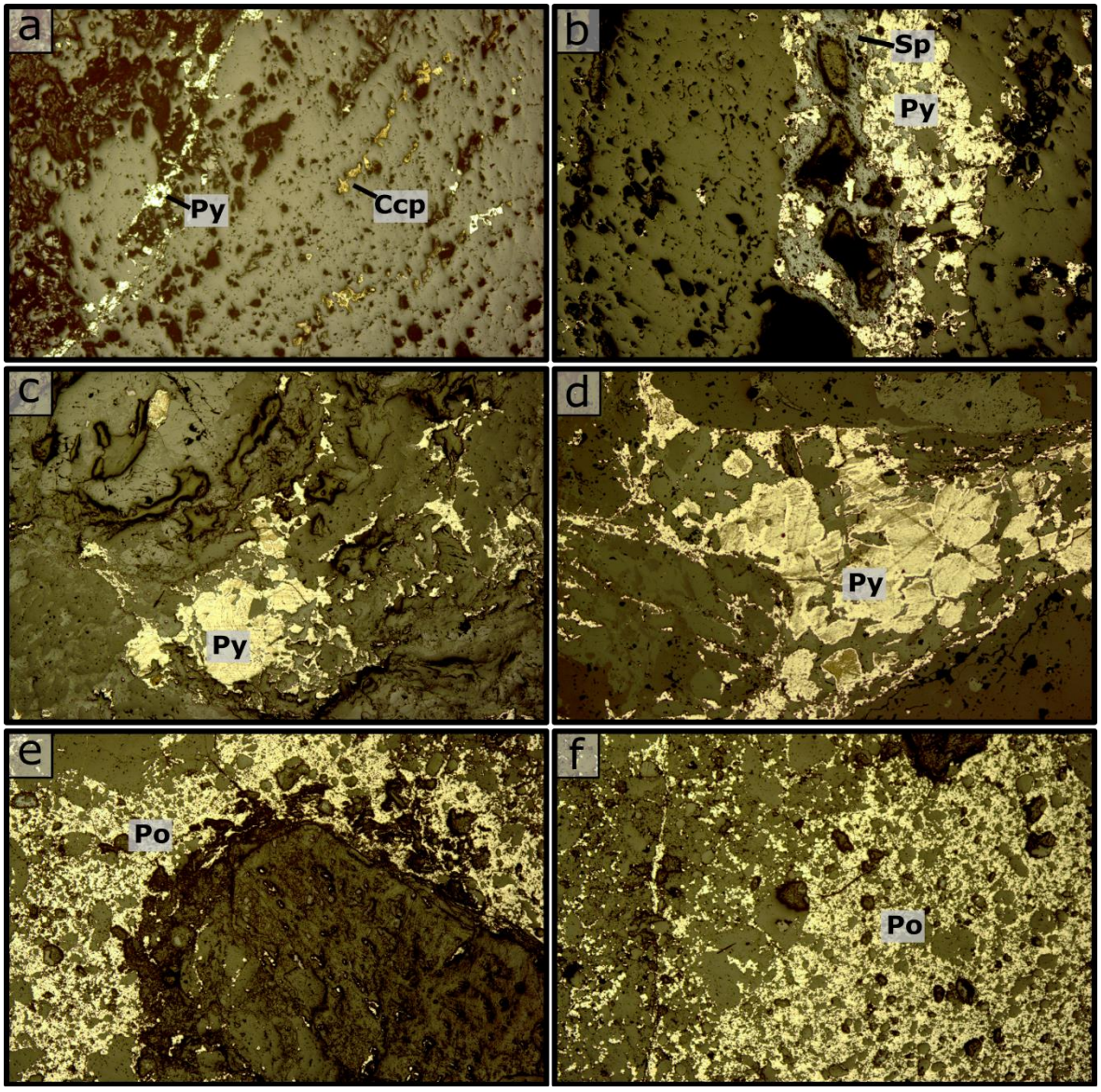

Figure 4.9. FOV in all photomicrographs – 4mm **a) K25266** Veined or disseminated pyrite and chalcopyrite parallel to foliation in host rock. **b) K25266** Pyrite and sphalerite. **c) K25268** Pyrite in heavily deformed host rock. **d) K25268** Pyrite showing exsolution laminae and alteration. **e) K25269** Massive pyrrhotite and host rock displaying durchbewegung texture of rounded gangue in a matrix or sulphides **f) K25269** Massive pyrrhotite with durchbewegung texture.

4.1.2 - Metallurgical assay

Table 3. Assay results for samples K25251 – K25262 via methods detailed in Section 3.3. <x indicates values below detection limits. Uncertainties are not reported due to the commercial nature of the analysis, as discussed in Section 3.3.

Samples (K25251 – K25262)

Element ppm	51	52	53	54	55	56	57	58	59	60	61	62
	Allt Na Cossaig			Lochside						Drium Na Fearna		
Au	<0.01	0.01	<0.01	<0.01	0.01	<0.01	0.05	0.01	<0.01	0.03	0.01	<0.01
Ag	2	1	<1	1	1	<1	1	<1	<1	<1	<1	<1
Al %	6.26	6.51	0.19	2.16	0.76	3.31	1.69	2.51	4.82	6.33	6.14	6.28
As	70	50	420	<50	<50	<50	<50	<50	<50	<50	<50	<50
Ba	160	330	<50	<50	<50	310	<50	<50	<50	100	70	700
Be	<10	<10	<10	<10	<10	<10	<10	<10	<10	<10	<10	<10
Bi	<20	<20	<20	<20	<20	<20	<20	<20	<20	<20	<20	<20
Ca %	0.55	0.46	34.1	3.85	0.69	0.74	2.64	2.89	3.59	3.16	5.01	7.14
Cd	10	<10	<10	<10	<10	<10	<10	<10	<10	<10	<10	<10
Co	30	20	10	100	70	30	110	80	80	40	40	30
Cr	80	150	<10	60	50	230	60	100	70	10	80	60
Cu	440	220	20	1610	250	60	710	870	380	110	180	110
Fe %	12.95	6.85	6.4	24	17.25	4.18	29.9	26.7	20.8	9.94	5.38	6.73
Ga	<50	<50	<50	<50	<50	<50	<50	<50	<50	<50	<50	<50
K %	0.7	0.6	<0.1	<0.1	<0.1	2.1	<0.1	<0.1	0.1	0.5	0.3	0.8
La	<50	<50	100	<50	<50	<50	<50	<50	<50	<50	<50	<50
Mg %	1.5	3.43	0.21	4.06	0.72	2.09	2.42	1.95	2.56	3.42	2.38	1.42
Mn	9050	6140	7550	1060	360	230	2600	1780	1410	620	730	940
Mo	20	70	20	10	10	<10	20	10	10	<10	30	<10
Na %	0.79	2.83	<0.05	0.33	<0.05	1.45	0.21	0.34	0.67	3.06	2.66	2.67
Ni	200	150	20	150	300	110	400	260	200	40	80	40
P	970	870	<50	1360	2260	580	2240	1080	1410	540	350	1000
Pb	320	70	540	<20	50	30	<20	<20	<20	<20	<20	<20
S %	1.17	2.48	6.6	>10	>10	2.32	>10	>10	7.26	<.05	2.48	0.47
Sb	<50	<50	<50	<50	<50	<50	<50	<50	<50	<50	<50	<50
Sc	10	20	<10	10	10	10	10	10	30	10	40	10
Sr	50	150	180	10	<10	90	10	10	20	140	100	600
Th	<50	<50	<50	<50	<50	<50	<50	<50	<50	<50	<50	<50
Ti %	0.3	0.61	<.05	0.18	0.16	0.29	0.13	0.23	0.61	0.59	0.2	0.65
Tl	<50	<50	280	<50	<50	<50	<50	<50	<50	<50	<50	<50
U	<50	<50	<50	<50	<50	<50	<50	<50	<50	<50	<50	<50
V	470	730	20	160	70	140	120	150	310	290	360	220
W	<50	<50	<50	<50	<50	<50	<50	<50	<50	<50	<50	<50
Zn	380	290	170	180	70	110	260	320	210	50	190	100

Table 3. Assay results for samples K25263 – K25274 via methods detailed in Section 3.3. <x indicates values below detection limits. Uncertainties are not reported due to the commercial nature of the analysis, as discussed in Section 3.3.

	Sample (K25263 – K25274)											
Element ppm	**63**	**64**	**65**	**66**	**67**	**68**	**69**	**70**	**71**	**72**	**73**	**74**
		Flowerdale							Sidean Mor			
Au	<0.01	<0.01	<0.01	0.2	0.17	0.06	0.03	<0.01	<0.01	<0.01	<0.01	<0.01
Ag	<1	1	1	1	<1	4	3	1	<1	<1	<1	<1
Al %	6.24	0.42	4.52	1.41	0.64	1.06	0.54	5.38	5.64	4.97	6.17	6.77
As	<50	<50	<50	750	140	110	80	<50	<50	120	<50	<50
Ba	90	<50	150	<50	<50	60	50	190	60	50	<50	<50
Be	<10	<10	<10	<10	<10	<10	<10	<10	<10	<10	<10	<10
Bi	<20	<20	<20	<20	<20	<20	<20	<20	<20	<20	<20	<20
Ca %	4.28	0.24	1.15	0.57	1.03	1.13	0.93	4.58	4.89	4.49	5.06	6.27
Cd	<10	<10	<10	<10	<10	<10	<10	10	<10	<10	<10	<10
Co	10	<10	20	40	20	30	90	50	60	10	10	80
Cr	180	20	100	40	30	30	50	130	100	150	120	990
Cu	60	50	140	300	80	340	240	180	210	150	130	240
Fe %	8.85	5.56	11.5	6.97	15.6	25	23.7	10.1	11	6.23	8.27	8.42
Ga	<50	<50	<50	<50	<50	<50	<50	<50	<50	<50	<50	<50
K %	0.6	0.1	0.4	<0.1	<0.1	0.1	0.1	0.3	0.1	0.2	0.1	0.1
La	<50	<50	<50	<50	<50	<50	<50	<50	<50	<50	<50	<50
Mg %	2.78	0.28	1.66	0.28	0.43	0.8	0.18	2.79	3.38	3.9	3.44	3.77
Mn	760	1270	1000	6080	3960	6020	570	2130	1430	960	1180	1150
Mo	10	<10	20	<10	<10	<10	10	10	<10	<10	<10	10
Na %	2.29	<0.05	1.86	<0.05	<0.05	<0.05	<0.05	1.79	1.51	1.15	1.64	1.23
Ni	30	10	70	110	50	110	270	120	220	30	30	480
P	460	800	1590	590	3700	3690	3900	590	450	320	340	380
Pb	<20	<20	20	<20	<20	<20	30	<20	<20	<20	<20	<20
S %	1.01	1.64	2.68	3.35	4.61	9.2	>10.0	2.2	3.11	0.48	1.04	1.56
Sb	<50	<50	<50	<50	<50	<50	<50	<50	<50	<50	<50	<50
Sc	40	<10	20	<10	<10	<10	<10	30	30	40	40	40
Sr	110	10	240	<10	20	30	20	290	110	70	100	110
Th	<50	<50	<50	<50	<50	<50	<50	<50	<50	<50	<50	<50
Ti %	0.69	<0.05	0.58	0.07	<0.05	<0.05	0.13	0.68	0.54	0.17	0.39	0.27
Tl	<50	<50	<50	<50	<50	<50	<50	<50	<50	<50	<50	<50
V	350	20	360	70	20	30	110	400	320	260	320	320
W	<50	<50	<50	<50	<50	<50	<50	<50	<50	<50	<50	<50
Zn	190	40	380	130	60	70	50	390	290	180	320	130

The oxidised amphibolite from the Allt na Cosaig (K25251/2) returned gold values below detection (Fig. 4.10). However Ag at 2 ppm and 1ppm, Cu at 440 ppm and 220 ppm, and Zn at 380 ppm and 290 ppm were all slightly elevated. The pyrite bearing vein, K25253, was low in base metals: 170 ppm Zn, 20 ppm Cu, 0.25% Al, and rich in Fe - 17.9%. The sample is dominated by calcite as is reflected in the Ca value of 68.5%. Post-transition metal values are the highest of any sample with 550 ppm Pb, 240 ppm Tl, and the second highest As values of any sample at 420 ppm. It is also the only sample to contain La, 100 ppm, at values above detection.

The float and outcrop samples from the east bank of Dubh Loch and Loch Bad an Sgalaig had gold above detection limits in three samples, K25255 – 0.01 ppm, K25257 – 0.05 ppm, and K25258 – 0.01 ppm. Silver was at 1 ppm in K25254, K25255, and K25257. The highest copper value of any sample was found in K25254 at 1640 ppm (0.16%) with values of 250 ppm, 60 ppm, 710 ppm, 870 ppm, and 380 ppm in K25255 – 59, respectively. Two samples, K25254 and K25257, had cobalt values over 100 ppm. Three samples recorded Zn levels above 200 ppm, K25257 – 260 ppm, K25258 – 320 ppm, and K25259 – 210 ppm. Iron was high in almost all the samples with all but K25256 recording values above 15%, and K252757 showing 29.9% Fe, while sulphur was above the maximum detection level (10 %) in K25254/5 and K25257/8. These high Fe and S values back up the optical identification of massive pyrite forming much of each sample.

Of the three amphibolites from the Druim na Fearna area, only K25260 recorded gold above detection, 0.03 ppm. Silver was below detection in all samples. Copper was low in all three at between 110 and 180 pmm, with higher Zn in the second two samples; 190 and 100 ppm as opposed to 50 ppm in the unit drilled by Jones et al., (1987).

All four samples from the Sidhean Mor gossan returned Au and Ag below detection. Base metal values are also low with averages of 230 ppm Zn, 180 ppm Cu, and Pb below detection. Iron ranges from 6.2% to 11% with sulphur from 0.48% to 3.11%.

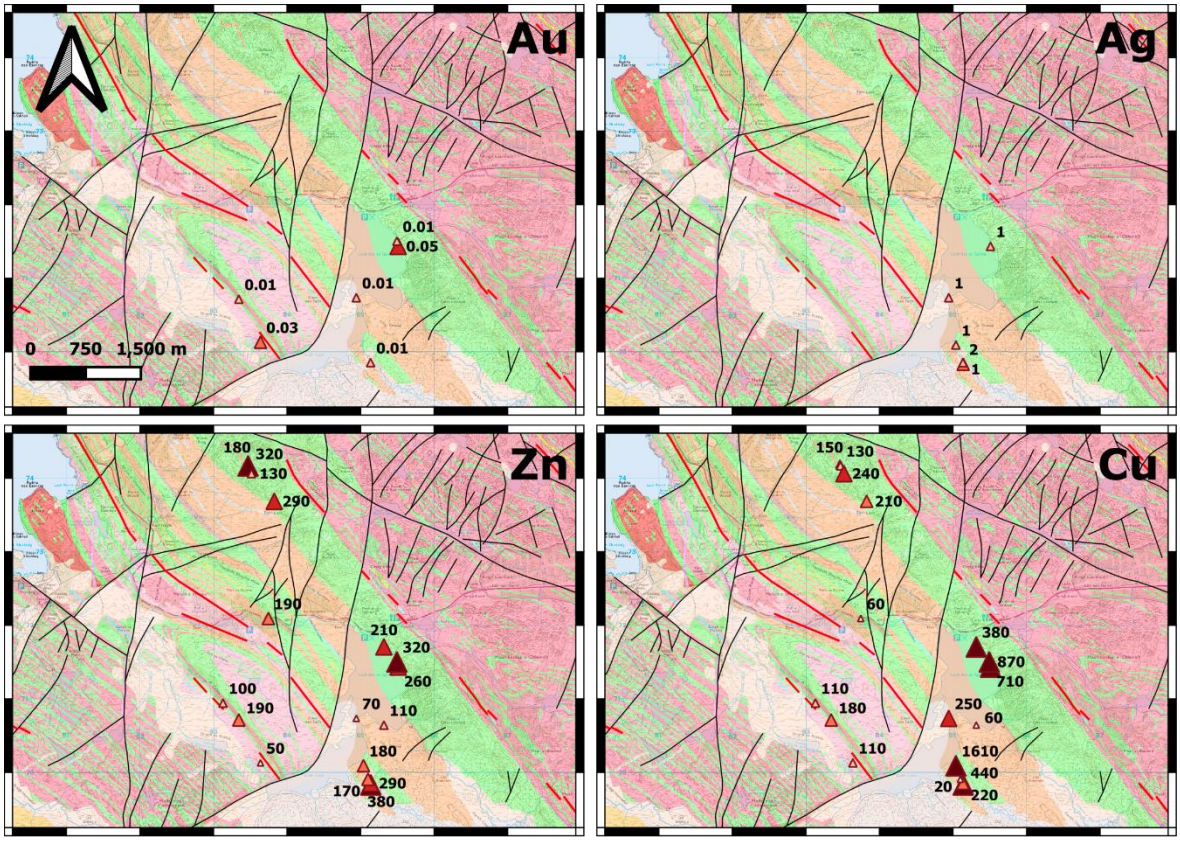

Fig. 4.10. Maps showing assay results for samples from the GSB above detection levels for elements Au, Ag, Zn, and Cu. Symbol sizes were automatically binned using equal ranges in QGIS. All values in ppm. Digimap (2020).

The Gorm-loch na Beinn inlier is the only location sampled to display significant precious metal mineralisation (Fig. 4.11). Precious metal values are above detection in 4 samples, K25266 – 69, that record Au values of 0.2 ppm, 0.17 ppm. 0.06 ppm, and 0.03 ppm respectively. These are the highest Au values of any samples, but significantly below the 4 ppm reported from the inlier by Coats et al., (1997). Silver values are similarly above detection in six of the seven samples with 1ppm in K25264-66 and K25270, 3 ppm in K25269, and 4 ppm in K25268. The only sample to record Ag below detection, K25267, records the highest gold value of 0.17 ppm. Base metal values from all samples are low with maximum values of 390 ppm Zn, 340 ppm Cu, 30 ppm Pb. Iron varies between 5.5% and 25% with S at between 2 and 5 % in all samples except K25268 – 9.2% and K25269 - >10%. The highest As values of any sample are found in K25266 with 750 ppm.

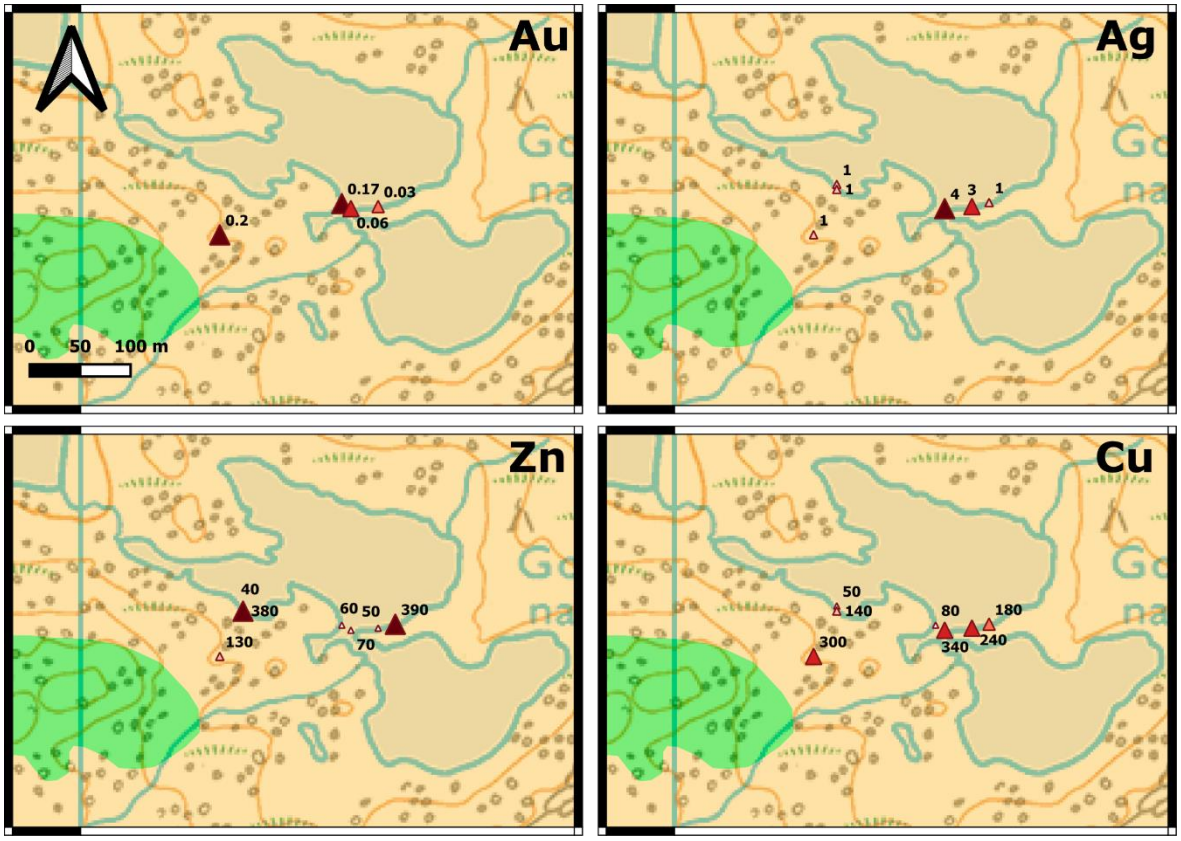

Fig. 4.11. Maps showing assay results for samples above detection lever from the Gorm-loch na Beinne inlier for elements Au, Ag, Zn, and Cu. Symbol sizes were automatically binned using equal ranges in QGIS. All values in ppm. Digimap (2020).

4.1.3 - Loch na Cabhaig

At Loch na Cabhaig a series of mafic and ultramafic rocks are exposed within Torridonian cover that bounds them on all sides (Fig. 4.12). These inliers were selected as a target of interest to this study due to their proximity to the Gorm-loch na Beinne inlier and the general rarity of ultramafic rocks within either the LMG or the LGC.

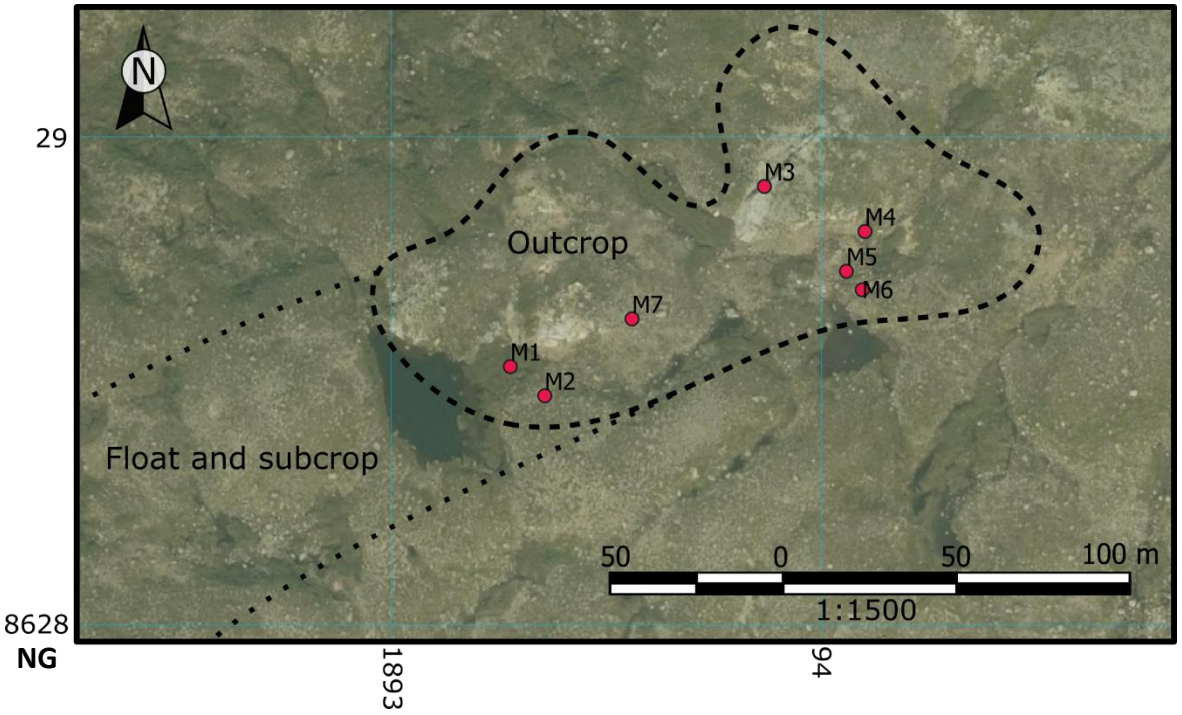

Figure 4.12. Aerial photograph showing the sample locations and approximate outline of the Loch na Cabhaig inlier. Digimap (2020).

The ultramafic inlier was briefly described by Coats et al (1997) as containing olivine rich ultramafic rocks but no further work was conducted. The inlier covers an area of c. 30,000 m² with a large area to the south-west that contains float boulders and possible outcrops. This train of float occurs leading away from the inlier towards the south-west and likely reflects glacial flow patterns in the region. The field relationships of the inlier are unclear due to the Torridonian cover, and its location could conceivably lie within the basement gneisses or within the GSB. Within the inlier exposure is generally good and contacts between units are apparent in some locations. The rocks are generally massive although fractures and quartz/calcite veining occur throughout. One exposure has evidence of a weak moderately SE dipping foliation. Units are easily visually separated by colour; green, grey/blue, or orange and each unit displays a unique weathering surface texture (Figures 4.13 and 4.14). Grey units have a generally fine grained and smooth surface appearance with some, but not all exposures, of soapstone displaying large unaligned ovoid megacrysts.

Green units display classic serpentinite weathering features and are heavily pitted, while orange units display prominent fanning needles of anthophyllite and surface oxidation.

A second inlier occurs c. 600 m to the south-west and is comprised of fine grained and well foliated amphibolite with fine banding defined by segregation between amphibole and plagioclase. At outcrop this foliation, 130/60, dips to the SW. Although exposure in this inlier is sparse, there appears to be very little internal variation and all exposures examined are of a similar lithology. A further 800 m to the SW a small ridge of quartzo-feldspathic gneiss occurs at the foot of the that closely resembles the Lewisian rocks exposed elsewhere in Torridon. In total nine samples (M1 - M9) were collected from the two inliers with M1 – M8 from the ultramafic inlier, and M9 from the amphibolite to the south-west.

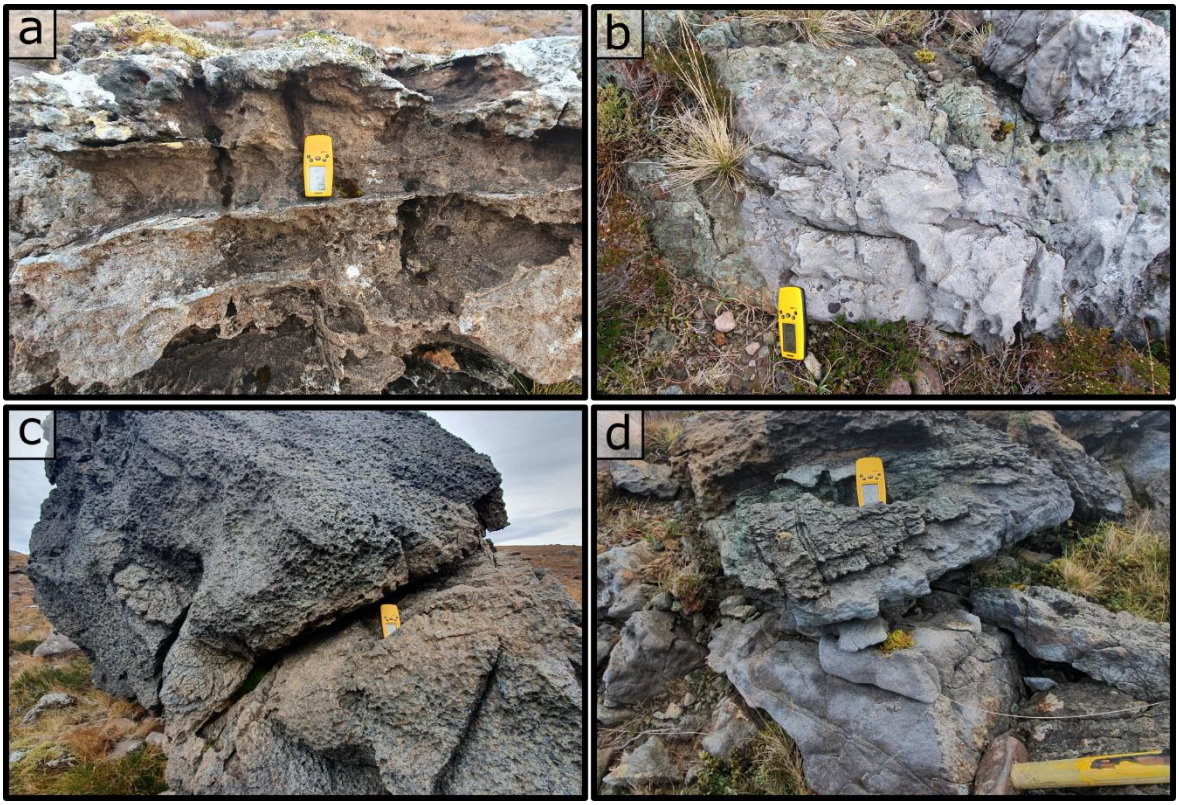

Figure 4.13. Field photographs of ultramafic lithologies at Loch na Cabhaig**a)** Distinctive orange weathering in anthophyllite bearing lithology. Horizontal resistant features are quartz veins. **b)** Contact between grey/pale-blue talk bearing units and a thin green tremolite bearing unit. **c)** Weathering-out layer in large 5 x 5 m block (M8). **d)** Sub-horitzontal contact between grey/blue lithology and green tremolite bearing unit.

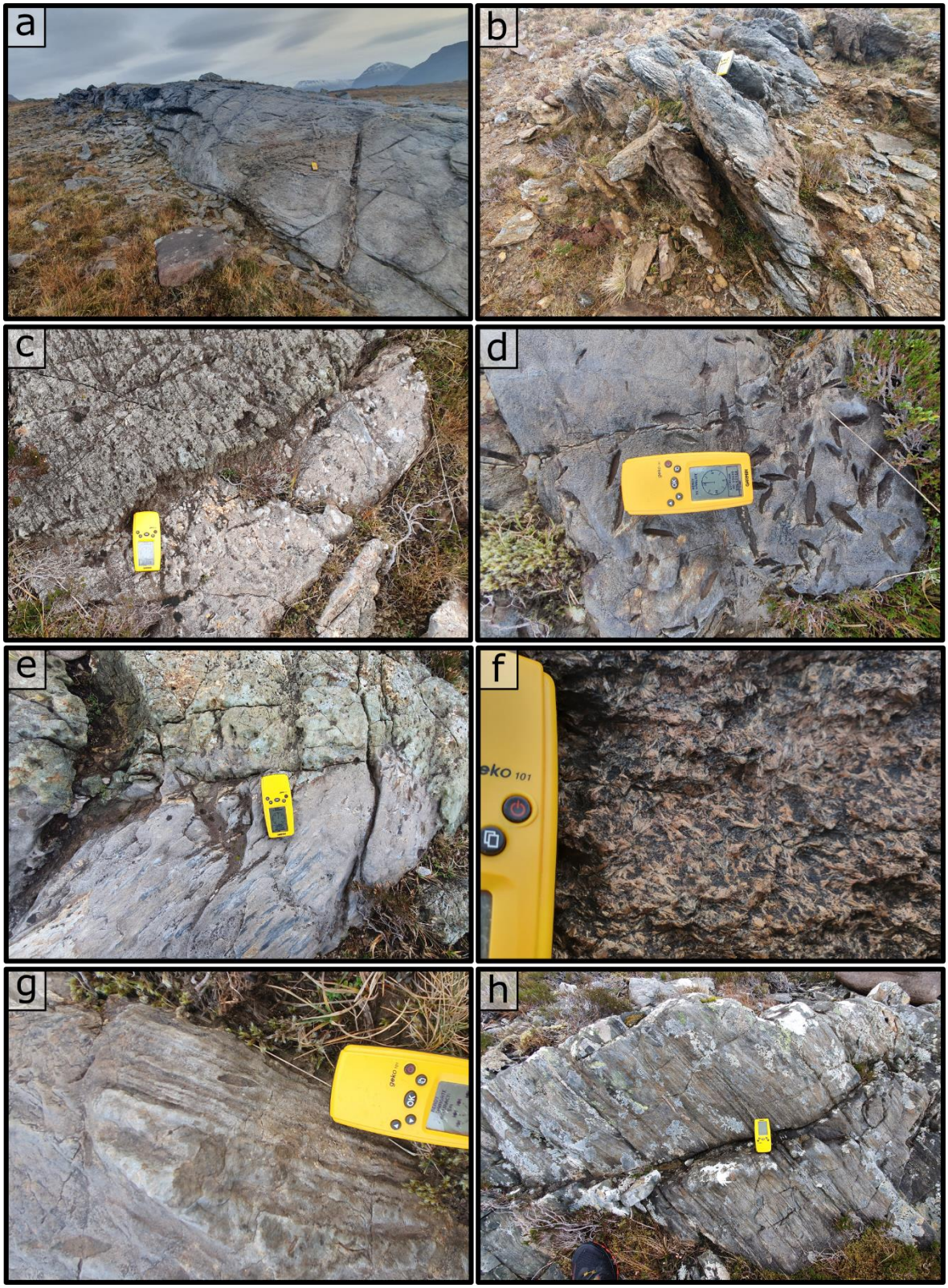

Figure 4.14. Field photographs of the Loch na Cabhaig ultramafic and mafic rocks. **a)** Large outcrop of tremolite + talc unit showing veining. **b)** Outcrop showing dipping fabric. **c)** sharp contact between tremolite bearing green unit and talc bearing grey unit. **d)** Large (up to 4 cm) unaligned megacryst in soapstone unit **e)** Boundary between green tremolite bearing units and grey soapstone unit with elongated and sheared megacrysts **f)** Anthophyllite fans prominent on surface of outcrop **g)** Weathering picking out potential igneous layering in talc + magnesite soapstone. Several megacrysts seen cutting this layering. **h)** Outcrop of amphibolite at M9 sample site showing strong foliation dipping to the south.

In thin section (Fig. 4.15) the ultramafic samples display no evidence of any primary igneous mineralogy, but display a range of alteration products. Serpentinite replacement textures were identified optically. However due to the difficulty in the identification of alteration products, six of the samples were prepared for X-ray powder diffraction (XRD) as detailed in section 3.6. The results of the XRD analysis are presented in Table 4 with matched peak graphs presented in the Appendix. No primary igneous mineralogy was identified in XRD analysis, suggesting alteration has been total. The minerals present are the low to medium temperature hydrous alteration products expected of an ultramafic protolith. These are, clays: vermiculite, kaolinite, and talc, asbestiform minerals: chrysolite, tremolite, and anthophyllite, carbonate minerals: dolomite and magnesite, along with clinochlore, zeolite, and lizardite.

Table 4. Results of XRD analysis on ultramafic samples from Loch na Cabhaig.

M1	Grey/Blue	Magnesite, Dolomite, Talc, Kaolinite, Vermiculite, Chrysotile
M2	Orange	Clinochlore, Talc, Anthophyllite
M3	Grey	Dolomite, Magnesite Talc, Clinochlore, Kaolinite
M4	Green	*No XRD*
M5	Green	Tremolite
M6	Orange	Clinochlore, Talc, Zeolite
M7	Grey	*No XRD*
M8	Green	Clinochlore, Lizardite, Dolomite, Magnetite
M9	Grey/Green	*No XRD*

M9 in thin section is dominated by subequal proportions of fine grained strongly aligned green pleochroic amphibole and altered plagioclase. Grain size is c. 0.25 - 0.5 mm with amphiboles occasionally up to 2 mm. Plagioclase displays rare relict twinning, although most grains display evidence of sericitic alteration. Weak banding is present formed by amphibole and plagioclase rich zones with these being c. 2 - 4 mm in width.

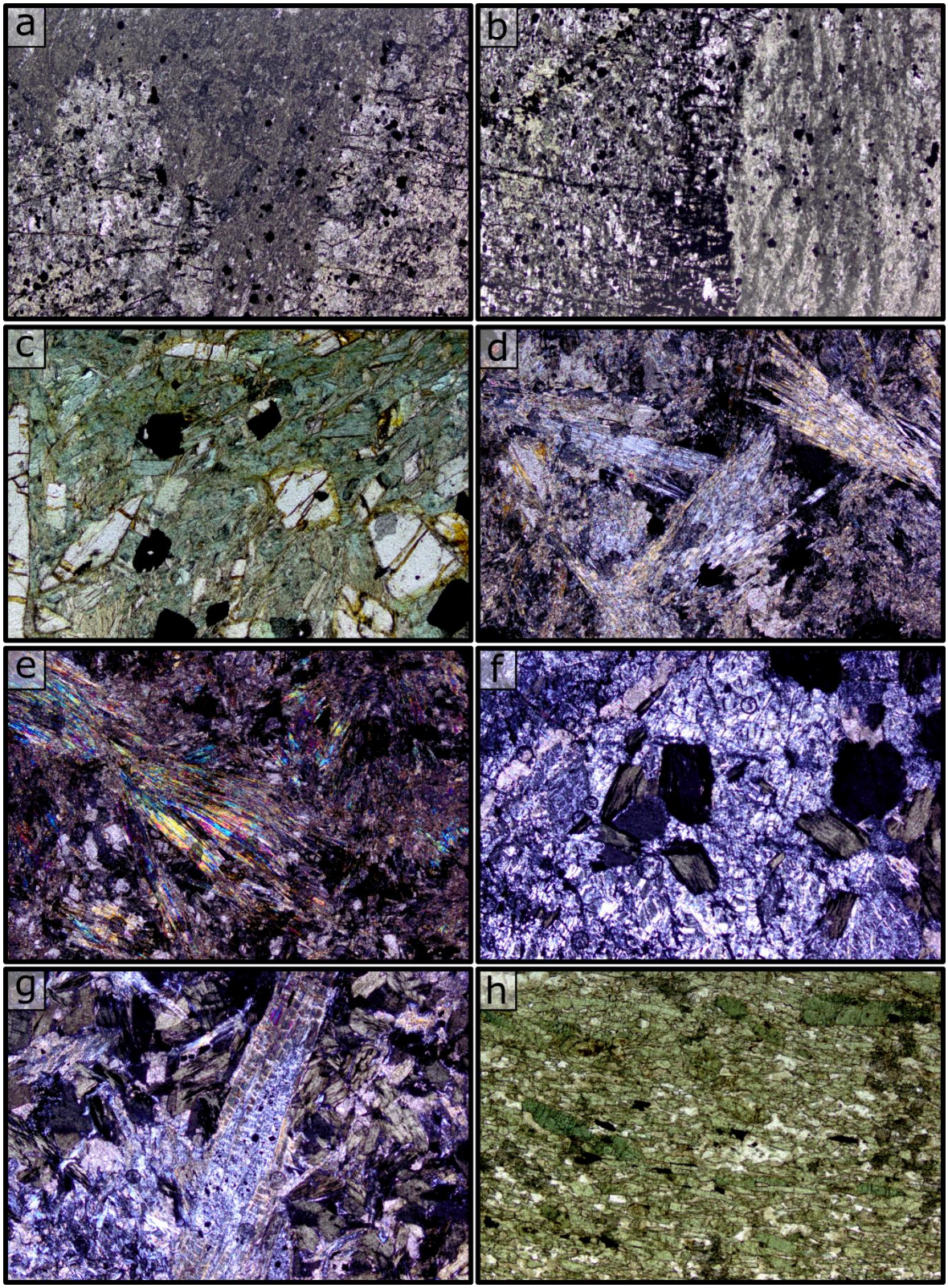

Figure 4.15 FOV in all photomicrographs – 4mm **a)** Boundary between megacryst (lower left and right) and fine grained carbonate dominate host rock (top) - M3 **b)** Altered megacryst (left) and banded host rock (left) - M3 **c)** Unidentified mineral seen in kite shaped cross section and elongate needle form within a serpentinite matrix - M4 **d)** Anthophyllite needles - M5 **e)** Anthophyllite needles and zeolite - M6 **f)** Lizardite with large opaques and altered chlorite - M8 **g)** Large needle (centre) altering to lizardite with altered chlorite - M8 **h)** Aligned green pleochroic amphibole - M9.

4.1.3.1 – Geochemistry

The origin and tectonic setting of the ultramafic and mafic rocks was of interest due to their proximity to known outcrops of the GSB and the general rarity of ultramafic lithologies within either it or the LGC. As such four samples, M3, M4, M8, and M9 were sent for major and trace element analysis as detailed in section 3.5. The results of this analysis are reported in Table 5.

Table 5. Results of geochemical analysis for samples M3, M4, M8, and M9. Major elements are reported in wt % oxide, while trace elements are reported in ppm. Uncertainties are reported by the lab as: **Major oxides** >100x detection limit - +/- 5%, **Minor/Trace element** >100x detection limit - +/- 10%. <x indicates values below detection limits.

Geochemistry of Flowerdale mafic/ultramafic samples

	SiO_2 %	Al_2O_3 %	Fe_2O_3%	MnO %	MgO %	CaO %	Na_2O %	K_2O %	TiO_2 %	P_2O_5 %
M3	38.06	2.22	9.4	0.197	26.02	7.7	0.03	< 0.01	0.051	0.01
M4	37.28	2.13	11.93	0.116	34.34	1.61	0.02	0.02	0.074	< 0.01
M8	37.3	3.51	11.37	0.118	32.63	1.86	0.08	0.08	0.202	0.02
M9	52.12	14.73	11.08	0.252	7.61	8.5	3.66	0.54	0.834	0.11

	LOI %	Total %	Sc (ppm)	Be	V	Ba	Sr	Y	Zr	Cr
	15.95	99.64	12	< 1	41	8	38	1	< 2	3920
	12.18	99.71	13	< 1	57	12	16	< 1	5	4350
	11.82	98.97	13	< 1	80	19	14	2	11	4510
	0.97	100.4	42	< 1	239	95	150	18	48	400

Co	Ni	Cu	Zn	Ga	Ge	As	Rb	Nb	Mo
129	2290	60	40	2	2	11	< 2	< 1	< 2
132	2270	< 10	40	2	1	< 5	< 2	< 1	< 2
114	2190	< 10	60	4	1	< 5	4	< 1	< 2
47	110	< 10	100	12	1	< 5	8	3	< 2

Ag	Sn	Sb	Cs	La	Ce	Pr	Nd	Sm	Eu
< 0.5	< 1	< 0.5	< 0.5	< 0.1	0.2	< 0.05	0.2	< 0.1	< 0.05
< 0.5	< 1	< 0.5	< 0.5	0.2	0.6	0.08	0.4	< 0.1	< 0.05
< 0.5	< 1	< 0.5	< 0.5	0.6	1.4	0.19	0.9	0.3	0.1
< 0.5	2	< 0.5	< 0.5	2.2	7	1.14	5.8	2	0.74

Gd	Tb	Dy	Ho	Er	Tm	Yb	Lu	Hf	Ta
< 0.1	< 0.1	< 0.1	< 0.1	< 0.1	< 0.05	< 0.1	0.01	< 0.2	< 0.1
< 0.1	< 0.1	0.2	< 0.1	< 0.1	< 0.05	< 0.1	0.02	< 0.2	< 0.1
0.4	< 0.1	0.5	< 0.1	0.3	< 0.05	0.3	0.05	0.3	< 0.1
2.9	0.5	3.3	0.7	2.2	0.32	2.3	0.38	1.3	0.2

W	Tl	Pb	Bi	Th	U
< 1	< 0.1	< 5	< 0.4	< 0.1	0.4
< 1	0.4	< 5	< 0.4	< 0.1	< 0.1
< 1	< 0.1	< 5	< 0.4	0.3	< 0.1
< 1	< 0.1	< 5	< 0.4	0.1	0.2

The geochemical data for the ultramafic samples, M3, M4, and M8, must be treated with scepticism and caution due to the major degrees of alteration detailed above. Major elements (CaO, SiO2 , MgO), and LREE can be mobilized during metasomatism (Paulick et al., 2006; Snow and Dick, 1995) while enrichment in fluid-mobile elements (e.g., B, Li, Cl, As, Sb, Pb, Th, U, Cs, Sr, Ba) may occur if these elements are sourced from surrounding lithologies. Despite this some value can be gained from the data and some potential origins can be considered more likely than others.

4.1.3.1 Major Elements

The silica contents of all three samples are low: 38% - M3, 37.3% - M4, and 37.3% in M8. MgO contents are 26% - M3, 34.3% - M4, and 32.6% - M8. Fe values in the form of total Fe oxides are 9.4% - M3, 11.9% - M4, and 11.1% - M8. Total alkalis in all three samples are very low at 0.03%, 0.04%, and 0.16% respectively. Al_2O_3 values are also low in all samples at 2.2%, 2.1%, and 3.5%. This low silica and Al in conjunction with low total alkali and high Mg and Fe confirms an ultramafic origin for all three samples. Sample M3 displays markedly lower MgO - c. 7%, and Fe - 2%, than M4 or M8. The deficit is primarily made up by an increase in CaO – 7.7% in M3 vs 1.6% and 1.8% in M4 and M8. These differences may reflect primary variations in the chemistry of the protolith, or the degree of metasomatism experienced by the samples. In thin section M3 displayed visible carbonate mineralogy and this, combined with the higher CaO values, suggest it as the most carbonate altered of the samples. Loss on ignition was 16%, 12.2%, and 11.8% in each sample.

The mafic amphibolite, M9 has a standard basaltic major element composition, with 52% silica, 4.2% total alkali, 7.6% MgO, 11.1% FeO (total oxides), 8.5% CaO and 14.7% Al_2O_3. On a standard TAS diagram it plots at the boundary between basalt and basaltic andesite.

Based on these major element results, the samples were plotted on an IUGS ultramafic classification diagram, Fig. 4.16, after the CIPW normative mineralogy method described in (Middlemost, 1989) and using the calculations of Hollocher, (2004). This plot suggest olivine rich protoliths in all case with normalised ol, opx, cpx values of; 55-10-33, 77-20-2, 73-26-0 for M3, M4, and M8. CIPW modal values for plagioclase are 5.5%, 6% and 9.2% respectively. Based on this, two samples, M4 and M8 fall into the hazburgite field and one sample, M3, plots in the lherzolite field.

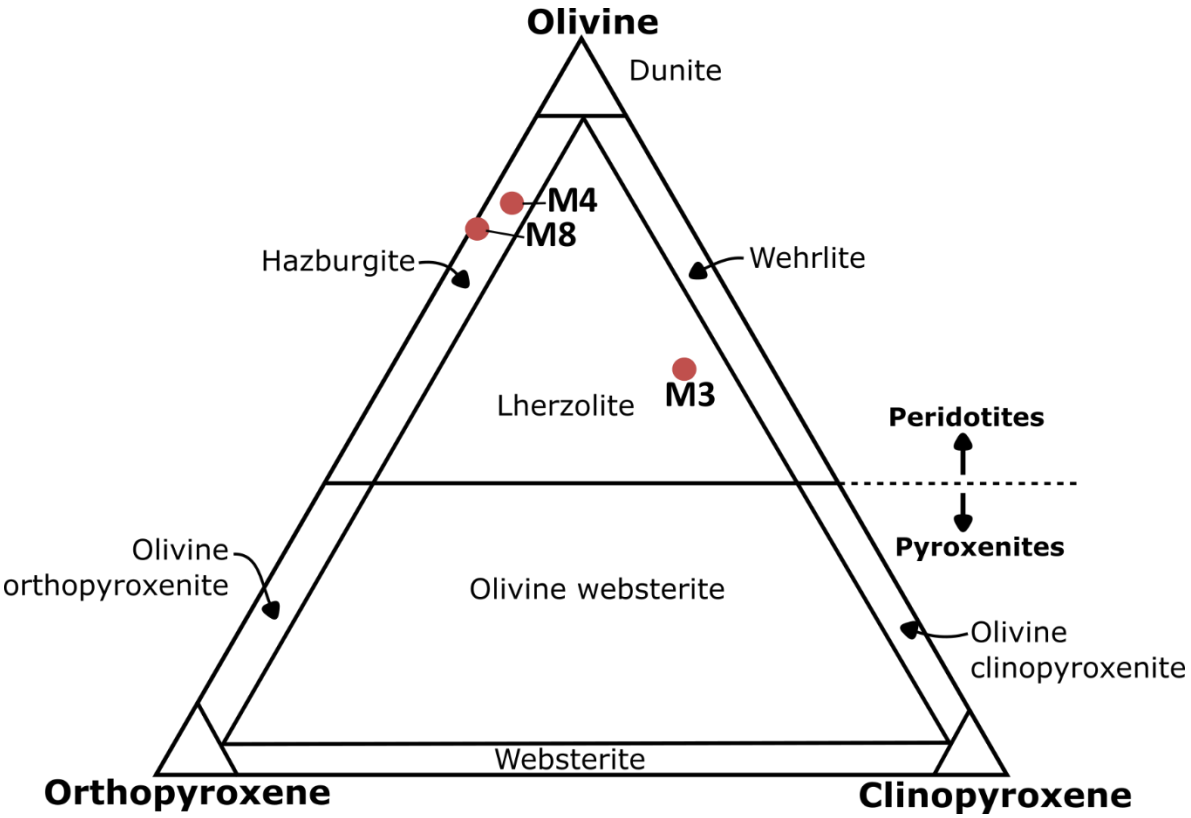

Figure 4.16. IUGS classification diagram for ultramafic samples after (Le Bas and Streckeisen, 1991). CIPW norms calculated via Hollocher, (2004)

5.2.1.2 - Trace Elements

Trace element values presented here are subject to a similar caveat as given above regarding mobility during metasomatism. Many are considerably less mobile than the major elements, however predicting the behaviour of each element in specific environments is difficult and many elements in some, or all, of the samples were below the detection levels of the analysis used. All three samples are enriched in trace elements associated with mafic/ultramafic igneous rocks: Cr at 3920 ppm, 4350 ppm, and 4510 ppm, Co at 129 ppm, 132 ppm, and 114 ppm, and Ni at 2290 ppm, 2270 ppm, and 2190 ppm for M3, M4, and M8 respectively. All other trace and REE were depleted with respect to typical crustal rocks.

All three ultramafic samples display flat to gently sloping REE profiles with chondrite normalised La/Lu values of 1.0 – 1.2 where data are available (Fig. 4.17). Samples M3 and M4 are heavily depleted in both LREE and HREE with many elements falling below the detection levels of the analysis. Primitive mantle normalised multi-element plots show

enrichment in some incompatible trace elements (Rb, Ba, Th, U) in all three samples. M9 has a negative REE profile with a normalised La/Lu value of 0.6.

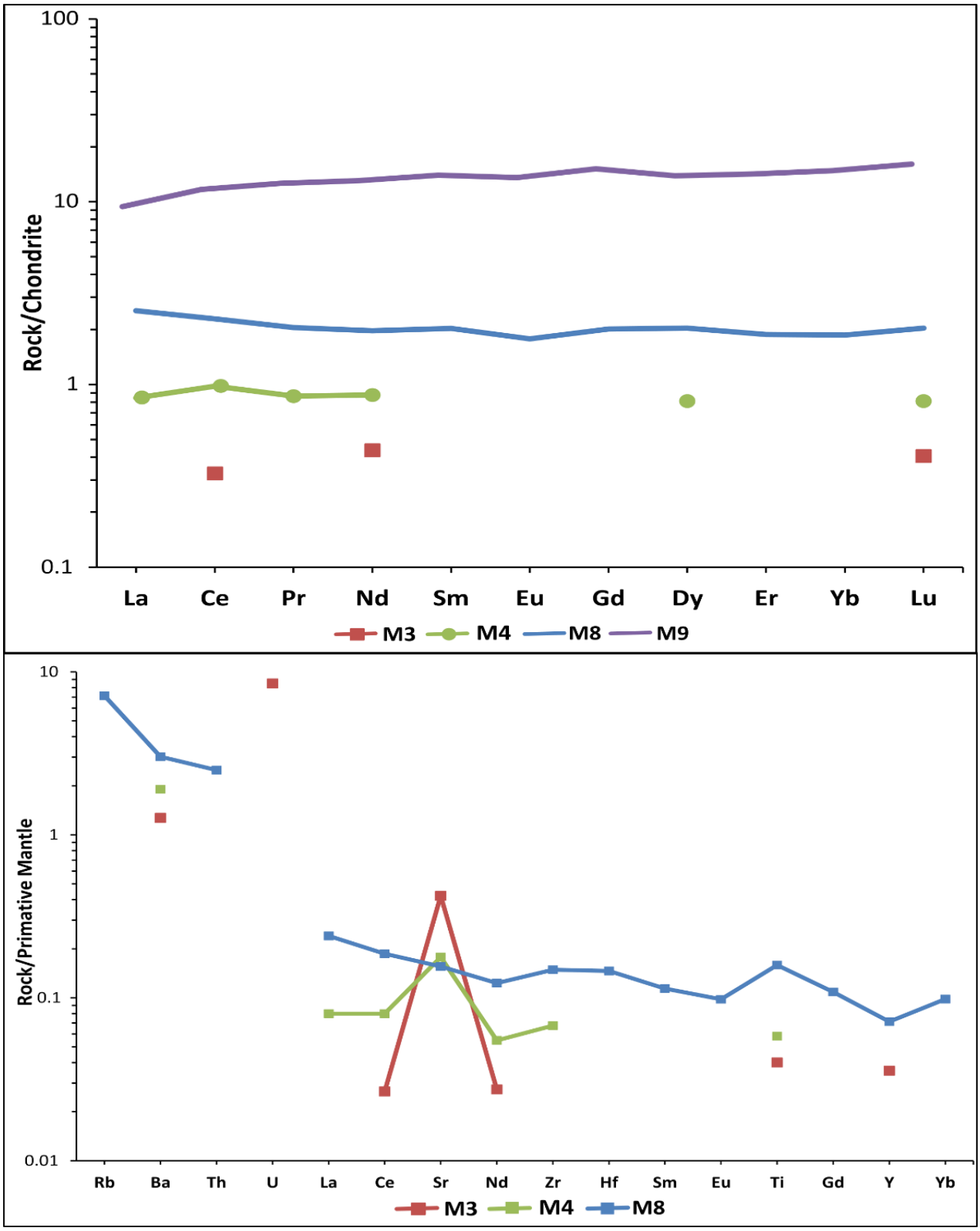

Figure 4.17. REE and Multi-element plots of sample M3, M4, M8 and M9. Uncertainties are not plotted as discussed in Section 3.3 and 3.5.

4.2 The Gruinard Belt

4.2.1 - Field Observations and Petrography

One sample, of c. 4 kg (**GB 1** NG 9581685515), was collected from a relatively pure quartzite in contact with amphibolites. Mapping of the area was not carried out due to time constraints at the sample location however the sampling site was located within the area mapped as metasediments by Crane (1972) and the BGS (Fig. 4.18). The sample is dominated, c. > 95 %, by coarse, c. 2 mm, quartz that displays extensive evidence of recrystalisation and granoblastic texture. Minor epidote occurs throughout and upon crushing a small fraction of garnet was recovered. After the confirmation of zircon in thin section, the sample was crushed and zircon separated from it following the procedure described in section 3.4. In total 49 zircon were extracted from the sample.

4.2.2 – Geochronology

A total of 67 U-Pb spot analyses were returned for sample GB1. Of these 34 were cores and 33 rims. The cores present three Archean ages, two highly discordant; 16%, and 32%, and one at 94% concordance (Fig. 4.19). These give $^{207}Pb/^{206}Pb$ ages of 2605 ± 105 Ma, 2731 ± 84 Ma, and 2600 ± 39 Ma. All cores within 5% concordance (n = 12) record a concordia age of 1702 ± 6 Ma with a mean squared weighted deviation (MSWD) of 3.9. This high MSWD and spread of concordant grains along the concordia curve from 1750 Ma to c. 1650 Ma as well as the suspected metasedimentary origin of the sample suggest that such a calculated age does not correspond to a discrete geologic event. A depositional age obtained from the youngest core is not possible due to the lack of CL-imaging and classification of detrital vs metamorphic zircon. A discordia through all core analysis, excluding inherited and highly discordant grains, gives an upper intercept of 1714 ± 16 Ma and lower intercept of 417 ± 94 Ma with an MSWD of 0.64.

A discordia anchored at 460 Ma through the two highly discordant Archean grains gives an approximate upper intercept of c. 2700 Ma. Three Mesoproterozoic cores at c. 1760 Ma are slightly above the concordia curve, concordances of -1% to -3%, and, as they lie along the discordia to the Caledonian may have suffered minor U-loss. One highly concordant core is found at a $^{207}Pb/^{206}Pb$ age of 1604 ± 64 Ma. Six cores cluster around a c. 1690 Ma age and

give a concordia age of 1690 ± 8 Ma with an MSWD of 0.5. Two cores record concordant Scandian $^{206}Pb/^{238}U$ ages of 442 ± 30 Ma and 424 ± 24 Ma.

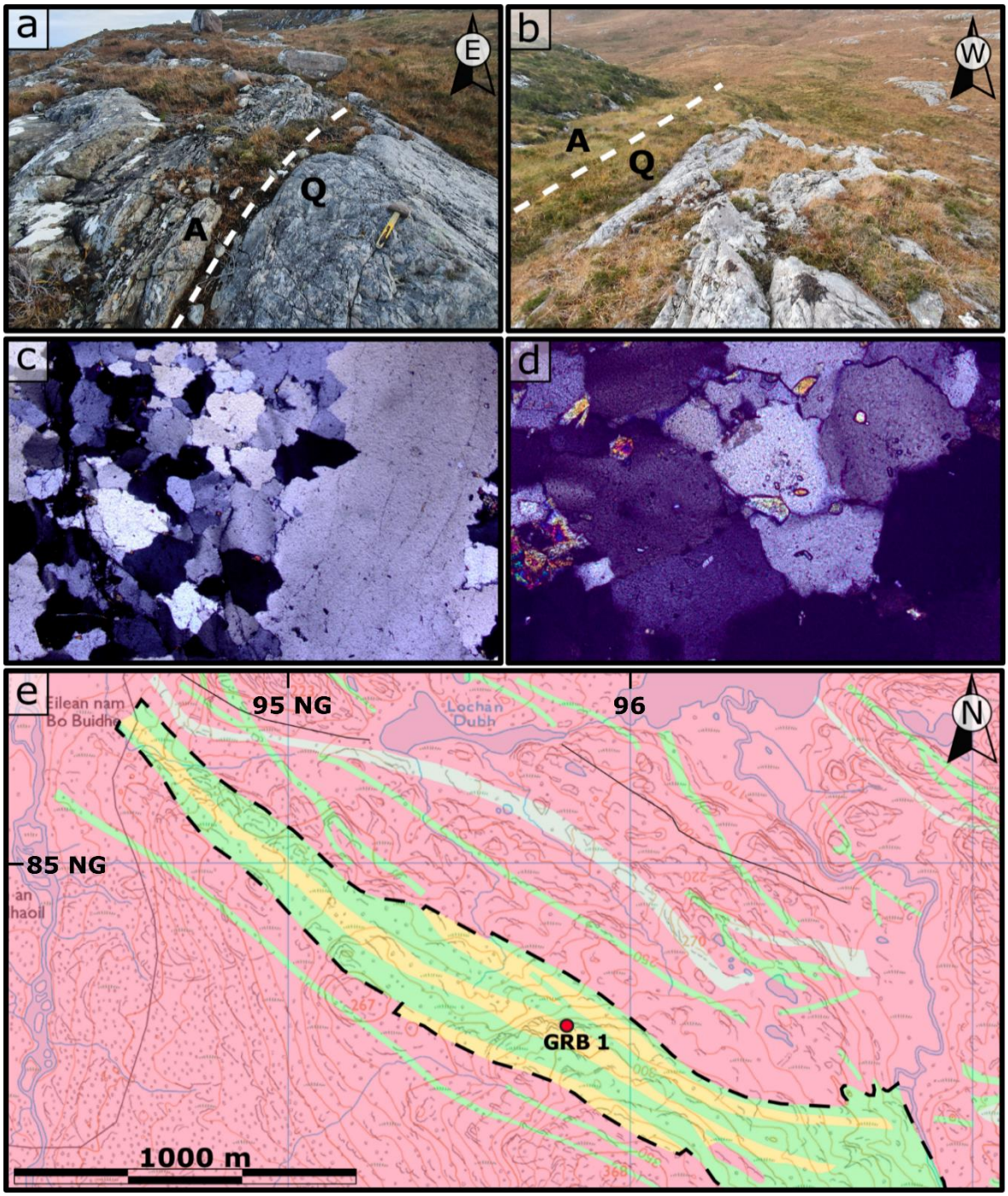

Figure 4.18. Field photographs of Gruinard Belt sample location. **a)** Sampled quartzite (Q) and northern contact with amphibolite (A) looking east. **b)** Looking west from the sample location. **c)** Thin section photomicrographs showing granoblastic quartz from 0.25 to 4 mm at 4x magnification. **d)** Small epidote and potential zircon grains at 20x magnification. **e)** Geologic map (Digimap, 2020) showing the location of sample GBR 1 collected from a quartzite. Outline of Gruinard Belt marked by black dashed line.

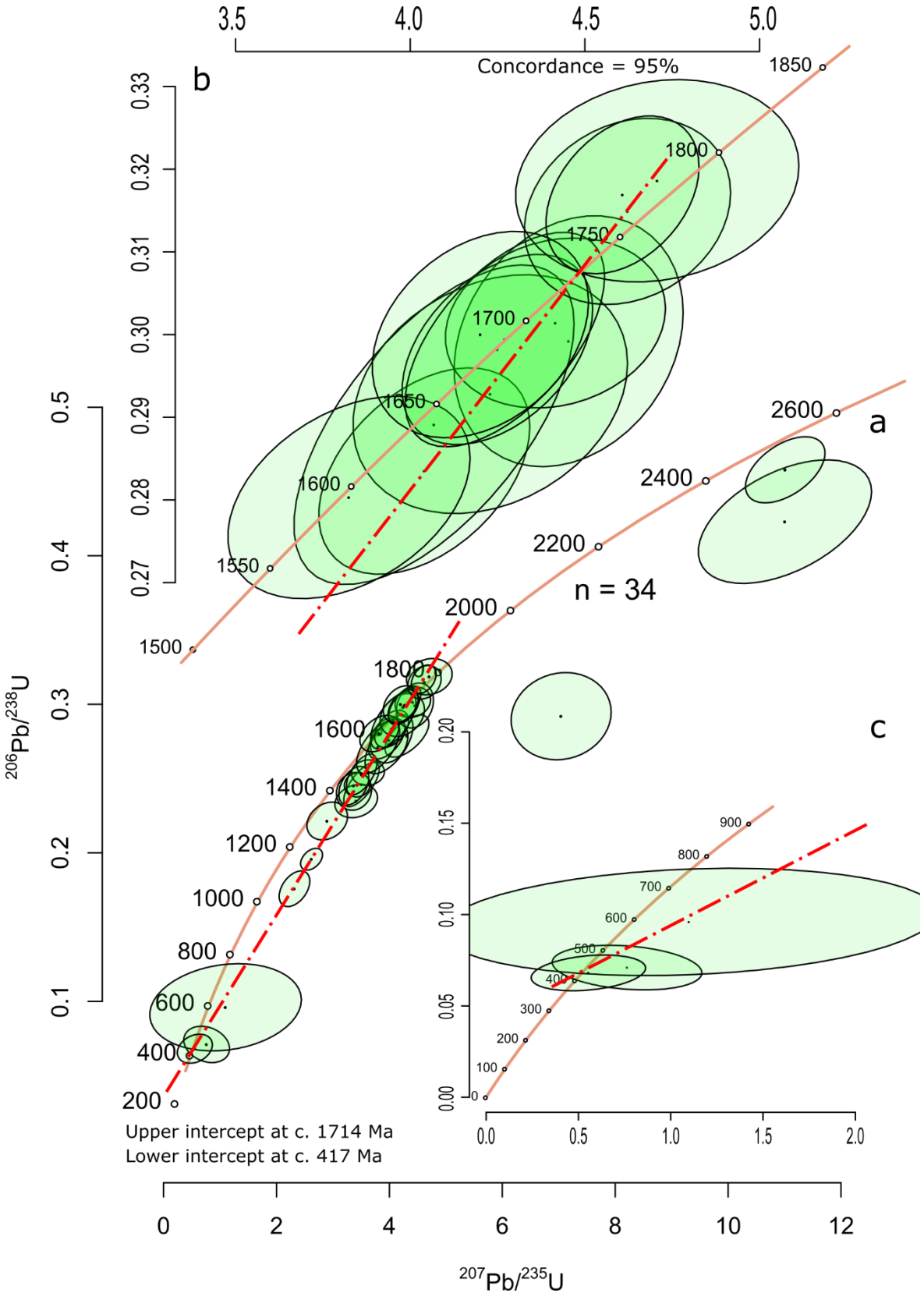

Figure 4.19. Wetherill concordia plots for cores from sample GB created with IsoplotR (Vermeesch, 2018). Red lines indicate approximate discordia between upper and lower intercepts. **A –** All core analyses showing three discordant Archean cores, a narrowly constrained Laxfordian age for most analyses, and a Caledonian aged Pb-loss and core grown event. **B -** Cores at > 95% concordance showing clusters at c. 1760 Ma and c. 1700 Ma. **C –** Caledonian aged cores.

The rims present a similar record to the cores. A discordia through all rim analyses gives an upper intercept of 1742 ± 12 Ma and lower intercept of 465 ± 31 Ma (Fig. 4.21). Three rims lie on the concordia at $^{207}Pb/^{206}Pb$ ages of 1770 ± 40 Ma, 1748 ± 49 Ma, and 1737 ± 70 Ma. The rim population (Fig. 4.20) is more unimodal with comparison to the three peaks present in core analyses. The main peak in rim $^{207}Pb/^{206}Pb$ ages occurs at c. 1740 – 1700 Ma, slightly younger than the first peak in core ages at c. 1760 – 1730 Ma. Following the procedure of Whitehouse and Kemp (2010), removing outliers until an MSWD of 1 is achieved, a concordia age of 1750 ± 10 Ma is obtained. Two rims, at 3% and 12% discordance, give Caledonian $^{206}Pb/^{238}U$ ages of 459 ± 9 Ma and 461 ± 10 Ma. One highly discordant rim gives an upper intercept of 2530 ± 130 Ma when the discordia is anchored at 465 Ma and as such may be an Archean rim that suffered major Caledonian aged Pb-loss.

Figure 4.20. KDE plots for cores and rims within 95% concordance. Main rim population centres around a c. 1730 Ma age while cores display three primary peaks at c. 1740 Ma, 1690 Ma, and 1660 Ma.

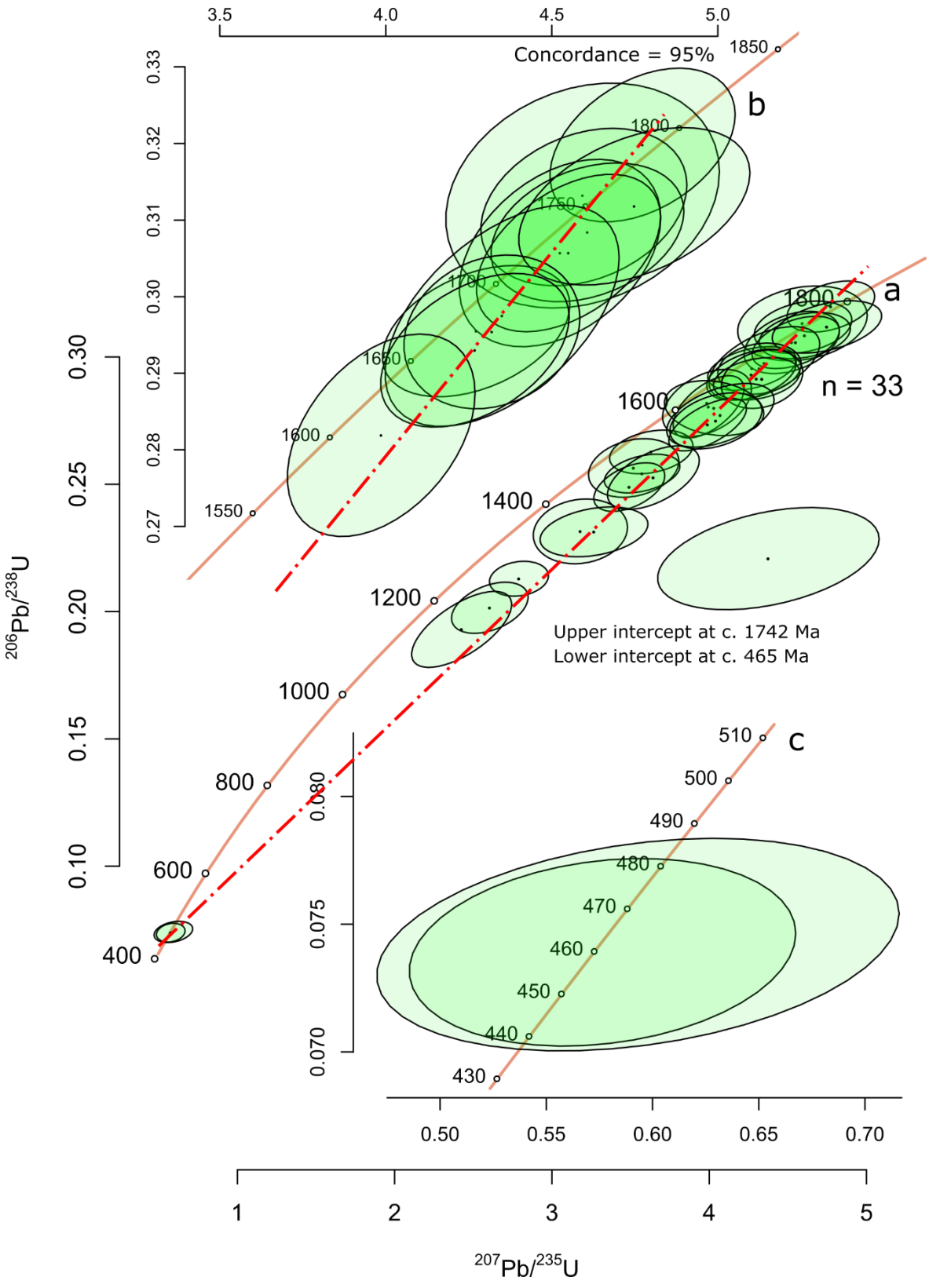

Figure 4.21. Wetherill concordia plots for rims from sample GB created with IsoplotR (Vermeesch, 2018). **A** – All rims displaying a Laxfordian age with a Caledonian aged Pb-loss and rim growth event. A single discordant rim may lie along a discordia to the Archean. **B** – Rims at > 95% concordance showing a discordia age of c. 1740 Ma. **C** – Two Caledonian ages rims at c. 460 Ma.

4.3 Scardroy and Orrin

Sampling from the Scardroy and Orrin inliers had two primary objectives; to collect gneisses for U-Pb zircon geochronology and to target mafic igneous bodies for comparison with potentially correlative lithologies in the foreland. Two samples of gneiss were collected from the Scardroy inlier - G1 and G3, while one was collected from Glen Orrin - G2 (Fig. 4.22). A previously collected sample, SCAR 2A was also analysed as part of this study. Igneous samples (M10 – M16, R1) were collected from a range of localities across both inliers. The igneous lithologies sampled include those classed by the BGS as Scourian amphibolite, Neoproterozoic hornblende schist, serpentinite, and several bodies not mapped at the scale of the BGS 1:50,000 sheets. Additionally several samples (PG, CG) were collected from the Scardroy inlier due to the evidence of mineralisation present within them.

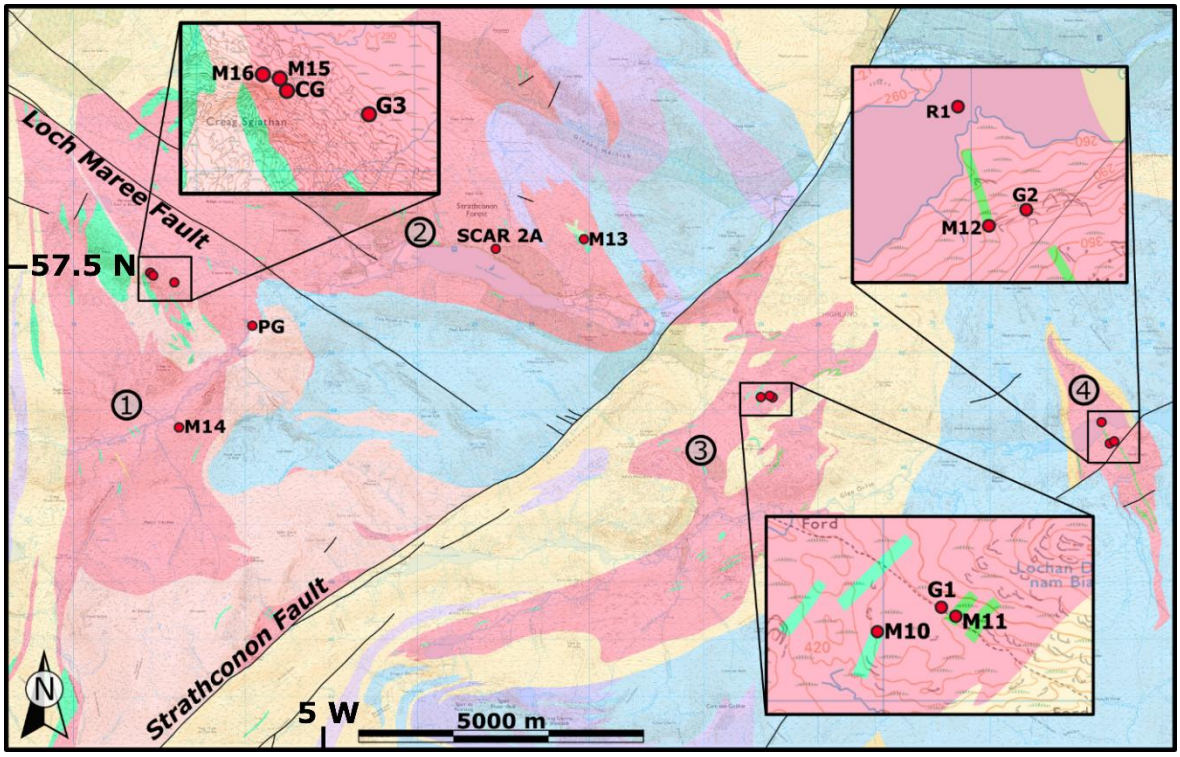

Figure 4.22. Sample map of the Scardroy area showing all samples collected for this study and the location of SCAR 2A collected prior. **1** – Scardroy inlier south of LMF, **2**- Scardroy inlier north of LMF, **3** – Inlier east of Strathconon Fault, **4** - Orrin Inlier. Basemap from Digimap, (2020)

Two large faults, the Strathconon Fault and the Loch Maree Fault, divide the inlier into three main areas; two west of the Strathconon Fault; north and south of the LMF, and one east of the Strathconon Fault (Fig 4.22). The Strathconon Fault runs NE-SW from Loch Hourn to Carn Chuinneag and is related to the larger and near-parallel GGF to the south-west. Hutton and McErlean, (1991) assign the fault a late Caledonian (425 – 395 Ma) sinistral movement history. A likely eastern continuation of the Loch Maree Fault terminates against the

Strathconon Fault at Scardroy (Peach et al., 1913). The Loch Maree Fault is a Neoproterozoic structure with limited Paleozoic reactivation (Stewart, 1993). Approximately five kilometres to the east of the easternmost portion of the Scardroy inlier is the Orrin Inlier. The Orrin Inlier outcrops over an area of c. 3 km^2 at the west end of the Orrin reservoir. It outcrops over a diamond shaped area with the long axis running NNW – SSE almost perpendicular to the trend of Glen Orrin. It is best exposed in the south side of the glen and along the banks of the River Orrin. The sampling strategy was designed to target all four of these areas and collect from as wide a geographical spread as practical.

In addition to the sampling of gneisses and minor intrusive bodies, and in order to approach the question of along strike basement mineralisation, samples of potentially mineralised lithologies were collected. This was supported by the work detailed in Coats et al., (1993), whom after the discovery of the mineralisation within the LMG (Jones et al., 1987) and because of the significant along strike potential of Besshi style VMS mineralisation as well as superficial similarities in lithology conducted exploratory geochemical stream and concentrate sampling at Scardroy. The Great Glen geochemical atlas (BGS, 1987) shows a zone of anomalous copper values in the Scardroy area that extends from the LMSB along the Loch Maree Fault. These anomalous values are related primarily to the Lewisianoid rocks of the inlier rather than the overlying Moine. The BGS Mineral Reconnaissance Program Summaries no. 12 (Coats et al., 1993) found minor copper mineralisation related to deformed chalcopyrite and pyrrhotite bearing podiform bodies of a few metres in size hosted in garnet amphibolites. Further minor mineralisation, including those returning the highest assays, was found related to crush zones along the Strathconon fault and is likely related to fluid migration along this structure.

4.3.1 - Field Observations and Petrography

4.3.1.1 - Gneisses

Two samples of gneiss from the Scardroy inlier, G1 and G3, were collected from east and west of the Strathconnon Fault respectively. Sample G1 (NH 28151 49251) was collected from a path-side exposure at the head of An Gleannan (Fig. 4.20). At hand specimen scale folded banding is formed by thin biotite rich layers in a felsic dominated gneiss. Thin section images (Fig. 4.24) show large k-feldspar, up to 3 mm, with relict tartan twinning, similarly coarse plagioclase, and quartz from 0.25 – 2 mm. Minor biotite (15%) makes up the rest of the sample. No metamorphic fabric is apparent at thin section scale, likely due to the generally coarse nature of the rock. However there is evidence of brittle deformation in the form of fine grained bands cutting the slide. Sample G3 (NH 17761 51230) was collected from a pale weathered coarsely banded gneiss from Choire Bhuic. Fresh surfaces show a strong pink colouration. In thin section the sample is dominated by quartz and plagioclase with minor K-feldspar. Grain size varies across the section from 0.25 mm to 1 mm. A third sample, Scar 2A (NH 2333 5174), was collected prior to this study by Dr. Iain Neill. It is a strongly banded gneiss comprising amphibole, plagioclase, and quartz. The dominance of feldspars in all three samples suggests a felsic to intermediate igneous origin.

A sample of gneiss, G2 (NH 34164 48455), was collected from the Orrin Inlier at a large whaleback exposure c. 30 m in length running parallel to the fall line of the hill near the centre of the inlier (Fig. 4.23). The exposure is distinctively banded, striking 150/60 SW, and differentially weathered based on grain size variation between bands at a centimetre to decimetre scale. Coarse layers are separated by bands of a finer grainsize. Finer layers are subordinate to the coarse and thicker layers at an approximate ratio of 10:1. Gentle open folding is present with a plunge and trend of 60→230, additionally evidence of isoclinal folding is present on some surfaces. Conjugate fracture sets and veins cut and occasionally displace banding. On initial inspection the outcrop appears similar to the surrounding strongly banded Moine metasedimentary rocks, however it lies almost centrally within the area marked as part of the Orrin inlier on BGS mapping. In thin section, taken from a coarse layer for mechanical reasons, the sample is dominated by coarse (up to 3 mm) quartz - 70%, with plagioclase displaying fresh twinning, altered k-feldspar, minor biotite (5%), and potential minor <1% Garnet, and sillimanite. Textures in thin section show areas of granoblastic grain boundaries and areas of finer grained (0.5 mm) quartz surrounding larger feldspars. It is unclear if these textures represent a primary igneous feature or are related to

extensive metamorphic recrystallization. A nearby exposure, c. 100 m downslope and along strike, is of more classically Lewisianoid banded and ptygmatically folded amphibole and k-feldspar gneiss. As such it is considered on the basis of field and thin section evidence that G2 represents either a metasedimentary lithology within the Orrin Inlier or a heavily deformed and foliated granitic body.

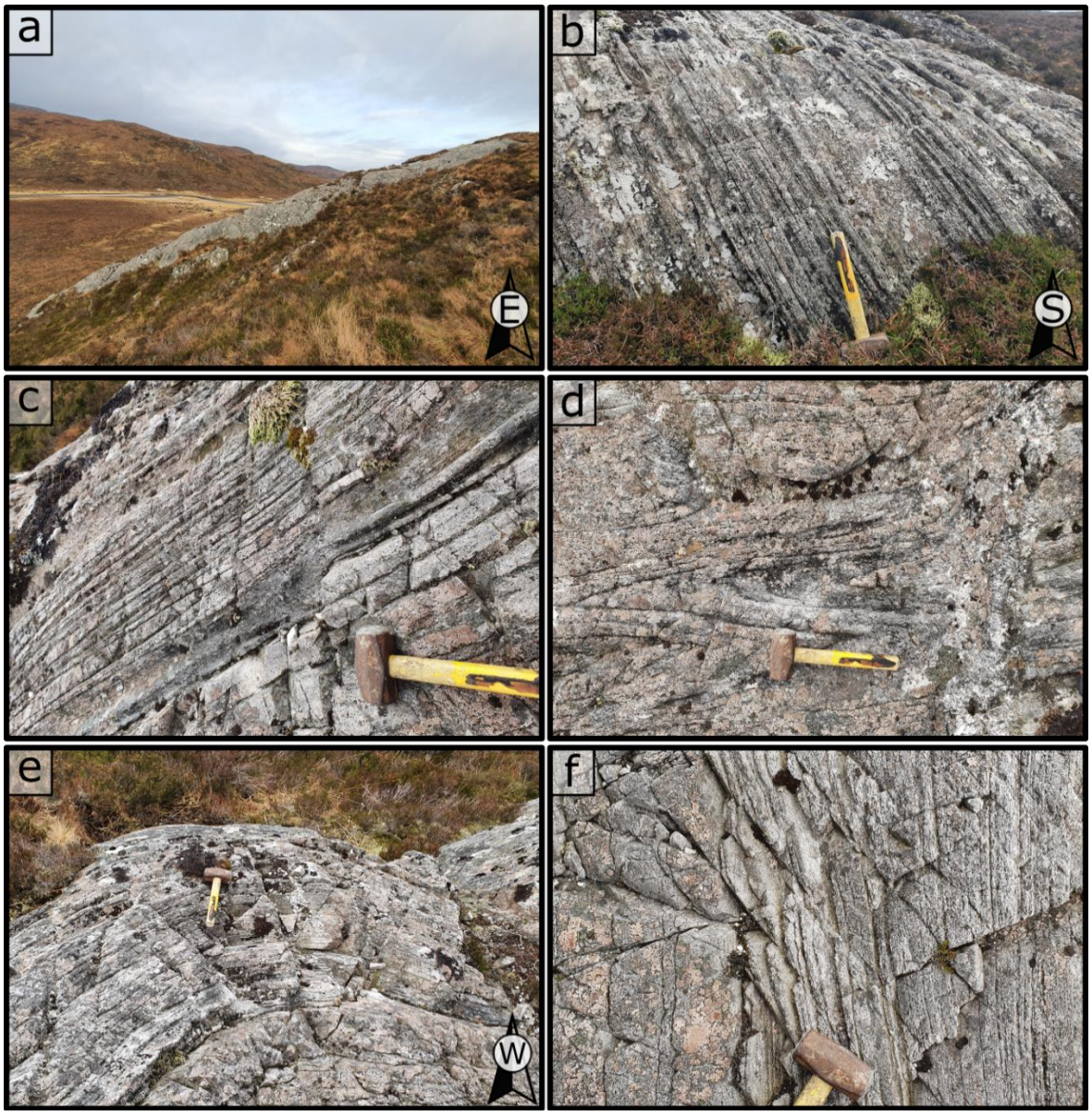

Figure 4.23. Field photos of exposure sampled for G2 **a)** Outcrop on north face of Meall Cosach c. 30 m in length. **b)** Fine scale cm/dm banding **c)** Layer offset across small fracture **d)** Isoclinal folding **e)** Open folding **f)** Conjugate fractures

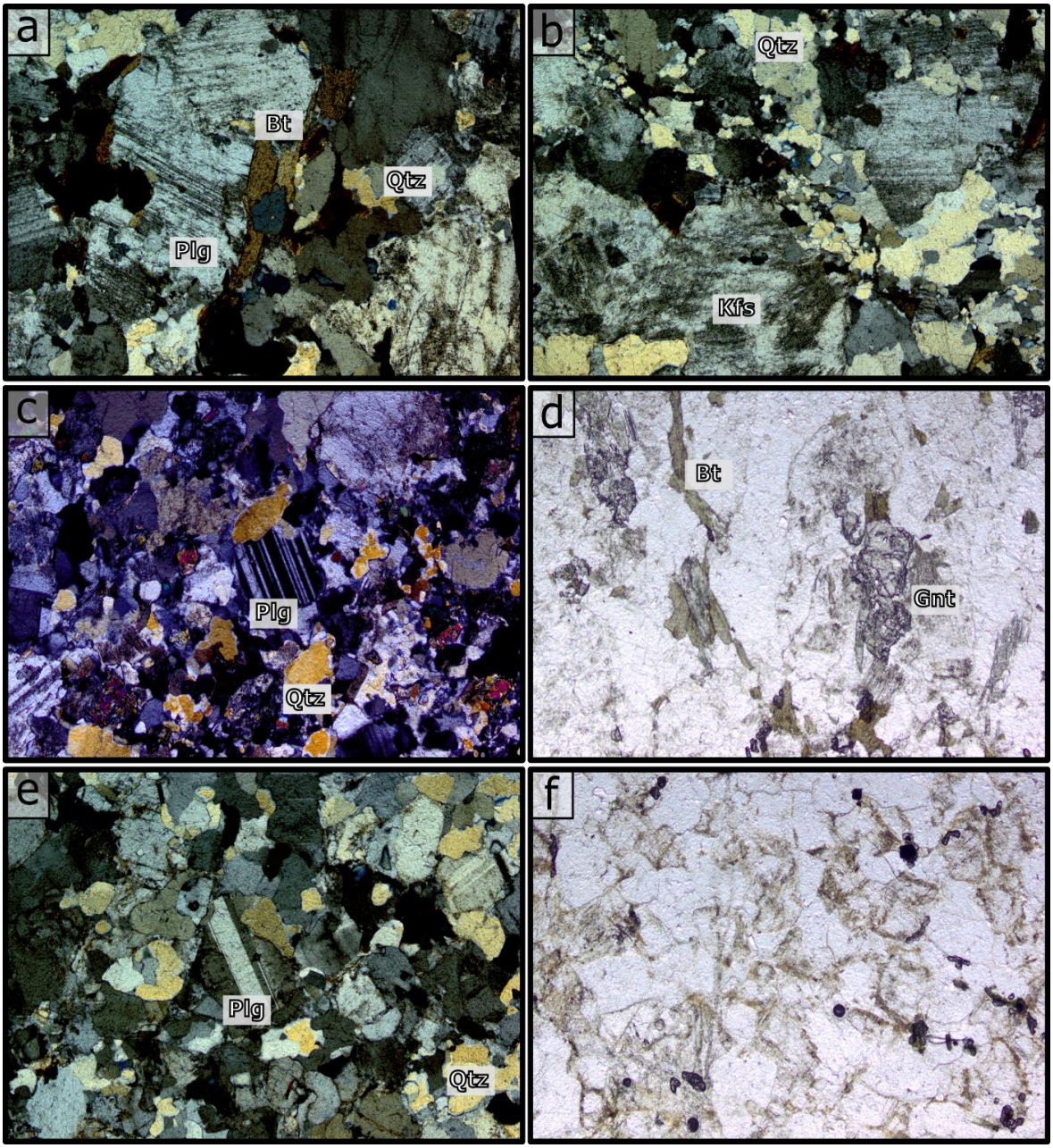

Figure 4.24. Thin section images of sampled gneisses – FOV 4 mm **a) G1 -** Coarse (2 mm) plagioclase and k-feldspar with minor quartz and biotite - xpl **b) G1 -** K-feldspar with quartz. Band of fine-grained quartz diagonally bisecting the image suggests brittle deformation - xpl. **c) G2 -** Plagioclase and quartz (0.5 – 1 mm) with K-feldspar -xpl. **d) G2 -** Minor biotite and garnet in low relief quartz and feldspars - ppl. **e) G3 -** Coarse plagioclase and quartz (1 mm) showing well preserved twinning – xpl. **f) G3 -** Alteration of feldspars in sample giving dusty texture - ppl.

4.3.1.2 – Intrusive bodies

Near to G1 two samples were collected from small bodies marked as hornblende schist and amphibolite on BGS mapping. Two samples, M10 and M11, were collected from dark grey to black outcrops, at the appropriate coordinates, that appeared distinct from the paler surrounding gneisses. M10 (NH 27995 49227) was collected from 50 m south-west of the stalking path through An Gleannan. Several small poorly exposed outcrops occurred in low cropped vegetation distinct from surrounding thick heather. In thin section (Fig. 4.25) the sample is foliated and dominated by quartz and plagioclase (80%), biotite (15%) with minor amphibole completes the mineralogy. Grainsize is up to 2 mm and commonly 0.75 to 1 mm. M11 (NH 28202 49221) is made up of fine grained, 0.25 mm, quartz and plagioclase with biotite and trace muscovite. A crude fabric is defined by alignment of biotite. Upon thin section examination, these samples appear relatively similar in mineralogy to the neighbouring gneisses - G1, being dominated by plagioclase and quartz, with a greater percentage of biotite, only minor amphibole, and a finer grainsize that is responsible for the darker colour. As such these samples do not seem to fit the definition of an amphibolite as mapped by the BGS and may represent either a slightly more mafic portion of the gneisses, or a relatively felsic intrusion miss-classified by the BGS. For this reason they are included in the interpretation of both the gneisses and igneous intrusions.

A series of small mafic intrusions from the Scardroy inliers and Orrin Inlier were sampled; M10, M11, M13, M14, M15, and M16 from Scardroy, with M12 and R1 collected from the Orrin inlier. M12 (NH 34085 48417) was collected from a dyke like body trending NNW-SSE for over 1.5 km through the inlier as mapped by the BGS. At the sample location, c 50 m west of G2, exposure is poor and no contact relationships between the igneous body and the surrounding gneisses were visible. At outcrop the body is black to dark green in colour and conspicuously coarse grained with a sharp surface texture. In hand sample it appears to consist of amphibole (c. 2 mm) with a minor interstitial pale green mineral, likely epidote or chlorite. In thin section it is dominated by pale to dark green pleochroic euhedral to subhedral amphibole (85%) with minor plagioclase (10%) and epidote. No obvious fabric or primary igneous textures are present at outcrop or thin section scale.

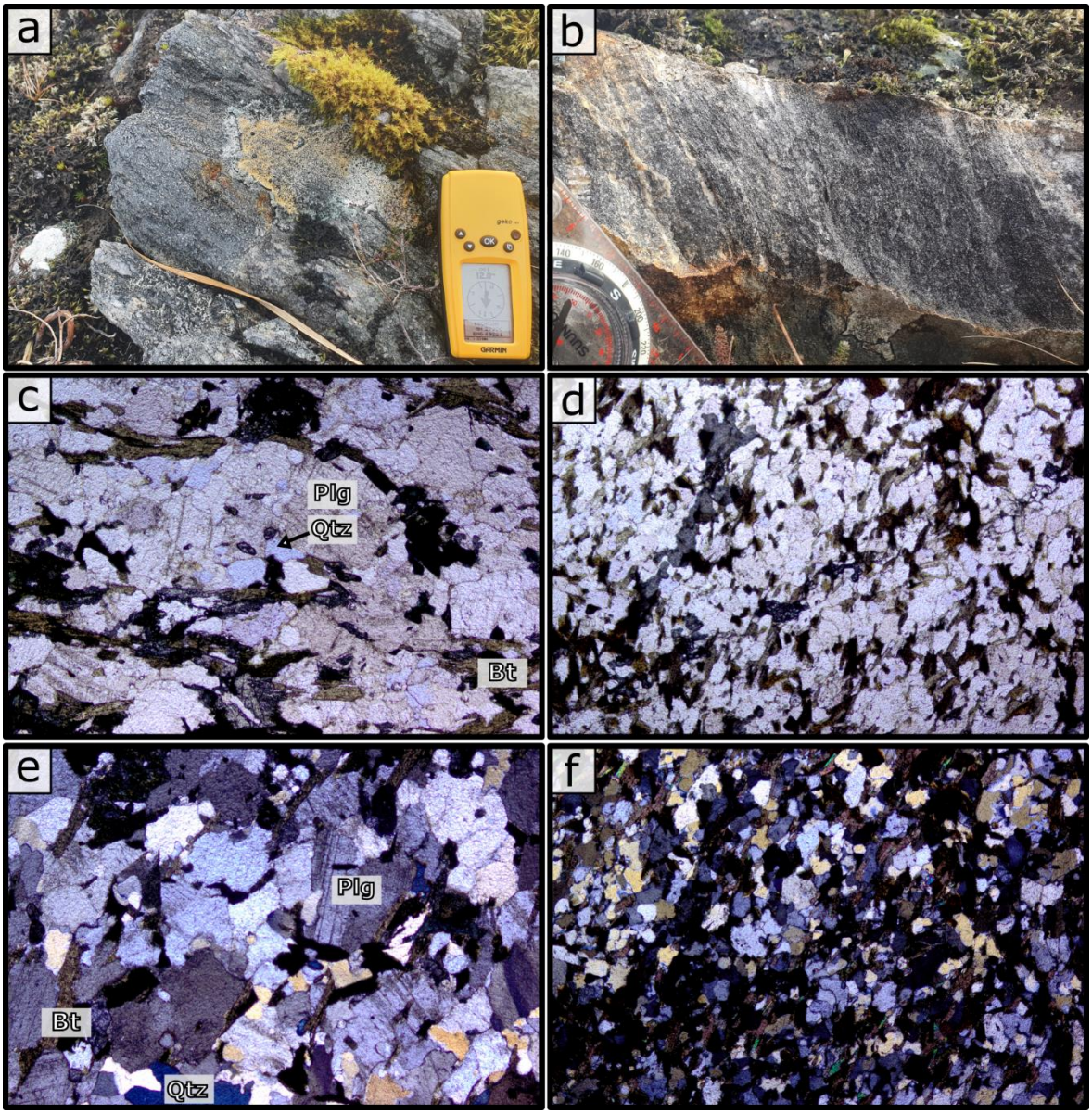

Figure 4.25 Field photographs and thin section images of samples M10 and M11 – FoV 4 mm on photomicrographs. **a) M10 -** Outcrop showing weak foliation and dark grey colouration. **b) M11 -** Outcrop showing strong steeply dipping foliation and banding of mafic and felsic minerals. **c) M10 -** Thin-section image showing biotite, plagioclase, and quartz up to 1 mm with weak alignment of biotite - ppl. **d) M11 -** Thin section image showing fine grained mineralogy comprising quartz, plagioclase, and biotite - ppl. **e) M10 –** Poorly developed twinning in plagioclase and weak alignment of biotite – xpl. **f) M11 -** image as d) - xpl.

Sample R1 (NH 33942 48790) was collected from a river section below the level of the Orrin reservoir recorded on Ordnance Survey mapping. Large, 3mm, feldspars are heavily altered, some display relict barcode twinning with some evidence of zoning (65%). Quartz is 2 – 3 mm (30%). Biotite was frequently altered (10%) and minor amounts of muscovite was observed. The sample contained no evident metamorphic textures or alignment. As such this may represent a younger intrusion into the inlier and relate to events recorded within the Moine.

M14 (NH 17843 48698) was collected from a gully near the western edge of the Scardroy inlier to the east of the Loch Maree Fault. The location was mentioned in Coats et al., (1993) as containing gossanous material however no material of this type was identified. Instead several minor mafic intrusions occurred within mixed mafic-felsic gneisses and alongside evidence of extensive faulting. The sample was collected from a dark coarse-grained lithology in the gully wall. At hand specimen scale it was dominated by large amphiboles of c. 2 mm. In thin section (Fig. 4.26) these large amphiboles are sheared and are wrapped by a fabric formed of small amphiboles of c. 0.25 mm. Intermediate, 0.5 mm, quartz and plagioclase make up c. 40% of the rock with amphiboles of both sizes making up the remaining c. 60%. The fabric within this intrusion may relate to the nearby faulting, with a band of cataclasite exposed c. 2 m above the sample.

Samples M15 (NH 17339 51396) and M16 (NH 17349 51396) were collected from within 50 m of one another and may sample the same unit. The location is marked as felsic gneiss on BGS 1 50,000 scale mapping, however the outcropping lithology is a large body of garnet amphibolite. Exposure is poor and the terrain is steep and very wet so it is unclear if the two samples collected are from one large body or are separate. In thin section M15 is formed of pleochroic green amphibole, 1 – 3 mm (45%), plagioclase (30%) is found between amphibole crystals. Large anhedral garnets (10 mm) 25% form a background to much of the sample. The garnets contain numerous inclusions of significantly finer quartz and amphibole than found outside areas of garnet. This perhaps indicates garnet formation at an early stage inhibited crystal growth in these regions. M16 (NH 17349 51396) was collected c. 50 m west of M15. The sample shows similarly coarse amphibole (3 mm) with occasionally zoning and plagioclase (2 mm). There is possible relict pyroxene showing replacement by amphibole, and chlorite. Large (8 mm) garnet is also present in the background with these areas having a smaller grain size and an alignment not present in the rest of the slide.

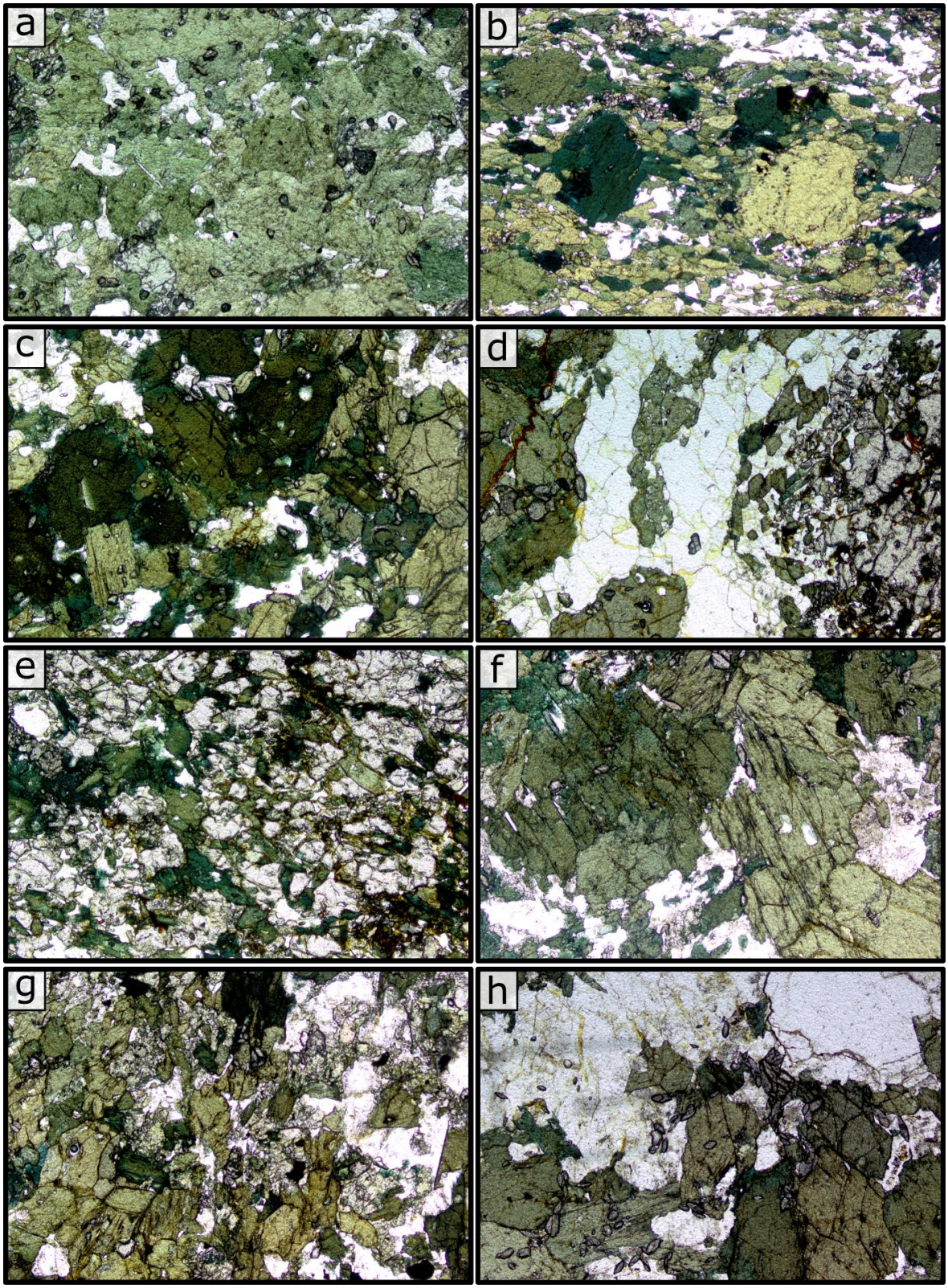

Figure 4.26. Thin section images of mafic samples collected from the Scardroy and Orrin inliers, all images in ppl – FoV 4mm. **a) M12 –** Coarse amphibole with minor plagioclase. **b) M14 –** Large rounded amphibole in a strong planar fabric defined by alignment of smaller amphiboles. **c) M15 –** Large amphibole with plagioclase and minor titanite. **d) M15 –** Boundary between coarse region (left) and fine inclusions in large garnet (right). **e) M15 –** Large garnet covering whole image with small amphibole and plagioclase inclusions. **f) M16 –** Large amphiboles with quartz and plagioclase. **g) M16 –** Boundary between coarse region (left) and larger garnet (right). **h) M16 –** Clusters of titanite along boundary between amphibole and plagioclase rich region.

One ultramafic sample M13 (NH 24908 51985) was collected from a deformed body containing serpentinised ultramafic material and garnet amphibolites c. 150 m in length within the gneisses. Initially the mafic portion of this targeted for sampling, however this was not identified in the field and instead a sample of the ultramafic portion was collected. This sample comprised serpentine and tremolite with rare relict olivine and pyroxene.

4.3.1.3 – Mineralised Samples

Two samples were collected from the Scardroy inlier due to their distinctive oxidative weathering patterns suggestive of potential mineralisation (Fig. 4.27). Near to M15 and M16 a large rockfall provided samples of CG (NH 17393 51350). These blocks displayed a strong orange to orange-green weathering pattern and were very friable. At hand specimen scale biotite occurs within a pale matrix commonly stained orange/green. In thin section euhedral biotite, 2 mm, form 25% of the sample and display weak alignment. Oxides form c. 5 – 10 % of the sample, and several large (0.5 – 1 mm) sphalerite crystal were observed. Subequal amounts of quartz and plagioclase form the majority of the rock (65%), grains range from 0.25 to 1 mm. These are commonly fractured and may originally have displayed a generally coarser texture. Large plagioclase grains are fractured into multiple grains with twinning matching across fractures. A thin oxide coating occurs along most fractures and grain boundaries.

A second sample, PG (NH 19123 5047), was collected due to distinctive orange oxidation at a cutting for the vehicle track in Gleann Fhiodhaig on the north bank of the River Meig. The rock is dominated by subequal proportions of quartz and plagioclase of 0.5 to 2 mm that display a strong fabric. Large, 1 – 4 mm, fractured generally euhedral garnets (15%) are wrapped by a later foliation defined by small biotites (10 %). Oxides and possible sulphides form c. 5% of the rock and are commonly found coating the curvy-planar fabric and fractures. It is suggested that these opaques are epigenetic and related to fluid movement during deformation due to their occurrence along fractures. Both the strong fabric and the mineralisation may relate to the proximity of the sample, c. 30m to the SE, with the boundary between the inlier and the Moine. This boundary is likely to have been a focus of deformation or may be purely tectonic in nature and hence facilitated fluid movement.

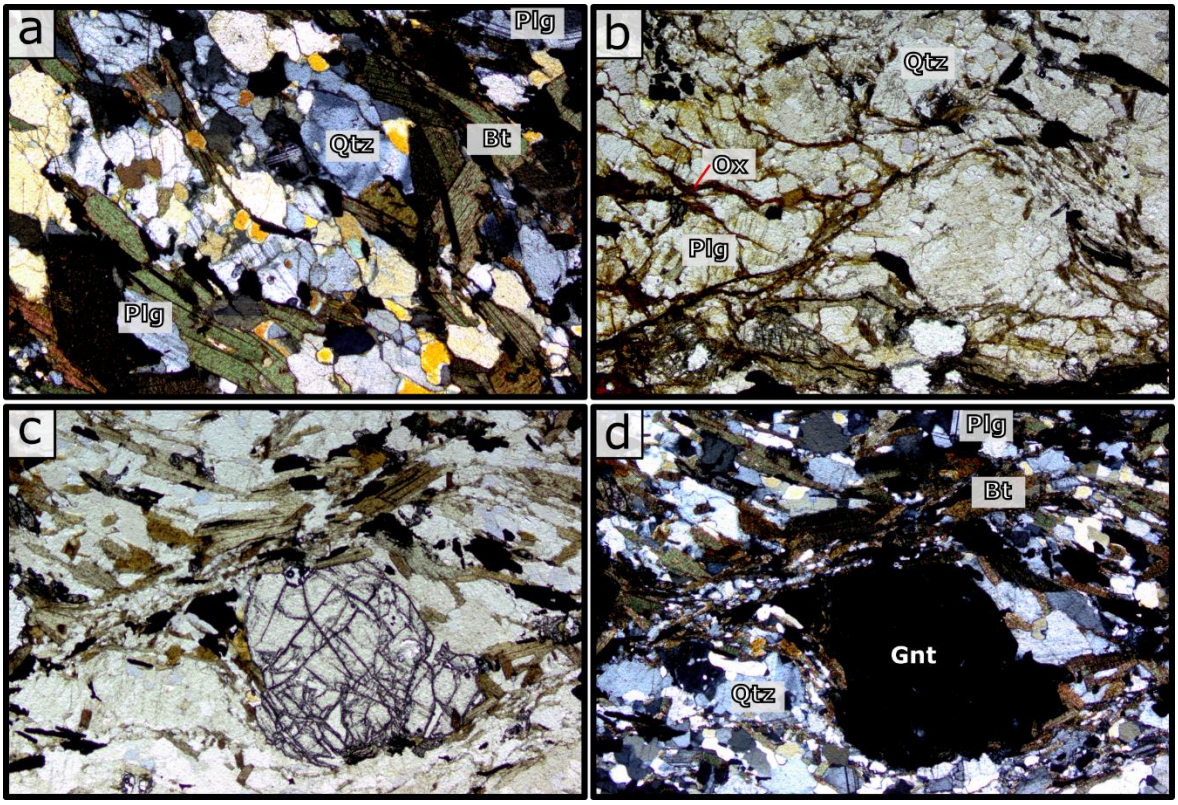

Figure 4.27. Thin section images of samples **PG** and **CG** – FOV - 4 mm. **a) CG** - Quartz, biotite and plagioclase showing alignment - xpl. **b) PG** - Evidence of deformation and oxide coating of fracture/fabric surfaces - ppl. **c) PG -** Garnet showing sinistral strain with biotite, plagioclase, and quartz - ppl. **d) PG** As in c) - xpl.

4.3.2 – Geochemistry

Table 6. Major and trace element analyses of samples from the Scardroy and Orrin inliers. Methods as detialed in Section 3.5. Major elements are reported in wt % oxide, while trace elements are reported in ppm. Uncertainties are reported by the lab as: **Major oxides** >100x detection limit - +/- 5%, **Minor/Trace element** >100x detection limit - +/- 10%. **<x** indicates values below detection limits.

Geochemistry of Scardroy Samples

	SiO_2	Al_2O_3	Fe_2O_3	MnO	MgO	CaO	Na_2O	K_2O	TiO_2	P_2O_5	LOI	Total	Sc	Be
M10	59.74	17.89	6.92	0.095	2.4	3.85	4.91	2.64	0.872	0.38	0.63	100.3	6	3
M11	63.5	13.96	8.12	0.099	3.63	2.33	2.37	3.5	0.802	0.14	0.83	99.28	20	2
M12	51.44	6.19	11.43	0.172	14.06	13.77	1.27	0.53	1.004	0.06	0.74	100.7	38	1
M13	35.98	1.98	10.98	0.114	31.42	1.14	0.04	0.01	0.134	<0.01	17.96	99.77	10	< 1
M14	49.67	12.38	15.67	0.158	5.41	8.91	3.22	0.91	2.038	0.11	0.49	98.96	20	2
M15	50.68	12.57	16.23	0.309	5.07	10.15	2.1	0.58	2.066	0.22	0.32	100.3	42	1
M16	47.97	12.46	15.45	0.267	6.13	12.81	2.22	0.49	1.553	0.12	1	100.5	50	1
R1	64.53	16.66	4.01	0.059	1.85	1.81	5.52	2.17	0.401	0.07	1.5	98.58	6	2
G2	82.64	7.76	1.21	0.032	0.72	1.29	1.38	2.92	0.087	0.05	0.42	98.5	2	1
SCAR 2A	70.29	15.78	2.17	0.038	0.81	3.27	4.96	0.88	0.208	0.08	0.23	98.7	2	2

V	Ba	Sr	Y	Zr	Cr	Co	Ni	Cu	Zn	Ga	Ge	As	Rb	Nb
100	312	441	16	218	< 20	17	< 20	10	90	23	1	< 5	119	12
175	509	176	16	156	290	24	80	20	120	18	1	< 5	182	7
187	27	63	12	61	1480	56	330	< 10	90	11	2	< 5	3	3
66	7	7	1	5	4550	127	2070	30	60	2	< 1	< 5	< 2	< 1
423	121	261	17	113	20	54	100	80	80	20	1	< 5	8	7
446	75	100	37	138	50	34	30	40	100	16	2	< 5	9	8
429	96	252	30	89	100	47	50	100	100	18	2	< 5	9	5
36	351	316	7	143	120	12	80	20	40	21	< 1	< 5	116	6
14	509	82	4	89	60	1	30	< 10	< 30	9	< 1	< 5	81	1
20	415	531	3	83	30	4	< 20	< 10	< 30	18	< 1	< 5	36	2

Mo	Ag	In	Sn	Sb	Cs	La	Ce	Pr	Nd	Sm	Eu	Gd	Tb	Dy
< 2	0.6	< 0.2	2	< 0.5	1.5	73.8	149	17.5	61	9.3	1.94	5.8	0.7	3.6
2	0.5	< 0.2	1	< 0.5	4.4	11.8	26	2.96	10.8	2.3	0.8	2.2	0.4	2.6
< 2	< 0.5	< 0.2	1	< 0.5	< 0.5	7.4	18.4	2.61	12.4	3.2	0.9	3.3	0.5	2.9
< 2	< 0.5	< 0.2	1	< 0.5	< 0.5	0.2	0.6	0.09	0.5	0.2	<0.05	0.2	< 0.1	0.3
< 2	< 0.5	< 0.2	1	< 0.5	< 0.5	12.4	30.6	4.22	19.2	4.8	1.42	4.7	0.7	4
< 2	0.5	< 0.2	1	< 0.5	< 0.5	10.3	28.1	4.14	19.7	5.8	2.07	6.9	1.3	7.3
< 2	< 0.5	< 0.2	10	< 0.5	< 0.5	9.1	20.4	2.84	14	4.3	1.46	5.4	1	5.7
< 2	< 0.5	< 0.2	1	< 0.5	3	12.8	28.7	3.03	10.8	1.9	0.5	1.4	0.2	1.3
< 2	< 0.5	< 0.2	< 1	< 0.5	< 0.5	9.5	19	2.12	7.5	1.1	0.39	0.9	0.1	0.6
< 2	< 0.5	< 0.2	1	< 0.5	0.5	11.9	23.8	2.65	8.8	1.3	0.43	0.8	< 0.1	0.4

Ho	Er	Tm	Yb	Lu	Hf	Ta	W	Tl	Pb	Bi	Th	U
0.6	1.5	0.21	1.3	0.2	5.2	1	< 1	0.7	7	< 0.4	7.9	3.2
0.6	1.8	0.28	1.9	0.31	4	0.7	1	1.2	7	< 0.4	10.7	2.9
0.5	1.4	0.19	1.3	0.18	1.7	0.3	< 1	< 0.1	< 5	< 0.4	1.6	0.6
< 0.1	0.1	<0.05	0.2	0.03	< 0.2	< 0.1	< 1	< 0.1	< 5	< 0.4	< 0.1	< 0.1
0.7	2	0.27	1.7	0.25	3	0.6	< 1	< 0.1	< 5	< 0.4	2.7	0.8
1.5	4.4	0.63	4.1	0.66	3.7	0.6	< 1	< 0.1	6	< 0.4	0.8	0.7
1.2	3.6	0.52	3.5	0.57	2.4	0.3	< 1	0.1	6	< 0.4	0.6	0.9
0.3	0.9	0.14	1	0.17	3.7	1	< 1	0.7	9	< 0.4	4.4	1.6
0.1	0.3	<0.05	0.3	0.04	2.2	0.3	1	0.3	6	< 0.4	4.1	0.8
< 0.1	0.2	<0.05	0.2	0.03	2.2	0.2	2	0.2	7	< 0.4	3.2	0.2

4.3.2.1 – Gneisses and Evolved Igneous Rocks

Major element geochemistry for samples G2 and SCAR 2A are: silica at 82.6% and 70.3%, Al_2O_3 at 7.8% and 15.8%, total Fe oxides are 1.2% and 2.2%, CaO values are 1.4% and 5%, and total alkalis are 4.3% and 5.8% respectively. MnO, MgO, TiO_2, and P_2O_5 are all <1%. LOI is 0.4% and 0.23% in each sample, indicative of very anhydrous rocks. Both contain significant amounts of feldspars in thin section and are therefore considered to be meta-igneous in origin. SCAR 2A falls into the range of major elements associated with tonalites. However G2 is significantly higher in silica and lower in Al. It may be that some of this silica is a feature of metasomatism and replacement. As detailed above there is the potential for M10 and M11 to have sampled gneissose rocks instead of the intrusive bodies targeted. As such they have been included in figure 4.28.

Normalised to the LGC complex compositions of Weaver and Tarney (1981) all four samples are enriched in Rb, Th, and U (Fig. 4.28). In the case of M10 and M11 this is up to 100x for U, while G2 and SCAR 2A are enriched at c. 10x the levels found in the foreland. Except for these mobile elements, G2 and SCAR 2A are depleted in most other elements and especially the HREE. M10 and M11 plot respectively in the monozite and granodiorite fields of a plutonic TAS diagram. Both have relatively high silica contents at 60% and 63% and are enriched in alkali elements with total alkali values of 7.6% and 5.9%. M10 displays a highly fractionated REE profile with a La/Lu ratio of 38 and a La value of 311x chondrite. M11 has a steep LREE slope and a flat HREE profile with a La/Lu ratio of 4. M10 and M11 display similar REE patterns to the LGC with M10 enriched in both LREE and HREE and M11 depleted in LREE but enriched in HREE compared to the LGC. Both M10 and M11 display Nb, Ta anomalies. On both Yb v. La/Yb and Y v. Sr/Y diagrams (Fig. 4.29) SCAR 2A falls into the low-HREE TTG field. G2 plots in this field for Yb, but falls below it for Y, potentially due to the increased mobility of Sr.

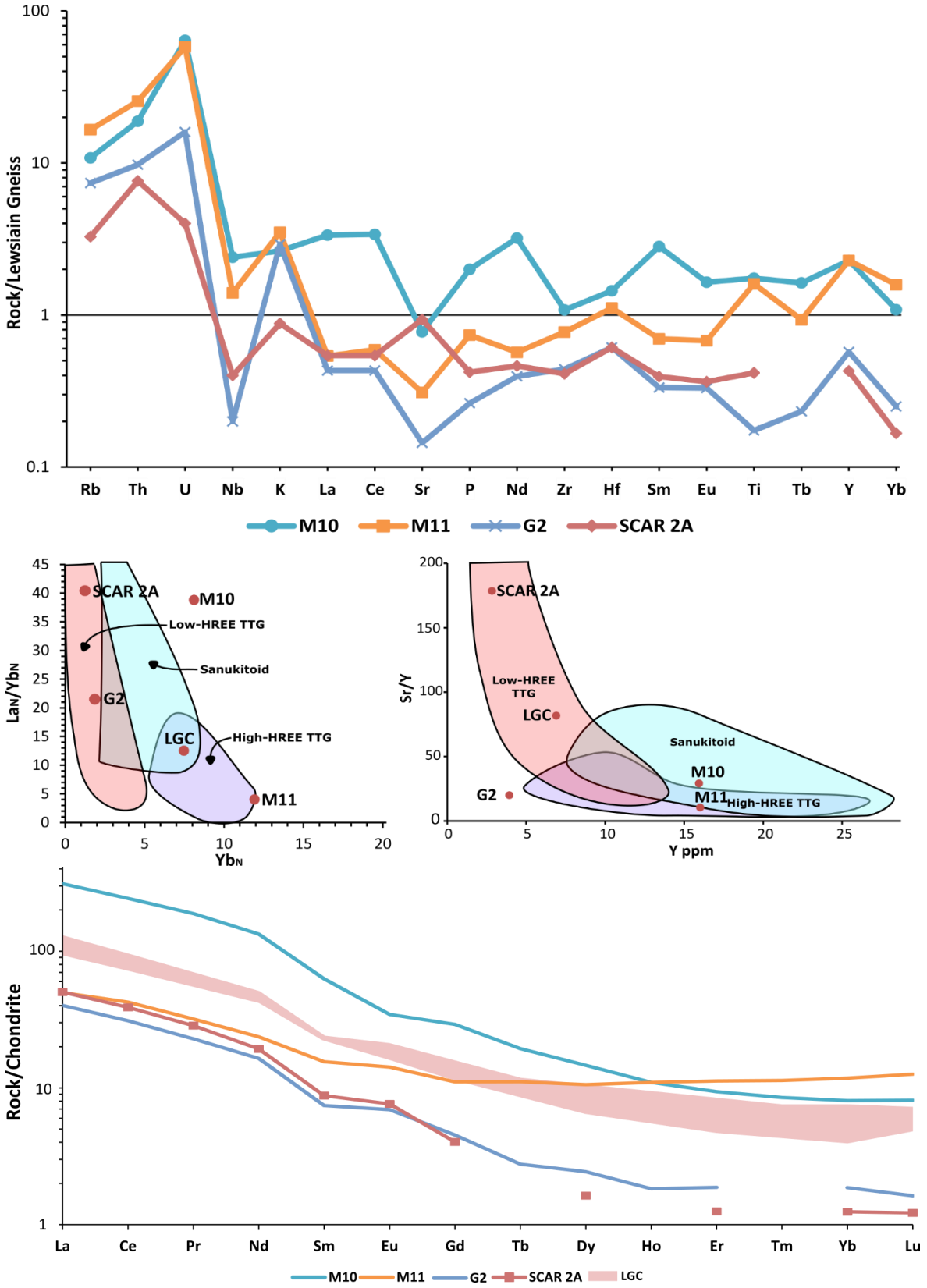

Figure 4.28. Multi-element Plot showing samples M10, M11, G2 and SCAR 2A normalised to values for the foreland Lewisian from Weaver and Tarney, (1981b). **La/Yb v. YbN plot** of samples along with Lewisian values (Weaver and Tarney, 1981b) with fields for typical Archean igneous rocks after Dey et al., (2014). **Sr/Y v. Y plot** with fields after Day et al., (2014) and LGC data from Weaver and Tarney, (1981b). **REE plot** showing samples M10, M11, G2, and SCAR 2A against LGC data from Weaver and Tarney, (1981b).

4.3.2.2 – Mafic Intrusions

Additional mafic and ultramafic samples SCAR 2 - 6 were collected by Emma Waters during an undergraduate dissertation in 2016 – 2017. These samples underwent whole rock geochemical analysis prior to this study at SUERC and the University of Edinburgh, see techniques in Milne (2019). Their results and locations are presented in appendix 8 and their interpretation is integrated into the discussion in Section 5.4.2.1; they are not discussed in detail here. Additionally, a single ultramafic sample, M13, was collected from a serpentinised body as part of this work. It has low, 35%, SiO_2, high, 31.5%, MgO, along with 11% FeO and very low total alkali. This sample is integrated into the discussion in section 5.4.2.1.

Four of the mafic samples collected as part of this study, M12 from Orrin, M14 – M16 from Scardroy, and SCAR 2 and SCAR 6 collected prior, plot within the gabbroic/basaltic field on a TAS diagram (Fig 4.29). All have silica contents between 45% – 52%. The mineralogy of M12 and M14 is distinct from that of M15 and M16 by the marked absence of garnet in M12 and M14. Major element geochemistry shows a marked divergence between M12 and M14 - M16; Al_2O_3 is lower – 6% in M12 vs c. 12% in all three Scardroy samples, MgO is higher - 14% vs 5% - 6%, $Fe_2O_{3(T)}$ is lower - 11% vs 15% - 16%, as is TiO_2 – 1% vs 1.5% - 2%, finally total alkali in M12 is lower than found in M14, M15, or M16 at 1.8% vs 2.7% - 4.13%. Trace element geochemistry also supports a distinction between the samples. M12 has less than half the V at 190 ppm than M14– 16 have at c. 420 ppm in all three samples. Ba - 75pppm – 120 ppm vs 30 ppm and Sr; 100 pmm – 250 ppm vs 60 ppm are also significantly lower in the Orrin sample. In M12 Cr is more than order of magnitude higher at 1480 ppm vs 20 ppm – 100 ppm, and Ni at 330 ppm vs 30 ppm – 100 ppm in the Scardroy samples.

The REE profile (Fig. 4.30) of M12 shows a moderately sloping profile with a La/Lu ratio of 5.1 and a La value of 30x chondrite. M14 displays a similar REE pattern to M12 with a similar slope, La/Lu = 4.2 from a higher initial La value of 50x chondrite. M15 and M16 display near flat REE patterns with normalised Lu/La values of 1.6 from a starting point of c. 40x chondrite La. M12 and M14 share a similar fractionated REE profile while the physically proximal M15 and M16 share a similar flat profile. All mafic samples show Nb, Ta anomalies. However as in the foreland Scourie Dykes this may be a signature of the

underling sub-continental mantle lithosphere from which they were derived (Hughes et al., 2019) rather than a direct signature reflecting the formation mechanism of the mafic samples. In comparison with the dykes of the foreland, M12 and M14 resemble the volumetrically minor olivine-gabbros, while M15 and M16 resemble the numerically dominant dolerites. When the fields for the Scourie Dykes of Hughes et al., (2014) are plotted on discrimination

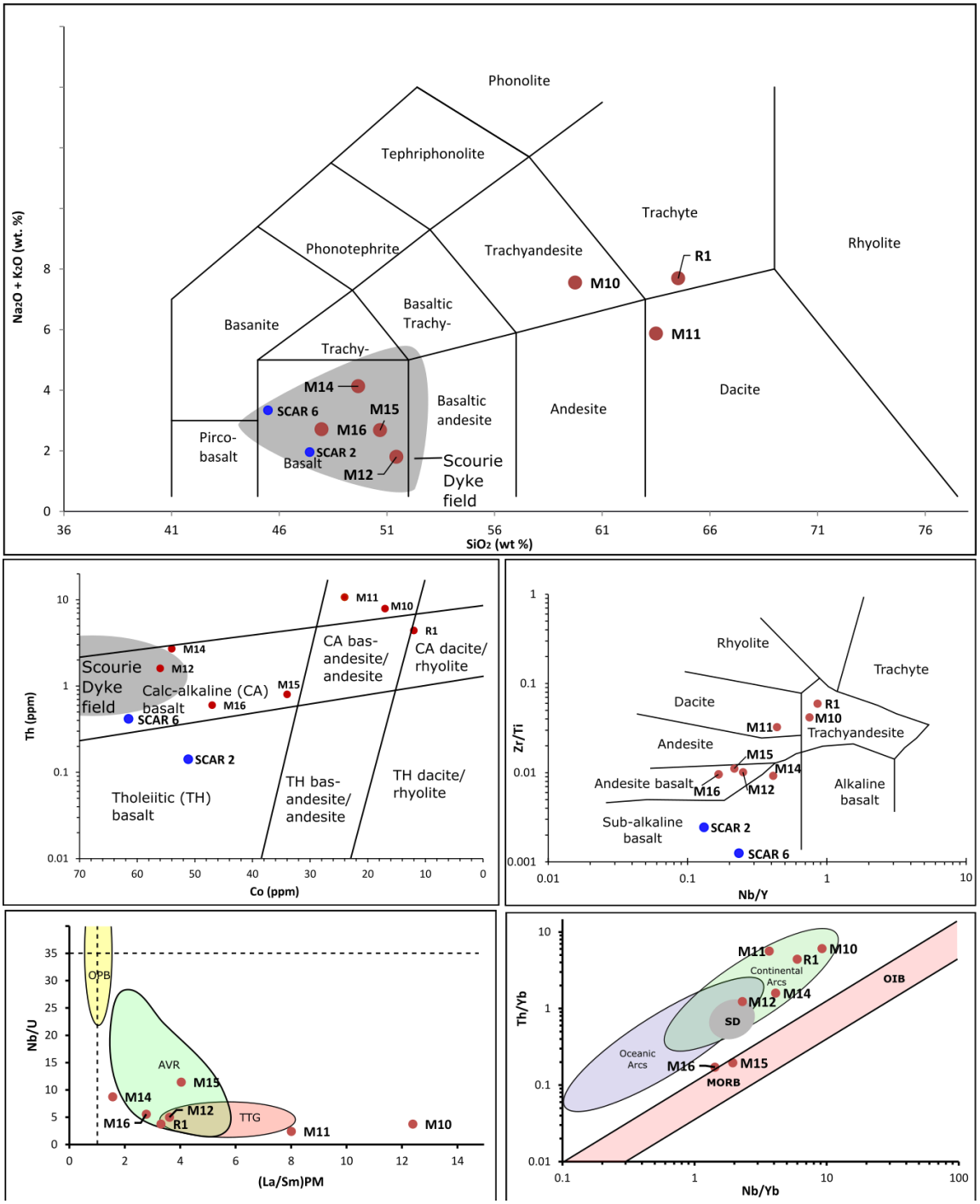

Figure 4.29. Geochemical analysis and discrimination of intrusive igneous samples. Fields for Scourie Dykes plotted from Hughes et al., (2014). SCAR 2 and SCAR 6 collected prior to this study by Emma Waters. **TAS Plot** - showing clear differentiation betweena grouping of basaltic samples and three more evolved samples. **Co – Th diagram** after Hastie et al., (2007). **Nb/Y – Zr/Ti** diagram after Winchester and Floyd, (1977). **La/Sm – Nb/U** plot **Nb/Yb – Th/Yb** plot after Pearce, (1982). REE

diagrams (Fig. 4.29) it is M12 and M14 that appear to resemble both one another, and the dykes of the foreland.

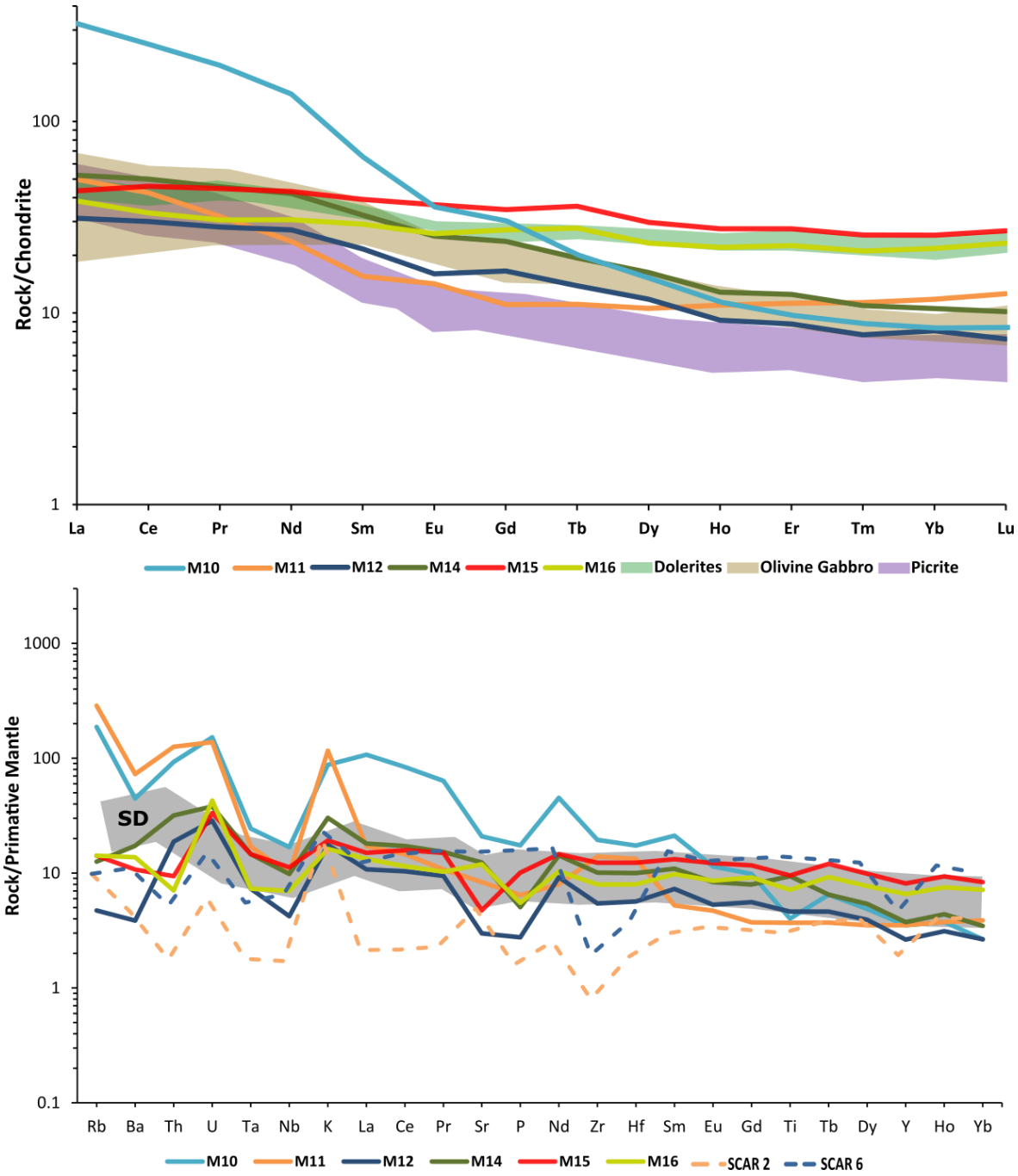

Figure 4.30 REE plot – Chondrite normalised values for mafic samples from Scardroy and Orrin plotted against Scourie Dyke fields from Hughes et al., (2014). **Multi-element plot –** Primitive mantle normalised values for mafic samples from Scardroy and Orrin. Dashed samples collected prior to this study by Emma Waters. Scourie Dyke, SD – grey, fields from Weaver and Tarney, (1981).

4.3.3 - Geochronology

LA-ICP-MS U-Pb dating of separated zircon from samples G1, G2, G3, and SCAR 2A is detailed below with data tables in appendix 4 - 7.

4.3.3.1 – Orrin (G2)

Concordant cores (5% discordance or less) with those interpreted as inherited and metamorphic cores omitted (n = 22) overlap the concordia curve, with a probability cut-off at 2σ, in the range 2750 Ma to 2850 Ma (Fig. 4.31). A population of c. 15 centre around a c. 2800 Ma age with a spread to lower ages considered to be the result of Pb loss due to later metamorphism. A weighted mean of these 15 cores gives an age of 2844 ± 16 Ma (MSWD of 0.51) and a concordia age of 2797 ± 9 Ma with a MSWD of 0.86. As such the protolith is interpreted to be c. 2800 – 2850 Ma in age. Cores recording a pre-2850 Ma age are interpreted as inherited due to a high degree of dispersion in the range c. 2850 – 3000 Ma and no sign of clustering. In total seven cores are interpreted as inherited: three very likely inherited, a further three being likely inherited, and one highly discordant but likely inherited. The three very likely inherited cores give $^{207}Pb/^{206}Pb$ ages of 2876 ± 26 Ma, 2921 ± 33 Ma, and 3007 ± 51 Ma, while the likely inherited cores record $^{207}Pb/^{206}Pb$ ages of 2868 ± 63 Ma, 2876 ± 66 Ma, and 2920 ± 76. All six are within 5% concordance, while one additional discordant (30%) core gives a $^{207}Pb/^{206}Pb$ age of 2825 ± 302 and a concordia age of 3122 ± 210.

Two cores present concordant ages at < 2500 Ma and are interpreted as metamorphic. One core gives a concordant (0.5% discordance) $^{207}Pb/^{206}Pb$ age of c. 2470 ± 40 Ma and a concordia age of c. 2475 ± 27 Ma. A second core presents a late-Paleoproterozoic $^{207}Pb/^{206}Pb$ age of c. 1770 ± 116 Ma and a concordia age of c. 1607 ± 34 Ma with a discordance of 11.2%. Two discordia exist within the analysed cores with both sharing a c. 2840 Ma upper intercept. The most prominent suggests major lead loss associated with a Neoproterozoic event at c. 900 Ma. A second less distinct discordia within these cores appears to relate to a c. 1700 Ma event.

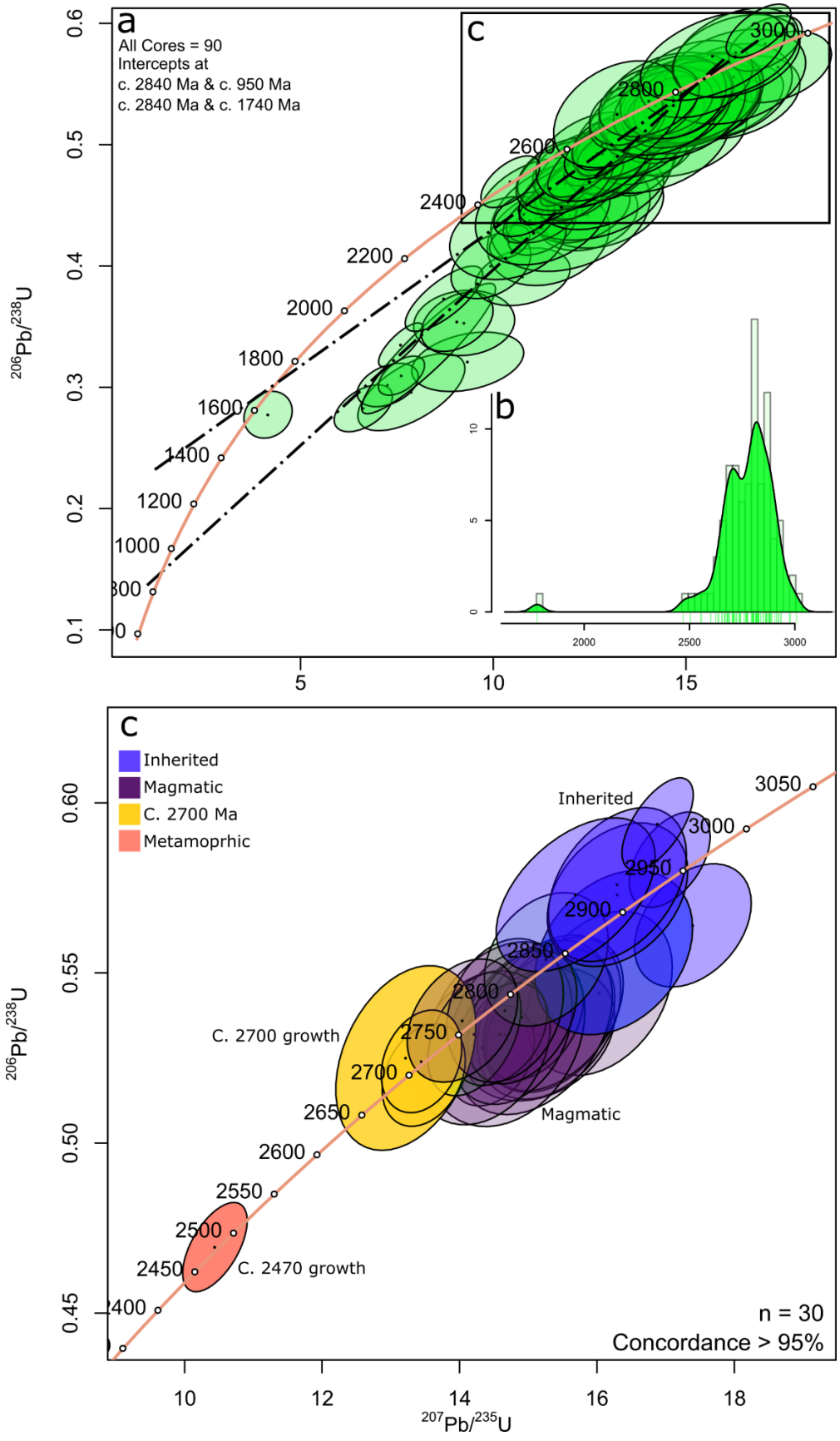

Figure 4.31. Wetherill concordia plots for G2 created with IsoplotR (Vermeesch, 2018). **A** – All cores at 2σ. showing concordance at c. 2800 Ma and discordia towards c. 900 Ma and c. 1700 Ma with single concordant cores at c. 2500 Ma and 1600 Ma. **B** – KDE plot of $^{207}Pb/^{206}Pb$ core ages. **C** – Concordant cores with error ellipses at 1σ. Showing inherited, magmatic, c. 2700 Ma, and c. 2480 Ma populations.

Two concordant (within 5%) rims occur between 2850 – 2900 Ma and as these pre-date the protolith age are considered to be inherited (Fig. 4.32). Seven rims (at > 95% concordance) occur at between c. 2750 – 2850 Ma with a concordia age of 2777 ± 12 Ma (MSWD = 0.32) and may be magmatic rims affected by minor lead loss. A cluster of concordant (within 5%) rims (n=17) occurs at between 2600 Ma and 2700 Ma with a weighted mean of c. 2670 Ma. In conjunction with four concordant cores: 2676 ± 84 Ma, 2708 ± 49 Ma, 2716 ± 42 Ma, and 2707 ± 40 Ma, this cluster may suggest a metamorphic event at c. 2700 Ma with minor later lead loss. However the proximity of this age to the interpreted protolith age and the high degree of uncertainty in the data makes this interpretation tentative. Alternatively, these cores and rims may represent drawn down primary cores and magmatic rims that have been affected by Archean lead loss and hence plot very close to the concordia curve. Three concordant rims occur at 2442 ± 53 Ma, 2475 ± 61 Ma, and 2489 ± 75 Ma, and in combination with the single c. 2470 core described above, may suggest a metamorphic event at c. 2470 Ma. These cores and rims are highly concordant (<5% discordance) and distinct from the discordia of both cores and rims related to later Proterozoic events. Six rims, at within 5% concordance and 12 at within 30% concordance, occur between c.1800 Ma and 1600 Ma with a further 5 rims occurring along a discordia from c. 1700 Ma towards the Neoproterozoic. The six most concordant record $^{207}Pb/^{206}Pb$ ages of 1647 ± 71 Ma, 1708 ± 28 Ma, 1627 ± 63 Ma, 1737 ± 55 Ma, 1780 ± 48 Ma, and 1857 ± 65 Ma. Together these give a concordia age of 1706 ± 9 Ma (MSWD = 2.40) and a weighted mean of 1724 ± 19 (MSWD = 1.88). Four rims are found at c. 850 – 900 Ma, with $^{206}Pb/^{238}U$ ages of 897 ± 17 Ma, 880 ± 17 Ma, 805 ± 15 Ma, and 755 ± 27 Ma with concordances of more than 80%. In addition, one rim is found at 598 ± 16 Ma with a discordance of 17%. These five rims may record several early Neoproterozoic metamorphic event, the ‘Renlandian’ at c. 900 Ma; the lower intercept of the main discordia, and distinct ‘knoydartian’ events at c. 830 – 780 and 725 Ma.

The rims display three, and potentially four, discordia. From an upper intercept of c. 2600 Ma two lower intercepts are present at c. 1700 Ma and c. 900 Ma. Additionally Laxfordian rims at c. 1700 - 1800 Ma show a trend towards a c. 900 Ma event. Early Neoproterozoic rims at c. 900 Ma may display a discordia towards a Caledonian age event although this is poorly defined due to the low number of results in this age range. Finally rims at c. 2600 - 2700 Ma may represent a drawdown of primary magmatic rims from c. 2800 Ma and hence a discordia from 2800 Ma towards 2400 Ma or may represent a separate c. 2700 Ma event themselves.

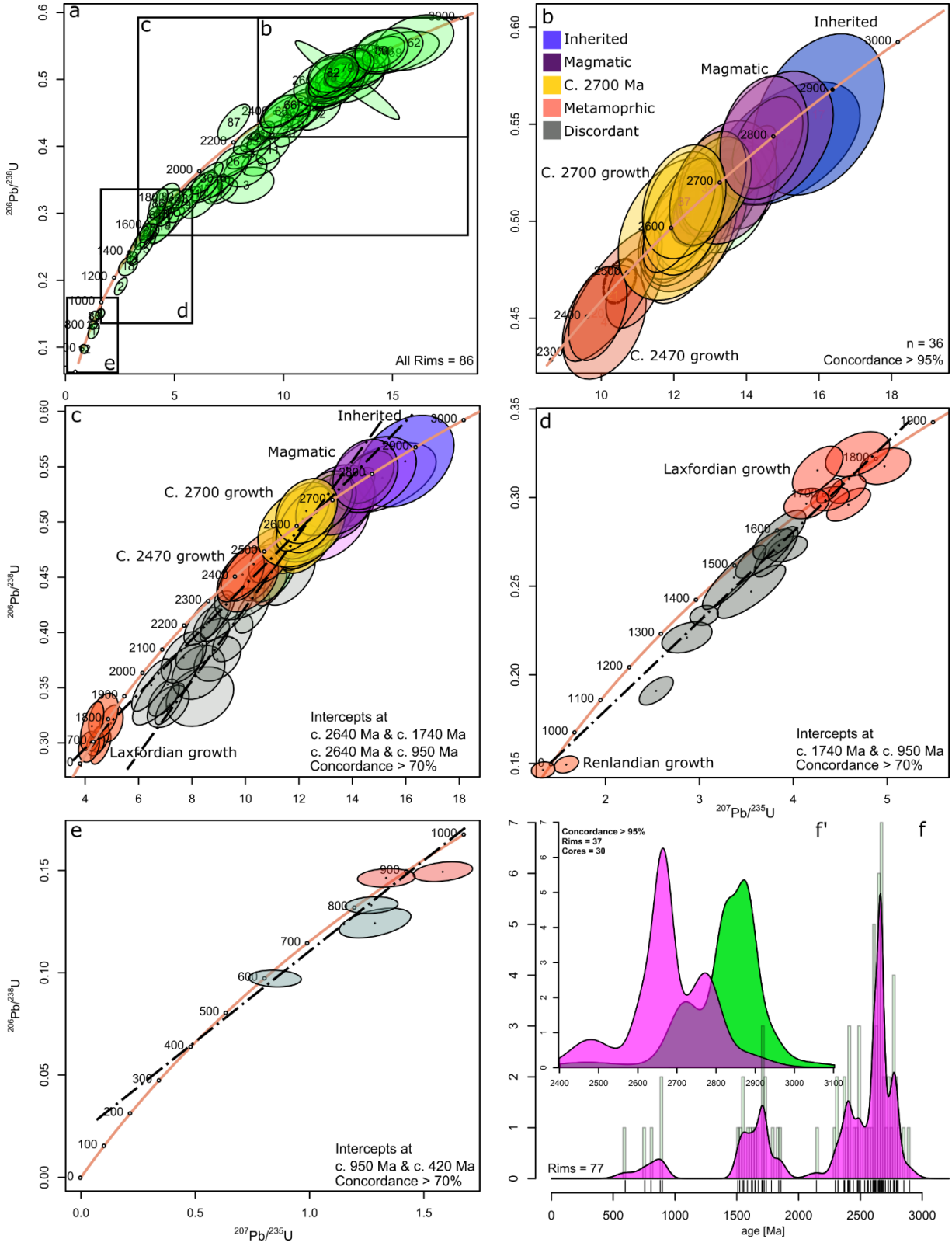

Figure 4.32. Wetherill concordia plots for sample G2 with error ellipses shown at 2σ unless otherwise specified. Plots created with IsoplotR (Vermeesch., 2018). **A –** All rims at 1σ showing the location of inset figures. **B –** Concordant Archean rims and colour legend. **C –** Archean and Laxfordian rims with discordia from c. 2640 to Laxfordian and Renlandian metamorphic events. **D -** Discordant rims between Laxfordian and Renlandian metamorphic populations. **E –** Neoproterozoic rims**. F –** KDE showing distribution of rim analyses. **F'** – KDE showing distinct populations of early concordant cores and rims suggesting a rim growth event distinct from the protolith age.

4.3.3.2 – Scardroy (SCAR 2A)

The analyses of zircon cores from sample SCAR 2A is dominated by discordant grains that define a prominent discordia, formed by over 90 cores with discordance > 5%, with an upper intercept at c. 2700 Ma and a lower intercept at c. 900 Ma (Fig. 4.33). Four cores occur above the concordia curve at pre-2800 Ma ages, this is interpreted as reflecting U-loss as they occur along the trend of the main discordia from c. 900 Ma to 2700 Ma when projected above the concordia. Few concordant cores are present with nine Archean analyses occurring within 2% concordance. These form two clusters, one of two grains that give $^{207}Pb/^{206}Pb$ ages of 2769 ± 52 Ma and 2774 ± 46 Ma and a second cluster formed of five analyses that gives a concordia age of 2631 ± 11 Ma with a MSWD of 0.37 and a weighted mean of 2636 ± 20 Ma with a MSWD of 0.55. In combination with the upper discordia intercept at c. 2700 Ma it is considered likely the protolith age for the sample lies in the range 2750 – 2800 Ma with minor draw down due to later Pb loss. Two concordant cores, within 5%, present ages of 2868 ± 33 Ma and 2852 ± 16 Ma and are interpreted as inherited. Four cores, within 5% discordance, record 'Laxfordian' $^{207}Pb/^{206}Pb$ ages of 1958 ± 62 Ma, 1702 ± 60 Ma, 1724 ± 36 Ma, and 1727 ± 167 Ma. The first falls within error of the "early-Laxfordian" at c. 1.91 – 1.85 Ga, while the subsequent three cores fall within the "late-Laxfordian" between c. 1.75 – 1.65 Ga. Additionally a second less distinct concordia appears to link a c. 2700 - 2750 Ma upper intercept with a c. 1700 Ma lead loss event. Four cores, within 30% discordance, record sub one Ga $^{206}Pb/^{238}U$ ages of 655 ± 15 Ma, 802 ± 16 Ma, 906 ± 11 Ma, and 940 ± 26 Ma. The two c. 900 Ma cores sit at the lower intercept of the main discordia and may represent zircon growth associated with this event.

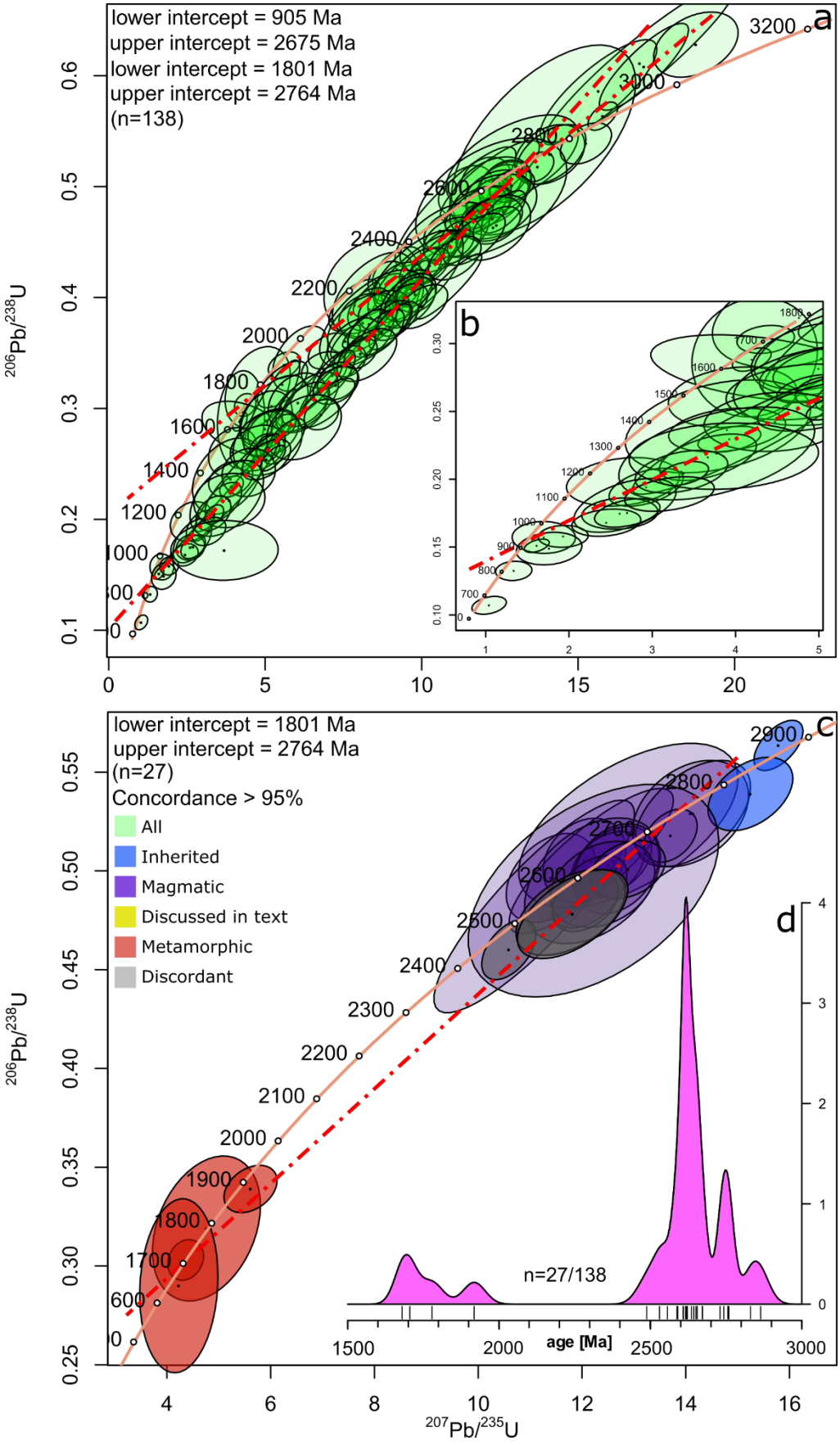

Figure 4.33. Wetherill concordia plots created with IsoplotR (Vermeesch, 2018). **A** – All cores at 2σ. showing concordance at c. 2700 Ma and discordia towards c. 900 Ma and c. 1700. **B –** Close up of A showing c. 900 Ma lower intercept and two younger grains. **C** – Concordant cores (> 95%) showing inherited, magmatic and metamorphic populations. **D** - KDE plot of > 95% concordant $^{207}Pb/^{206}Pb$ core ages

One rim presents a $^{207}Pb/^{206}Pb$ age of 2899 ± 46 Ma and may be inherited (Fig. 4.34). Five concordant rims, within 2%, cluster around concordia age of 2725 ± 12 Ma with a MSWD of 1.5 and a weighted mean of 2726 ± 18 with MSWD of 1.03. These overlap with the c. 2700 – 2750 Ma age interpreted as the protolith age from the core cluster and discordia and are interpreted as related to emplacement of the igneous protolith. A series of discordia exists within the rim analyses. A discordia with a c. 2700 Ma upper intercept trends to a point slightly below a late-Laxfordian lower intercept. This appears to have been slightly drawn down towards a later c. 900 Ma event. A second prominent discordia links the same upper intercept with a c. 900 Ma lower intercept. These discordia are tied to metamorphic events as evidenced by the presence of concordant rims at each of these intervals. A third discordia exists between a c. 1700 Ma late-Upper Laxfordian upper intercept and a poorly defined Neoproterozoic or Paleozoic lower intercept.

Five rims, three within 5% and one within 10% concordance, present Laxfordian'$^{207}Pb/^{206}Pb$ ages of 1995 ± 81 Ma, 1683 ± 51 Ma, 1683 ± 41 Ma, 1711 ± 94 Ma, and 1782 ± 184 Ma. Four of these analyses fall within error of the late-Laxfordian at c. 1.75 – 1.65 Ga while one may relate to the early Laxfordian. These analyses match those of zircon cores that also showed a stronger late-Laxfordian signature. Five rims occur above the main discordia trend, and within 4% discordance, and record ages of 2428 ± 54 Ma, 2407 ± 64 Ma, 2339 ± 79 Ma, 2237 ± 34 Ma, and 2324 ± 56 Ma. These all fall slightly below the concordia curve, but above the discordia from c. 2700 to c. 1700. They may lie along a discordia to the c. 1900 early Laxfordian or relate to a separate episode of rim growth.

Three rims, within 30% discordance, record sub one Ga $^{206}Pb/^{238}U$ ages, with two at c. 900 Ma, 912 ± 36 Ma and 939 ± 24 Ma, and one at 775 ± 10 Ma. The two rims a c. 900 Ma occur at the lower intercept of the discordia from both c. 2700 Ma and c. 1700 Ma and as such are interpreted as recording zircon growth associated with this event. The 775 Ma rim falls outwith error of the c. 900 Ma event and may relate to a separate, younger, Knoydartian event.

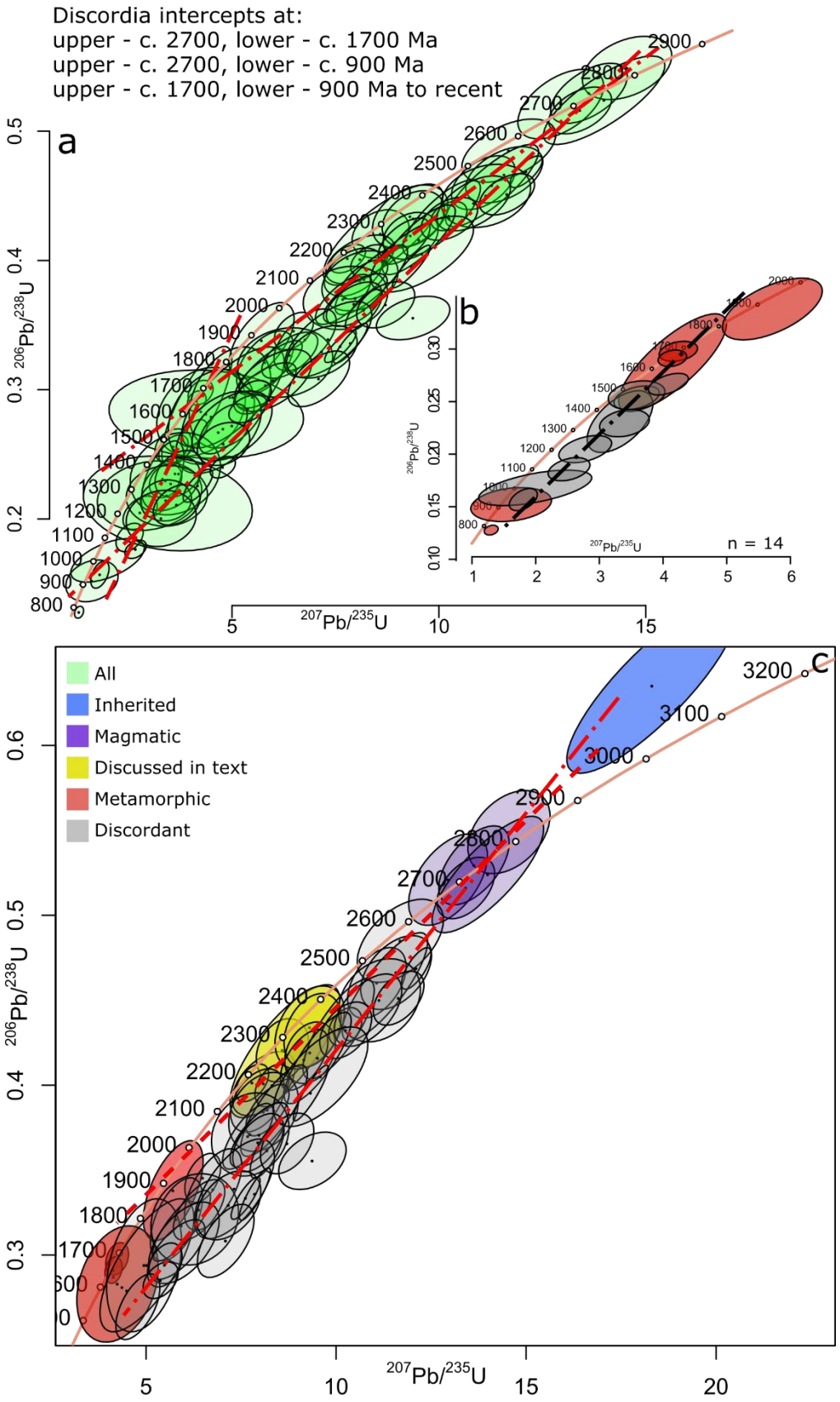

Figure 4.34. Rim analyses for sample SCAR 2A. **A –** All rims at 2σ showing concordance at c. 2700 Ma and discordia towards c. 900 Ma and c. 1700 Ma. **B –** Laxfordian concordant rims with discordia towards an unclear Neoproterozoic to Paleozoic intercept. **C –** Interpreted Archean and Proterozoic rims showing upper intercepts and interpreted protolith age at c. 2700 – 2750 Ma.

4.3.3.3 – Scardroy (G3)

A total of 27 analyses (Fig 4.35) were recorded from sample G3: 16 cores, and 11 rims. Two cores give a concordia age of 2744 ± 20 Ma with an MSWD of 0.59. One core records a $^{207}Pb/^{206}Pb$ age of 2884 ± 48 Ma and may be inherited. Two cores give early-Laxfordian $^{207}Pb/^{206}Pb$ ages of 1937 ± 98 Ma and 1949 ± 74 Ma, whilst one core gives an age of 1803 ± 64 Ma. A discordia though all core analyses, excluding concordant Laxfordian cores, gives an upper intercept at 2779 ± 21 Ma and lower intercept at 983 ± 51 Ma. A concordia through only the most concordant (> 95%) analyses gives an upper intercept of 2816 ± 45 Ma and lower intercept of 1795 ± 53 Ma. As such G3 is interpreted to record a protolith age of c. 2740 to c. 2810 Ma.

One rim within records an $^{207}Pb/^{206}Pb$ age of 2740 ± 14 Ma, within the range of the interpreted protolith age. No rims record Laxfordian ages although one rim (85% concordance) records a $^{206}Pb/^{238}U$ age of 1281 ± 63 Ma and $^{207}Pb/^{206}Pb$ age of 1501 ± 107 Ma and may be a Laxfordian rim with later Neoproterozoic or Paleozoic Pb-loss. A single rim records a sub one Ga $^{206}Pb/^{238}U$ age of 764 ± 18 Ma. A discordia through the rim analyses, excluding the concordant core at c. 760 ma, gives an upper intercept at 2776 ± 23 Ma and a lower intercept at c. 925 ± 38 Ma. Two possible discordia exist between c. 2750 Ma and the Laxfordian, and the Laxfordian and the Neoproterozoic to Paleozoic, however these are based on very few analyses.

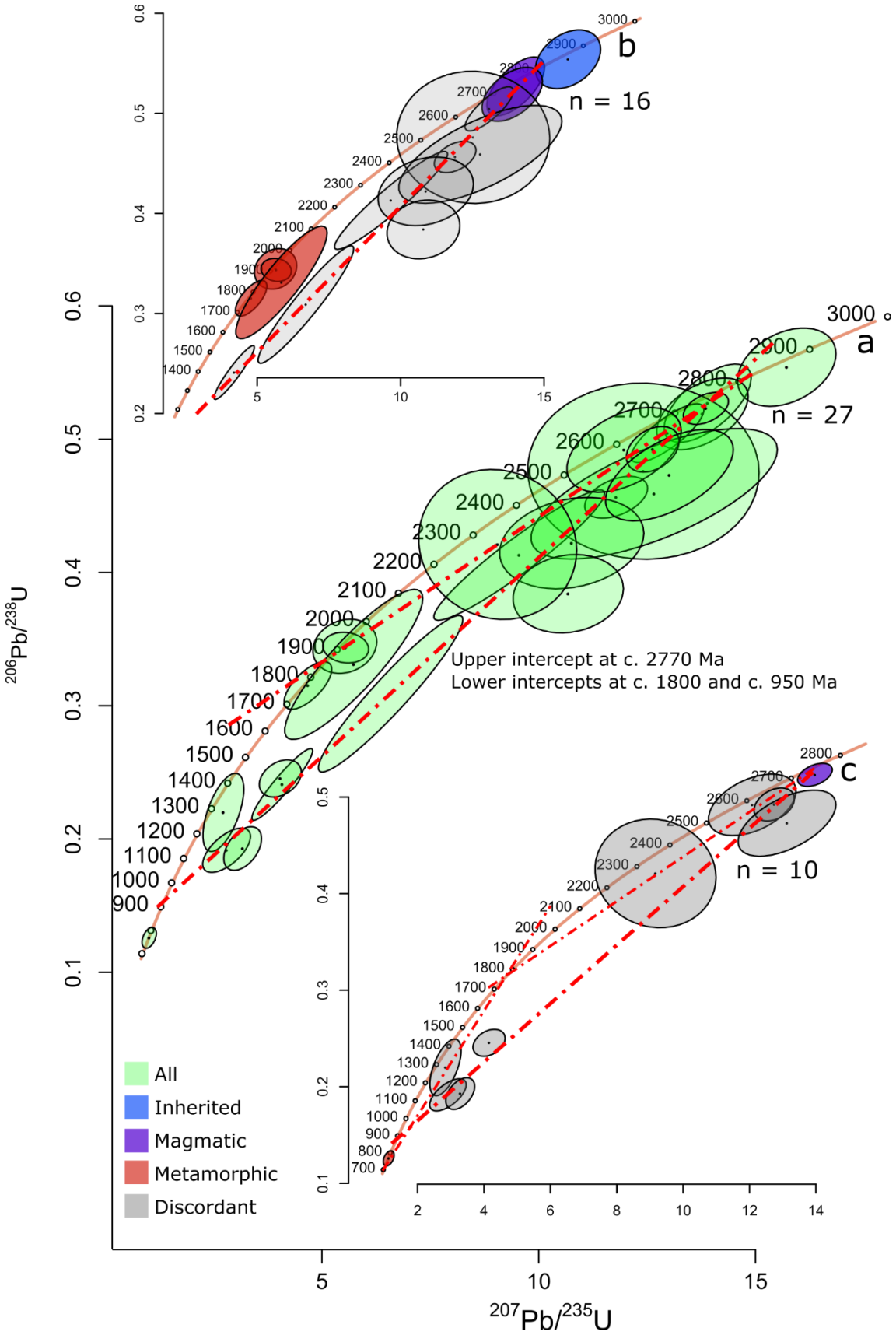

Figure 4.35. Core and rim analyses for sample G3. **A** – All analyses showing an Archean protolith with Laxfordian growth and discordia pointing to a Neoproterozoic event. **B** – All cores showing a single inherited core, magmatic cores, and metamorphic growth associated with the Laxfordian. **C** – All rim analyses showing a single magmatic rim, a concordant Neoproterozoic rim, and ill defined discordia.

4.3.3.4 – Scardroy (G1)

Analyses for cores from G1 give a well constrained Mesoproterozoic protolith age with extensive evidence of Caledonian aged Pb-loss and zircon growth (Fig. 4.36). A discordia through all cores, minus the single inherited core, gives an upper intercept of 1776 ± 8 Ma and a lower intercept of 470 ± 24 Ma. A discordia through only the Proterozoic cores gives a composite lower intercept at c. 600 Ma while one through only cores within 80% concordance gives an intercept at c. 800 Ma. This c. 800 Ma lower intercept may be related to the single concordant rim found at c. 830 Ma and suggests Pb-loss associated with both c. 830 Ma and 470 Ma. A concordia age for cores within 2% concordance (n = 10) gives an age of 1772 ± 5 Ma with an MSWD of 1.3. While a weighted mean of all cores within 5% concordance gives an age of 1776 ± 10 Ma with an MSWD of 0.4. As such the protolith is considered to have been emplaced at c. 1775 ± 10 Ma. One core presents a $^{207}Pb/^{206}Pb$ age of 2731 ± 68 Ma and is considered to be inherited. Thirteen cores within 50% concordance record Caledonian $^{206}Pb/^{238}U$ ages with a concordia age of 463 ± 3 Ma and a MSWD of 0.88. While a weighted mean of all Caledonian aged cores (n = 21) gives 463 ± 2 Ma.

The rims of G1 zircon show a similar pattern to the cores (Fig. 4.37). Rims within 2% concordance, excluding a single Caledonian aged analysis, give a concordia age of 1731 ± 5 Ma with a MSWD of 1.5, n = 11. A discordia through all rim analyses, discounting one concordant Neoproterozoic grain, gives an upper intercept of 1697 ± 7 Ma and lower intercept of 488 ± 11 Ma with an MSWD of 0.93. With Caledonian and concordant Neoproterozoic analyses omitted a discordia through only Mesoproterozoic rims yields a lower intercept of c. 780 Ma. A weighted mean of analyses within 5% concordance gives a value of 1717 ± 16 Ma with a MSWD of 0.96. Within these concordant analyses, two subgroups appear to form overlapping clusters. The first centred around a c. 1780 Ma age and a second younger cluster around a c. 1730 Ma age. Taken together this c. 40 Ma younger age for the rims and evidence of two population supports a metamorphic growth at c. 1730 Ma. Both the c. 1775 Ma emplacement age and this c. 1730 Ma metamorphic age are within the period of the late-Laxfordian event. A single concordant rim, 94% concordance, gives a Neoproterozoic $^{206}Pb/^{238}U$ age of 829 ± 17 Ma. A concordia age for all Caledonian aged rims, within 50% concordance (n = 14) gives a value of 462 ± 2 Ma and a MSWD of 0.9. While a weighted mean of all Caledonian aged rims (n = 22) yields and age of 463 ± 3 Ma with an MSWD of 1.2. This is in agreement with the age determined from core analyses and within the range of the Grampian event at c. 470 Ma – 460 Ma.

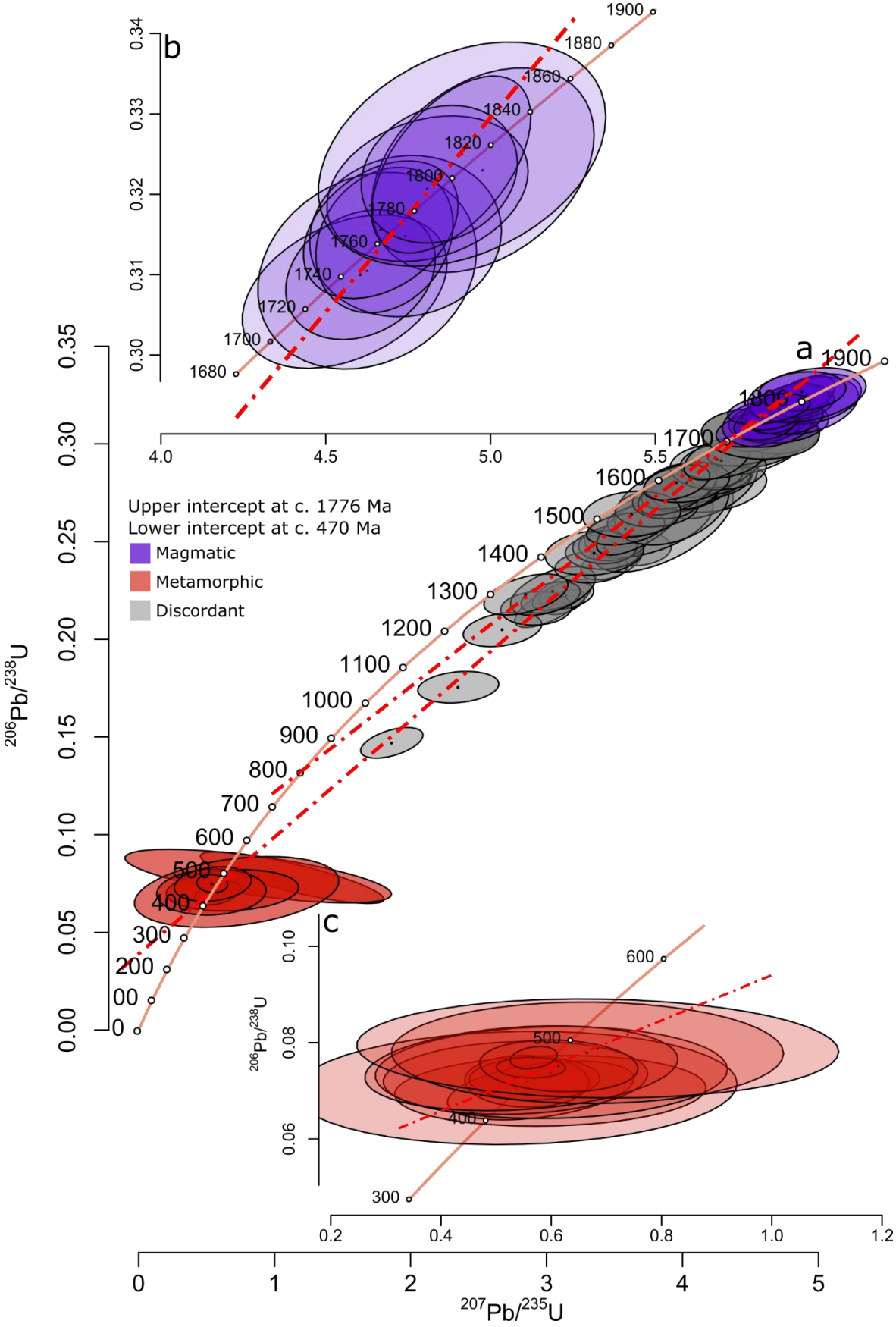

Figure 4.36. Core analyses of sample G1. **A –** All cores showing a Mesoproterozoic protolith age, Caledonian aged growth, and composite discordia towards the Neoproterozoic and Paleozoic. **B –** Cores within 2% concordance. **C –** All Caledonian analyses showing a Grampian (470 Ma) age.

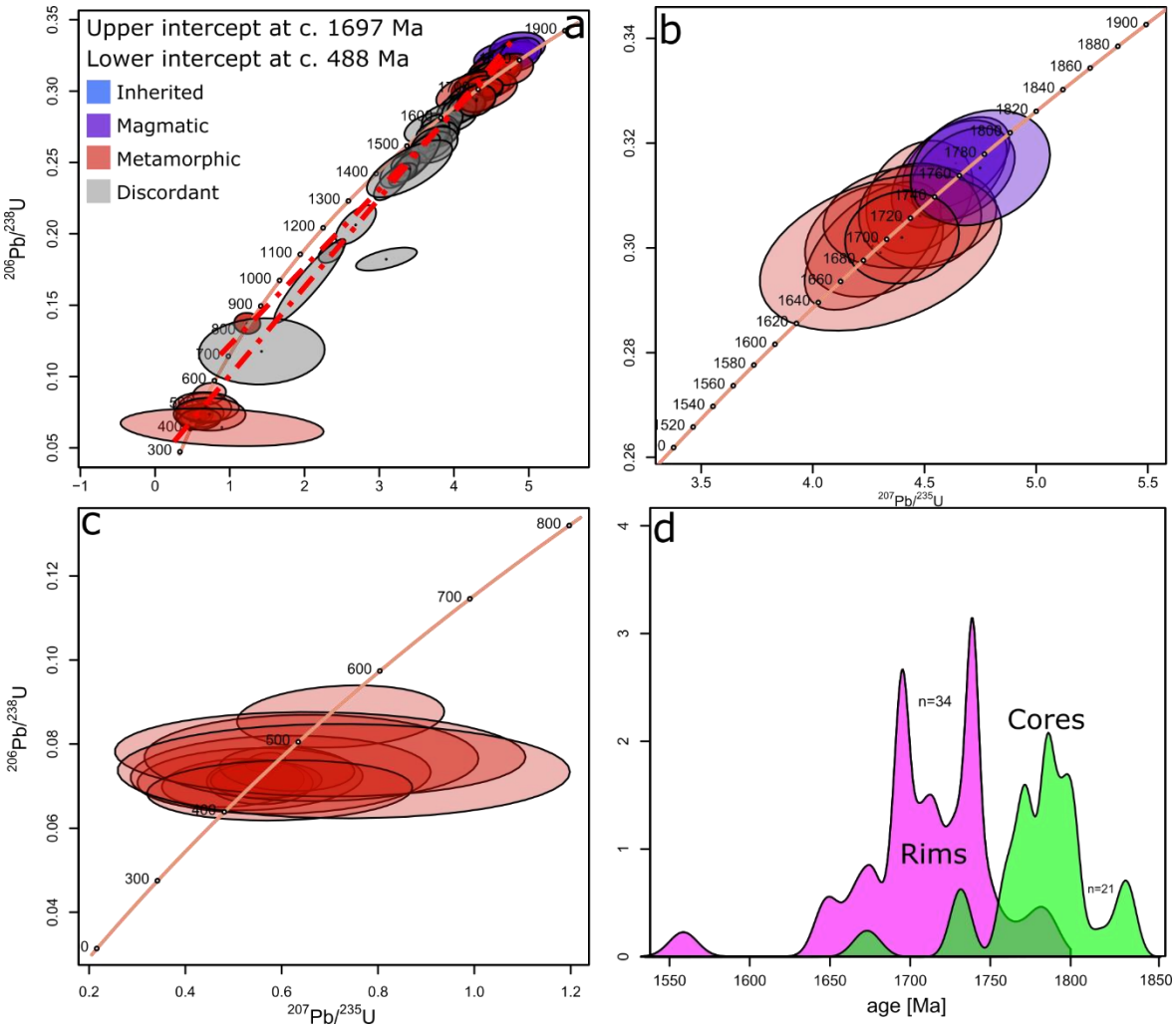

Figure 4.37. Rim analyses for sample G1. **A –** All rims. **B –** Analyses within 2% concordance showing populations overlapping with interpreted protolith age, and younger c. 1700 Ma population. **C** – Caledonian rims showing dominantly Grampian aged growth. **D –** KDE plots for concordant core and rim populations showing older cores interpreted as protolithic, and younger rims potentially grown during Laxfordian metamorphism.

Chapter 5. Discussions and Conclusions

5.1 - Loch Maree Group

5.1.1. – Mineralisation

5.1.1.1 – Allt na Cosaig

The Allt na Cosaig and Druim na Fearna sample sites show similar styles of mineralisation, small scale dissemination of sulphides within an amphibolite interpreted to represent an originally mafic-igneous host rock. The exact igneous origin of the amphibolites sampled is unclear, with any primary intrusive or extrusive features overprinted by metamorphism. Park, (2002) suggests that intercalation with marine sediments and variations in geochemistry suggest sub-aqueous basalt, intrusive sills, and minor tuffs are all present within the sequence. The marine nature of these rocks suggests that significant post eruptive low-grade alteration typical of sea floor volcanics may have occurred prior to their accretion to the Lewisian. This low-grade alteration of marine basalts can generate pyrite as an accessory phase to the primary albite, actinolite, chlorite, epidote assemblage (Humphris and Thompson, 1978; Oliva-Urcia et al., 2011). Later prograde metamorphism would overprint this zeolite facies assemblage with an amphibolite facies one but leave disseminated pyrite throughout the rock. This may be a mechanism through which the low levels of disseminated sulphides found in samples from the Allt na Cosaig and Druim Na Fearna localities formed. These display only slightly elevated base metal values and so limited hydrothermal alteration could form sparsely disseminated sulphides. The possibility that these sulphides were formed during Laxfordian metamorphism is considered unlikely due to their tectonisation and limited remobilisation. Additionally, their disseminated nature is suggestive of a pervasive alteration where later formation of sulphides during Laxfordian aged metamorphism may have favoured a vein or foliation parallel formation.

5.1.1.2 – Carbonate/Pyrite Veins

The only evidence of syn- or post-metamorphic mineralisation sampled by this study, are the calcite and pyrite veins sampled in the Allt na Cosaig (K25253). This set of veins occur along the boundary between mineralised amphibolite and schists and may relate to minor faulting along or near this boundary. The veins are straight and appear undeformed suggesting they were formed after the major phases of deformation. As such they may date

to the Late-Laxfordian, and relate to the greenschist facies retrogressive features that characterise this event (Park, 2002). Alternatively they may relate to the brittle deformation and pseudotachylyte formation that occurred during the Grenvillian (Campbell et al., 2019; Sherlock et al., 2008). The only other noted example of mineralised veining from the LMG is reported in Coats et al., (1997) from the LMSB where two sets of NE trending 10 – 20 cm pyrite bearing carbonate veins are recorded. Comparison to the LMSB veins: 0.03% Zn, 0.08% Cu, 0.19% Pb, appear superficially similar in base metal values. The strike of the Allt na Cosaig veins at 320° is offset c. 90° from the NE trend for the LMSB veins reported by Coats et al., (1997). They suggest the veins may be related to movement along the Loch Maree Fault or Mesozoic extension parallel to the Minch fault. As with the LMSB veins there is no evidence of scavenging and upgrading of primary mineralisation within the Allt na Cosaig veins, and they are deemed of little economic importance.

5.1.1.3 - Sidhean Mor

The Sidhean Mor locality likely represent primary syngenetic sulphide mineralisation. The metamorphic mobilisation and deformation of sulphide minerals means they must predate said metamorphic event. The banding of the samples, comprised of alternating coarse quartz rich and fine-grained mica rich layers, is likely to be a primary depositional feature. These interpretations fit with the conclusions of Jones et al., (1987) who proposed an exhalative origin for the sulphide horizon. The distal exhalative portion of a VMS deposit is characterised by the precipitation and deposition of silica and pyrite from suspension (Lydon, 1984). This forms a laterally extensive but thin deposit that during periods of quiescence will become interbedded with other marine sediments or igneous material. This exhalate horizon cannot be related to the main orebody at Kerry Road as c. 1000 m of stratigraphy interrupted by the Flowerdale shear zone separate the two. The Sidhean Mor sulphide horizon may extend into the LMSB. Coats et al., (1997) suggested a correlation between it and similar bands of quartz actinolite hosted stratiform pyrite/pyrrhotite deposits within the Ben Lair Hornblende Schist, an amphibolite they correlate with the Aundrary Amphibolite. The laterally extensive nature of this deposit suggests that any original feeder zone or zones are likely to be significantly above or below current exposure levels and so unlikely to be an economic target. Extensive sampling of the band may elucidate geochemical indicators that would indicate the more proximal and distal zones, however this is unlikely to lead to any significant metalliferous deposits and it is not considered a priority of any future exploration.

5.1.1.4 - Float

The origin of the float samples (K25254 – 55, 57 – 58) collected along the shore of Loch Bad an Sgalaig is of interest as they contain the highest sulphide proportions, c. 50%, of any collected samples. The sulphides in these samples are dominated by py, with minor ccp, sp, and gn in a host rock comprised predominantly of quartz and amphibole. The two largest source of brecciated sulphide rich rocks within the GSB is the Sidean Mor exhalative horizon and the Kerry Road orebody.

Comparison with the Kerry road site suggests float samples have not been sourced from it due to the significant differences in mineralisation. Host rock mineralogy differs between the sample sets; the float is a quartz-amphibole schist, the host rock at Kerry Road is a quartz-carbonate schist. This is reflected in the Ca content, with the average Ca values of the float being 2.5 % and the Kerry Road ore being 8.5 %. Base metal values are at least an order of magnitude lower and precious metal values are either below detection level or very low in the float, with K25257 recording the highest Au value of 0.05ppm. Fe contents of float samples, 17 – 30 %, are above the range for the Kerry Road site - 4.5 – 20 % with a mean of 10.2 %. Additionally, trace element concentrations in the float samples are significantly higher in certain key elements: P, Ni, Ti, V, and Cr. For these reasons it is considered very unlikely these samples were sourced from the Kerry Road deposit.

The second potential source for these samples is the Sidean Mor sulphide horizon. The Aundrary Amphibolite that hosts the Sidean Mor sulphide horizon outcrops to the east of the loch on the slopes of Meall a' Ghlas-Leothaid. As such the material would have a relatively short downslope distance to migrate. The host rock mineralogy of each set of samples is similar, a deformed quartz-amphibole, likely actinolite, schist with banding defined by coarse quartz zones and fine grained amphibole rich zones. Folding is evident at thin section scale in both sets of samples. Extensive brecciation has affected both the host rock and sulphide mineralogy in both sets of samples and so postdates the sulphide mineralisation. Variation in metal content and mineralisation are to be expected in a horizon that runs for over 6 km; Coats et al., (1997) report variation in the sulphide content of the LMSB exhalative horizon that they correlate with the one at Sidean Mor from c. 10% to 90 %. Additionally sampling bias of float samples may have had an effect, as the collection of more heavily oxidised and hence sulphide bearing samples would skew the set towards the most heavily mineralised. The degree of brecciation and deformation appears to be greater in the

float samples than those from Sidean Mor, however this may be due to the high proportion of sulphides within these samples, and therefore their decreased strength.

The third possibility, that the float samples are sourced from a yet undiscovered sulphide rich unit within the GSB is considered unlikely. If the float was sourced from an exposed or near surface outcrop then the exploration, geochemical sampling, and geophysical analysis conducted over the belt would likely have discovered it (Jones et al., 1987; Coats et al., 1997). The possibility that the float is weathering out of a secondary position within the Torridonian cover rocks is possible, as coarse basal conglomerates with large locally derived clasts are common near the unconformity surface. This possibility does not however preclude a correlation with the Sidean Mor horizon, as it is likely material from this unit would have been incorporated into the Torridonian.

5.1.1.5 - Gorm-Loch na Beinne

The Gorm-Loch na Beinne inlier is the only site to record significant precious metal assay values, 0.2 ppm Au and 4 ppm Ag. These are significantly lower than the up to 4 ppm Au recorded by Coats et al., (1997) but this may be due to relatively poor sample availability at the time of this study. Only one sample was recovered from the central peat gully, compared to the 14 samples collected in 1997 from this area. This disparity in sample density may relate to overzealous collecting by Coats et al., (1997) or changes in the morphology of the peat gully in the intervening c. 20 years. K25266 was collected from a bank that showed evidence of recent slumping, and so may have been exposed in the interval between 1997 and this study. No samples from the loch-bed are reported as being collected by Coats et al., (1997). The loch on the western side is shallow and the bed dominated by abundant cobble sized clasts and orange weathered sediments. Due to the difficulty in recovering samples from the peat cover this sub-aqueous float is considered the most prospective site for any future sampling. The occurrence of sulphide bearing float and subcrop on both sides of the loch suggests that these lithologies may underly the loch itself.

The low base metal values, maximums of 390 ppm Zn, 340 ppm Cu, 30 ppm Pb, within the inlier match that reported by Coats et al., (1997), and are at least an order of magnitude below that of the Kerry Road deposit. This is reflected in the dominance of iron-sulphides, pyrite and pyrrhotite, and a near absence of chalcopyrite and sphalerite. No gold was observed in reflected light, however Coats et al., (1997) observed several small occurrences of electrum within samples from the inlier. These significant disparities in mineralisation style between

the two locations may be due to sampling bias or a more fundamental difference in the style of the deposits and may preclude direct correlation between the two. If the correlation of the An Lungard amphibolite with the Aundrary amphibolite (Coats et al., 1997) is correct then the inlier likely occurs at a similar stratigraphic position, within the GSB, as the Kerry Road site. The distance, c. 11 km, between the two localities is significant and even if they are related stratigraphically and temporally to the same mineralising episode, major differences in the hydrothermal system may have existed across the intervening distance. Despite these differences, the range of exhalative and sulphide bearing lithologies found at Gorm-loch na Beinne mark it as the only occurrence within the GSB or LMSB that bears any resemblance to the Kerry Road deposit and as such the only other potentially economic prospect within the belt.

5.1.1.6 - Future work

Within the main exposure of the LMG near Gairloch, all previously examined localities have been revisited by GreenOre. None returned economic values of Au, Ag, Cu, or Zn and it is judged that the likelihood of larger deposits existing at the near surface in these areas is low. It is therefore considered that besides the development of the Kerry Road deposit, any future work should focus on the Gorm-loch na Beinne inlier.

The deep peat cover at the Gorm-loch na Beinne inlier makes any additional follow up sampling difficult. However on the basis of historic results of up to 4 g/ton, geologic and geophysical data, further work is warranted. The small scale of the area makes a modern geophysical survey a practical task that would give an indication of the possible location and orientation of any deposit. Deep overburden sampling would allow for the recovery of material from below cover of up to 5 m depth. The remote location of the inlier would require delivery of the machinery via quadbike or ATV and hence the support of the estate. The rig is then portable over the several hundred metre distance from the end of the vehicle track at Poca Buidhe. A series of closely spaced lines at c 20 m with sampling every 10 m would result in c. 120 samples over 1200 m of line (Fig. 5.1). Lithological examination of samples would allow for coarse mapping of lithologies below the cover and in combination with geophysics create a far greater understanding of the structure of the inlier than that currently based on fairly limited float sampling. The sampling would take three or four days dependent on ground conditions, additional time for transport of machinery would mean the sampling could be completed inside a working week in ideal conditions.

Additional geochemical sampling may help to constrain comparisons between the inlier and the Kerry Road deposit. The best exposed units at the Gorm-loch na Beinne inlier are amphibolites that make up the hillock and two low ridges to the north and south of the central peat gully. Analysis of the amphibole chemistry in these rocks may be a useful proxy and guide to the potential scale of mineralisation present. Systematic variation in amphibole chemistry within host amphibolites from Mg and Si limited ferrotschermakite to Mg and and Si rich actinolite has been recorded with decreasing distance to the Kerry Road VMS deposit (Drummond et al, 2020). This is believed to represent the primary alteration to host rock chemistry by the fluids responsible for the formation of the deposit. During metamorphism these chemical gradients controlled the resulting amphibole chemistry, and so may be used as a vector towards mineralisation.

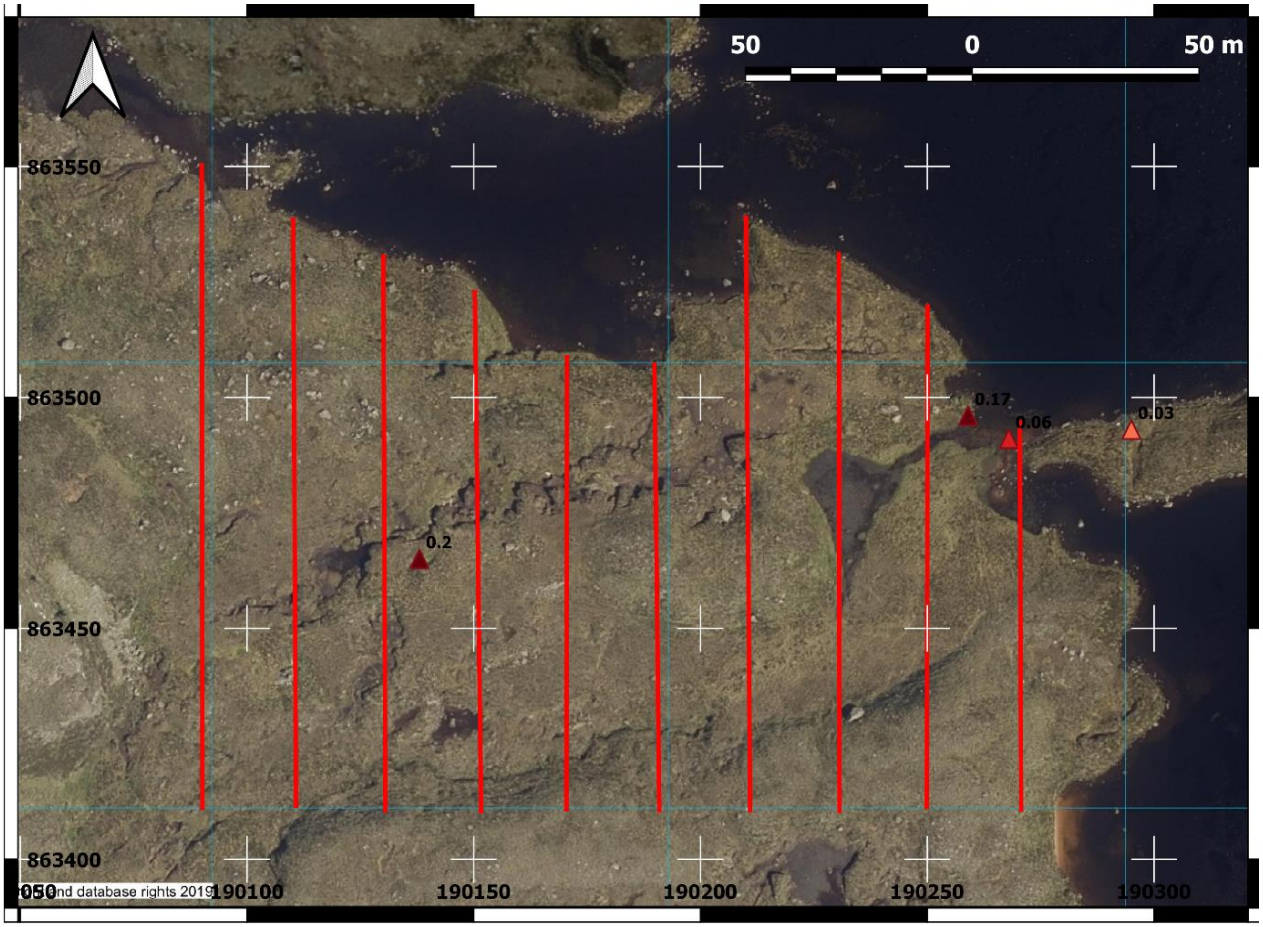

Figure 5.1. Schematic map showing how the area of poor exposure within the Gorm-loch na Beinne inlier could be covered with 20 m spaced deep overburden sampling lines. Samples from this study recording anomalous gold values also shown.

5.1.2 – Conclusions

1) Mineralisation within the GSB likely formed as the result of several spatially and temporally separate systems and reflects a variety of formation processes that were dominantly syngenetic with only minor epigenetic occurrences. The significant tectonic disruption and possible assembly of the GSB from distinct oceanic plateau, volcanic arc, and near continental sedimentary sources, means any correlation across boundaries within the belt is potentially impossible.

2) The majority of sampled mineralisation is pre-metamorphic as evidenced by varying degrees of sulphide remobilisation. Remobilisation occurs in Sp, Ccp, and Po, but not Py which retains a generally euhedral crystal shape. This indicates the maximum thermal conditions of metamorphism were not enough to cross the brittle ductile boundary for pyrite and as such have not exceeded lower amphibolite facies (Marshall and Gilligan, 1987). This is in broad agreement with the estimates of metamorphic conditions for the late-Laxfordian within the LMG obtained by other methods.

3) The Sidean Mor gossan and float samples potentially sourced from this horizon likely records the exhalative and distal zones of a hydrothermal system that *may* increase in grade within more proximal deposits. However the widespread nature of this deposit within both the GSB and LMSB suggests that any original feeder zones and related higher-grade proximal deposits may have been significant distances from current exposures. As such they are likely to be considerably above or below current exposure levels or have been tectonically removed during Laxfordian thrusting.

4) The Gorm-loch na Beinne inlier is the only sampled locality, in addition to the Kerry Road deposit, within the GSB to record significant levels of Au mineralisation. The site likely occupies a similar stratigraphic position to Kerry Road. However significant differences occur between the two sites in precious and base metal mineralisation and host rock lithology.

5.2 – Loch Na Cabhaig Mafic/Ultramafic Rocks

5.2.1 – Mafic inlier

A key to understanding the origins of the nearby ultramafic rocks is ascertaining their relationship to the LGC and LMG. The amphibolite (M9) to the south of Loch na Cabhaig is the closest non-Torridonian outcrop. It is therefore compared to a range of possible candidates: the Scourie Dykes (or other dyke suites), LMG amphibolites, and mafic portions of layered mafic/ultramafic intrusions. Its mineralogy and texture are poor separators as examples of all could resemble M9, at outcrop and thin section, in being a strongly foliated amphibolite. This penetrative foliation is uncommon within mafic/ultramafic complexes found elsewhere within the LGC that are commonly massive. The ultramafic rocks at Loch na Cabhaig are generally massive to occasionally weakly foliated, however the amphibolite of M9 displays a very prominent foliation. This foliation is a more common feature in LMG amphibolites or Scourie Dykes that experienced significant strain during the Laxfordian. The field relationships of both inliers to one another, the LGC, and the LMG are obscured by Torridonian cover. The two closest exposures of known origin are the Gorm-loch na Beinne inlier of the GSB c. 700 m to the NE of the ultramafic rocks, and an outcrop of felsic gneiss, likely Lewisian, c. 800 m to the SE of the amphibolite (M9). Somewhere within the c. 2.5 km between these rocks of known affinity must lie the southern margin of the GSB and the boundary with the Lewisian gneisses. However the position of this boundary is not known and the relationship of either inlier to it is unclear.

The outcrop pattern of M9 may suggest difficulty in correlation with the Scourie Dykes. The amphibolite is observed in outcrop over a width of c. 200 m. If it represents a portion of a Scourie Dyke it is significantly above the thickness they reach without apparent width increases. When the geochemistry of M9 is compared to the Scourie Dyke data of Weaver and Tarney, (1981) and Mason and Brewer, (2004) there are major differences. The Nb/Th ratio is significantly different with the Scourie Dykes of Weaver and Tarney, (1981) displaying an average ratio of 2.4 and a range of 1.7 – 3, while M9 has a Nb/Th ratio of 30. This is due to the order of magnitude lower Th values in this sample (0.1 ppm) compared to the average dyke (3.4 ppm). In figure 5.2, M9 plots outside the field of dykes from Weaver

and Tarney (1981) on all discrimination diagrams. The samples geochemistry generally suggests a less evolved melt or a more depleted mantle source.

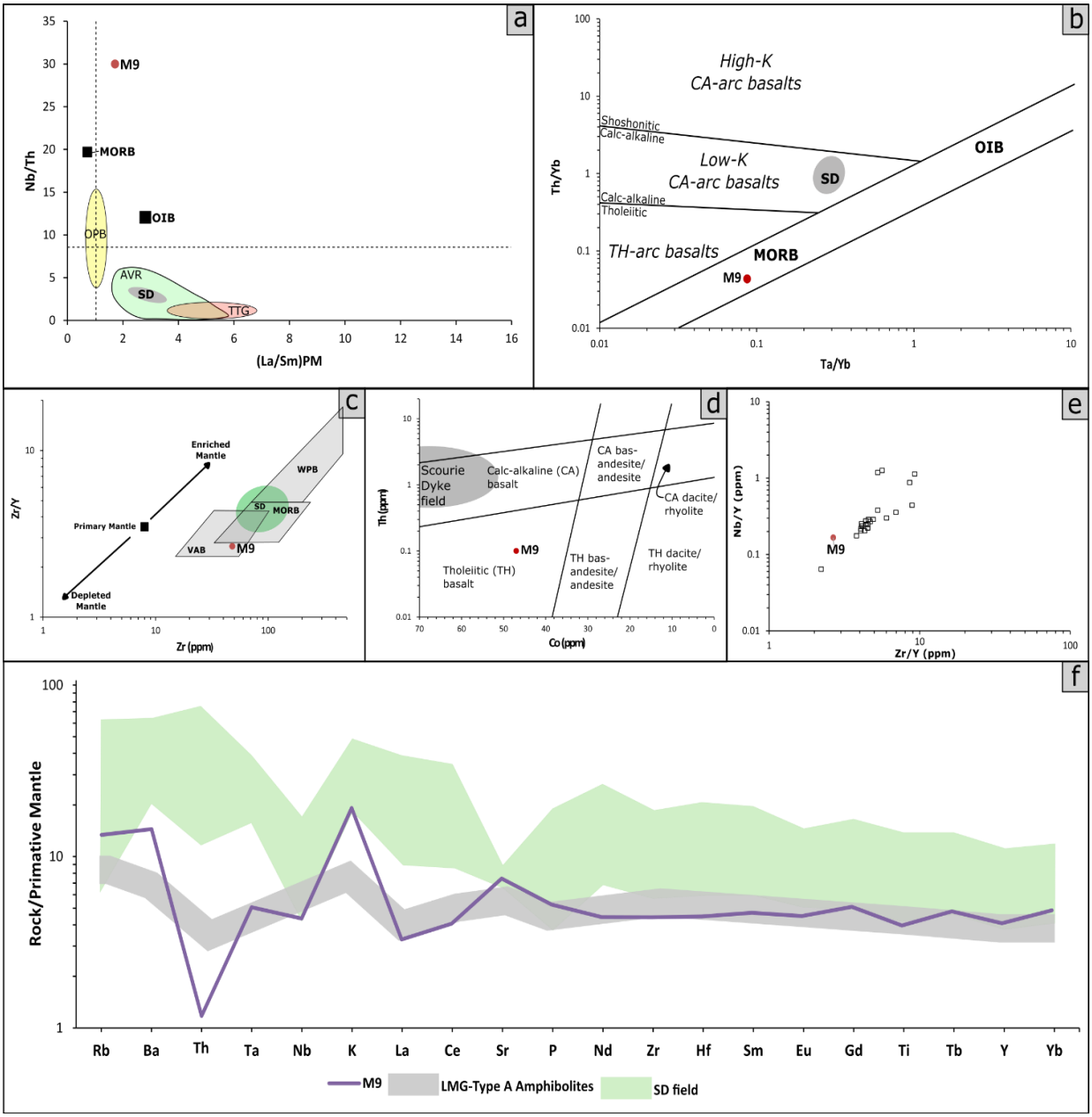

Figure 5.2 Plots showing geochemical analysis of sample M9 compared to a range of other LGC lithologies**. a)** (La/Sm)PM - Nb/Th - Dashed lines indicate primitive mantle values (McDonough and Sun, 1995) OPB, AVR, and TTG fields from (Polat and Kerrich, 2000). **b)** Ta/Yb – Th/Yb diagram after (Pearce, 1982) **c)** Zr – Zr/Y diagram after Pearce and Norry (1979). **d)** Co – Th diagram after Hastie et al., (2007) **e)** Zr/Y – Nb/Y diagram with Scourie Dykes from Mason and Brewer (2004). **f)** Mulit-element plot showing M9 with the fields of the Scourie Dykes and Type-A LMG amphibolites (Park, 2002). Scourie Dyke fields in all diagrams except e) from Weaver and Tarney (1981). MORB - Mid-ocean ridge basalt, OIB – Oceanic island basalt, OPB – Oceanic plateau basalt, AVR – Arc volcanic rocks, TTG – Tonalite-trondhjemite-granodiorite, VAB – Volcanic arc basalt, WPB – Within plate basalt.

M9 has a negative MORB-like REE profile with a normalised La/Lu value of 0.6, although it is comparatively enriched in LREE compared to a true MORB. This is similar to the LMG-Type-A amphibolites that show flat REE profiles with chondrite normalised values of c. 10, and near flat multi-element primitive mantle profiles. Park, (2002) concludes these amphibolites are of basaltic igneous origin due to their MORB geochemical signatures and intercalation with marine sediments. Their REE profiles do not display the characteristic LREE depletion associated with true MORBs and as such resemble ocean plateau basalts (Kerr et al., 1998). The REE profile of M9 closely resembles that of these Type-A amphibolites of the LMG. The multi-element plot (Fig. 5.2f) shows M9 plotting slightly below the Scourie Dykes of the central and southern regions that are geochemically similar to one another and display a continental basaltic trend with enrichment in LREE (Park, 2002). Compared to the dykes, M9 is LREE depleted, but displays similar HREE values to the dykes of all regions as well as the Type-A amphibolites of the LMG. M9 displays a positive Sr anomaly that is not present in any of the Scourie dyke samples of Weaver and Tarney, (1981), Park, (2002), or Mason and Brewer, (2004) from the northern, central or southern regions that all display negative Sr anomalies. A smaller positive Sr anomaly is present in the type-A amphibolites. These amphibolites also display a negative Th anomaly (Park, 2002) again smaller than but similar to that in M9. As such it is concluded that the amphibolite sampled by M9 is unlikely to represent a Scourie Dyke.

Comparison with mafic portions of mafic/ultramafic layered intrusions into the LMG is the third option for consideration for M9. They appear mineralogically different, with the amphibole, plagioclase, and minor quartz assemblage of M9 distinct from the amphibole, garnet, plagioclase, pyroxene assemblage of Ben Strome and similar complexes (Guice, 2019). The significant tectonisation and hydration that have occurred may have replaced this original mineralogy, however it would have had to have been near total and leave no evidence of the previous gabbroic texture/mineralogy. The position near to the southern boundary of the GSZ may have resulted in sufficient strain and hydration to accomplish this, and large areas of mafic rocks with no interleaved ultramafic are reported from other complexes within the Lewisian (Guice, 2019; Guice et al., 2020). The geochemistry of M9 does not rule out correlation with the ultramafic rocks as part of a larger ultramafic/mafic complex. The Ben Strome Complex mafic rocks show gently positive to gently negative REE patterns with chondrite normalised values between 4 and 62 compared to the M9 values of 9 to 16. However based on comparison with the three possible corelates it is, speculatively, proposed that M9 represents part of the amphibolites of the LMG.

5.2.3 – Ultramafic Inlier

The ultramafic rocks at Loch an Cabhaig have experienced total metasomatic alteration. No evidence of any original primary igneous mineralogy was observed in thin section or detected via XRD. This makes any interpretation of these rocks fraught with difficulty as the large volumes of fluid flushed through these rocks is likely to have affected their geochemistry.

The mineral assemblage of the Loch na Cabhaig inlier as determined by XRD and optical examination of thin sections is within that expected of a highly altered and hydrated ultramafic protolith. The sequence of magnesite, anthophyllite, chrysotile, dolomite, lizardite, talc, tremolite, magnetite, and clays suggests this alteration occurred in an environment containing a mixed H_2O/CO_2 fluid phase. It may also suggest two phases of alteration as a range of P-T conditions are recorded from low temperature hydrous lizardite, to higher P-T favouring anthophyllite. It is unclear in what order this alteration took place. Serpentinite minerals may be the remnants of an early low temperature alteration now largely replaced by a later prograde talc + magnesite + tremolite + anthophyllite assemblage. This potentially early serpentinisation comprises the replacement of original igneous mineralogy by serpentinite group minerals and the associated production of magnetite. Serpentine group minerals include the low temperature, below middle greenschist facies, chrysotile and lizardite, and the higher temperature and less hydrous antigorite. The prograde metamorphism of serpentinised rocks involves the breakdown of these phases to be replaced, during purely isochemical metamorphism, by an assemblage comprising tremolite, talc, and anthophyllite (Frost and Frost, 2019). Talc formation in isochemical or fluid free systems occurs at temperatures associated with upper amphibolite facies, higher than the commonly found greenschist facies alteration of ultramafic rocks to talc + magnesite bearing soapstones. The temperature of talc formation is lowered to upper greenschist facies by the presence of a CO_2 bearing phase. In the presence of this phase the assemblage talc + magnesite + dolomite becomes common (Frost and Frost, 2019). The large volumes of fluid involved in these reactions can have significant effects on the overall chemistry, most commonly seen in the formation of carbonate minerals and the increase in silica required for extensive talc formation.

This total alteration and overprinting of any primary igneous mineralogy at Loch na Cabhaig makes interpretation difficult. Their position near to the likely southern boundary of the GSZ will have been a focus for major fluid migration during the Laxfordian and Grenvillian events (Sherlock et al., 2008).

The major element Mg/Si and Al/Si ratios for all samples plot near or to the left of primitive mantle values (Fig. 5.3). The abyssal peridotites field to the left of the primitive mantle value represents increasing extraction of melt with the lowest Al/Si ratios in the most depleted rocks. This mantle depletion trend is curved, with higher Mg/Si ratios at lower Al/Si ratios likely representing the exhaustion of cpx and then opx during melting of peridotite (Wasylenki et al., 2003). Samples M4 and M8 plot near this mantle depletion trend, with M8 very close to the primitive mantle value and M4 in the abyssal peridotite field. M3 falls below these fields due to its reduced Mg%. Archean ultramafic rocks have the potential to be komatiitic in origin, and the fields of both low-Al (Parman et al., 2004) and high-Al (Rollinson, 1999) komatiiites has been plotted on Figure 5.3. Samples M8 and M3 plot outside but near to the low-Al komatiites field, although it is considered highly unlikely that these samples have a komatiitic origin. Yb v Ce/Sm values (Fig. 5.3) normalised to primitive mantle values for sample M8 plots in the orogenic peridotite and close to the sub-arc and abyssal peridotite fields of Rollinson, (2007). Samples M3 and M4 had Ce or Sm values below detection level and so can only be plotted as lying to the left of their indicated Yb_N line.

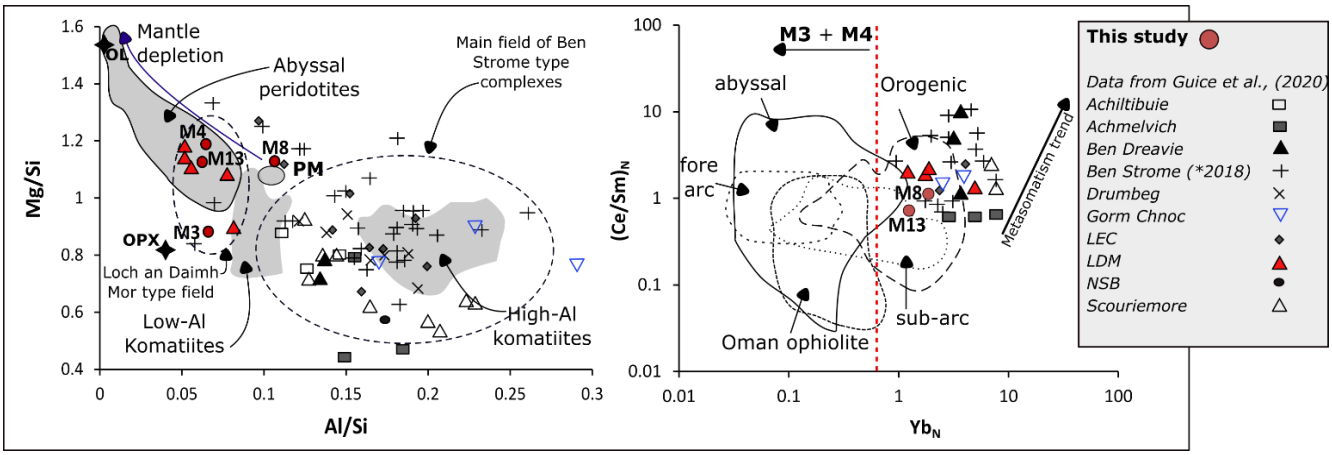

Figure 5.3. Al/Si v. Mg/Si and Yb_N v. $(Ce/Sm)_N$ for ultramafic samples analyised in this study. Data for other LGC mafic/utramafic complexes and classification of complex types from Guice et., (2018; 2020). Fields for peridotite type from Rollinson, (2007). Komatiite fields from Parman et al., (2004) and Rollinson, (1999). Primitive mantle (PM) values from McDonough and Sun, (1995).

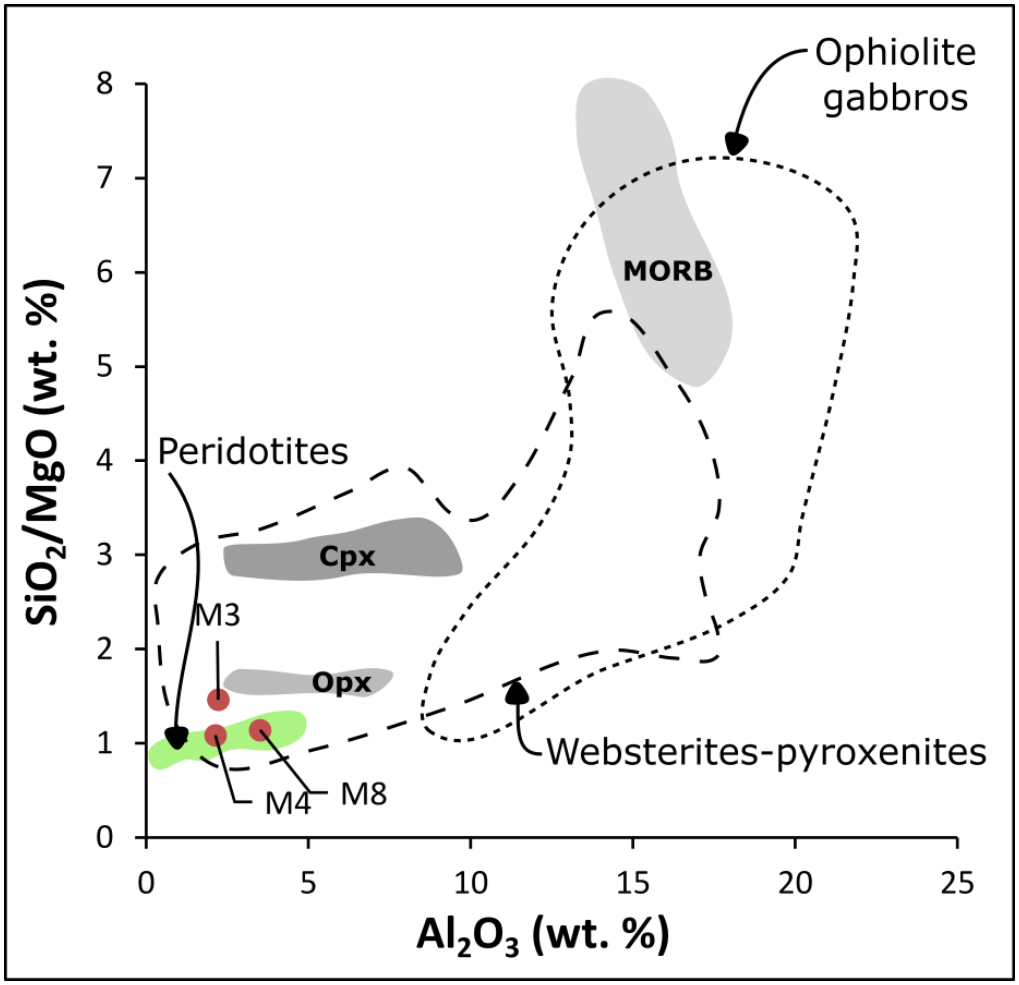

Figure 5.4 Al v Si/Mg oxide plot for ultramafic samples. Samples plot in the peridotite field.

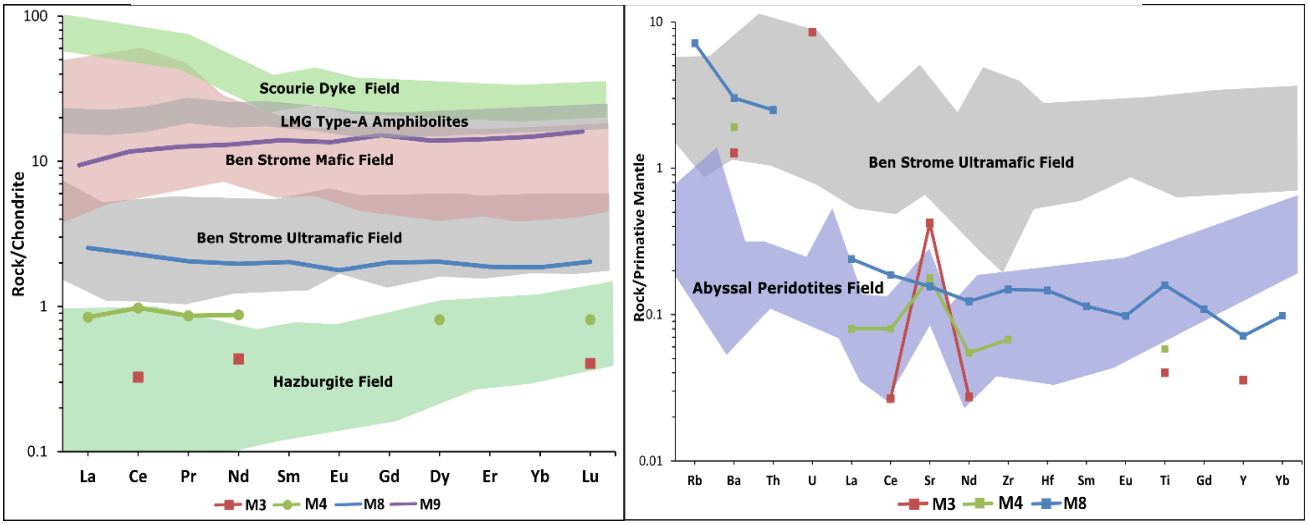

Figure 5.5. REE chondrite normalised and multi-element primitive mantle normalised plots for the Loch na Cabhaig ultramafic and mafic rocks. Where elements were below the detection levels they have been omitted. Fields for Ben Strome mafic and ultramafic rocks and abyssal peridotites from Guice et al., (2020). Harzburgite field from Bodinier and Godard, (2003). Chondrite and primitive mantle normalising values from McDonough and Sun (1995)

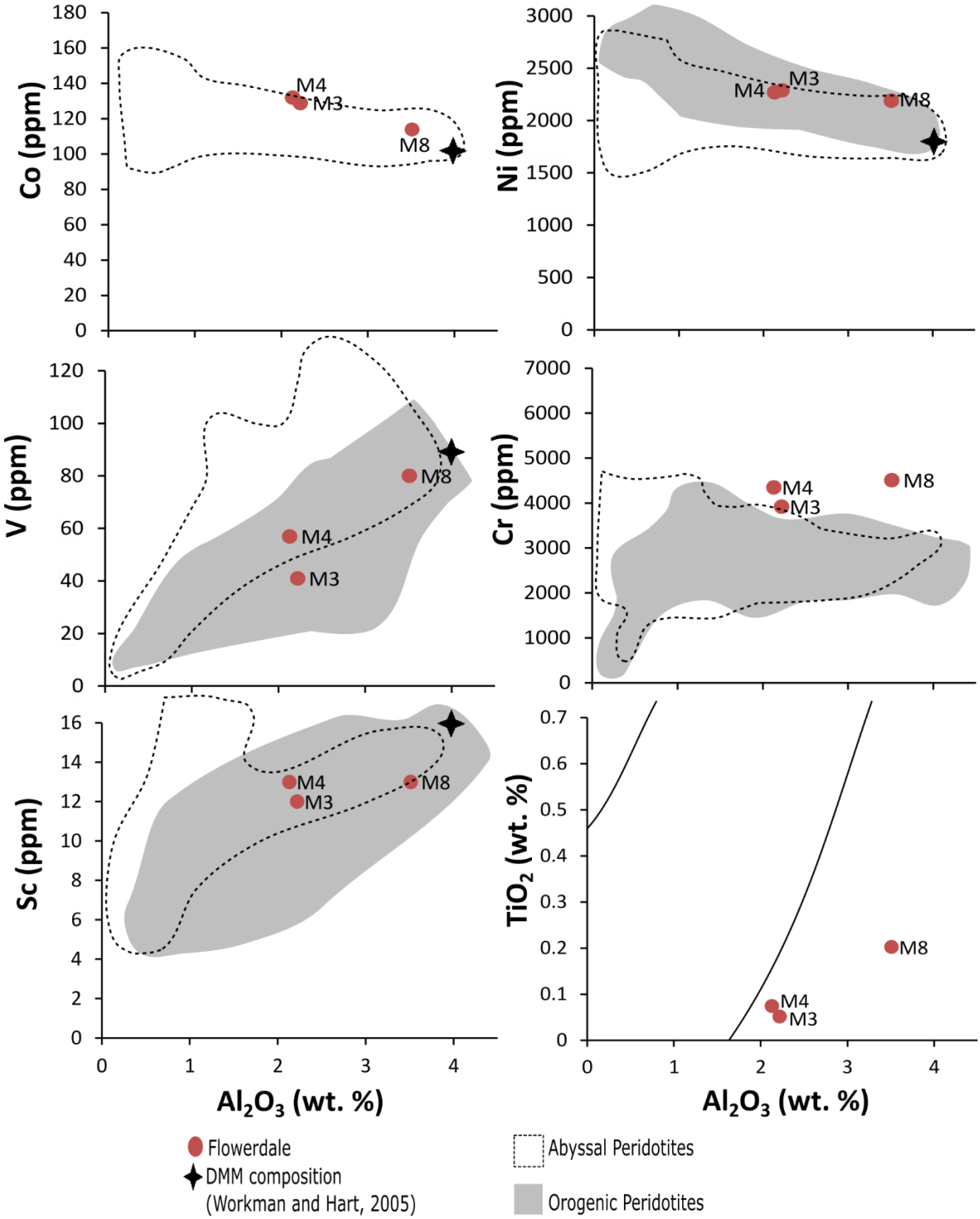

Figure 5.6. Aluminium oxide v. trace element plot for ultramafic samples. Fields for abyssal and orogenic peridotites shown.

All three ultramafic samples display flat to gently sloping REE profiles with chondrite normalised La/Lu values of 1.0 – 1.2 where data are available. This differs from the Loch an Daimh Mor rocks that show enriched LREE and depleted HREE profiles. This may be a primary difference in protolith chemistry or may reflect LREE mobility during hydrothermal alteration. M8 plots within the Ben Strome ultramafic field of Guice et al., (2020). Samples M3 and M4 are heavily depleted in both LREE and HREE with many elements falling below the detection levels of the analysis. Where values are plotted for samples M3 and M4 they fall into the harzburgite field of Bodinier and Godard, (2003). Primitive mantle normalised multi-element plots show enrichment in some incompatible trace elements (Rb, Ba, Th, U) in all three samples. This is potentially due to metasomatic processes with these elements sourced from the surrounding rocks. Other than the previously mentioned elements, the samples plot near or in the abyssal peridotite field (Guice et al., 2020). All three samples plot primarily below the field for the Ben Strome Complex ultramafic rocks on multi-element diagrams.

The tectonic position of the inlier is unclear as Torridonian cover conceals the boundary between the Lewisian Gneisses and the LMG in Flowerdale. If the correlation of the Gorm-Loch na Beinne and An Lungard inliers with the Kerry Road and Aundrary Amphibolite are correct, then the potential for the Loch na Cabhaig inlier to lie within the LMG exists as the distance from the An Lungard inlier to Loch na Cabhaig is less than the width of the GSB at Gairloch. This would imply a Paleoproterozoic rather than Archean age to the ultramafic rocks. The nearby amphibolite M9 displays textural and mineralogical characteristics that are not discriminatory between an origin as a LMG amphibolite, or within the LGC as either a pre-Laxfordian dyke or a larger mafic intrusion linked to the ultramafic rocks. It is therefore only on the basis of its geochemistry that any discrimination can be made. Its negatively sloping REE profile, negative Th and positive Sr anomalies, generally LREE depleted MORB-like geochemistry, along with strong foliation and similarity at outcrop, suggest that a correlation with the LMG type-A amphibolites of Park et al., (2001) is the more likely of the possibilities. This potential correlation of the amphibolite with the Mill na Claise amphibolite that outcrops along the southern boundary of the GSB would place the ultramafic rocks of the Loch na Cabhaig inlier within the GSB. The subduction-accretion model for the origin of the LMG includes the possibility of tectonic intercalation of abyssal peridotites or sub-arc cumulates into the sequence of oceanic plateau basalts and marine sediments (Dilek and Flower, 2004; Greene et al., 2003; Jagoutz and Schmidt, 2011; Kerr et al., 1996). This would be the first reported occurrence of ultramafic rocks from the LMG,

although ultramafic pods occur in the Paleoproterozoic Langavat Belt of Harris (Mason et al., 2004; Mason and Brewer, 2005) that likely forms part of the same subduction-accretion complex (Park, 2010)

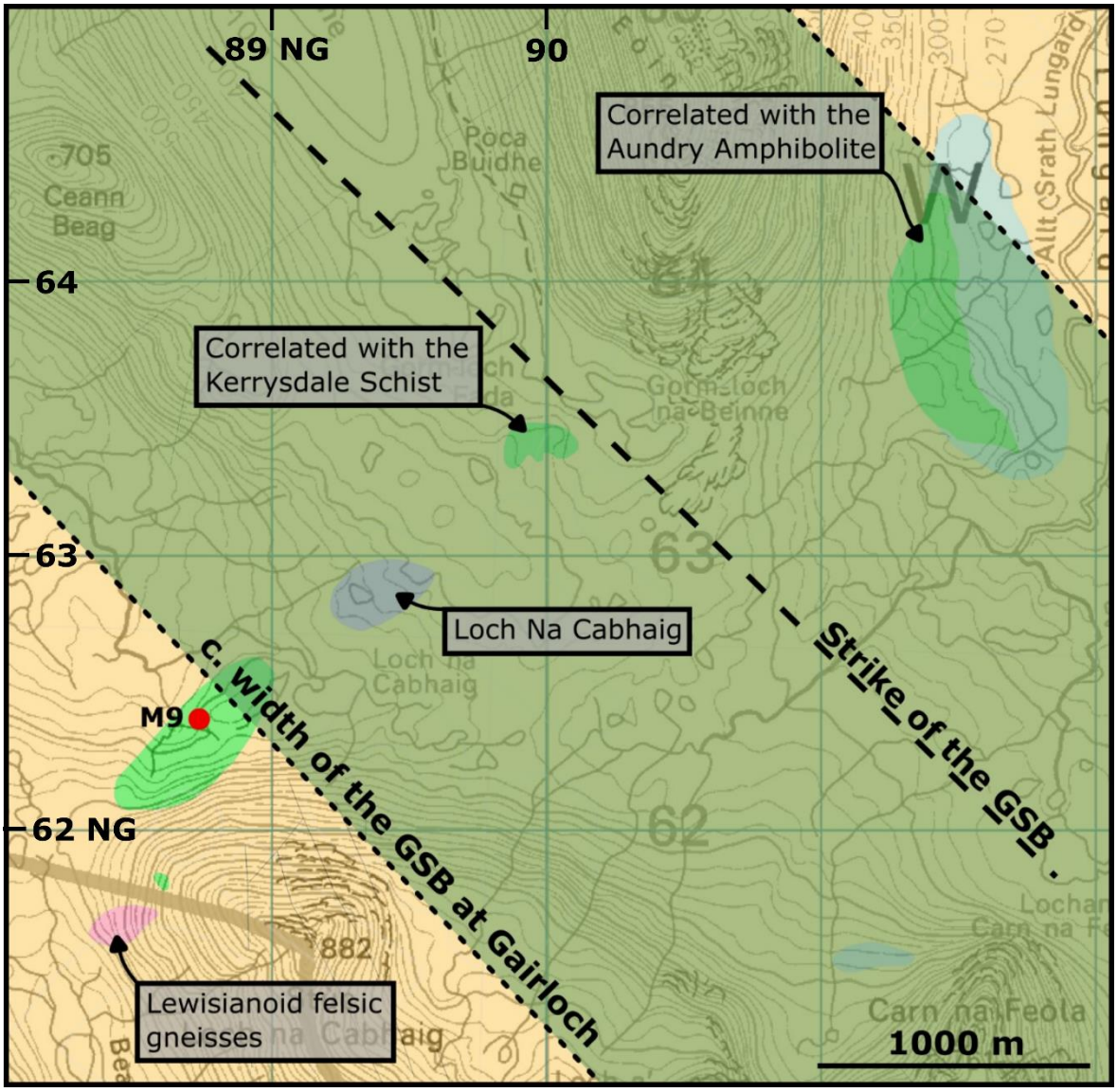

Figure 5.7. Sketch map showing the Flowerdale inliers, their tentative corelations with the GSB from Coats et al., (1997) along with the approximate strike and strike perpendicular width of the belt as seen at Gairloch. This places the Loch na Cabhaig and M9 inliers near the potential edge of the belt and conceivably within either the basement gneisses or the GSB.

If the inlier lies within basement Lewisian rocks, two correlative possibilities exist. It could represent a highly altered layered intrusive complex similar to the Ben Strome type (Guice et al., 2020) found at multiple locations throughout the LGC. However several lines of evidence argue against this as a likely option. There is a distinct lack of layering throughout the inlier, with possible layering only present at one small outcrop that may be a feature of alteration, exposure, or deformation. The Al and Mg/Si ratios of the rocks are also significantly different from those of all Ben Strome type intrusions, although caveats should

be attached to these data due to the mobility of major elements, including Al at deep crustal levels (Manning et al., 2012). Less mobile elements suggest a similar relationship and together with the more heavily depleted REE and trace element profiles provide enough evidence to suggest that correlation with Ben Strome type layered intrusive complexes is a less likely option.

If the potential for correlation with the Ben Strome type complexes is considered unlikely, it is possible to compare the inlier to the Loch an Daimh Mor complex. All three samples show similar geochemical analyses to the Loch an Daimh Mor rocks of Guice et al., (2020) and plot in or near the abyssal peridotite fields. This body is significantly different from the Ben Strome type complexes interpreted as intrusive into the LGC. Using geochemical data and field evidence Guice et al., (2020) argue for a pre-TTG emplacement age for the complex and that it represents the strongest candidate within the LGC for a fragment of Archean mantle. Even with the significant caveats attached to the geochemical evidence for both localities, correlation with the Loch an Daimh complex is considered more likely than to the Ben Strome type based on Al/Si ratios, depleted REE and incompatible element profiles. If this is the case, it would be only the second occurrence of this type recorded within the LGC. An interpretation as a fragment of mantle material is compatible with the alternate position within the LMG. In this scenario it represents a fragment of Paleoproterozoic oceanic crust intercalated within the supracrustal sequence during the Laxfordian. Either tectonic interpretation would suggest these rocks are of significant importance within the Hebridean Terrane and worthy of further study.

5.2.3 - Conclusions

1) The Loch na Cabhaig inlier consists of a suite of highly altered and hydrated rocks displaying a range of serpentinite and hydrous alteration products of originally peridotitic ultramafic origin.

2) These rocks are depleted in REE, comparatively low in Fe2O3 and Al2O3, high in MgO, and generally massive. In these aspects they resemble ophiolitic hazburgites, abyssal peridotites, and residual mantle rocks.

3) The mafic inlier to the south-west of Loch na Cabhaig is considered to geochemically resemble the type-A amphibolites of the Loch Maree Group, and therefore may place the southern boundary of the Gairloch Schist Belt to the south-west of this locality.

4) This structural interpretation would place the Loch na Cabhaig ultramafic rocks within the Gairloch Schist Belt. As such they may represent the sub-arc to mantle portion of the arc to oceanic plateau assemblage represented by the rest of the LMG.

5) Alternately the ultramafic rocks are comparable with the Loch an Daimh Mor locality, considered to represent the best candidate within the Hebridean terrane for a fragment of pre-TTG emplacement Archean mantle.

5.3 - The Gruinard Belt

5.3.1 - Discussion

The results from the Gruinard Belt quartzite, a late-Laxfordian age and Caledonian Pb-loss, are novel and unexpected with respect to the rest of the foreland LGC. The dominance of late-Laxfordian ages, c. 1800 – 1650 Ma, suggests either an overwhelmingly dominant Paleoproterozoic source for detrital zircons, or near total metamorphic zircon growth and/or resetting (Carson et al., 2002) during the Laxfordian. Three discordant grains recording likely Archean ages and are the only evidence of potential detrital input from the LGC. The c. 1750 Ma age of the oldest non-Archean cores is c. 100 Ma younger than the next youngest metasedimentary unit presently dated within the LGC, the c. 1.87 Ga Leverburgh metasediments (Whitehouse et al., 1997).

Without cathodoluminescent imaging of zircon grains, an important area for future work, it is hard to attribute zircon core or rim analyses to detrital or metamorphic events. As such the possibility that almost all zircon is metamorphic or has suffered total resetting is considered possible. If only the three Archean analyses are of truly detrital zircon then all other analyses may represent zircon growth and resetting of the U-Pb system associated with the late-Laxfordian, perhaps catalysed by major fluid flow along the zone of shear that the Gruinard Belt lies within. The spread of zircon ages with respect to the dating of the late-Laxfordian in the southern mainland LGC is closely matched, with metamorphism dated at between c. 1740 and 1670 Ma (Love et al., 2010 and references therein). This interpretation would require only three detrital zircons, from a separated population of 49, to have survived resetting and alone been separated from over 4 kg of crushed quartzite. Furthermore no early-Laxfordian ages are recorded, this would require that metamorphic growth or resetting of Archean zircon was associated exclusively with the later event. Additionally no other locality known to have experienced late-Laxfordian deformation in the LGC had its U-Pb system completely reset by the amphibolite facies event.

If it is assumed that at least some of the Paleoproterozoic zircons are detrital and have not been fully reset, then a maximum depositional age of c. 1700 Ma can be assigned to the Belt. For this model a major source of c. 1700 - 1800 Ma zircons is required. Within the mainland Lewisian, late-Laxfordian felsic intrusions are generally small scale pegmatitic or granitic intrusive sheets. These are dated at c. 1790 - 1770 Ma for granites near and within the

Laxford Shear Zone (Goodenough et al., 2013), and c. 1695 Ma for pegmatites within the Gairloch block (Park et al., 2001). The Outer Hebrides contains c. 1675 – 1655 Ma granite pegmatites within the Langavat Belt (Mason, 2012) along with the larger scale Harris Injection Complex emplaced at c. 1705 – 1655 Ma (Friend and Kinny, 2001). However none of these are a singular candidate and good match for the dominant c. 1770 – 1690 Ma age recorded within the Gruinard Belt and all lack the scale required to provide a dominant source of Paleoproterozoic material while masking the Archean signature of Lewisian gneisses they are emplaced into.

A more promising source may be found when considering the driver of the late-Laxfordian event. It is generally considered that the early-Laxfordian represents the development of an active continental margin and the accretion of arc material, at c. 1.91 Ga to 1.85 Ga, now represented by the LMG, Langavat, and Leverburgh Belts (Mason, 2016). A c. 100 Ma hiatus in metamorphism is then followed by the late-Laxfordian, an event likely triggered by the accretion of the Malin block, juvenile Paleoproterozoic crust to the SW of the Lewisian, at c. 1.75 to 1.65 Ga. The Malin block is postulated to form much of the basement south of the Great Glen (Park, 2005), however it is presently poorly exposed in only a few small inliers within the Caledonides of Scotland and Ireland. The Rhinns Complex, an association of meta-igneous gneisses exposed on the islands of Islay and Colansay, records an arc-like geochemical signature and a c. 1.8 Ga emplacement age (Muir et al., 1994). The Irish Annagh Gneiss Complex comprises Paleoproterozoic crust dated to c. 1755 Ma (Daly, 1996). The Inishtrahull gneiss, Donegal, records a very well constrained emplacement age of 1779 ± 3 Ma (Daly et al., 1991) and a metamorphic age of c. 1710 Ma obtained from $^{39}Ar/^{40}Ar$ dating in amphibole (Roddick and Max, 1983). The offshore Rockall and Hatton Highs comprise a juvenile Paleoproterozoic terrane with an age of c. 1750 Ma (Morton et al., 2014) and a very strong unimodal age signature including no primary or inherited Archean zircon. The continuity of these offshore locations with the onshore expression of the Malin block is unclear, but they likely all form part of the extensive Labradorian - Gothian Belts that lay along the active southern margin of Laurentia-Baltica between c. 1.8 and 1.6 Ga (Park, 1995).

Sediment shed from these Paleoproterozoic blocks during collision with the LGC would have an appropriate age signature to match that within the Gruinard Belt and the potential to be quickly buried syn-orogenically during late-Laxforidan thrusting. The three Archean grains may suggest a very minor component derived from the LGC. The location of the suture between the Malin block and the LGC lies some way to the south of the Gruinard Belt

and has been extensively modified, displaced, or erased by later Grenvillian and Caledonian tectonism and faulting e.g. the significant sinistral displacement along the Great Glen Fault between the southernmost outcrop of the LGC and the northernmost outcrop of the Malin block. If this model is assumed to be true, then both core and rim populations at between c. 1760 – 1700 Ma may represent detrital populations derived from this juvenile Paleoproterozoic source. Burial and metamorphism within the Lewisian may then be recorded by the younger c. 1680 – 1670 Ma core grouping. Although highly speculative due to the error range of the data, this age matches the titanite ages of c. 1670 Ma interpreted to date amphibolite facies metamorphism within the Rona and Gruinard blocks (Love et al., 2010). It should additionally be noted that these late-Laxfordian ages are remarkably similar to those recently recorded from the Loch Shin inlier by Strachan et al., (2020). Here two meta-igneous lithologies give crystallisation ages of 1711 ± 19 Ma and c. 1655 Ma, while a meta-sedimentary schist gave a maximum depositional age of 1802 ± 51 Ma. Strachan et al., (2020) suggests these anonymously young ages indicate the basement to the NHT is Baltic in origin and was sutured to the Lewisian during the Grenvillian. It is however possible that they represent late-Laxfordian aged intrusions and sedimentary material related to the collision with the Malin block, now that similar material may be recognised as present within the foreland Lewisian.

Either model likely precludes correlation of the belt with the LMG due to either the c. 200 Ma younger depositional age, the absence of evidence for early-Laxfordian metamorphism, no evidence of the c. 2200 – 2000 Ma detrital component present within LMG metasediments, or total resetting of the U-Pb system indicative of a higher metamorphic grade than that achieved anywhere in the LMG. Previous correlation has been based primarily on proximity and similarity in strike of the belt to the two major outcrops of the LMG. However lithological differences are present between the two; true quartzites are very rare within the LMG and no evidence of the diverse range of schistose, exhalative, and mineralised lithologies present in both the GSB and LMSB is evident in the Gruinard Belt. If this potential correlation with the LMG (Park, 2001; 2005, Love et al., 2010) is discounted, then significant changes to the local structure of the Lewisian is possible. The LMSB does not need to extend above the present ground surface across the Carnmore antiform, and the upper/lower plate model for the Laxfordian of Park (2005) would need at least minor modification. The Gruinard belt may still represent a boundary between the generally granulite facies Assynt and Gruinard blocks, and dominantly amphibolite facies southern

region as Park, (2005) suggests, however this boundary would be a late-Laxfordian feature marked with a thin zone of detritus from that self-same event.

The second point of note about the U-Pb data from the Gruinard Belt is the prominent Caledonian discordia and associated zircon growth. As the sample lies to the west of the Moine Thrust, and within the 'foreland' to the Caledonian, this requires explanation. Other authors have reported significant Paleozoic Pb-loss from samples within the LGC of the foreland. Corfu et al., (1994) report "*many ages that have been disturbed by younger cryptic events*" and suggest this is the result of "*local low-grade processes*" comparable to that observed "*in basement units overthrust by Caledonian nappes in southern Norway*". Corfu et al., (1998) find "*post-Laxfordian Pb-loss*" in titanites from Gruinard Bay. Two samples from Love et al., (2004), GL01-08 from Inverkirkaig and GL01-10 from Loch an Daimh, display recent Pb-loss with poorly defined lower intercepts at c. 500 and 300 Ma. Two samples from Love et al., (2010) collected from Diabaig show 'Caledonian' discordia that are described as "*marked recent Pb-loss*" by the authors. Sample GL00/03 records a lower intercept of 462 ± 17 Ma and well defined discordia while sample GL00/04 records a lower intercept of 478 ± 11 Ma along a poorly defined discordia. Whitehouse et al., (1997) report a lower intercept of 427 ± 24 Ma in a Paleoproterozoic diorite from the Butt of Lewis. Fischer et al., (2021) identify a number of Paleozoic discordia in their data that they choose to anchor at a Grampian (470 Ma) age.

It should be noted that none of these studies report Paleozoic core or rim growth associated with these lower intercepts and Pb-loss events. To what extent individual data points may have been discounted as contamination or simply irrelevant to the mainly Archean focus of the work is not clear. In the Gruinard Belt, the age of this Pb-loss and zircon growth appear to be Grampian rather than Scandian. This is evidenced by the rim growth occurring at 460 ± 10 Ma and the discordia of all analyses give a lower intercept of 450 ± 28 Ma, although the comparatively more discordant core analyses give younger ages of 442 ± 30 Ma and 424 ± 24 Ma and a lower intercept of 417 ± 94 Ma. A Grampian age would predate movement on the Moine thrust, dated to c. 430 Ma (Goodenough et al., 2011) and the Outer Isles Thrust, c. 430 Ma (Kelley et al., 1994). The Outer Isles Thrust is perhaps the most promising structure for allowing Caledonian fluids to infiltrate the Lewisian from below, potentially then focused along pre-existing zones of weakness such as the Gruinard Front. If significant Caledonian fluid circulation occurred along this zone of weakness it may have caused Pb-loss and zircon growth. This model of 'modern' fluid driven alteration of the U-Pb system

within the Lewisian is supported by large scale Mesozoic Pb-loss within offshore samples of Holdsworth et al., (2018) that they subscribe to "*thermal events associated with Phanerozoic basin development*".

To test the veracity of either proposed model; total metamorphic zircon growth within an Archean protolith, or a late-Laxfordian depositional age, significant future work is envisioned. Cathodoluminescence imaging of zircon would allow textural analysis that may discriminate between detrital and metamorphic origins. Detailed mapping of the belt would constrain the relationship between the belt and the surrounding gneisses, some authors suggest that "Scourie Dykes" cut the belt and so assign a pre-2400 Ma age (Crane, 1972) while others dismiss this while arguing for correlation with the c. 2000 Ma LMG. The separated garnet fraction may allow for Lu – Hf or Sm – Nd geochronology to be conducted that would shed further light on the Paleoproterozoic and Paleozoic history of the belt. Geochemical analysis of the amphibolites would permit comparisons with those of the LMG and LGC and potentially determine their tectonic setting.

5.3.2 - Conclusions

1) U-Pb data from extracted zircon from the Gruinard Belt are open to interpretation:

- **a.** A near total resetting of the U-Pb system, or growth of a population of near-entirely metamorphic zircon, during the late-Laxfordian with a potentially Archean depositional age evidenced by three discordant grains.

- **b.** A Paleoproterozoic depositional age with detrital zircons sourced dominantly from outside the LGC, perhaps the Paleoproterozoic Malin block, and metamorphosed during the late-Laxfordian soon after deposition.

2) The sample shows evidence of Grampian aged Pb-loss and zircon growth, perhaps related to the movement of Caledonian fluids along a pre-existing line of weakness.

3) Significant further work is required to better constrain the history and significance of the Gruinard Belt.

5.4 – Scardroy and Orrin inliers

5.4.1 – Orrin

5.4.1.1 – Discussion

The gneisses of the Orrin inlier display a tight cluster of U-Pb ages associated with zircon cores that strongly suggests an igneous protolith with an age of c. 2800 – 2850 Ma. A relatively small number (n=7) of cores range from c. 2850 to c. 3000 Ma and are considered to be inherited. This protolith age is typical of those found within many foreland Lewisian blocks (Kinny et al., 2005). The < 2900 Ma age suggests that correlation with the Assynt (2960 – 3030 Ma protolith) or Rona terranes (c. 3000 - 3125 Ma protolith) is unlikely, but most other foreland regions including the Gruinard, Gairloch, and Rhiconich blocks (c. 2825 Ma and c. 2680 – 2840 Ma respectively) display similar protolith ages in the range (Kinny and Friend, 1997; Love et al., 2004).

Early metamorphic events in the collected data are difficult to distinguish from primary magmatic ages due to the relative closeness of events and a general spread of ages due to later Pb loss. Evidence of a possible metamorphic event at c. 2700 Ma would closely match the major granulite facies event recorded in the Gruinard terrane and the Outer Hebrides, dated at c. 2730 Ma (Love et al., 2004, Kelly et al., 2008). Additionally, rim and core growth is associated with a c. 2470 Ma age that closely matches that of c. 2480 Ma "Inverian" retrogressive metamorphism related to the docking of the Assynt and Gruinard blocks (Love et al., 2010) or the c. 2490 Ma peak metamorphic age recorded within the Assynt terrane (Kinny et al., 2005; MacDonald et al., 2015). There is uncertainty associated with the c. 2700 Ma rims in the Orrin data as to whether it is a distinct event or instead a near concordant draw down of magmatic rims associated with the clearer c. 2470 event. As such it can only be stated with confidence that an early metamorphic event occurred, likely at c. 2470 Ma, with the potential for another earlier event at c. 2700 Ma within 100 Ma of the emplacement of the protolith. If indeed both c. 2700 Ma and c. 2470 Ma events are present within the Orrin inlier it would strongly suggest a direct correlation with the along strike Gruinard block of the foreland that records c. 2800 – 2860 Ma protolith ages with metamorphism at c. 2730 Ma, 2480 Ma, and c. 1750 Ma may be possible (Love et al., 2004).

Laxfordian aged metamorphism within the inlier is supported by concordant cores and rims at c. 1700 Ma as well as a clear discordia in pre-1900 Ma rims with a c. 1700 Ma intercept.

This c. 1700 – 1750 Ma event matches the 1750 – 1650 Ma second phase of the Laxfordian associated with regionally extensive amphibolite facies metamorphism of Mason (2015). Early Neoproterozoic metamorphism is evident both in concordant rims and a clear discordia in analysed cores with a c. 900 Ma lower intercept. There is no evidence of Grenvillian aged, c.1200 – 1000 Ma, events and instead the discordia and rims appear to suggest Renlandian aged, 950 – 910 Ma, rim growth and extensive Pb loss from Archean cores. Previous evidence of the Renlandian has been limited to granulite facies reworking of Archean gneisses and Proterozoic metasediments in Shetland (Jahn et al., 2017) and amphibolite metamorphism of the Moine rocks of the far north coast (Bird et al., 2018). Its occurrence in the zircon from Glen Orrin is therefore the most southerly record of this event in Scotland. The Orrin inlier lies within Glenfinnan group rocks deposited at c. 880 Ma (Cawood et al., 2004) that postdate the Renlandian (Bird, 2017). The relationship between the inlier and cover rocks is unclear and may be either a depositional unconformity or a faulted boundary. Only weak evidence of any post c. 900 Ma events is present in the form of Neoproterozoic rims. Whether this is related to Knoydartian or Caledonian events is unclear.

A commonly cited factor limiting the correlation of NHT inliers directly with the Lewisian has been the lack of intrusive igneous bodies that resemble either the Scourie dykes, or the later granitic sheets (Friend et al., 2008). In this regard the mafic body sampled by M12 is of interest. In addition to its mapped elongate and dyke like outcrop, it bears a geochemical similarity to the Scourie Dykes of the foreland LGC, plotting in or near the field of the Scourie Dykes on most discrimination diagrams (Fig 4.29). The foreland Scourie Dykes fall mainly into the basaltic field on a TAS plot with some overlap into the picrobasalt, trachybasalt, and basaltic andesite fields. Three suites of foreland dykes are recognised: numerically dominant dolerites, picrites, and olivine gabbros. Co levels show a clear distinction between the foreland picrites and dolerites, with average values of 157 ppm and 72 ppm respectively. By this measure M12 resembles the dolerite dykes with Co values of 56 ppm. However high Cr, Ni, and MgO, in combination with lower TiO_2, V, and Y suggest that, if a correlation between M12 and the foreland is made, it is more similar to the picrite or olivine gabbro suite than to the dolerites.

All three foreland dyke suites are depleted in HFSE and enriched in Th, LREE, and LILE with this Th and select LILE (e.g. Rb and K) enrichment, in contrast with the LGC, which is notably depleted in these elements. Dyke suites show a chondrite normalised REE pattern enriched in LREE with between 20 – 100x La. Dolerites show flat middle REE patterns and

no fractionation of heavy REE, while picrite and olivine gabbros show lower and more fractionated HREE patterns (Fig. 4.30). In comparison to the Scourie dolerites M12 displays a depleted REE profile (30x La) with more fractionated and lower HREE values that closely resembles the other suites. In the multi-element plot M12 displays marked Rb and Ba depletion in comparison to the Scourie Dykes, although how much this is a feature of greater alteration is unclear. It displays a similar prominent negative Ta-Nb anomaly as well as a negative Sr anomaly. All foreland dykes display a prominent negative Nb-Ta anomaly with the picrites displaying a negative Nb-Ta-Ti anomaly. In Paleozoic and Cenozoic rocks this is a strong indicator of subduction involvement in melt generation, however applying this to Archean and Paleoproterozoic aged rocks is controversial. Hughes et al., (2014) suggest that the presence of this anomaly in Scottish mantle xenoliths along with accompanying Th and LREE enrichment in both xenoliths and Scourie Dykes indicates that it is a primary feature of the Scottish sub-continental lithospheric mantle (SCLM). This enriched geochemistry of the SCLM may be a relict signature of shallow subduction and associated alteration of the overlying mantle during the formation of the LGC. Alternately it may be coeval with the dykes and related to metasomatism associated with the rifting event that controlled their generation and emplacement. In either case a direct subduction signature within the dykes is discounted. Due to these similarities it is considered that M12 is either correlatable with the dykes of the foreland – likely the picrite or olivine gabbro suite - or formed through similar processes from a similarly enriched SCLM. The geochemistry of sample G2 is enriched in Rb, Th, and U in comparison to the granulite facies gneisses of the Lewisian. However this depletion is not a marked a feature of the amphibolite facies gneisses of the northern region and the Outer-Hebrides and as such is not representative of the Lewisian as a whole

On the basis of these similarities in geochemistry and geochronology, there is no evidence to suggest that the Orrin inlier is exotic with regards to the foreland Lewisian. No evidence of the c. 1772–1655 Ma magmatic component or the c. 1800 Ma depositional age as recognised in the Loch Shin inlier by Strachan et al., (2020) is present at Orrin. As such there is no reason to suggest a Baltican origin for this section of the NHT basement and a Laurentian affinity is considered the most probable option.

5.4.1.2 – Conclusions

(1) U-Pb ages support an Archean (c. 2800 – 2850 Ma) igneous protolith for the Orrin inlier.

(2) There is good evidence for at least one early metamorphic event at c. 2470 Ma and potentially an earlier event at c. 2700 Ma. Both are comparable with dated events within the central region of the foreland.

(3) Proterozoic metamorphism occurred during both the late-Laxfordian (c. 1750 Ma) and Renlandian (c. 950 Ma) events, with this being the most southerly record of the Renlandian yet known in Scotland.

(4) No evidence of Grenvillian metamorphism is present suggesting that this event is patchily expressed within the basement east of the Moine thrust.

(5) Mafic rocks from the Orrin inlier bear a strong geochemical similarity to the picrite or olivine gabbro dykes of the foreland.

(6) There is no evidence that suggests the Orrin inlier is exotic with respect to the foreland and indeed it appears to bear strong similarity in the timings of all key events to the Lewisian

5.4.2 – Scardroy

5.4.2.1 – Discussion

Both Scardroy samples, SCAR 2A and G3, record Archean protolith ages of c. 2750 – 2800 Ma and c. 2740 – 2810 Ma respectively. These are slightly, although not significantly, younger than the c. 2850 age interpreted as the protolithic age of the sample from the Orrin inlier. These U-Pb zircon protolith ages are a close match to the 2,810 ± 120 Ma whole rock age obtained by Moorbath and Taylor (1974), 2741 ± 120 Ma when adjusted for a modern ^{87}Rb decay constant (Bird, 2017). These ages are within the younger grouping of igneous crystallisation ages common across the foreland at c. 2840 – 2680 Ma from most major blocks of the northern, central, and southern regions (Fischer et al., 2021; Goodenough et al., 2013; Love et al., 2010). SCAR 2A is enriched in Rb, Th, and U in comparison to the granulite facies gneisses of the central Lewisian. However this depletion is not as marked a feature of the amphibolite facies gneisses of the northern region or the Outer-Hebrides and is not representative of the Lewisian as a whole. As such the protolith age is not diagnostic of any direct correlation with an individual foreland block or 'terrane', however there is no evidence to suggest an exotic origin for the inlier.

Neither sample displays convincing evidence of the c. 2480 Ma, or c. 2730 Ma events recorded in the Orrin inlier. A weak cluster of rims occurs above the main discordia at c. 2430 – 2320 Ma in sample SCAR 2A. It is unclear however if these lie along a discordia between the protolith age and the early-Laxfordian or are drawn down from a c. 2480 Ma metamorphic age as recorded at Orrin. These rims are the only potential evidence of any pre-Laxfordian tectono-thermal event within the Scardroy samples. This absence of early high-grade events matches the findings of Friend et al., (2008) who find these events absent from the more northerly Borgie and Farr inliers or those of Storey (2008) in which the eastern Glenelg gneisses record their earliest metamorphism during the Laxfordian before extensive Grenvillian reworking. It therefore may be a feature of much of the Lewisianoid basement east of the Moine Thrust to lack these early metamorphic events. This may suggest large parts of its present configuration were separate from the foreland blocks recording these events during the late Archean.

Laxfordian aged metamorphism is present in each sample with core and/or rim growth associated with early and late-Laxfordian events at c. 1900 Ma and c. 1750 - 1670 Ma. The

late-Laxfordian dominates this evidence in SCAR 2A with the majority of rim and core growth and the discordia intercepts relating to the later event. However in G3 the more limited evidence appears to favour a stronger effect from the earlier phase of the Laxfordian. This lack of early high-grade metamorphism and dominance of the Laxfordian suggests the gneisses at Scardroy more closely resemble the foreland Rhiconich or Tarbert blocks (Kinny et al., 2005) or the Type B crust of Park (2005). These blocks lack the early high-grade metamorphism present in the Assynt, Gruinard, and Rona blocks, and are dominated by Laxfordian events.

No evidence is present for the Grenvillian event in either sample. This matches with its non-expression in the Orrin inlier and again suggest evidence of this event is patchily distributed within the basement of the NHT. As at Orrin, both samples record evidence of Pb-loss associated with a c. 950 - 900 Ma event, while SCAR 2A presents rim growth associated with this event at 912 ± 36 Ma and 939 ± 24 Ma. Both samples show single analyses at c. 800 - 770 Ma, while SCAR 2A also records a single c. 650 Ma age. The earlier of these ages may relate to the c. 825 – 780 'Knoydartian' event recorded within the overlying Moine (Cutts et al., 2010).

Neither Scardroy sample records zircon growth nor distinct Pb-loss associated with the Caledonian. Moorbath and Taylor (1974) present K-Ar ages from hornblende and biotite of c. 460 Ma and c. 425 Ma that they suggest is indicative of Caledonian age resetting of these systems. This may be due to the relatively large size of the inlier, compared to that containing sample G1, limiting the influence of Caledonian deformation. Further work, including structural mapping, may help to constrain the limits of any Caledonian structures or deformation and the relative intensity of these at Scardroy and within the Moine.

Without either absolute or relative dating of the meta-mafic rocks from Scardroy, any correlation with lithologies of the foreland is tentative at best. It is unclear how many generations of mafic and ultramafic bodies are represented within the inlier. Three general classes are present, small amphibolite bodies of generally < 10 m width, large amphibolite bodies > 100 m such as that found in Coire a' Bhuic, and ultramafic rocks with or without associated mafic material. To what extent these bodies are tectonically disrupted and once formed larger contiguous bodies is unclear without improved mapping and structural understanding of the inlier. The large mafic bodies and multiple occurrences of ultramafic material that outcrop at Scardroy is relatively uncommon within much of the foreland where

felsic gneisses are more dominant. The samples from Scardroy that may represent dismembered mafic-ultramafic complexes are M13, and SCAR 2 – 5. On Figure 5.8 these plot in or near the fields of mafic and ultramafic lithologies from the foreland Ben Strome complex. Samples SCAR 3, 4, and 5 also display a prominent europium anomaly suggesting fractional crystallisation. The degree of alteration these bodies have undergone appears to be generally higher than within the foreland, although this may be a function of additional Proterozoic and Paleozoic deformation and fluid influx. The relationship of these bodies to the gneisses at Scardroy is unclear, but ultramafic/mafic associations from the foreland are thought to be generally intrusive into the felsic gneisses but predate early metamorphic events (Guice et al., 2020).

With the exception of M13, samples collected during this study are significantly more evolved than SCAR 2 – 5. Additionally, no, to only very minor, europium anomalies are present suggesting a distinct origin from the mafic-ultramafic associations. These samples can be further subdivided by two sets of REE profiles, those showing a generally flat profile – the three garnet amphibolites: SCAR 5, M15, and M16, and those showing a sloping REE profile – the two amphibolites: M12 and M14. In comparison to the Scourie Dykes of the foreland, M12 and M14 resemble the olivine gabbros, whilst the three garnet amphibolites are comparatively HREE enriched and hence resemble the dolerites of the foreland. This superficial geochemical resemblance is not in itself enough to suggest they are one and the same without more detailed field work and geochronology. However with the dominant Laxfordian signature within the inlier it is conceivable that the now highly altered and tectonically disrupted mafic bodies are the equivalent of the better preserved dykes of the foreland, or share a similar tectonic environment of formation with a similarly enriched sub-continental lithospheric mantle source. The single sample of gneiss analysed, SCAR 2A, is comparatively enriched in Rb, Th, and U and depleted in HREE with regards to the central region of the LGC. However it can be considered a TTG based on its geochemistry and is not dissimilar from the gneisses of the northern or southern regions of the foreland, as such there is no evidence against correlation with the LGC.

At least two phases of mafic igneous activity are therefore present within the inlier: the intrusion of associated ultramafic-mafic bodies, and the separate intrusion of more evolved and generally smaller mafic bodies. Whether both are the direct correlates of their foreland counterparts is unclear, however there is presently no evidence to firmly exclude this possibility. When the geochemistry is considered in addition to the geochronology, there is

no evidence to suggest that the Scardroy inlier is exotic to the Lewisian, or Laurentia. The dominance of the Laxfordian along with the geochemistry of SCAR 2A suggests it resembles the peak amphibolite facies upper plate gneisses of Park (2005) and therefore the northern or southern regions of the mainland and the majority of the Outer Hebridean gneisses.

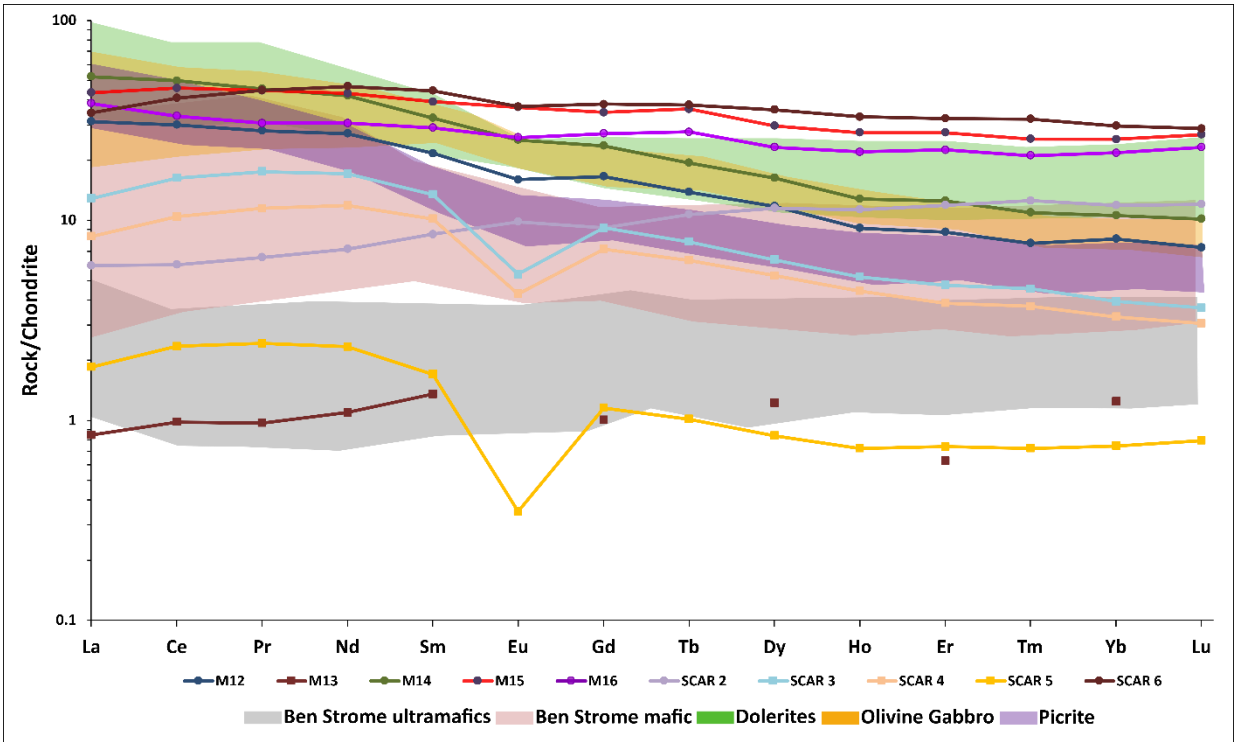

Figure 5.8. REE plot showing mafic and ultramafic samples from the Scardroy and Orrin (M12) inliers. Fields for foreland comparators, Scourie Dykes and Ben Strome complex from Hughes et al., (2014) and Guice et al., (2020)

5.4.2.2 – Conclusions

1) The Scardroy inlier records an Archean protolith age of c. 2750 – 2800 Ma in SCAR 2A and c. 2740 – 2810 in G3. No evidence is present for early metamorphic events at c. 2700 Ma or 2480 Ma recorded within the Orrin inlier or much of the foreland.

2) Evidence for metamorphic events within the Scardroy inlier is found for: early and late-Laxfordian events at c. 1900 and 1700 Ma, Renlandian aged events at c. 950 – 900 Ma, and Knoydartian events at c. 830 – 780 Ma. No evidence of the Grenvillian or Caledonian is present in the Scardroy samples.

3) Geochemical analysis of igneous bodies from the inlier suggests at least two classes of intrusion are present. Firstly those that may represent dismembered mafic-ultramafic complexes and, secondly a more evolved suite that bear some resemblance to the dykes of the foreland and *may* be their equivalent.

4) On the basis of this history the inlier appears to strongly resemble the Lewisian of the foreland and there is no evidence to suggest it is exotic with regards to Laurentia.

5.4.3 - Loch Airigh Inlier (G1)

5.4.3.1 - Discussion

While the Scardroy inlier records an Archean age the 'Loch Airigh' inlier, a name suggested and used by this study, east of the Strathconon fault containing sample G1 has a well constrained protolith age of c. 1775 Ma with only a single inherited Archean (c. 2730 Ma) grain. This age predates the late-Laxfordian, c. 1750 – 1670, by some 25 Ma but compares well with granitic intrusive rocks within the foreland dated at c. 1790 - 1770 Ma near and within the Laxford Shear Zone (Goodenough et al., 2013). The c. 1775 Ma age of G1 compares very closely with a 1772 ± 38 Ma age that Strachan et al., (2020) obtained from an intermediate orthogniess from the Loch Shin inlier. Strachan et al., (2020) use this age along with a c. 1800 Ma metasedimentary age from the same area to argue for a Baltic heritage for the inlier. However on the basis of a single age from sample G1 it is considered premature to suggest an exotic origin for the body as a whole rather than a geologically simpler interpretation of the sample as a Laxfordian granitic intrusive body. Zircon rims display extensive growth at c. 1730 Ma, around 40 Ma after the crystallisation of the igneous protolith. This is interpreted to record metamorphism associated with the late-Laxfordian after the emplacement of the igneous protolith.

No evidence of the c. 950 Ma Renlandian event prominent within the Orrin and Scardroy inliers is observed. There is some evidence of a c. 800 Ma 'Knoydartian' Pb-loss event in the discordant analyses and one concordant rim is found at c. 830 Ma. G1 is the only sample to show a strong Caledonian (Grampian) signature. The age of this event is c. 463 ± 3 Ma as constrained by both core and rim populations. This age is a near exact match for the 463 ± 4 Ma age obtained from a syntectonic pegmatite by Cutts et al., (2010) from Glen Urquhart and within the range of regional scale migmatisation in East Sutherland at c. 470 - 460 Ma (Kinny et al., 1999). This places metamorphism of G1 within the Grampian event at likely pressure-temperature conditions of c. 7 kbar and 650 °C (Cutts et al., 2010).

Two samples, M10 and M11, were collected from within 100 m of sample G1. Based on similar petrography and unclear field relations may in fact sample the same or similar lithology. They plot as monzonites to granodiorites with relatively LREE enriched profiles and geochemistry suggestive of an origin in a continental-arc to collisional setting. On several discrimination diagrams they fall within or near to TTG fields and in some respects

resemble the geochemistry of SCAR 2A. The lack of field relations between M10/M11 and G1 hinders a broader integration of the geochronology with the geochemistry. If however all three samples share the c. 1775 Ma age, then the continental-arc tectonic setting implied by their geochemistry would be a conceivable environment for the margin of the Lewisian prior to the late-Laxfordian and the final collision of the outboard Malin arc.

The position of the Loch Airigh inlier is unclear with regards to the main Scardroy inlier lying west of the Strathconon Fault. The Airigh gneisses lie in the same tectonic position just above the SBT as those at Scardroy, however the Strathconon Fault has experienced a period of sinistral motion at c. 430 – 425 Ma synchronous with the emplacement of the Ratagain granite (Stewart et al., 2001). It is unclear if this is the only direction of slip upon the fault as its history is poorly constrained; however if so, this would place the G1 gneisses significantly to the south-west once this motion is restored. Numerous small Lewisianoid inliers occur either side of the Strathconon fault as far south as Morar, with prominent inliers such as those at Glenelg truncated by it. A better understanding of the offset across the fault would aid in potential correlation of inliers either side. Additionally the position of the Loch Airigh relative to the Orrin inlier is unclear as the two are separated by the Sgurr Na Cairbe Slide, a feature of unknown Neoproterozoic to Paleozoic age (Tobisch et al., 1970).

The Loch Airigh inlier is considered to be of interest for future work, especially further geochronology and mapping to determine whether the entire mass bears a Laxfordian age. If other samples within the inlier record an Archean age similar to that at Scardroy and Orrin, then G1 likely represents a small scale Laxfordian intrusion into these gneisses. If however the inlier as a whole carries this age signature then a different model for its formation and correlation may be required, potentially supporting the work of Strachan et al., (2020) in suggesting an exotic origin for at least some of the basement to the Northern Highlands.

5.4.3.2 – Conclusions

1) The Airigh inlier records a tightly constrained c. 1775 Ma, crystallisation age.

2) Evidence of metamorphism during the late-Laxfordian is present some 40 Ma later at c. 1730 Ma. There is limited evidence of a Knoydartian aged event at c. 830 Ma.

3) Prominent Pb-loss and zircon growth are found at c. 463 Ma associated with the Grampian event.

4) Geochemical analysis of intermediate to felsic samples from the inlier suggest formation in a continental-arc to collisional setting.

5) The relationship of the Airigh inlier with the main Scardroy inlier is unclear due to displacement along the Strathconon fault, however it may originally have lain to the south-west.

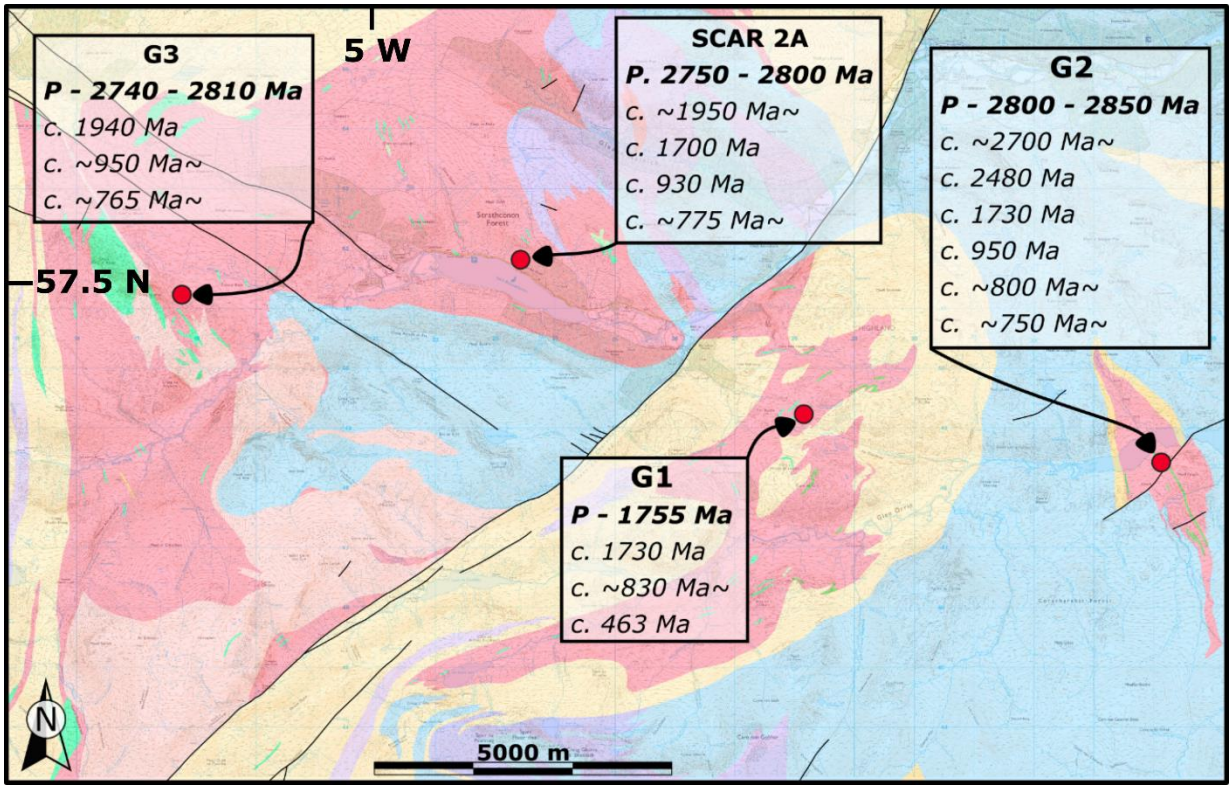

Figure 5.9. Map showing dates of events recorded at each sample site across the Strathconon inliers. Protolith age in bold with metamorphic events indicated by either Pb-loss or zircon growth in italics. ~indicates~ an event with low evidence of or uncertainty in presence.

Chapter 6. Summary and Concluding Remarks

The work conducted here has opened several new and interesting lines of study within both the Hebridean and Northern-Highlands terranes. Within the foreland it reinforces the importance of volumetrically small but geologically critical occurrences of ultramafic and metasedimentary material in unravelling the history of the LGC. Within the Northern Highlands the degree of heterogeneity between basement inliers, both of this and other studies, is becoming increasingly apparent. However, that heterogeneity is no greater than that found within the foreland and is not itself diagnostic of a non-Lewisian association.

Continued detailed study of the LMG and mineralisation present within it has the potential to provide important insights into the tectonic regimes and environments present during the Paleoproterozoic. The possibility that the Loch na Cabhaig ultramafic rocks form a part of the oceanic sequence presents a rare opportunity to study what may be a c. 2.0 Ga obducted sliver of lower oceanic crust. This would be unique within Scotland and rare globally for rocks of an important age for the evolution of plate tectonics. It further reinforces the importance of ultramafic rocks within the Lewisian in unravelling the history of the complex. The confirmation of precious metal mineralisation at Gorm-loch na Beinne extends the potential for economic mineralisation along strike significantly from the Kerry Road deposit and adds an important avenue for expansion of any future mining operation. The economic importance of the mineralisation within the LMG may not be world class in the scale of deposits. It none-the-less represents an important segment within the current resurgence of interest, exploration, and investment in Scottish gold with potential benefits for the local community and the international recognition of the industry within Scotland.

The potential and tentative late-Laxfordian age, and hence non-correlation with the LMG, for the Gruinard belt is an important addition to the history of supracrustal material within the LGC. It may extend the range of occurrence of these lithologies from the early-Laxfordian LMG and Outer-Hebridean belts an extra c. 200 Ma into the late-Laxfordian. It could therefore provide an important window into the upper-crustal evolution and processes of an orogenic event presently dominated by study of its lower-crustal roots. It would also significantly improve the understanding of the nature of boundaries within the LGC and its assembly along them.

The continuation of these features, structures, and geologic history from the Hebridean Terrane to the Northwest Highlands Terrane depends on the continuity of basement across the Moine Thrust. To this end the similarities of the Scardroy and Orrin inliers to the Lewisian of the foreland is considered (Fig. 6.1, Fig. 6.2). The Rhiconich block is the only mainland 'terrane' to provide a close match for the protolith age, absence of early high-grade metamorphism, and the dominantly Laxfordian metamorphic signature present within the Scardroy inlier (Kinny et al., 2005). Meanwhile the Orrin inlier records a similar series of events, including early metamorphic zircon growth, to that present within the Gruinard and Assynt blocks of the central region. Despite these similarities it is considered that attempting to directly correlate between the studied inliers and regions within the foreland is fraught with difficulty. This is especially evident once the intervening shortening across the Moine and Sgurr Beag thrusts, lateral displacements along the Strathconon Fault, and deformation associated with a series of Neoproterozoic and Paleozoic metamorphic events not expressed within the foreland are considered. It is however apparent that the differences present between individual inliers and between inliers and the foreland are no larger than that found across similar distances within the foreland. A factor of increasing relevance as a growing body of work recognises heterogenous ages within individual foreland blocks (Fischer et al., 2021; Goodenough et al., 2013; Love et al., 2010) greater than that proposed between separate blocks. This combined with the increasing recognition of coincident metamorphic events shared across the complex is reshaping and refining the terrane model of Kinny et al., (2005). Taking the simpler two plate model of Park, (2005) the Scardroy inlier fits the model of a lower 'type B' plate that reached peak metamorphism during the Laxfordian, while the Orrin inlier matches that of the upper 'type A' plate variably retrogressed during the Laxfordian from an earlier high-grade event.

This widespread evidence of the Laxfordian across the foreland is usually taken as evidence of the final assembly of the LGC during this event, either from a series of disparate blocks, or in a simpler continental collision with later modification. The similar expression of the Laxfordian across many of the Lewisianoid inliers suggests that, whatever differences may be present in their Archean history, by the Mesoproterzoic both the foreland and the modern day sub-Moine basement had been assembled. This would suggest that the sub-Moine basement, at least within the Strathconon area, appears distinctly Laurentian and Lewisian in nature. Later events have since modified its structure, however no evidence of later larger scale additions such as a Grenvillian aged suture or exotic terranes are observed. The expression of individual Proterozoic to Paleozoic events differs between samples, with

variable evidence of Renlandian, 'early' and 'late' Knoydartian, and Caledonian events present across the inliers. This variable and patchy expression of Neoproterozoic to

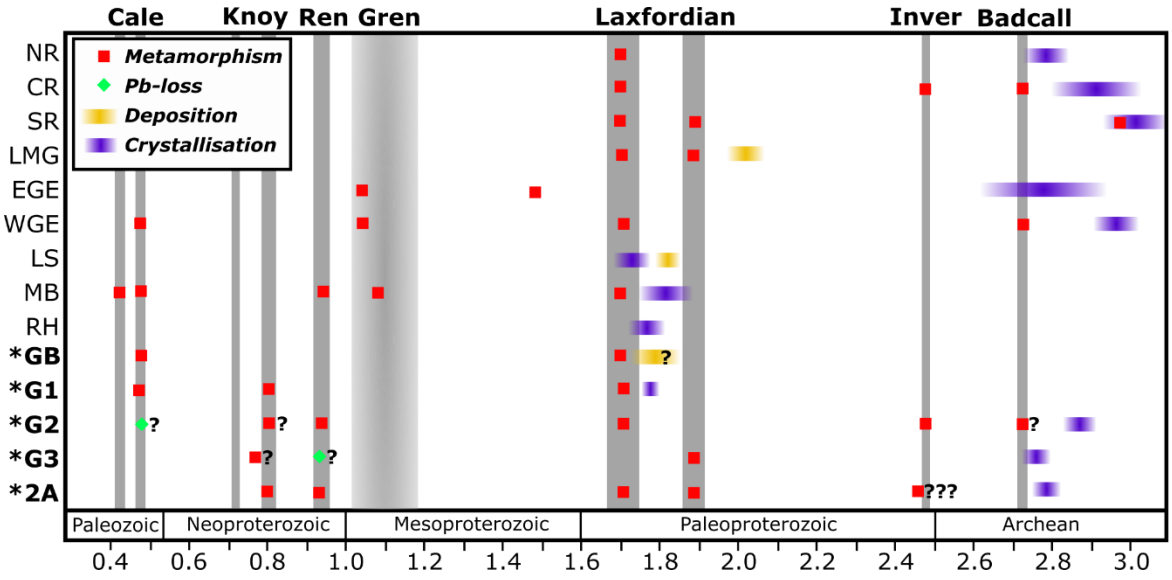

Figure 6.1. Comparison of protolithic and metamorphic ages recorded in samples from this study (***bold**) with various comparators from both onshore and offshore Scotland. Events abbreviations: Cale – Caledonian, Knoy – Knoydartian, Ren – Renlandian, Gren – Grenvillian, Inver – Inverian, Badcall – Badcallian. Location abbreviations: NR – Northern region, CR – Central Region, SR – Southern Region, LMG – Loch Maree Group, EGE – Eastern Glenelg, WGE – Western Glenelg, LS – Loch Shin, MB – Malin Block, RH – Rockall High Dates for protolith ages from; Daly et al., (1991), Fischer et al., (2021), Goodenough et al., (2013), Kinny et al., (2005), Love et al., (2010), Morton et al., (2014), Muir et al., 1994), Strachan et al., (2020).

Paleozoic events may relate to the immediate setting of each with regards to local Knoydartian or Caledonian structures.

This shared basement between Hebridean and Northwest Highland terranes, as evidenced by correlation of Lewisianoid inliers with the foreland, allows for the LMG, associated mineralisation, and late-Laxfordian supracrustal rocks to exist east of the Moine Thrust. Although exactly along strike there is no evidence of LMG like rocks at Scardroy, likely due to lateral displacement across the Moine thrust, however the belt may exist at depth below overlying Moinian cover. South-west of the Scardroy inliers a series of small and discrete occurrences of Lewisianoid gneisses occur within remote and mountainous country. Similar study of these may improve any potential correlation between inliers and individual blocks of the foreland and hence constrain the relative and potential location of foreland boundaries and potential supracrustal sequences within the basement to the Moine.

Despite the relative accessibility and long history of study of Scotland's geology it is evident that much work remains to be done and many questions are still to be answered. Its compact size, range in variety and age of rocks along with positioning at the margins of many global events make it a prime candidate for modern research and debate around important controversies within the study of poly-orogenic systems, global tectonics, deep time and major earth processes. The contribution this work may make is hopefully a small part of the process towards a fuller understanding of these important questions.

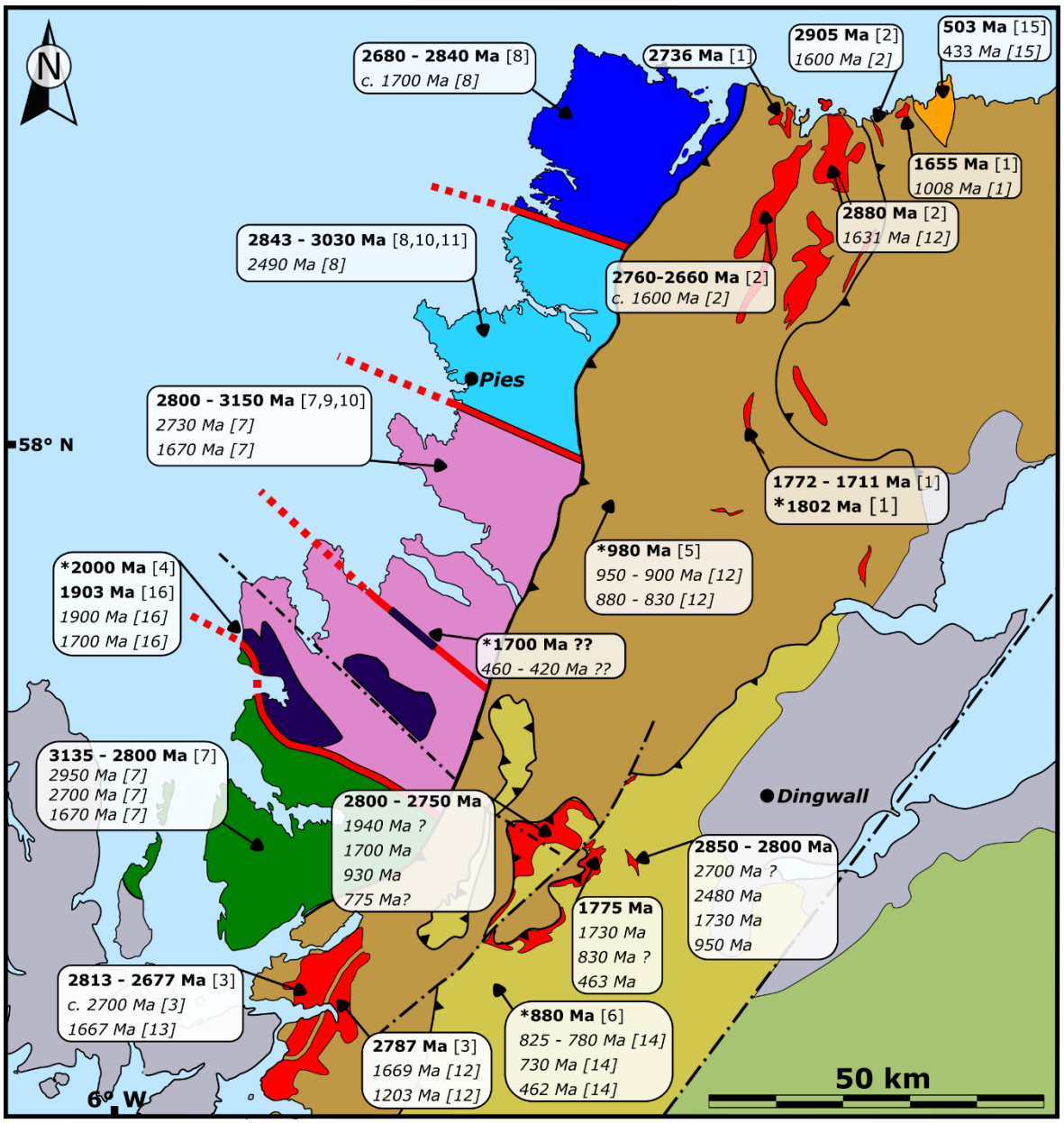

Figure 6.2 Map showing selected key dates, from this study and others, across the Northern Highlands and Hebridean terranes. **Bold** indicated magmatic protolith ages *** ages** are metasedimentary depositional ages whilst *italic* ages are metamorphic ages. [1] (Strachan et al., 2020) [2] (Friend et al., 2008) [3](Storey, 2002) [4] (Whitehouse et al., 1997) [5] (Cawood et al., 2007) [6] (Cawood et al., 2004) [7] (Love et al., 2010) [8] (Kinny and Friend, 1997) [9] (Love et al., 2004) [10] (Fischer et al., 2021) [11] (Goodenough et al., 2013) [12] (Bird, 2011) [13] (Storey, 2008) [14] (Cutts et al., 2010) [15] (Dunk et al., 2019) [16] (Park et al., 2001)

List of References

Alderman, A.R., 1936. Eclogites from the neighbourhood of Glenelg, Inverness-shire. Quarterly Journal of the Geological Society, 92(1-4), pp.488-530.

Baker, T.R., Prave, A.R. and Spencer, C.J., 2019. 1.99 Ga mafic magmatism in the Rona terrane of the Lewisian Gneiss Complex in Scotland. Precambrian Research, 329, pp.224-231.

Barrie, C.T. and Hannington, M.D., 1999. Classification of volcanic-associated massive sulfide deposits based on host-rock composition. Reviews in economic geology, 8, pp.1-11.

Bird, A., Cutts, K., Strachan, R., Thirlwall, M.F. and Hand, M., 2018. First evidence of Renlandian (c. 950–940 Ma) orogeny in mainland Scotland: Implications for the status of the Moine Supergroup and circum-North Atlantic correlations. Precambrian Research, 305, pp.283-294.

Bird, A.F., 2011. Age resolution of peak metamorphism within the Caledonides of northern Scotland and Shetland (Doctoral dissertation, Royal Holloway, University of London).

Bodinier, J.L. and Godard, M., 2003. Orogenic, ophiolitic, and abyssal peridotites. Treatise on geochemistry, 2, p.568.

Bonsor, H.C., Strachan, R.A., Prave, A.R. and Krabbendam, M., 2012. Sedimentology of the early Neoproterozoic Morar Group in northern Scotland: implications for basin models and tectonic setting. Journal of the Geological Society, 169(1), pp.53-65.

British Geological Survey, Regional Geochemical Atlas, Great Glen, Keyworth, Nottinghamshire, UK, 1987, 16 pp. plus 28 maps plus descriptions.

Burns, I.M., Fowler, M.B., Strachan, R.A. and Greenwood, P.B., 2004. Geochemistry, petrogenesis and structural setting of the meta-igneous Strathy Complex: a unique basement block within the Scottish Caledonides?. Geological Magazine, 141(2), pp.209-223.

Burton, C.J., 2016. Discussion on "The Neoproterozoic to Mid-Devonian evolution of Scotland: a review and unresolved issues." Scottish Journal of Geology 51, 5–30.

Butler, R.W.H. and Coward, M.P., 1984. Geological constraints, structural evolution, and deep geology of the Northwest Scottish Caledonides. Tectonics, 3(3), pp.347-365.

Campbell, L.R., Phillips, R.J., Walcott, R.C. and Lloyd, G.E., 2019. Rupture geometries in anisotropic amphibolite recorded by pseudotachylytes in the Gairloch Shear Zone, NW Scotland. Scottish Journal of Geology, 55(2), pp.75-92.

Carson, C.J., Ague, J.J., Grove, M., Coath, C.D. and Harrison, T.M., 2002. U–Pb isotopic behaviour of zircon during upper-amphibolite facies fluid infiltration in the Napier Complex, east Antarctica. Earth and Planetary Science Letters, 199(3-4), pp.287-310.

Cawood, P.A., Nemchin, A.A. and Strachan, R., 2007. Provenance record of Laurentian passive-margin strata in the northern Caledonides: Implications for paleodrainage and paleogeography. Geological Society of America Bulletin, 119(7-8), pp.993-1003.

Cawood, P.A., Nemchin, A.A., Strachan, R.A., Kinny, P.D. and Loewy, S., 2004. Laurentian provenance and an intracratonic tectonic setting for the Moine Supergroup, Scotland, constrained by detrital zircons from the Loch Eil and Glen Urquhart successions. Journal of the Geological Society, 161(5), pp.861-874.

Coats, J.S., Shaw, M.H., Gunn, A.G., Rollin, K.E. and Fortey, N.J., 1997. Mineral exploration in Lewisian supracrustal and basic rocks of the Scottish Highlands and Islands. Mineral Reconnaissance Programme Report, 146.

Coats, J.S., Shaw, M.H., Smith, R.T., 1993. Mineral Investigation in the Scardroy Area, Highland Region, Scotland. Mineral Reconnaissance Programme Open File Report no. 12.

Colman, T.B., 2000. Exploration for metalliferous and related minerals in Britain: a guide. Great Britain. Department of Trade and Industry., British Geological Survey Minerals Group.

Coney, P.J., Jones, D.L. and Monger, J.W., 1980. Cordilleran suspect terranes. Nature, 288(5789), pp.329-333.

Corfu, F., Crane, A., Moser, D. and Rogers, G., 1998. U-Pb zircon systematics at Gruinard Bay, northwest Scotland: implications for the early orogenic evolution of the Lewisian complex. Contributions to Mineralogy and Petrology, 133(4), pp.329-345.

Corfu, F., Heaman, L.M. and Rogers, G., 1994. Polymetamorphic evolution of the Lewisian Complex, NW Scotland, as recorded by U-Pb isotopic compositions of zircon, titanite and rutile. Contributions to Mineralogy and Petrology, 117(3), pp.215-228.

Crane, A., 1972. The geology of the Lewisian complex near Poolewe, Ross-shire (Doctoral dissertation, Keele University).

Crowley, Q.G., Key, R. and Noble, S.R., 2015. High-precision U–Pb dating of complex zircon from the Lewisian Gneiss Complex of Scotland using an incremental CA-ID-TIMS approach. Gondwana Research, 27(4), pp.1381-1391.

Cutts, K.A., Kinny, P.D., Strachan, R.A., Hand, M., Kelsey, D.E., Emery, M., Friend, C.R.L. and Leslie, A.G., 2010. Three metamorphic events recorded in a single garnet: Integrated phase modelling, in situ LA-ICPMS and SIMS geochronology from the Moine Supergroup, NW Scotland. Journal of Metamorphic Geology, 28(3), pp.249-267.

Daly, J.S., 1996. Pre-Caledonian history of the Annagh Gneiss Complex North-Western Ireland, and correlation with Laurentia-Baltica. Irish Journal of Earth Sciences, pp.5-18.

Daly, J.S., Muir, R.J. and Cliff, R.A., 1991. A precise U-Pb zircon age for the Inishtrahull syenitic gneiss, County Donegal, Ireland. Journal of the Geological Society, 148(4), pp.639-642.

Davies, J.H.F.L. and Heaman, L.M., 2014. New U–Pb baddeleyite and zircon ages for the Scourie dyke swarm: A long-lived large igneous province with implications for the Paleoproterozoic evolution of NW Scotland. Precambrian Research, 249, pp.180-198.

Dewey, J.F., Dalziel, I.W., Reavy, R.J. and Strachan, R.A., 2015. The Neoproterozoic to Mid-Devonian evolution of Scotland: a review and unresolved issues. Scottish Journal of Geology, 51(1), pp.5-30.

Dewey, J.F., Dalziel, I.W., Reavy, R.J. and Strachan, R.A., 2016. Reply to Discussion on 'The Neoproterozoic to Mid-Devonian evolution of Scotland: a review and unresolved issues' Scottish Journal of Geology, 51, 5–30. Scottish Journal of Geology, 52(2), pp.112-112.

Dewey, J.F., Strachan, R.A., 2003. Changing Silurian-Devonian relative plate motion in the Caledonides: Sinistral transpression to sinistral transtension. Journal of the Geological Society 160, 219–229.

Dey, S., Nandy, J., Choudhary, A.K., Liu, Y. and Zong, K., 2014. Origin and evolution of granitoids associated with the Kadiri greenstone belt, eastern Dharwar craton: a history of orogenic to anorogenic magmatism. Precambrian Research, 246, pp.64-90.

Dilek, Y. and Flower, M.F., 2003. Arc-trench rollback and forearc accretion: 2. A model template for ophiolites in Albania, Cyprus, and Oman. Geological Society, London, Special Publications, 218(1), pp.43-68.

Droop, G., Fernandes, L. and Shaw, S., 1999. Laxfordian metamorphic conditions of the Palaeoproterozoic Loch Maree Group, Lewisian Complex, NW Scotland. Scottish Journal of Geology, 35(1), pp.31-50.

Drummond, D.A., Cloutier, J., Boyce, A.J. and Prave, A.R., 2020. Petrogenesis and geochemical halos of the amphibolite facies, Lower Proterozoic, Kerry Road volcanogenic massive sulfide deposit, Loch Maree Group, Gairloch, NW Scotland. Ore Geology Reviews, 124, p.103623.

Dubé, B., Gosselin, P.A.T.R.I.C.E., Mercier-Langevin, P., Hannington, M. and Galley, A., 2007. Gold-rich volcanogenic massive sulphide deposits. Geological Association of Canada, Mineral Deposits Division, pp.75-94.

Dunk, M., Strachan, R.A., Cutts, K.A., Lasalle, S., Storey, C.D., Burns, I.M., Whitehouse, M.J., Fowler, M., Moreira, H., Dunlop, J. and Pereira, I., 2019. Evidence for a late Cambrian juvenile arc and a buried suture within the Laurentian Caledonides of Scotland: Comparisons with hyperextended Iapetan margins in the Appalachian Mountains (North America) and Norway. Geology, 47(8), pp.734-738.

Elliott, D. and Johnson, M.R.W., 1980. Structural evolution in the northern part of the Moine thrust belt, NW Scotland. Earth and Environmental Science Transactions of The Royal Society of Edinburgh, 71(2), pp.69-96.

Evans, C.R., 1965. Geochronology of the Lewisian basement near Lochinver, Sutherland. Nature, 207(4992), pp.54-56.

Fischer, S., Prave, A.R., Johnson, T.E., Cawood, P.A., Hawkesworth, C.J. and Horstwood, M.S., 2021. Using zircon in mafic migmatites to disentangle complex high-grade gneiss terrains–Terrane spotting in the Lewisian complex, NW Scotland. Precambrian Research, 355, p.106074.

Fletcher, T.P. and Rushton, A.W., 2008. The Cambrian fauna of the Leny Limestone, Perthshire, Scotland. Earth and Environmental Science Transactions of the Royal Society of Edinburgh, 98(2), pp.199-218.

Fleuty, M.J., 1961. The three fold-systems in the metamorphic rocks of upper Glen Orrin, Ross-shire and Inverness-shire. Quarterly Journal of the Geological Society, 117(1-4), pp.447-479.

Floyd, P.A., Winchester, J.A. and Park, R.G., 1989. Geochemistry and tectonic setting of Lewisian clastic metasediments from the Early Proterozoic Loch Maree Group of Gairloch, NW Scotland. Precambrian Research, 45(1-3), pp.203-214.

Freeland, G.L. and Dietz, R.S., 1973. Rotation history of Alaskan tectonic blocks. Tectonophysics, 18(3-4), pp.379-389.

Friend, C. and Kinny, P., 2001. A reappraisal of the Lewisian Gneiss Complex: geochronological evidence for its tectonic assembly from disparate terranes in the Proterozoic. Contributions to Mineralogy and Petrology, 142(2), pp.198-218.

Friend, C.R.L. and Kinny, P.D., 1995. New evidence for protolith ages of Lewisian granulites, northwest Scotland. Geology, 23(11), pp.1027-1030.

Friend, C.R.L., Kinny, P.D., Rogers, G., Strachan, R.A. and Paterson, B.A., 1997. U-Pb zircon geochronological evidence for Neoproterozoic events in the Glenfinnan Group (Moine Supergroup): the formation of the Ardgour granite gneiss, north-west Scotland. Contributions to Mineralogy and Petrology, 128(2), pp.101-113.

Frost, B.R., Frost, C.D., 2019. Metamorphism of Peridotitic Rocks, in: Essentials of Igneous and Metamorphic Petrology. Cambridge University Press, pp. 217–233.

Galley, A.G., Hannington, M.D., Jonasson, I.R., 2007. Mineral Deposits of Canada: A Synthesis of Major Deposit-Types, District Metallogeny, the Evolution of Geological Provinces, and Exploration Methods: Geological Association of Canada, Mineral Deposits Division, Special Publication.

Goodenough, K.M., Crowley, Q.G., Krabbendam, M. and Parry, S.F., 2013. New U-Pb age constraints for the Laxford Shear Zone, NW Scotland: Evidence for tectono-magmatic processes associated with the formation of a Paleoproterozoic supercontinent. Precambrian Research, 233, pp.1-19.

Goodenough, K.M., Millar, I., Strachan, R.A., Krabbendam, M., Evans, J.A., 2011. Timing of regional deformation and development of the Moine Thrust Zone in the Scottish Caledonides: constraints from the U–Pb geochronology of alkaline intrusions. Journal of the Geological Society 168, 99–114.

Goodenough, K.M., Park, R.G., Krabbendam, M., Myers, J.S., Wheeler, J., Loughlin, S.C., Crowley, Q.G., Friend, C.R.L., Beach, A., Kinny, P.D., Graham, R.H., 2010. The Laxford Shear Zone: an end-Archaean terrane boundary? Geological Society, London, Special Publications 335, 103–120.

Greene, A.R., DeBARI, S.M., Kelemen, P.B., Blusztajn, J. and Clift, P.D., 2006. A detailed geochemical study of island arc crust: the Talkeetna arc section, south–central Alaska. Journal of Petrology, 47(6), pp.1051-1093.

Guice, G., 2019. Origin and geodynamic significance of ultramafic-mafic complexes in the North Atlantic and Kaapvaal Cratons (Doctoral dissertation, Cardiff University).

Guice, G.L., McDonald, I., Hughes, H.S.R., MacDonald, J.M., Blenkinsop, T.G., Goodenough, K.M., Faithfull, J.W., Gooday, R.J., 2018. Re-evaluating ambiguous age relationships in Archean cratons: Implications for the origin of ultramafic-mafic complexes in the Lewisian Gneiss Complex. Precambrian Research 311, 136–156.

Guice, G.L., McDonald, I., Hughes, H.S.R., MacDonald, J.M., Faithfull, J.W., 2020. Origin(s) and geodynamic significance of Archean ultramafic–mafic bodies in the mainland Lewisian Gneiss Complex, North Atlantic Craton. Journal of the Geological Society jgs2020-013.

Hastie, A.R., Kerr, A.C., Pearce, J.A., Mitchell, S.F., 2007. Classification of Altered Volcanic Island Arc Rocks using Immobile Trace Elements: Development of the Th–Co Discrimination Diagram. Journal of Petrology 48, 2341–2357.

Heaman, L.M., Tarney, J., 1989. U-Pb baddeleyite ages for the Scourie dyke swarm, Scotland: Evidence for two distinct intrusion events. Nature 340, 705–708.

Holdsworth, R.E., Dempsey, E., Selby, D., Darling, J.R., Feely, M., Costanzo, A., Strachan, R.A., Waters, P., Finlay, A.J., Porter, S.J., 2015. Silurian–Devonian magmatism, mineralization, regional exhumation and brittle strike-slip deformation along the Loch Shin Line, NW Scotland. Journal of the Geological Society 172, 748–762.

Holdsworth, R.E., Morton, A., Frei, D., Gerdes, A., Strachan, R.A., Dempsey, E., Warren, C., Whitham, A., 2019. The nature and significance of the Faroe-Shetland Terrane: Linking Archaean basement blocks across the North Atlantic. Precambrian Research 321, 154–171.

Holdsworth, R.E., Selby, D., Dempsey, E., Scott, L., Hardman, K., Fallick, A.E. and Bullock, R., 2020. The nature and age of Mesoproterozoic strike-slip faulting based on Re–Os geochronology of syntectonic copper mineralization, Assynt Terrane, NW Scotland. Journal of the Geological Society, 177(4), pp.686-699.

Hollocher, K., 2004. CIPW norm calculation program. Geology Department, Union College.

Hughes, H.S., McDonald, I., Goodenough, K.M., Ciborowski, T.J.R., Kerr, A.C., Davies, J.H. and Selby, D., 2014. Enriched lithospheric mantle keel below the Scottish margin of the North Atlantic Craton: Evidence from the Palaeoproterozoic Scourie Dyke Swarm and mantle xenoliths. Precambrian Research, 250, pp.97-126.

Humphris, S.E. and Thompson, G., 1978. Hydrothermal alteration of oceanic basalts by seawater. Geochimica et Cosmochimica Acta, 42(1), pp.107-125.

Hutton, D.H.W. and McErlean, M., 1991. Silurian and Early Devonian sinistral deformation of the Ratagain granite, Scotland: constraints on the age of Caledonian movements on the Great Glen fault system. Journal of the Geological Society, 148(1), pp.1-4.

Irwin, W.P., 1972. Terranes of the western Paleozoic and Triassic belt in the southern Klamath Mountains, California.

Jagoutz, O. and Schmidt, M.W., 2012. The formation and bulk composition of modern juvenile continental crust: The Kohistan arc. Chemical Geology, 298, pp.79-96.

Jahn, I., Strachan, R.A., Fowler, M., Bruand, E., Kinny, P.D., Clark, C. and Taylor, R.J., 2017. Evidence from U–Pb zircon geochronology for early Neoproterozoic (Tonian) reworking of an Archaean inlier in northeastern Shetland, Scottish Caledonides. Journal of the Geological Society, 174(2), pp.217-232.

Johnson, T.E., Brown, M., Goodenough, K.M., Clark, C., Kinny, P.D. and White, R.W., 2016. Subduction or sagduction? Ambiguity in constraining the origin of ultramafic–mafic bodies in the Archean crust of NW Scotland. Precambrian Research, 283, pp.89-105.

Johnson, Y.A., Park, R.G., Winchester, J.A., 1987. Geochemistry, Petrogenesis and Tectonic Significance of the Early Proterozoic Loch Maree Group Amphibolites of the Lewisian Complex, NW Scotland. Geological Society Special Publication 33, 255–269.

Jones, E.M., Rice, C.M. and Tweedie, J.R., 1987. Lower Proterozoic stratifrom sulphide deposits in Loch Maree group, Gairloch, northwest Scotland. Transactions of the Institution of Mining and Metallurgy. Section B. Applied earth science, 96, pp.128-140.

Kelley, S.P., Reddy, S.M. and Maddock, R., 1994. Laser-probe 40Ar/39Ar investigation of a pseudotachylyte and its host rock from the Outer Isles thrust, Scotland. Geology, 22(5), pp.443-446.

Kelly, N.M., Hinton, R.W., Harley, S.L. and Appleby, S.K., 2008. New SIMS U–Pb zircon ages from the Langavat Belt, South Harris, NW Scotland: implications for the Lewisian terrane model. Journal of the Geological Society, 165(5), pp.967-981.

Kerr, A.C., Marriner, G.F., Arndt, N.T., Tarney, J., Nivia, A., Saunders, A.D. and Duncan, R.A., 1996. The petrogenesis of Gorgona komatiites, picrites and basalts: new field, petrographic and geochemical constraints. Lithos, 37(2-3), pp.245-260.

Kinny, P.D., Friend, C.R.L. and Love, G.J., 2005. Proposal for a terrane-based nomenclature for the Lewisian Gneiss Complex of NW Scotland. Journal of the Geological Society, 162(1), pp.175-186.

Kinny, P.D., Friend, C.R.L., Strachan, R.A., Watt, G.R. and Burns, I.M., 1999. U–Pb geochronology of regional migmatites in East Sutherland, Scotland: evidence for crustal melting during the Caledonian orogeny. Journal of the Geological Society, 156(6), pp.1143-1152.

Krabbendam, M., Leslie, A.G. and Goodenough, K.M., 2014. Structure and stratigraphy of the Morar Group in Knoydart, NW Highlands: implications for the history of the Moine Nappe and stratigraphic links between the Moine and Torridonian successions. Scottish Journal of Geology, 50(2), pp.125-142.

Le Bas, M.J. and Streckeisen, A.L., 1991. The IUGS systematics of igneous rocks. Journal of the Geological Society, 148(5), pp.825-833.

Love, G.J., Friend, C.R.L. and Kinny, P.D., 2010. Palaeoproterozoic terrane assembly in the Lewisian Gneiss Complex on the Scottish mainland, south of Gruinard Bay: SHRIMP U–Pb zircon evidence. Precambrian Research, 183(1), pp.89-111.

Love, G.J., Kinny, P.D. and Friend, C.R.L., 2004. Timing of magmatism and metamorphism in the Gruinard Bay area of the Lewisian Gneiss Complex: comparisons with the Assynt Terrane and implications for terrane accretion. Contributions to Mineralogy and Petrology, 146(5), pp.620-636.

Lydon, J.W., 1984. Ore deposit models-8. Volcanogenic massive sulphide deposits Part I: A descriptive model. Geoscience Canada.

MacDonald, J.M., Goodenough, K.M., Wheeler, J., Crowley, Q., Harley, S.L., Mariani, E. and Tatham, D., 2015. Temperature–time evolution of the Assynt Terrane of the Lewisian Gneiss Complex of Northwest Scotland from zircon U-Pb dating and Ti thermometry. Precambrian Research, 260, pp.55-75.

Manning, C.E., Thomas, R. and Tropper, P., 2012, April. Aluminum Mobility in Crustal Fluids: the Role of Al-Si Complexing. In EGU General Assembly Conference Abstracts (p. 3460).

Marshall, B. and Gilligan, L.B., 1987. An introduction to remobilization: information from ore-body geometry and experimental considerations. Ore Geology Reviews, 2(1-3), pp.87-131.

Mason, A.J. and Brewer, T.S., 2004. Mafic dyke remnants in the Lewisian Complex of the Outer Hebrides, NW Scotland: a geochemical record of continental break-up and re-assembly. Precambrian Research, 133(1-2), pp.121-141.

Mason, A.J., 2012. Major early thrusting as a control on the Palaeoproterozoic evolution of the Lewisian Complex: evidence from the Outer Hebrides, NW Scotland. Journal of the Geological Society, 169(2), pp.201-212.

Mason, A.J., 2016. The Palaeoproterozoic anatomy of the Lewisian Complex, NW Scotland: evidence for two 'Laxfordian'tectonothermal cycles. Journal of the Geological Society, 173(1), pp.153-169.

Mason, A.J., Parrish, R.R. and Brewer, T.S., 2004. U–Pb geochronology of Lewisian orthogneisses in the Outer Hebrides, Scotland: implications for the tectonic setting and correlation of the South Harris Complex. Journal of the Geological Society, 161(1), pp.45-54.

McDonough, W.F. and Sun, S.S., 1995. The composition of the Earth. Chemical geology, 120(3-4), pp.223-253.

Middlemost, E.A., 1989. Iron oxidation ratios, norms and the classification of volcanic rocks. Chemical geology, 77(1), pp.19-26.

Milne, E.J.M., 2019. The Great Glen Caledonian Igneous Suite: New geochemical and geochronological insights into the final stages of the Caledonian Orogeny (Doctoral dissertation, University of Glasgow).

Moorbath, S. and Taylor, P.N., 1974. Lewisian age for the Scardroy Mass. Nature, 250(5461), pp.41-43.

Morton, A., Frei, D., Stoker, M. and Ellis, D., 2014. Detrital zircon age constraints on basement history on the margins of the northern Rockall Basin. Geological Society, London, Special Publications, 397(1), pp.209-223.

Muir, R.J., Fitches, W.R. and Maltman, A.J., 1994. The Rhinns Complex: Proterozoic basement on Islay and Colonsay, Inner Hebrides, Scotland, and on Inishtrahull, NW Ireland. Earth and Environmental Science Transactions of The Royal Society of Edinburgh, 85(1), pp.77-90.

Noble, S.R., Hyslop, E.K. and Highton, A.J., 1996. High-precision U–Pb monazite geochronology of the c. 806 Ma Grampian Shear Zone and the implications for the evolution of the Central Highlands of Scotland. Journal of the Geological Society, 153(4), pp.511-514.

Oliva-Urcia, B., Kontny, A., Vahle, C. and Schleicher, A.M., 2011. Modification of the magnetic mineralogy in basalts due to fluid–rock interactions in a high-temperature geothermal system (Krafla, Iceland). Geophysical Journal International, 186(1), pp.155-174.

Park, R.G., 1995. Palaeoproterozoic Laurentia-Baltica relationships: a view from the Lewisian. Geological Society, London, Special Publications, 95(1), pp.211-224.

Park, R.G., 2005. The Lewisian terrane model: a review. Scottish Journal of Geology, 41(2), pp.105-118.

Park, R.G., 2010. Structure and evolution of the Lewisian Gairloch shear zone: variable movement directions in a strike-slip regime. Scottish Journal of Geology, 46(1), pp.31-44.

Park, R.G., Kinny, P.D., Friend, C.R.L. and Love, G.J., 2005. Discussion on a terrane-based nomenclature for the Lewisian Gneiss Complex of NW Scotland Journal, Vol. 162, 2005, pp. 175–186. Journal of the Geological Society, 162(5), pp.893-895.

Park, R.G., Tarney, J. and Connelly, J.N., 2001. The Loch Maree Group: Palaeoproterozoic subduction–accretion complex in the Lewisian of NW Scotland. Precambrian Research, 105(2-4), pp.205-226.

Park, RG (ed.) 2002. The Lewisian Geology of Gairloch, NW Scotland. Geological Society Memoir no. 26. London, Bath: Geological Society of London. ISBN1862391165. Geological Magazine, 140(5), 614-615.

Parman, S.W., Grove, T.L., Dann, J.C. and De Wit, M.J., 2004. A subduction origin for komatiites and cratonic lithospheric mantle. South African Journal of Geology, 107(1-2), pp.107-118.

Paton, C., Hellstrom, J., Paul, B., Woodhead, J. and Hergt, J., 2011. Iolite: Freeware for the visualisation and processing of mass spectrometric data. Journal of Analytical Atomic Spectrometry, 26(12), pp.2508-2518.

Peach, B.N., 1907. The geological structure of the North-West Highlands of Scotland. HM Stationery Office.

Peach, B.N., Hinxman, L.W., Horne, J., Crampton, C.B. and Carruthers, R.G., 1913. The Geology of Central Ross-shire:(Explanation of Sheet 82) (Vol. 82). HM Stationery Office.

Pearce, J.A., 1982. Trace element characteristics of lavas from destructive plate boundaries. Andesites, 8, pp.525-548.

Polat, A. and Kerrich, R., 2000. Archean greenstone belt magmatism and the continental growth–mantle evolution connection: constraints from Th–U–Nb–LREE systematics of the 2.7 Ga Wawa subprovince, Superior Province, Canada. Earth and Planetary Science Letters, 175(1-2), pp.41-54.

Ramsay, J.G., 1957. Moine-Lewisian relations at Glenelg, Inverness-shire. Quarterly Journal of the Geological Society, 113(1-4), pp.487-524.

Rivers, T., 1997. Lithotectonic elements of the Grenville Province: review and tectonic implications. Precambrian Research, 86(3-4), pp.117-154.

Roddick, J.C. and Max, M.D., 1983. A Laxfordian age from the Inishtrahull Platform, County Donegal, Ireland. Scottish Journal of Geology, 19(1), pp.97-102.

Rollinson, H., 1999. Petrology and geochemistry of metamorphosed komatiites and basalts from the Sula Mountains greenstone belt, Sierra Leone. Contributions to Mineralogy and Petrology, 134(1), pp.86-101.

Rollinson, H., 2007. Recognising early Archaean mantle: a reappraisal. Contributions to Mineralogy and Petrology, 154(3), pp.241-252.

Sanders, I.S., Daly, J.S. and Davies, G.R., 1987. Late Proterozoic High-pressure granulite facies meta-morphism in the north-east Ox inlier, north-west Ireland. Journal of Metamorphic Geology, 5(1), pp.69-85.

Sherlock, S.C., Jones, K.A. and Park, R.G., 2008. Grenville-age pseudotachylite in the Lewisian: laserprobe 40Ar/39Ar ages from the Gairloch region of Scotland (UK). Journal of the Geological Society, 165(1), pp.73-83.

Smith, D.I. and Watson, J., 1983. Scale and timing of movements on the Great Glen fault, Scotland. Geology, 11(9), pp.523-526.

Soper, N.J. and Barber, A.J., 1982. A model for the deep structure of the Moine thrust zone. Journal of the Geological Society, 139(2), pp.127-138.

Stewart, A.D., 1993. Late Proterozoic and Late Palaeozoic movement on the Coigach fault in NW Scotland. Scottish Journal of Geology, 29(1), pp.21-28.

Stewart, M., Strachan, R.A., Martin, M.W. and Holdsworth, R.E., 2001. Constraints on early sinistral displacements along the Great Glen Fault Zone, Scotland: structural setting, U–Pb geochronology and emplacement of the syn-tectonic Clunes tonalite. Journal of the Geological Society, 158(5), pp.821-830.

Storey, C., 2008. The Glenelg-Attadale Inlier, NW Scotland, with emphasis on the Precambrian high-pressure metamorphic history and subsequent retrogression: an introduction and review. Scottish Journal of Geology, 44(1), pp.1-16.

Storey, C.D., 2002. Tectono-metamorphic evolution of the Glenelg-Attadale Inlier, northwest Scotland (Doctoral dissertation, University of Leicester).

Storey, C.D., Brewer, T.S. and Temperley, S., 2005. P–T conditions of Grenville-age eclogite facies metamorphism and amphibolite facies retrogression of the Glenelg–Attadale Inlier, NW Scotland. Geological Magazine, 142(5), pp.605-615.

Strachan, R.A., Johnson, T.E., Kirkland, C.L., Kinny, P.D. and Kusky, T., 2020. A Baltic heritage in Scotland: Basement terrane transfer during the Grenvillian orogeny. Geology, 48(11), pp.1094-1098.

Stubblefield, C.J., 1956. Cambrian palaeogeography in Britain.

Sutton, J. and Watson, J., 1950. The pre-Torridonian metamorphic history of the Loch Torridon and Scourie areas in the North-West Highlands, and its bearing on the chronological classification of the Lewisian. Quarterly Journal of the Geological Society, 106(1-4), pp.241-307.

Tanner, P.W.G., 1970. The Sgurr Beag Slide–a major tectonic break within the Moinian of the Western Highlands of Scotland. Quarterly Journal of the Geological Society, 126(1-4), pp.435-463.

Taylor, R.J., Johnson, T.E., Clark, C. and Harrison, R.J., 2020. Persistence of melt-bearing Archean lower crust for> 200 my—an example from the Lewisian Complex, northwest Scotland. Geology, 48(3), pp.221-225.

Tobisch, O.T., Fleuty, M.J., Merh, S.S., Mukhopadhyay, D. and Ramsay, J.G., 1970. Deformational and metamorphic history of Moinian and Lewisian rocks between Strathconon and Glen Affric. Scottish Journal of Geology, 6(3), pp.243-265.

Trewin, N.H. ed., 2002. The geology of Scotland. Geological Society of London.

Vermeesch, P., 2018. IsoplotR: A free and open toolbox for geochronology. Geoscience Frontiers, 9(5), pp.1479-1493.

Vernon, R., Holdsworth, R.E., Selby, D., Dempsey, E., Finlay, A.J. and Fallick, A.E., 2014. Structural characteristics and Re–Os dating of quartz-pyrite veins in the Lewisian Gneiss Complex, NW Scotland: Evidence of an Early Paleoproterozoic hydrothermal regime during terrane amalgamation. Precambrian Research, 246, pp.256-267.

Wasylenki, L.E., Baker, M.B., Kent, A.J. and Stolper, E.M., 2003. Near-solidus melting of the shallow upper mantle: partial melting experiments on depleted peridotite. Journal of Petrology, 44(7), pp.1163-1191.

Weaver, B.L. and Tarney, J., 1981. Lewisian gneiss geochemistry and Archaean crustal development models. Earth and Planetary Science Letters, 55(1), pp.171-180.

Whitehouse, M.J., Bridgwater, D. and Park, R.G., 1997. Detrital zircon ages from the Loch Maree Group, Lewisian Complex, NW Scotland: confirmation of a Palaeoproterozoic Laurentia—Fennoscandia connection. Terra Nova, 9(5-6), pp.260-263.

Whitehouse, M.J., Claesson, S., Sunde, T. and Vestin, J., 1997. Ion microprobe U□ Pb zircon geochronology and correlation of Archaean gneisses from the Lewisian Complex of Gruinard Bay, northwestern Scotland. Geochimica et Cosmochimica Acta, 61(20), pp.4429-4438.

Winchester, J.A. and Floyd, P.A., 1977. Geochemical discrimination of different magma series and their differentiation products using immobile elements. Chemical geology, 20, pp.325-343.

Workman, R.K. and Hart, S.R., 2005. Major and trace element composition of the depleted MORB mantle (DMM). Earth and Planetary Science Letters, 231(1-2), pp.53-72.

Zirkler, A., Johnson, T.E., White, R.W. and Zack, T., 2012. Polymetamorphism in the mainland Lewisian complex, NW Scotland–phase equilibria and geochronological constraints from the Cnoc an t'Sidhean suite. Journal of Metamorphic Geology, 30(8), pp.865-885.

Sample No.	Grid Ref	Easting	Northing	Latitude	Longitude	Sample Type	Description
K25251	NG 8513969831	185139	869831	57.666913	-5.6041739	Outcrop	Folded oxidised unit in burn
K25252	NG 8513669851	185136	869851	57.667091	-5.6042419	Outcrop	Likely continuation of above unit
K25253	NG 8510169906	185101	869906	57.667567	-5.6048764	Outcrop	Qtz veining/breccia with large brassy pyrite in stream bed
K25254	NG 8504070091	185040	870091	57.669196	-5.6060617	Float	Dominated by sulphides, brecciated textures, pyrite
K25255	NG 8494270734	184942	870734	57.674914	-5.6082745	Float	Sulphide rich boulder from lochside brecciated textures
K25256	NG 8531770642	185317	870642	57.674268	-5.6019179	Outcrop	Oxidised schist from lochside
K25257	NG 8551171433	185511	871433	57.681451	-5.5993755	Float	Sulphide rich boulder from lochside brecciated textures
K25258	NG 8549471503	185494	871503	57.682071	-5.5997222	Float	Sulphide rich boulder from lochside brecciated textures
K25259	NG 8531771707	185317	871707	57.683815	-5.6028662	Outcrop	Band of oxidised rock at lochside near road
K25260	NG 8363970129	183639	870129	57.668866	-5.6295337	Outcrop	Massive amphibolite with minor pyrite and Qtz veining
K25261	NG 8334470713	183344	870713	57.673959	-5.6349933	Float	Minor pyrite in amphibolite from stream
K25262	NG 8312970942	183129	870942	57.675908	-5.6387965	Outcrop	Finely dissemated pyrite in banded amphibolite
K25263	NG 8374672092	183746	872092	57.686514	-5.6295042	Outcrop	Sulphur stained roadside outcrop
K25264	NG 9016163491	190161	863515	57.612441	-5.5146514	Subcrop	possible subcrop, pyrite
K25265	NG 9016163491	190161	863510	57.612441	-5.5146514	Subcrop	pyrite+Hematite, adjactent to '264
K25266	NG 9013863443	190138	863465	57.612	-5.5149941	Float	Massive sulphides, central peat gully
K25267	NG 9026863491	190259	863496	57.61249	-5.512864	Float	In Loch, Massive pyrite + hematite + illminite
K25268	NG 9026863491	190268	863491	57.61249	-5.512864	Float	In Loch, Pyrite - orange/yellow colour to loch floor
K25269	NG 9029563475	190295	863493	57.612359	-5.512399	Float	Massive pyrite, east side of loch on promontary
K25270	NG 9031263477	190312	863497	57.612385	-5.5121168	Outcrop	Pyrite at east side of loch
K25271	NG 8382673686	183826	873686	57.700841	-5.6295957	Outcrop	5m wide gossan with pyrite
K25272	NG 8346374190	183463	874190	57.705185	-5.636127	Outcrop	Iron stained, pyrite and quartz, folded 40m gossan
K25273	NG 8347074168	183470	874168	57.704991	-5.63599	Outcrop	Iron stained, pyrite and quartz, folded 40m gossan
K25274	NG 8351774062	183517	874062			Outcrop	pyrite pyrrotite in amphibolite
KR 1	NG 8377772521	183777	872521	57.690375	-5.6293702	Outcrop	3 samples from surface exposure at kerry road
GRB 1	NG 9581685515	195816	885515	57.812504	-5.4388693	Outcrop	
M1	NG 8933962850	189339	862850	57.606311	-5.5278256	Outcrop	
M2	NG 8935262839	189352	862839	57.606218	-5.5275989	Outcrop	
M3	NG 8943562918	189435	862918	57.606965	-5.5262813	Outcrop	
M4	NG 8947362901	189473	862901	57.606831	-5.5256318	Outcrop	
M5	NG 8946662886	189466	862886	57.606693	-5.5257357	Outcrop	
M6	NG 8947262879	189472	862879	57.606633	-5.5256294	Outcrop	
M7	NG 8938562868	189385	862868	57.606494	-5.5270729	Outcrop	
M8	NG 8926162720	189261	862720	57.605109	-5.5290153	Boulder	
M9	NG 8878362385	188783	862385	57.5441	-7.203745	Outcrop	

M10	NH 27995 49227	227995	849227	57.500492	-4.872173	Outcrop
M11	NH 28202 49221	228202	849221	57.500516	-4.8687191	Outcrop
M12	NH 34085 48417	234085	848417	57.495496	-4.7701266	Outcrop
M13	NH 24908 51985	224908	851985	57.524051	-4.925596	Outcrop
M14	NH 17843 48698	217843	848698	57.491779	-5.0409357	Outcrop
M15	NH 17339 51396	217339	851396	57.515777	-5.0513522	Outcrop
M16	NH 17349 51396	217349	851396	57.515781	-5.0511855	Outcrop
G1	NH 28151 49251	228151	849251	57.500766	-4.8695902	Outcrop
G2	NH 34164 48455	234164	848455	57.495865	-4.768836	Outcrop
G3	NH 17761 51230	217761	851230	*57.514458*	*-5.0441937*	Outcrop
PG	NH 19123 50473	219123	850473	57.508214	-5.0209291	Outcrop
CG	NH 17393 51350	217393	851350	57.515386	-5.0504176	Outcrop
GULLY	NH 17843 48698	217843	848698	57.491779	-5.0409357	Outcrop
RIVER	NH 33942 48790	233942	848790	57.49879	-4.7727635	Outcrop

Appendix 2 - XRD

Pattern List - M1

Visible	Ref.Code	Score	Compound Name	Displ.[°2Th]	Scale Fac.	Chem. Formula
*	01-075-8840	59	Magnesite, syn	-0.108	0.465	Mg (C O3)
*	01-075-3686	58	Dolomite	-0.043	0.400	Ca Mg (C O3)2
*	01-073-9904	70	Trimagnesium disil..	0.107	0.172	Mg3 (Si2 O5) (O..
*	00-058-2028	53	Kaolinite-1A	-0.019	0.132	Al2 Si2 O5 (O H)4
*	00-019-0770	45	Talc-2M	-0.016	0.749	Mg3 Si4 O10 (O H)2

Graphics

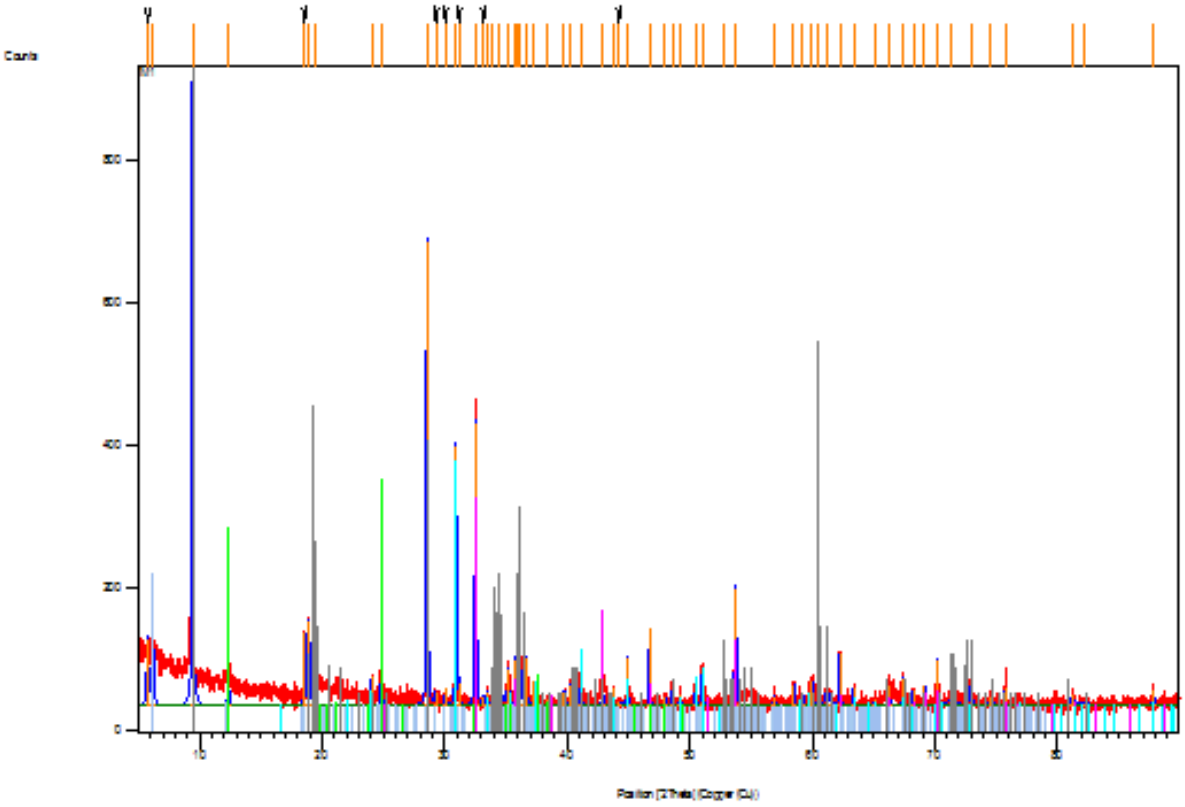

Pattern List - M2

Visible	Ref.Code	Score	Compound Name	Displ.[°2Th]	Scale Fac.	Chem. Formula
*	00-007-0077	58	Clinoclore	-0.093	0.580	Mg - Fe - Al - Si ..
*	00-029-1493	39	Talc-2M	-0.089	0.507	Mg3 Si4 O10 (O H)2
*	00-042-0544	38	Anthophyllite	-0.030	0.410	Mg5 Fe2 +2 Si8 O22..

Graphics

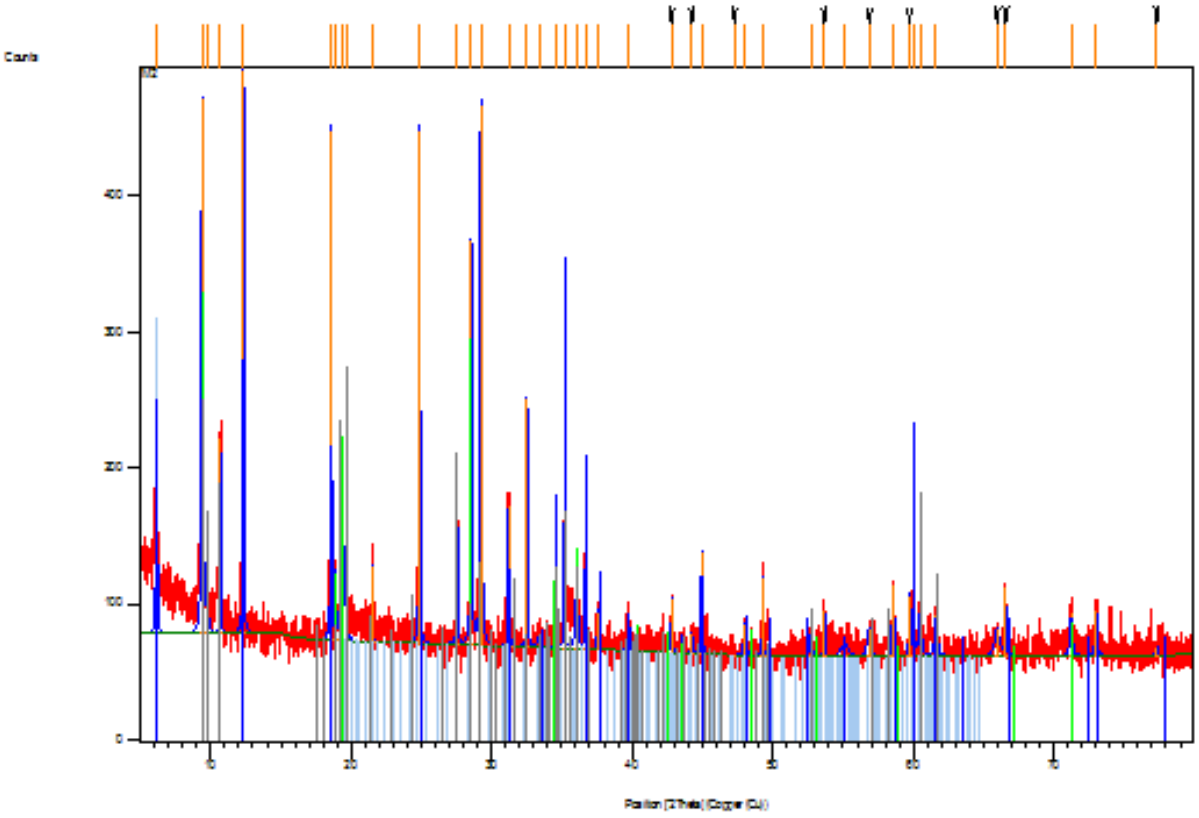

Pattern List - M3

Visible	Ref.Code	Score	Compound Name	Displ.[°2Th]	Scale Fac.	Chem. Formula
*	00-029-0853	58	Clinochlore-1MIIb	-0.025	0.190	Mg5 Al (Si3 Al) ..
*	00-058-2028	55	Kaolinite-1A	0.000	0.185	Al2 Si2 O5 (O H)4
*	00-019-0770	50	Talc-2M	-0.017	0.677	Mg3 Si4 O10 (O H)2
*	00-034-0517	49	Dolomite, ferroan	0.078	0.182	Ca (Mg , Fe) (C..

Graphics

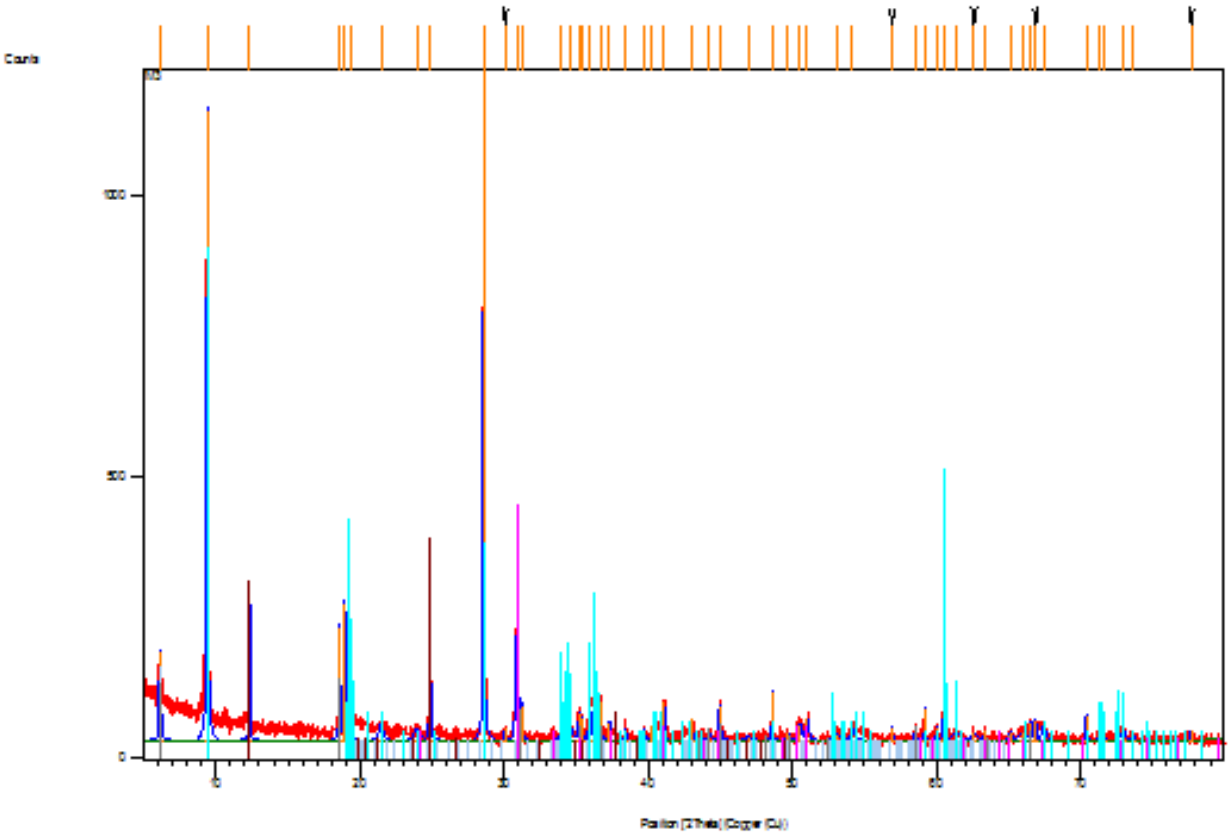

Pattern List - M5

Visible	Ref.Code	Score	Compound Name	Displ.[°2Th]	Scale Fac.	Chem. Formula
*	00-013-0437	72	Tremolite	-0.055	0.315	Ca2 Mg5 Si8 O22 (..

Graphics

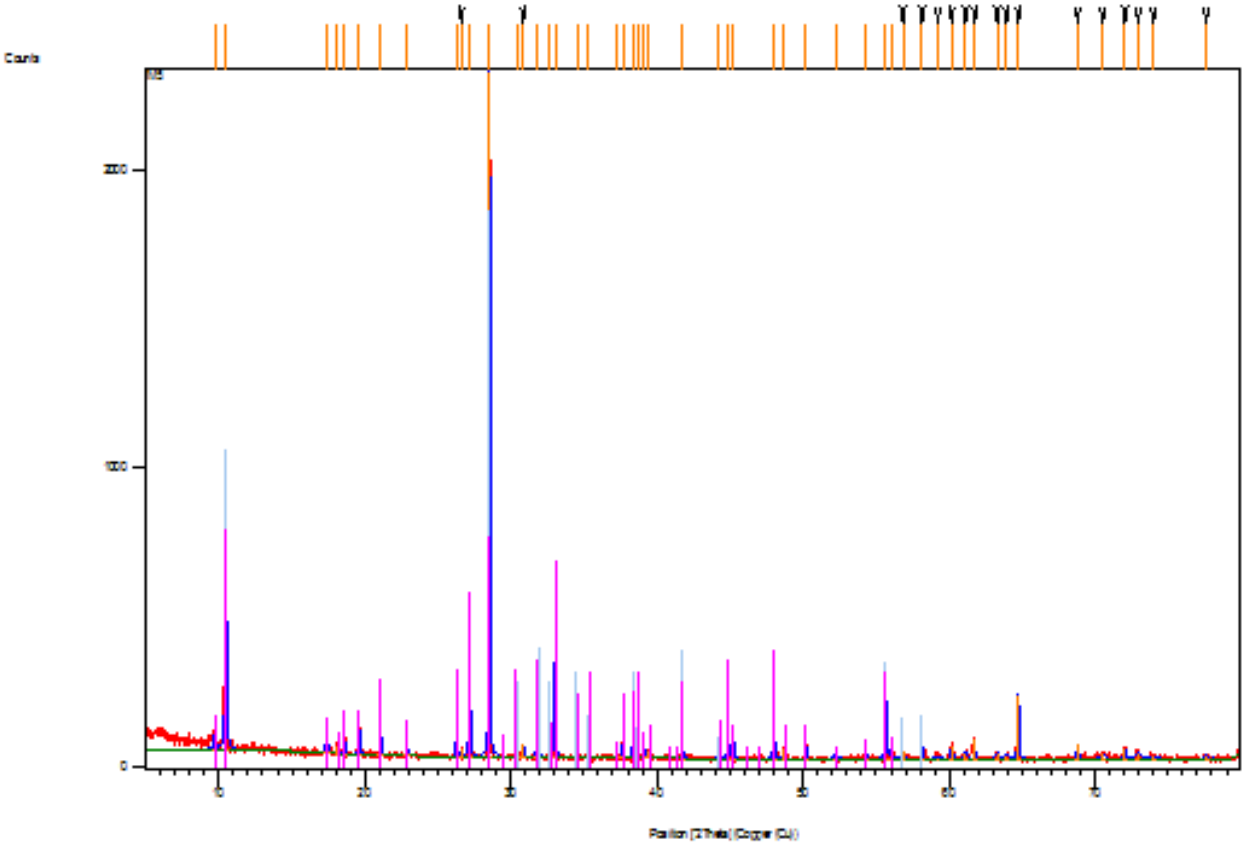

Pattern List - M6

Visible	Ref.Code	Score	Compound Name	Displ.[°2Th]	Scale Fac.	Chem. Formula
	00-012-0185	76	Clinochlore	-0.048	0.601	(Mg , Fe , Al)6 ..
	01-071-0936	45	Calcium tecto-alum..	-0.003	0.179	Ca40 Al80 Si112 O3..
	01-085-0594	39	calcium alumosilic..	0.008	0.207	Ca1.95 Al3.9 Si8.1..
	00-029-1493	26	Talc-2M	-0.015	0.150	Mg3 Si4 O10 (O H)2

Graphics

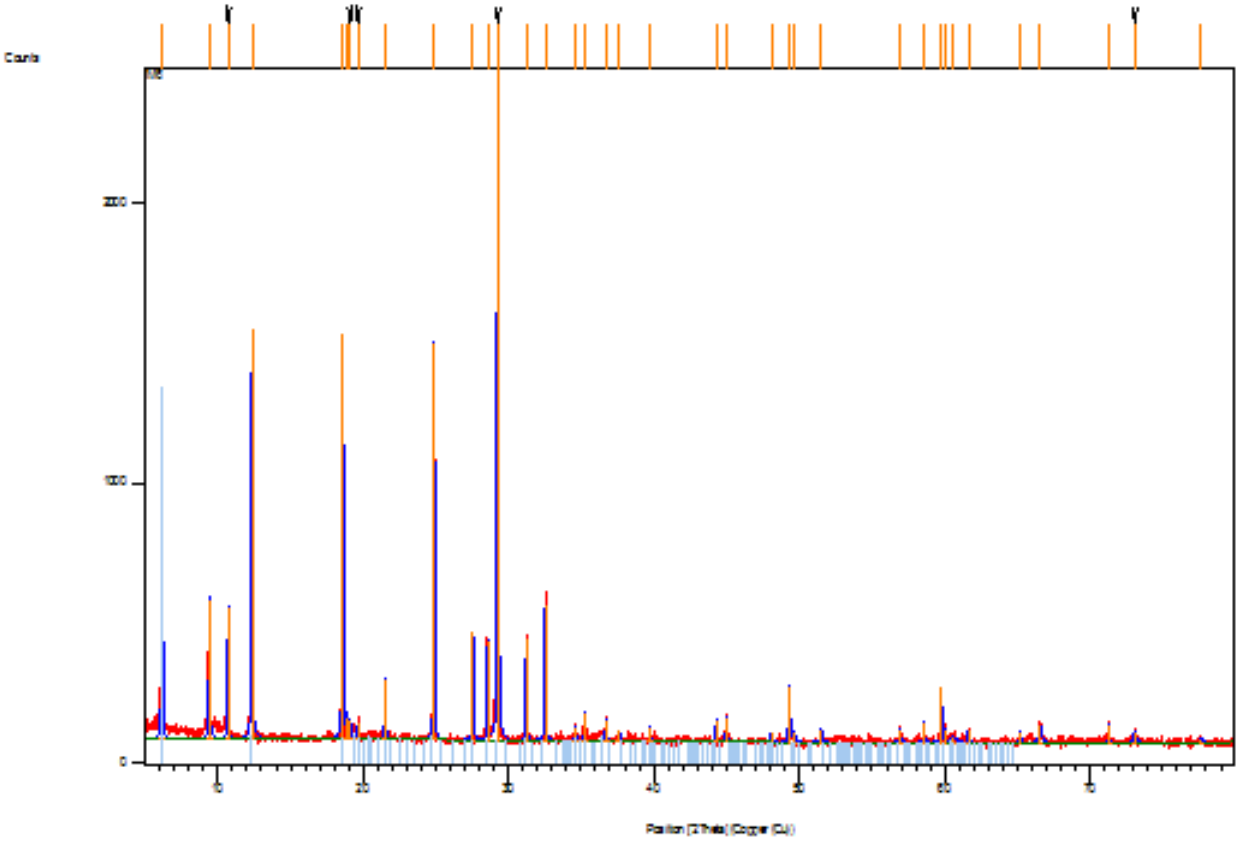

Pattern List - M8

Visible	Ref.Code	Score	Compound Name	Displ.[°2Th]	Scale Fac.	Chem. Formula
*	00-012-0185	75	Clinochlore	-0.087	0.844	(Mg , Fe , Al)6 ..
*	00-050-1606	47	Lizardite-1M	-0.029	0.623	(Mg , Fe)3 Si2 O..
*	00-034-0517	45	Dolomite, ferroan	0.109	0.511	Ca (Mg , Fe) (C..
*	01-087-0246	43	Magnetite, syn	-0.076	0.497	Fe2.9 O4

Graphics

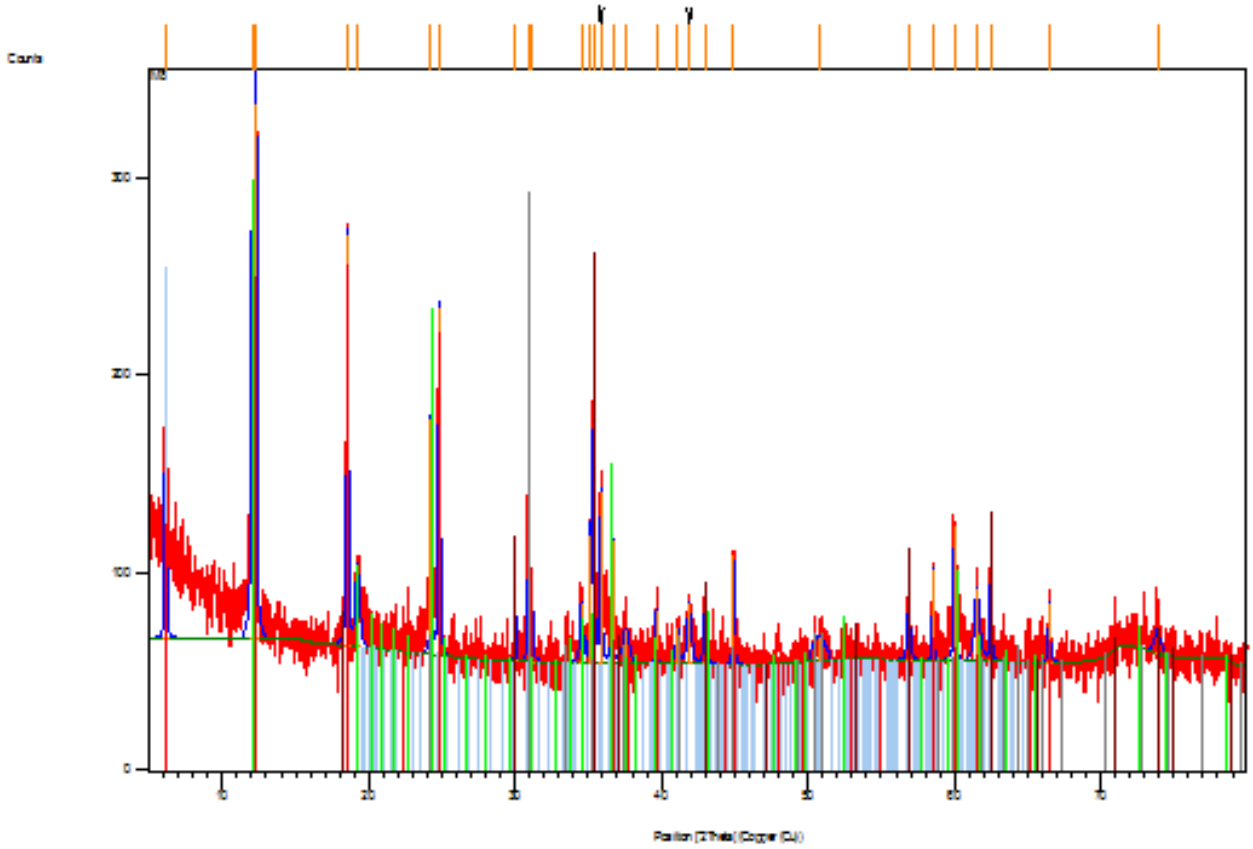

Sample GB		Final 207_235	± (2σ)	Final 206_238	± (2σ)	rho	Final 238_206	± (2σ)	Final 207_206	± (2σ)	rho
GB29	**Core**	0.72	0.14	0.071	0.005	0.014368	14.08451	0.991867	0.078	0.019	0.49973
GB8	**Core**	0.99	0.45	0.096	0.012	0.17728	10.41667	1.302083	0.083	0.041	0.079456
GB11	**Core**	6.71	0.34	0.292	0.012	0.015005	3.424658	0.140739	0.175	0.011	0.57984
GB18	**Core**	2.24	0.1	0.1758	0.0049	0.39954	5.688282	0.158547	0.0957	0.0042	0.1697
GB28	**Core**	2.582	0.084	0.1957	0.003	0.50198	5.109862	0.078332	0.0972	0.0027	0.10397
GB27	**Core**	0.53	0.12	0.0681	0.004	0.11541	14.68429	0.862513	0.059	0.013	-0.01595
GB12	**Core**	3.36	0.15	0.2349	0.0046	0.23596	4.257131	0.083367	0.1054	0.0048	0.22918
GB31	**Core**	10.61	0.59	0.423	0.017	0.47564	2.364066	0.09501	0.1888	0.0097	0.24425
GB1	**Core**	3.58	0.14	0.246	0.0061	0.70212	4.065041	0.1008	0.1034	0.0027	-0.03942
GB2	**Core**	2.85	0.14	0.2214	0.0052	0.23374	4.516712	0.106084	0.095	0.0048	0.2252
GB24	**Core**	3.31	0.13	0.2414	0.0052	0.16158	4.142502	0.089234	0.1014	0.0042	0.42482
GB23	**Core**	3.326	0.091	0.2457	0.0033	0.1018	4.070004	0.054664	0.1013	0.003	0.40639
GB33	**Core**	4.24	0.14	0.2786	0.0058	0.57874	3.589375	0.074725	0.1123	0.0033	-0.04817
GB32	**Core**	3.56	0.12	0.254	0.0035	0.097739	3.937008	0.05425	0.1034	0.0036	0.33284
GB20	**Core**	3.35	0.11	0.2452	0.0053	0.46603	4.078303	0.088153	0.0997	0.003	0.25341
GB22	**Core**	3.43	0.12	0.2528	0.0056	0.64994	3.955696	0.087626	0.1007	0.0026	0.14452
GB5	**Core**	3.92	0.16	0.2731	0.0081	0.54788	3.661662	0.108603	0.1061	0.0037	0.1012
GB26	**Core**	3.85	0.13	0.2758	0.0062	0.14907	3.625816	0.081509	0.1051	0.0039	0.43857
GB10	**Core**	3.9	0.14	0.2766	0.0055	0.60667	3.615329	0.071888	0.1037	0.0029	0.065126
GB15	**Core**	10.65	0.29	0.4579	0.0091	0.59135	2.183883	0.043401	0.1745	0.0041	0.2833
GB7	**Core**	3.81	0.17	0.2711	0.0073	0.66976	3.688676	0.099326	0.1017	0.0033	0.051072
GB13	**Core**	4	0.13	0.2835	0.0051	0.49628	3.527337	0.063455	0.1034	0.0029	0.17513
GB30	**Core**	4.34	0.12	0.2992	0.0062	0.14511	3.342246	0.069258	0.108	0.0035	0.42757
GB16	**Core**	4.13	0.16	0.2928	0.0059	0.33118	3.415301	0.068819	0.1048	0.004	0.27342
GB19	**Core**	4.34	0.11	0.3014	0.0042	0.18796	3.31785	0.046234	0.1063	0.0032	0.29848
GB17	**Core**	4.06	0.18	0.2891	0.0079	0.6468	3.459011	0.094522	0.1021	0.0032	0.062145
GB21	**Core**	3.76	0.14	0.2803	0.005	0.33226	3.567606	0.063639	0.099	0.0034	0.10179
GB4	**Core**	4.31	0.11	0.2982	0.0047	0.36427	3.353454	0.052855	0.1034	0.0025	0.19041
GB3	**Core**	4.27	0.12	0.2994	0.0053	0.62632	3.340013	0.059125	0.1035	0.0023	0.077556
GB25	**Core**	4.57	0.12	0.3149	0.0046	0.29405	3.175611	0.046389	0.1065	0.0029	0.34415
GB6	**Core**	4.63	0.16	0.3186	0.005	0.14626	3.138732	0.049258	0.1072	0.0039	0.28883
GB9	**Core**	4.19	0.13	0.3	0.0051	0.29248	3.333333	0.056667	0.1016	0.003	0.25297
GB14	**Core**	4.581	0.093	0.3169	0.0039	0.39514	3.15557	0.038835	0.1055	0.002	0.28548
GB61	**Rim**	4.47	0.16	0.3132	0.006	0.20458	3.192848	0.061166	0.1064	0.004	0.30276
GB36	**Rim**	4.73	0.12	0.3198	0.0041	0.44208	3.126954	0.040089	0.1083	0.0024	0.15076
GB55	**Rim**	4.57	0.13	0.3117	0.0042	0.30138	3.208213	0.043229	0.107	0.0029	0.21275
GB37	**Rim**	4.45	0.13	0.3057	0.005	0.43526	3.271181	0.053503	0.1074	0.0028	0.23045
GB64	**Rim**	4.49	0.1	0.3084	0.0037	0.32534	3.242542	0.038902	0.1084	0.0027	0.16971

Sample GB		Final 207_235	± (2σ)	Final 206_238	± (2σ)	rho	Final 238_206	± (2σ)	Final 207_206	± (2σ)	rho
GB48	**Rim**	4.45	0.11	0.3057	0.0042	0.45422	3.271181	0.044943	0.108	0.0024	0.10267
GB59	**Rim**	4.24	0.13	0.2975	0.0059	0.46692	3.361345	0.066662	0.1061	0.003	0.086592
GB54	**Rim**	4.68	0.13	0.3118	0.0042	0.38857	3.207184	0.043201	0.1105	0.003	0.027974
GB51	**Rim**	0.57	0.038	0.0739	0.0015	0.21043	13.5318	0.274664	0.0566	0.0036	0.11643
GB62	**Rim**	4.26	0.11	0.2954	0.0041	0.25518	3.38524	0.046985	0.1061	0.0028	0.35658
GB57	**Rim**	4.21	0.11	0.293	0.0041	0.4095	3.412969	0.047758	0.1057	0.0026	0.090457
GB34	**Rim**	3.93	0.12	0.2819	0.0054	0.32978	3.547357	0.067952	0.1026	0.0028	0.26007
GB56	**Rim**	3.95	0.1	0.2804	0.005	0.62088	3.566334	0.063594	0.1034	0.002	0.2341
GB46	**Rim**	4.26	0.11	0.2914	0.0034	0.28618	3.431709	0.040041	0.1071	0.0027	0.15025
GB53	**Rim**	4.255	0.099	0.2913	0.0047	0.30381	3.432887	0.055388	0.108	0.0028	0.40036
GB39	**Rim**	3.94	0.14	0.2799	0.0044	-0.21289	3.572705	0.056163	0.1045	0.004	0.57116
GB66	**Rim**	3.56	0.11	0.2627	0.0035	0.30082	3.806624	0.050716	0.1003	0.0029	0.1606
GB52	**Rim**	3.46	0.13	0.2564	0.0047	0.29319	3.900156	0.071493	0.0996	0.0034	0.31126
GB44	**Rim**	3.98	0.14	0.2771	0.0051	0.48765	3.608805	0.06642	0.1066	0.0032	0.059509
GB47	**Rim**	3.902	0.098	0.2734	0.0042	0.58781	3.657644	0.056189	0.1059	0.0021	-0.01798
GB38	**Rim**	3.96	0.12	0.2749	0.0045	0.36542	3.637686	0.059547	0.1067	0.003	0.19727
GB41	**Rim**	3.514	0.093	0.2542	0.0031	0.35987	3.93391	0.047975	0.102	0.0026	0.06975
GB35	**Rim**	0.578	0.05	0.0742	0.0017	0.25297	13.47709	0.308774	0.058	0.0047	-0.0225
GB49	**Rim**	3.366	0.09	0.2489	0.0039	0.53246	4.017678	0.062953	0.1018	0.0024	0.13922
GB45	**Rim**	3.64	0.11	0.2526	0.0051	0.49328	3.958828	0.079929	0.1047	0.0029	0.091848
GB42	**Rim**	3.07	0.12	0.2315	0.0052	0.20904	4.319654	0.097029	0.0997	0.0042	0.42162
GB50	**Rim**	2.719	0.08	0.2129	0.0028	0.17394	4.697041	0.061774	0.0951	0.0027	0.30015
GB65	**Rim**	3.2	0.14	0.2313	0.004	0.31653	4.32339	0.074767	0.1025	0.0042	0.096935
GB40	**Rim**	2.58	0.095	0.2015	0.0041	0.40762	4.962779	0.10098	0.0938	0.0033	0.13511
GB58	**Rim**	2.37	0.13	0.193	0.0061	0.67861	5.181347	0.163763	0.0912	0.0037	-0.08711
GB63	**Rim**	4.27	0.29	0.2208	0.0082	0.41455	4.528986	0.168196	0.1438	0.0089	0.1923
GB60	**Rim**	2.44	0.96	0.091	0.016	0.2778	10.98901	1.932134	0.225	0.09	0.37246
Z_Plesovice_1	**Std**	0.435	0.027	0.05437	0.00089	0.13997	18.3925	0.301073	0.0568	0.0035	0.10738
Z_Plesovice_2	**Std**	0.426	0.025	0.05525	0.00096	0.19801	18.09955	0.31449	0.055	0.0032	0.13663
Z_Plesovice_3	**Std**	0.398	0.021	0.05373	0.0009	0.11532	18.61158	0.311752	0.0527	0.0028	0.18737
Z_Plesovice_4	**Std**	0.388	0.023	0.05451	0.00094	0.12134	18.34526	0.316356	0.0509	0.003	0.14193
Z_Plesovice_5	**Std**	0.384	0.021	0.05216	0.00082	0.070406	19.17178	0.301397	0.053	0.003	0.1933
Z_Plesovice_6	**Std**	0.379	0.022	0.05282	0.00089	-0.01391	18.93222	0.319002	0.0511	0.0031	0.30899
Z_Plesovice_7	**Std**	0.398	0.025	0.05383	0.00087	0.17842	18.577	0.300241	0.0521	0.0031	0.066861
Z_Plesovice_8	**Std**	0.395	0.024	0.05285	0.00085	0.17969	18.92148	0.304319	0.0529	0.0032	0.008735
Z_Plesovice_9	**Std**	0.4	0.026	0.05329	0.00095	0.070997	18.76525	0.334528	0.0538	0.0035	0.15589
Z_Plesovice_10	**Std**	0.382	0.026	0.05281	0.00083	0.12635	18.93581	0.297609	0.0519	0.0034	0.11846
Z_Plesovice_11	**Std**	0.462	0.029	0.05335	0.00087	0.19461	18.74414	0.305668	0.0612	0.0037	0.083479

Sample GB		Final 207_235	± (2σ)	Final 206_238	± (2σ)	rho	Final 238_206	± (2σ)	Final 207_206	± (2σ)	rho
Z_Plesovice_13	**Std**	0.411	0.021	0.05314	0.00077	0.15487	18.81822	0.272676	0.0556	0.0029	0.10751
Z_Plesovice_14	**Std**	0.398	0.022	0.0542	0.00076	-0.05648	18.45018	0.258711	0.0517	0.0028	0.31126
Z_Plesovice_15	**Std**	0.413	0.022	0.05414	0.00076	-0.07877	18.47063	0.259285	0.0548	0.003	0.31898
Z_Plesovice_16	**Std**	0.383	0.022	0.05419	0.00076	0.07251	18.45359	0.258807	0.0501	0.0028	0.18917
Z_Plesovice_17	**Std**	0.383	0.021	0.05453	0.00074	0.11661	18.33853	0.248863	0.0501	0.0028	0.063343
Z_Plesovice_18	**Std**	0.415	0.022	0.05501	0.00077	0.16764	18.17851	0.254453	0.0541	0.0029	0.10741
Z_Plesovice_19	**Std**	0.414	0.024	0.05567	0.0009	0.051847	17.963	0.290402	0.0532	0.0031	0.24279
Z_Plesovice_20	**Std**	0.416	0.022	0.05495	0.00089	0.055115	18.19836	0.294751	0.0542	0.003	0.23949
Z_91500_1	**Std**	1.96	0.16	0.1858	0.0051	0.17629	5.382131	0.147733	0.075	0.006	0.15423
Z_91500_2	**Std**	1.91	0.16	0.1818	0.005	0.23246	5.50055	0.15128	0.0767	0.0061	0.16059
Z_91500_3	**Std**	1.84	0.15	0.1849	0.0049	0.11533	5.408329	0.143325	0.0721	0.006	0.19736
Z_91500_4	**Std**	1.96	0.17	0.181	0.0051	0.063865	5.524862	0.155673	0.0784	0.0067	0.1895
Z_91500_5	**Std**	1.91	0.16	0.1831	0.0049	0.082978	5.461496	0.146157	0.0761	0.0064	0.24515
Z_91500_6	**Std**	1.72	0.14	0.1755	0.0047	-0.04076	5.698006	0.152596	0.0715	0.0063	0.35415
Z_91500_7	**Std**	1.86	0.16	0.1779	0.0045	0.03568	5.621135	0.142187	0.0758	0.007	0.29212
Z_91500_8	**Std**	1.83	0.17	0.1765	0.0049	0.050848	5.665722	0.157292	0.0739	0.007	0.12152
Z_91500_9	**Std**	1.75	0.16	0.1703	0.0049	0.075481	5.871991	0.168953	0.0755	0.0069	0.24973
Z_91500_10	**Std**	1.91	0.15	0.1722	0.0047	0.18479	5.807201	0.158501	0.079	0.0061	0.21149
Z_91500_11	**Std**	1.78	0.15	0.1768	0.0045	0.078305	5.656109	0.143962	0.0721	0.0062	0.29634
Z_91500_12	**Std**	1.85	0.15	0.1754	0.0048	0.15812	5.701254	0.156021	0.0781	0.0062	0.22939
Z_91500_13	**Std**	1.67	0.15	0.1756	0.0048	0.21411	5.694761	0.155665	0.0691	0.0063	0.12274
Z_91500_14	**Std**	1.68	0.15	0.1776	0.0055	0.12845	5.630631	0.174372	0.0698	0.0068	0.26117
Z_91500_15	**Std**	2.01	0.17	0.1823	0.005	0.12743	5.485464	0.150452	0.0779	0.0069	0.25866
Z_91500_16	**Std**	1.83	0.15	0.1758	0.0048	0.10063	5.688282	0.155312	0.0739	0.0062	0.2653
Z_91500_17	**Std**	1.82	0.16	0.183	0.0053	0.008843	5.464481	0.158261	0.0718	0.0063	0.30001
Z_91500_18	**Std**	1.93	0.17	0.1829	0.0048	0.088168	5.467469	0.143487	0.0779	0.0071	0.25235
Z_91500_19	**Std**	1.99	0.16	0.1848	0.005	0.12415	5.411255	0.146408	0.0776	0.0063	0.26429
Z_91500_20	**Std**	1.94	0.17	0.1828	0.0046	0.13998	5.47046	0.137659	0.0766	0.0069	0.10502
G_NIST612_1	**glass**	30.5	2	0.223	0.014	0.5378	4.484305	0.281526	1.007	0.068	0.60723
G_NIST612_2	**glass**	29.1	2	0.221	0.014	0.3694	4.524887	0.286644	1.008	0.077	0.62053
G_NIST612_3	**glass**	27.6	1.6	0.232	0.014	0.35191	4.310345	0.260107	0.924	0.066	0.67018
G_NIST612_4	**glass**	27.8	2.2	0.235	0.016	0.37868	4.255319	0.289724	0.867	0.071	0.42808
G_NIST612_5	**glass**	28.7	2	0.241	0.015	0.36	4.149378	0.25826	0.92	0.071	0.58635
G_NIST612_6	**glass**	29.9	1.9	0.239	0.016	0.34363	4.1841	0.280107	0.952	0.071	0.58119
G_NIST612_7	**glass**	28.8	2.1	0.231	0.015	0.31942	4.329004	0.281104	0.976	0.082	0.40543
G_NIST612_8	**glass**	28	2.3	0.229	0.017	0.23179	4.366812	0.324174	0.96	0.1	0.70763
G_NIST612_9	**glass**	29.3	1.9	0.225	0.015	0.28332	4.444444	0.296296	1.001	0.078	0.59705
G_NIST612_10	**glass**	28.2	1.9	0.245	0.017	0.38124	4.081633	0.283215	0.9	0.073	0.59019

Sample GB		Final 207_235	± (2σ)	Final 206_238	± (2σ)	rho	Final 238_206	± (2σ)	Final 207_206	± (2σ)	rho
G_NIST612_12	**glass**	28.8	2.5	0.24	0.018	0.55688	4.166667	0.3125	0.913	0.077	0.44129
G_NIST612_13	**glass**	29.5	2.2	0.242	0.015	0.41428	4.132231	0.25613	0.919	0.069	0.40664
G_NIST612_14	**glass**	29.8	1.9	0.238	0.017	0.41671	4.201681	0.30012	1.007	0.085	0.71823
G_NIST612_15	**glass**	31.7	2.5	0.245	0.018	0.42796	4.081633	0.299875	1.015	0.093	0.75844
G_NIST612_16	**glass**	30.5	2.2	0.248	0.018	0.39702	4.032258	0.292664	0.982	0.086	0.59603
G_NIST612_17	**glass**	30.5	2.1	0.251	0.021	0.28563	3.984064	0.333328	1.01	0.11	0.88751
G_NIST612_18	**glass**	32.4	2.6	0.259	0.022	0.38894	3.861004	0.327962	1.005	0.099	0.67473
G_NIST612_19	**glass**	30.2	2.5	0.24	0.017	0.33519	4.166667	0.295139	1	0.1	0.63242
G_NIST612_20	**glass**	29.6	2.1	0.255	0.022	0.51395	3.921569	0.338331	0.916	0.074	0.55555

Sample		Final 207_235	± (2σ)	Final 206_238	± (2σ)	Rho	Final 238_206	± (2σ)	Final 207_206	± (2σ)	Rho
G1	**core**	12.4	2	0.171	0.022	0.38067	5.847953	0.752368	0.7	0.14	0.52558
G1	**core**	10.5	1.5	0.162	0.016	0.3063	6.17284	0.609663	0.535	0.087	0.51919
G1	**core**	0.75	0.19	0.078	0.0054	0.05421	12.82051	0.887574	0.105	0.032	0.89606
G1	**core**	0.52	0.19	0.0788	0.0056	0.034358	12.69036	0.901853	0.081	0.041	0.74756
G1	**core**	0.65	0.25	0.0707	0.0074	0.22784	14.14427	1.480447	0.074	0.03	-0.07579
G1	**core**	0.6	0.15	0.0715	0.0043	-0.12154	13.98601	0.841117	0.07	0.02	0.059364
G1	**core**	1.826	0.094	0.147	0.0032	0.53156	6.802721	0.148086	0.0919	0.004	-0.0858
G1	**core**	2.31	0.12	0.1755	0.0033	0.15532	5.698006	0.107142	0.0972	0.005	0.1643
G1	**core**	0.571	0.066	0.0701	0.0025	0.37334	14.26534	0.50875	0.0601	0.0066	-0.1076
G1	**core**	3.07	0.067	0.219	0.0026	0.46312	4.56621	0.054211	0.1036	0.0019	0.13153
G1	**core**	2.99	0.1	0.2183	0.005	0.67209	4.580852	0.104921	0.1013	0.0027	-0.15331
G1	**core**	3.133	0.078	0.2225	0.0029	0.30724	4.494382	0.058578	0.1026	0.0026	0.20554
G1	**core**	2.65	0.12	0.205	0.0036	0.3133	4.878049	0.085663	0.0947	0.004	0.097387
G1	**core**	2.85	0.1	0.2158	0.0035	0.11321	4.63392	0.075156	0.0983	0.0038	0.34044
G1	**core**	3.11	0.1	0.2243	0.0039	0.64544	4.458315	0.077519	0.1011	0.0024	-0.04212
G1	**core**	2.989	0.093	0.2214	0.0033	0.4529	4.516712	0.067322	0.0993	0.0027	0.12593
G1	**core**	3.416	0.098	0.2399	0.0039	0.52592	4.168404	0.067765	0.1052	0.0025	0.15419
G1	**core**	3.55	0.1	0.2464	0.0036	0.19224	4.058442	0.059295	0.1076	0.0034	0.38136
G1	**core**	2.98	0.12	0.2247	0.0051	0.49403	4.450378	0.10101	0.0984	0.0035	0.017021
G1	**core**	3.28	0.11	0.237	0.0033	0.113	4.219409	0.058751	0.1019	0.0035	0.30951
G1	**core**	3.82	0.21	0.2581	0.0097	0.60791	3.874467	0.145612	0.1084	0.0048	0.11441
G1	**core**	3.36	0.11	0.2446	0.0036	0.048775	4.088307	0.060171	0.1013	0.0036	0.37141
G1	**core**	3.65	0.18	0.2591	0.0071	0.39747	3.859514	0.105761	0.1051	0.0047	0.041291
G1	**core**	3.43	0.1	0.2493	0.0037	0.2429	4.011231	0.059533	0.1015	0.0031	0.31423
G1	**core**	3.381	0.095	0.247	0.0034	0.035521	4.048583	0.055729	0.1007	0.0031	0.41089
G1	**core**	3.3	0.15	0.2442	0.0047	0.18525	4.095004	0.078815	0.0996	0.0045	0.26791
G1	**core**	4.14	0.15	0.2777	0.0052	0.20725	3.601008	0.06743	0.1107	0.004	0.22288
G1	**core**	2.8	0.11	0.2229	0.0043	0.4646	4.486317	0.086546	0.0927	0.0036	-0.05637
G1	**core**	4.26	0.15	0.2781	0.0067	0.56857	3.595829	0.086631	0.1099	0.0032	0.25309
G1	**core**	3.7	0.14	0.259	0.0065	0.70086	3.861004	0.096898	0.1033	0.0027	0.042039
G1	**core**	3.82	0.18	0.2683	0.0082	0.37901	3.727171	0.113913	0.106	0.0047	0.35496
G1	**core**	3.64	0.096	0.261	0.0032	0.2352	3.831418	0.046975	0.1027	0.0028	0.20062
G1	**core**	3.51	0.11	0.2566	0.0034	0.28436	3.897116	0.051638	0.1013	0.0031	0.041308
G1	**core**	4.03	0.14	0.2758	0.0041	0.40436	3.625816	0.053901	0.1066	0.003	0.08899
G1	**core**	4.11	0.12	0.28	0.0042	0.52882	3.571429	0.053571	0.1078	0.0029	0.14219
G1	**core**	4.13	0.11	0.2826	0.0042	0.1936	3.53857	0.05259	0.1085	0.0031	0.32237
G1	**core**	3.74	0.12	0.2671	0.0039	0.10698	3.743916	0.054666	0.1035	0.0035	0.28319
G1	**core**	3.96	0.12	0.2747	0.0039	0.26665	3.640335	0.051683	0.1057	0.0029	0.24852

Sample		Final 207_235	± (2σ)	Final 206_238	± (2σ)	Rho	Final 238_206	± (2σ)	Final 207_206	± (2σ)	Rho
G1	**core**	4.18	0.12	0.2833	0.0039	0.28731	3.529827	0.048593	0.1082	0.003	0.28897
G1	**core**	3.99	0.11	0.2757	0.0038	0.18692	3.627131	0.049993	0.1056	0.0028	0.38271
G1	**core**	4.23	0.15	0.2864	0.0057	0.61827	3.49162	0.069491	0.1081	0.0027	-0.0483
G1	**core**	3.92	0.1	0.2762	0.0039	0.4069	3.620565	0.051123	0.1044	0.0026	0.038493
G1	**core**	4.164	0.089	0.2857	0.0033	-0.06073	3.500175	0.040429	0.1071	0.0027	0.50663
G1	**core**	3.9	0.13	0.2763	0.0052	0.56631	3.619254	0.068115	0.1041	0.0026	0.092372
G1	**core**	4.47	0.14	0.2989	0.006	0.58612	3.345601	0.067158	0.1112	0.0031	0.085102
G1	**core**	4.55	0.1	0.2991	0.0036	0.37861	3.343363	0.040241	0.1112	0.0024	0.10802
G1	**core**	4.55	0.14	0.2994	0.0047	0.43333	3.340013	0.052432	0.1113	0.0029	0.18875
G1	**core**	4.17	0.14	0.2882	0.0048	0.021936	3.469813	0.05779	0.1073	0.004	0.41391
G1	**core**	3.56	0.14	0.264	0.0048	0.11942	3.787879	0.068871	0.0997	0.0042	0.29808
G1	**core**	3.98	0.12	0.2803	0.0042	0.24162	3.567606	0.053457	0.1044	0.0033	0.23222
G1	**core**	4.557	0.082	0.301	0.0031	0.22825	3.322259	0.034216	0.1104	0.0021	0.23316
G1	**core**	12.47	0.51	0.49	0.01	0.35698	2.040816	0.041649	0.1889	0.0078	0.1893
G1	**core**	4.53	0.13	0.2985	0.004	0.42553	3.350084	0.044892	0.1093	0.0028	0.018936
G1	**core**	4.24	0.12	0.2915	0.0038	0.27275	3.430532	0.04472	0.1067	0.003	0.17865
G1	**core**	4.59	0.13	0.3059	0.0045	0.032342	3.269042	0.04809	0.1112	0.0035	0.46426
G1	**core**	4.05	0.1	0.2803	0.0037	0.33327	3.567606	0.047093	0.1024	0.0024	0.14214
G1	**core**	4.2	0.1	0.2923	0.0044	0.38721	3.421143	0.051499	0.1056	0.0023	0.23462
G1	**core**	4.68	0.13	0.3069	0.0044	0.59969	3.25839	0.046715	0.1099	0.0024	-0.0133
G1	**core**	4.729	0.095	0.3117	0.0033	0.30057	3.208213	0.033966	0.1108	0.0022	0.30922
G1	**core**	4.45	0.17	0.3052	0.0053	-0.09129	3.27654	0.056899	0.1087	0.0047	0.44272
G1	**core**	4.64	0.14	0.3111	0.0044	0.13804	3.214401	0.045462	0.1098	0.0036	0.27743
G1	**core**	4.83	0.16	0.3194	0.006	0.26735	3.13087	0.058814	0.1119	0.0033	0.26267
G1	**core**	4.62	0.12	0.3107	0.0039	0.30917	3.218539	0.0404	0.1089	0.0024	0.24446
G1	**core**	4.5	0.13	0.3079	0.0039	0.38732	3.247808	0.041138	0.1074	0.0028	0.096413
G1	**core**	4.55	0.14	0.3105	0.005	0.12843	3.220612	0.051862	0.1081	0.0033	0.33867
G1	**core**	4.87	0.14	0.323	0.0052	0.31169	3.095975	0.049842	0.1118	0.003	0.24493
G1	**core**	4.65	0.12	0.3148	0.0041	0.010717	3.17662	0.041373	0.1093	0.003	0.41083
G1	**core**	4.586	0.096	0.31	0.0033	0.32348	3.225806	0.034339	0.1078	0.0022	0.28623
G1	**core**	4.641	0.087	0.3143	0.0037	0.2046	3.181674	0.037455	0.108	0.0021	0.40637
G1	**core**	4.72	0.12	0.3207	0.0037	0.18375	3.118179	0.035975	0.1088	0.0028	0.20611
G1	**core**	4.599	0.096	0.3156	0.0035	0.3805	3.168568	0.035139	0.1073	0.0021	0.19275
G1	**core**	4.91	0.11	0.3237	0.0045	0.5992	3.08928	0.042946	0.1094	0.0019	0.17746
G1	**core**	4.805	0.097	0.3225	0.0035	0.26837	3.100775	0.033652	0.109	0.0023	0.35773
G1	**core**	4.81	0.17	0.325	0.0057	0.34208	3.076923	0.053965	0.1097	0.0038	0.15838
G1	**core**	4.84	0.13	0.3269	0.0041	0.1388	3.059039	0.038367	0.1083	0.003	0.28264
G1	**core**	4.58	0.12	0.3179	0.0032	0.33989	3.145643	0.031664	0.1058	0.0026	-0.01673

Sample		Final 207_235	± (2σ)	Final 206_238	± (2σ)	Rho	Final 238_206	± (2σ)	Final 207_206	± (2σ)	Rho
G1	**core**	0.52	0.1	0.0747	0.0036	0.012194	13.38688	0.645151	0.053	0.011	0.01033
G1	**core**	0.524	0.045	0.075	0.0019	-0.11962	13.33333	0.337778	0.0523	0.0048	0.37232
G1	**rim**	4.78	0.15	0.33	0.0046	0.20296	3.030303	0.042241	0.1066	0.0034	0.25086
G1	**rim**	4.71	0.12	0.3266	0.0042	0.31326	3.061849	0.039375	0.1052	0.0024	0.2399
G1	**rim**	4.84	0.13	0.3258	0.0048	0.34211	3.069368	0.045221	0.1088	0.0026	0.33478
G1	**rim**	4.74	0.11	0.3251	0.0049	0.57816	3.075977	0.046362	0.1064	0.0022	0.19513
G1	**rim**	4.71	0.13	0.3244	0.0042	0.37292	3.082614	0.039911	0.1072	0.0028	0.09527
G1	**rim**	4.52	0.13	0.3238	0.0042	0.25097	3.088326	0.040059	0.1034	0.0031	0.15502
G1	**rim**	4.59	0.11	0.3194	0.0036	0.28883	3.13087	0.035288	0.1057	0.0025	0.2704
G1	**rim**	4.47	0.15	0.3186	0.0046	0.42044	3.138732	0.045318	0.1048	0.003	0.18456
G1	**rim**	4.47	0.11	0.3173	0.0035	0.09308	3.151592	0.034764	0.104	0.0027	0.32701
G1	**rim**	4.574	0.095	0.3162	0.0036	0.47539	3.162555	0.036006	0.1065	0.002	0.085623
G1	**rim**	4.74	0.14	0.3153	0.0045	0.26213	3.171583	0.045265	0.1093	0.003	0.30169
G1	**rim**	4.47	0.14	0.3146	0.0046	0.41512	3.17864	0.046477	0.1039	0.0028	0.13625
G1	**rim**	4.54	0.11	0.3141	0.0042	0.4999	3.183699	0.042571	0.1065	0.0022	0.14874
G1	**rim**	4.627	0.099	0.3141	0.0036	0.35223	3.183699	0.036489	0.1079	0.0021	0.20988
G1	**rim**	4.43	0.14	0.3126	0.0044	0.44834	3.198976	0.045027	0.1052	0.0028	-0.05788
G1	**rim**	4.391	0.097	0.3097	0.0044	0.20685	3.228931	0.045874	0.1049	0.0024	0.38603
G1	**rim**	4.38	0.13	0.3083	0.005	0.35736	3.243594	0.052605	0.1041	0.0029	0.18372
G1	**rim**	4.41	0.11	0.3061	0.0041	0.037374	3.266906	0.043758	0.1062	0.003	0.46421
G1	**rim**	4.34	0.16	0.3059	0.004	0.12895	3.269042	0.042747	0.1052	0.0038	0.21291
G1	**rim**	4.18	0.1	0.3029	0.0037	0.399	3.30142	0.040328	0.1012	0.0022	0.19483
G1	**rim**	4.421	0.086	0.3021	0.0028	0.32956	3.310162	0.03068	0.1069	0.002	0.2414
G1	**rim**	4.33	0.11	0.302	0.0036	0.13922	3.311258	0.039472	0.1057	0.0027	0.38377
G1	**rim**	4.23	0.13	0.3014	0.0044	0.27885	3.31785	0.048436	0.1029	0.0031	0.28079
G1	**rim**	4.25	0.14	0.3004	0.005	0.62519	3.328895	0.055408	0.1031	0.0025	0.018087
G1	**rim**	4.19	0.21	0.2991	0.0061	0.31108	3.343363	0.068186	0.1044	0.005	0.035664
G1	**rim**	4.5	0.31	0.2977	0.0081	0.20605	3.359086	0.091396	0.1125	0.0077	0.227
G1	**rim**	4.25	0.11	0.2948	0.0039	0.17494	3.39213	0.044876	0.106	0.0027	0.36591
G1	**rim**	4.23	0.1	0.2935	0.0045	0.23384	3.407155	0.052239	0.1064	0.0027	0.37212
G1	**rim**	4.14	0.11	0.2915	0.0037	0.34905	3.430532	0.043544	0.1037	0.0025	0.23462
G1	**rim**	4.134	0.083	0.2913	0.0037	0.30959	3.432887	0.043603	0.1045	0.0023	0.39719
G1	**rim**	4.07	0.12	0.2912	0.0057	0.54842	3.434066	0.067219	0.1025	0.0025	0.24761
G1	**rim**	4.05	0.12	0.2884	0.004	0.33634	3.467406	0.048092	0.104	0.0028	0.10945
G1	**rim**	4.012	0.085	0.2871	0.0039	0.21899	3.483107	0.047315	0.1037	0.0021	0.38001
G1	**rim**	3.95	0.11	0.287	0.0047	0.4578	3.484321	0.05706	0.1022	0.0027	0.21843
G1	**rim**	3.86	0.14	0.2813	0.0044	0.26368	3.554924	0.055605	0.1015	0.0037	0.12643

Sample		Final 207_235	± (2σ)	Final 206_238	± (2σ)	Rho	Final 238_206	± (2σ)	Final 207_206	± (2σ)	Rho
G1	**rim**	3.81	0.11	0.2739	0.0053	0.71988	3.650968	0.070647	0.1026	0.002	0.12788
G1	**rim**	3.69	0.1	0.2726	0.0045	0.045951	3.668379	0.060557	0.1014	0.0032	0.4585
G1	**rim**	3.71	0.1	0.2705	0.0045	0.46489	3.696858	0.0615	0.1012	0.0025	0.25653
G1	**rim**	3.663	0.074	0.2699	0.0031	0.53048	3.705076	0.042556	0.1001	0.0017	0.12845
G1	**rim**	3.71	0.12	0.2698	0.0038	0.22681	3.706449	0.052204	0.1015	0.0031	0.24789
G1	**rim**	3.685	0.097	0.2666	0.0038	0.63147	3.750938	0.053464	0.1016	0.0019	0.00874
G1	**rim**	3.61	0.13	0.2633	0.0066	0.79252	3.797949	0.095201	0.1005	0.0021	0.014112
G1	**rim**	3.64	0.13	0.2624	0.0052	0.3323	3.810976	0.075522	0.1033	0.0035	0.26345
G1	**rim**	3.66	0.12	0.2616	0.0041	0.38722	3.82263	0.059911	0.1025	0.0029	0.092318
G1	**rim**	3.435	0.075	0.2562	0.0041	0.66406	3.903201	0.062463	0.0985	0.0017	-0.04816
G1	**rim**	3.46	0.14	0.2531	0.007	0.7941	3.951008	0.109273	0.1005	0.0024	0.040697
G1	**rim**	3.344	0.093	0.2492	0.0034	0.20006	4.012841	0.05475	0.0989	0.0028	0.22312
G1	**rim**	3.34	0.21	0.2456	0.0082	0.66033	4.071661	0.135943	0.1006	0.0052	-0.26493
G1	**rim**	3.254	0.097	0.2453	0.0048	0.65533	4.076641	0.079771	0.0986	0.0019	0.16024
G1	**rim**	3.167	0.099	0.2434	0.0046	0.53938	4.108463	0.077646	0.0967	0.0026	0.20651
G1	**rim**	3.285	0.066	0.243	0.0027	0.29448	4.115226	0.045725	0.0994	0.002	0.16421
G1	**rim**	3.13	0.11	0.2362	0.0052	0.73474	4.2337	0.093206	0.0975	0.0022	-0.01074
G1	**rim**	2.65	0.11	0.2063	0.0056	0.71239	4.84731	0.13158	0.0945	0.003	0.0311
G1	**rim**	2.302	0.062	0.1867	0.0029	0.38794	5.356186	0.083197	0.0914	0.0024	0.13466
G1	**rim**	3.05	0.17	0.1823	0.0033	0.59017	5.485464	0.099298	0.1232	0.0056	-0.3085
G1	**rim**	1.98	0.17	0.167	0.012	0.9149	5.988024	0.430277	0.0899	0.0035	-0.39618
G1	**rim**	1.225	0.08	0.1373	0.003	0.10912	7.283321	0.15914	0.0652	0.0041	0.38446
G1	**rim**	1.4	0.35	0.1177	0.0095	0.003118	8.496177	0.685758	0.088	0.022	0.26983
G1	**rim**	0.71	0.089	0.088	0.0031	0.093738	11.36364	0.40031	0.06	0.0074	0.12625
G1	**rim**	0.63	0.17	0.0788	0.0042	-0.01761	12.69036	0.67639	0.063	0.017	0.26059
G1	**rim**	0.63	0.13	0.0779	0.0043	-0.00719	12.83697	0.708588	0.062	0.014	0.25667
G1	**rim**	0.557	0.016	0.07691	0.00094	0.33243	13.00221	0.158914	0.0536	0.0016	0.14255
G1	**rim**	0.6	0.06	0.0752	0.0022	-0.03392	13.29787	0.389034	0.0592	0.0061	0.38546
G1	**rim**	0.552	0.026	0.07484	0.00088	-0.01565	13.36184	0.157114	0.0546	0.0026	0.28535
G1	**rim**	0.56	0.12	0.0738	0.0039	0.070051	13.55014	0.716064	0.059	0.013	0.17306
G1	**rim**	0.67	0.18	0.0736	0.0047	-0.06214	13.58696	0.867645	0.072	0.02	0.24597
G1	**rim**	0.512	0.087	0.0727	0.0031	0.12049	13.75516	0.586534	0.0534	0.0098	0.12467
G1	**rim**	0.556	0.048	0.0725	0.0018	0.022735	13.7931	0.34245	0.057	0.005	0.25497
G1	**rim**	0.547	0.047	0.072	0.0022	-0.0458	13.88889	0.424383	0.056	0.005	0.36933
G1	**rim**	0.483	0.059	0.0718	0.0024	0.17295	13.92758	0.465546	0.0504	0.0062	0.10717
G1	**rim**	0.6	0.11	0.07	0.003	0.071369	14.28571	0.612245	0.062	0.012	0.12507
G1	**rim**	0.8	0.24	0.0644	0.0054	0.029113	15.52795	1.302033	0.101	0.065	0.34581

Sample		Final 207_235	± (2σ)	Final 206_238	± (2σ)	Rho	Final 238_206	± (2σ)	Final 207_206	± (2σ)	Rho
Z_Plesovice_2	**Std**	0.398	0.028	0.0537	0.001	0.1083	18.62197	0.346778	0.0529	0.0037	0.1058
Z_Plesovice_3	**Std**	0.423	0.03	0.05308	0.00096	0.078286	18.83949	0.340729	0.0579	0.0043	0.20459
Z_Plesovice_4	**Std**	0.407	0.026	0.05229	0.00088	0.023877	19.12412	0.321844	0.0563	0.0038	0.29131
Z_Plesovice_5	**Std**	0.394	0.026	0.0525	0.001	0.029054	19.04762	0.362812	0.0536	0.0037	0.20923
Z_Plesovice_6	**Std**	0.387	0.028	0.0525	0.001	-0.09183	19.04762	0.362812	0.0524	0.0039	0.32972
Z_Plesovice_7	**Std**	0.398	0.031	0.052	0.0011	0.093028	19.23077	0.406805	0.0548	0.0042	0.19759
Z_Plesovice_8	**Std**	0.403	0.028	0.0524	0.0012	0.070858	19.08397	0.437038	0.0556	0.0041	0.22262
Z_Plesovice_9	**Std**	0.392	0.026	0.0515	0.001	0.21079	19.41748	0.377038	0.0542	0.0036	0.088551
Z_Plesovice_10	**Std**	0.385	0.029	0.052	0.0011	0.1023	19.23077	0.406805	0.0523	0.004	0.12803
Z_Plesovice_11	**Std**	0.383	0.03	0.053	0.0011	0.081365	18.86792	0.391598	0.0517	0.0041	0.17451
Z_Plesovice_12	**Std**	0.405	0.028	0.0527	0.001	0.055443	18.97533	0.360063	0.0559	0.0042	0.18688
Z_Plesovice_13	**Std**	0.407	0.025	0.05253	0.00097	0.099982	19.03674	0.351526	0.0544	0.0032	0.24159
Z_Plesovice_14	**Std**	0.39	0.026	0.0532	0.0011	0.077596	18.79699	0.38866	0.0521	0.0035	0.23811
Z_Plesovice_15	**Std**	0.368	0.027	0.0528	0.0011	0.076719	18.93939	0.394571	0.0499	0.0037	0.24001
Z_Plesovice_16	**Std**	0.388	0.026	0.0528	0.0011	0.081226	18.93939	0.394571	0.0528	0.0037	0.16255
Z_Plesovice_17	**Std**	0.401	0.023	0.0533	0.001	0.21484	18.76173	0.352002	0.0543	0.0031	0.088069
Z_Plesovice_18	**Std**	0.4	0.024	0.05405	0.00097	0.048574	18.50139	0.332032	0.0534	0.0032	0.26272
Z_Plesovice_19	**Std**	0.348	0.027	0.0527	0.001	-0.01013	18.97533	0.360063	0.0481	0.0039	0.26545
Z_Plesovice_20	**Std**	0.413	0.028	0.0525	0.0011	0.053397	19.04762	0.399093	0.0566	0.0041	0.21391
Z_Plesovice_21	**Std**	0.361	0.026	0.0533	0.001	-0.13184	18.76173	0.352002	0.05	0.0038	0.38478
	Std										
Z_91500_1	**Std**	1.82	0.17	0.1797	0.0052	0.062621	5.56483	0.16103	0.0715	0.007	0.24362
Z_91500_2	**Std**	1.95	0.18	0.1839	0.0056	0.14699	5.437738	0.165586	0.0765	0.007	0.3986
Z_91500_3	**Std**	1.92	0.19	0.1793	0.0054	0.16036	5.577245	0.167971	0.0777	0.0075	0.087583
Z_91500_4	**Std**	1.86	0.18	0.1785	0.0048	0.080419	5.602241	0.150649	0.0744	0.0071	0.20535
Z_91500_5	**Std**	2	0.2	0.1816	0.0058	0.054722	5.506608	0.175872	0.0808	0.0086	0.24558
Z_91500_6	**Std**	1.82	0.19	0.1813	0.0058	0.16816	5.51572	0.176454	0.0754	0.008	0.16255
Z_91500_7	**Std**	1.92	0.17	0.1731	0.0053	-0.00747	5.777008	0.176881	0.0836	0.0082	0.32743
Z_91500_8	**Std**	1.61	0.18	0.1774	0.0056	0.02761	5.636979	0.177943	0.069	0.0082	0.27566
Z_91500_9	**Std**	1.88	0.16	0.1787	0.0055	0.10106	5.595971	0.172232	0.0745	0.0064	0.406
Z_91500_10	**Std**	1.76	0.17	0.1718	0.0059	0.30067	5.820722	0.199897	0.0735	0.0067	0.097948
Z_91500_11	**Std**	1.81	0.17	0.1807	0.0054	0.078013	5.534034	0.165378	0.0711	0.0065	0.23689
Z_91500_12	**Std**	1.98	0.17	0.1811	0.0054	0.004211	5.521811	0.164648	0.0807	0.0073	0.32078
Z_91500_13	**Std**	1.74	0.19	0.1767	0.0053	0.098514	5.65931	0.169747	0.0725	0.0079	0.1366
Z_91500_14	**Std**	1.78	0.17	0.1808	0.005	0.10772	5.530973	0.152958	0.0697	0.0068	0.13909
Z_91500_15	**Std**	1.73	0.16	0.1758	0.0059	0.00104	5.688282	0.190904	0.0729	0.0074	0.30781
Z_91500_16	**Std**	1.86	0.17	0.1823	0.0054	0.0995	5.485464	0.162488	0.0734	0.0067	0.1845
Z_91500_17	**Std**	1.81	0.17	0.1845	0.0058	0.064902	5.420054	0.170387	0.0736	0.0069	0.26477

Sample		Final 207_235	± (2σ)	Final 206_238	± (2σ)	Rho	Final 238_206	± (2σ)	Final 207_206	± (2σ)	Rho
Z_91500_19	**Std**	1.82	0.19	0.181	0.0056	0.12628	5.524862	0.170935	0.0719	0.0074	0.11333
Z_91500_20	**Std**	1.97	0.17	0.1758	0.0049	0.1889	5.688282	0.158547	0.0798	0.007	0.20818
Z_91500_21	**Std**	2.04	0.18	0.1815	0.0056	-0.04159	5.509642	0.169995	0.0825	0.0075	0.2792
G_NIST612_1	**glass**	30.5	2.6	0.236	0.02	0.40632	4.237288	0.359092	1.05	0.12	0.71053
G_NIST612_2	**glass**	29.4	2.4	0.234	0.018	0.39936	4.273504	0.328731	0.966	0.085	0.5385
G_NIST612_3	**glass**	29.9	2.2	0.226	0.018	0.24959	4.424779	0.352416	1.09	0.11	0.65993
G_NIST612_4	**glass**	28.1	2.2	0.238	0.022	0.39883	4.201681	0.388391	1.02	0.14	0.85075
G_NIST612_5	**glass**	32	2.4	0.235	0.018	0.38057	4.255319	0.325939	1.04	0.1	0.78759
G_NIST612_6	**glass**	33.8	3.1	0.248	0.019	0.34453	4.032258	0.308923	1.05	0.11	0.58361
G_NIST612_7	**glass**	30.7	2.9	0.252	0.018	0.24164	3.968254	0.283447	0.903	0.091	0.53435
G_NIST612_8	**glass**	31.2	2.7	0.252	0.02	0.24233	3.968254	0.314941	0.99	0.1	0.74484
G_NIST612_9	**glass**	31.1	2.2	0.235	0.016	0.28633	4.255319	0.289724	0.991	0.086	0.73201
G_NIST612_10	**glass**	29.8	2.3	0.254	0.017	0.21186	3.937008	0.263501	0.923	0.081	0.45869
G_NIST612_11	**glass**	29.2	2.7	0.257	0.023	0.40799	3.891051	0.348226	0.93	0.12	0.99425
G_NIST612_12	**glass**	30.1	2	0.241	0.018	0.26197	4.149378	0.309912	0.981	0.088	0.64578
G_NIST612_13	**glass**	29.1	2.1	0.252	0.019	0.21446	3.968254	0.299194	0.893	0.081	0.6249
G_NIST612_14	**glass**	30.8	2.5	0.253	0.022	0.33839	3.952569	0.343702	0.98	0.1	0.6658
G_NIST612_15	**glass**	32.1	2.6	0.27	0.02	0.25753	3.703704	0.274348	0.923	0.092	0.69784
G_NIST612_16	**glass**	30.3	2.5	0.262	0.021	0.38857	3.816794	0.305926	0.886	0.072	0.65142
G_NIST612_17	**glass**	30	2.5	0.253	0.019	0.45196	3.952569	0.296833	0.929	0.085	0.89108
G_NIST612_18	**glass**	30.1	2.4	0.268	0.025	0.35056	3.731343	0.348073	0.904	0.091	0.68105
G_NIST612_19	**glass**	28.5	2.4	0.248	0.019	0.28509	4.032258	0.308923	0.901	0.086	0.62866
G_NIST612_20	**glass**	32.1	3.1	0.279	0.022	0.17965	3.584229	0.282627	0.92	0.1	0.60297
G_NIST612_21	**glass**	26.5	1.7	0.232	0.018	0.20176	4.310345	0.334423	0.94	0.089	0.70007

Sample		Final 207_235	± (2σ)	Final 206_238	± (2σ)	Rho	Final 238_206	± (2σ)	Final 207_206	± (2σ)	Rho
G2	Core	6	1.4	0.12	0.015	-0.06383	8.333333	1.041667	0.26	0.3	0.41084
G2	Core	2.01	0.55	0.09	0.01	-0.09947	11.11111	1.234568	0.15	0.17	0.49468
G2	Core	8.13	0.59	0.296	0.013	0.58891	3.378378	0.148375	0.193	0.011	-0.00473
G2	Core	9.24	0.59	0.321	0.01	0.39482	3.115265	0.097049	0.211	0.013	0.18585
G2	Core	6.71	0.31	0.2827	0.0079	0.48548	3.537319	0.09885	0.1701	0.0069	0.11116
G2	Core	7.43	0.35	0.3019	0.0073	0.38241	3.312355	0.080093	0.1745	0.0073	0.16725
G2	Core	7.68	0.25	0.3096	0.0066	0.52074	3.229974	0.068856	0.1785	0.0049	0.14757
G2	Core	8.6	0.63	0.332	0.022	0.94592	3.012048	0.199594	0.1818	0.0067	-0.31732
G2	Core	9.07	0.52	0.353	0.011	0.18564	2.832861	0.088276	0.19	0.012	0.40665
G2	Core	9.16	0.42	0.354	0.01	0.41003	2.824859	0.079798	0.1857	0.0076	0.30116
G2	Core	7.75	0.24	0.3349	0.0074	0.78842	2.985966	0.065978	0.1647	0.0033	-0.08971
G2	Core	10.75	0.47	0.3911	0.0097	0.29149	2.556891	0.063416	0.1997	0.0093	0.26525
G2	Core	9.01	0.41	0.373	0.011	0.69743	2.680965	0.079063	0.1696	0.0054	-0.18119
G2	Core	11.24	0.62	0.423	0.016	0.32508	2.364066	0.089421	0.196	0.012	0.42589
G2	Core	10.14	0.44	0.4	0.011	0.37432	2.5	0.06875	0.1803	0.0075	0.29528
G2	Core	12.52	0.57	0.442	0.012	0.35835	2.262443	0.061424	0.2043	0.0092	0.38179
G2	Core	12.6	0.65	0.449	0.014	0.34045	2.227171	0.069444	0.207	0.011	0.35263
G2	Core	12.47	0.52	0.446	0.011	0.4329	2.242152	0.0553	0.2004	0.0079	0.2607
G2	Core	11.95	0.84	0.442	0.019	0.33396	2.262443	0.097254	0.197	0.014	0.31605
G2	Core	11.63	0.41	0.4312	0.0091	0.47811	2.319109	0.048942	0.1895	0.0056	0.22855
G2	Core	10.44	0.22	0.4199	0.0056	0.35777	2.381519	0.031761	0.1801	0.0036	0.30434
G2	Core	12.65	0.78	0.458	0.015	0.26187	2.183406	0.071509	0.199	0.012	0.2668
G2	Core	10.42	0.64	0.423	0.014	0.38889	2.364066	0.078243	0.178	0.011	0.33784
G2	Core	11.33	0.37	0.4402	0.0086	0.39437	2.271695	0.044381	0.1856	0.0058	0.18493
G2	Core	14.16	0.34	0.4806	0.0093	0.4519	2.080732	0.040264	0.21	0.0047	0.3136
G2	Core	11.13	0.3	0.4374	0.0075	0.4839	2.286237	0.039202	0.1816	0.0042	0.20267
G2	Core	11.16	0.69	0.445	0.018	0.69347	2.247191	0.090898	0.184	0.012	0.35335
G2	Core	12.55	0.41	0.4618	0.0095	0.54278	2.16544	0.044547	0.1937	0.0052	0.16679
G2	Core	14.53	0.32	0.4936	0.0078	0.4543	2.025932	0.032014	0.2122	0.0042	0.22425
G2	Core	4.19	0.28	0.2774	0.0079	0.15125	3.604903	0.102663	0.1087	0.0069	0.29281
G2	Core	12.56	0.36	0.464	0.011	0.57817	2.155172	0.051092	0.1927	0.0046	0.19365
G2	Core	12.86	0.77	0.474	0.018	0.29673	2.109705	0.080115	0.197	0.011	0.29601
G2	Core	13.29	0.33	0.4782	0.0086	0.34586	2.091175	0.037608	0.1991	0.0051	0.34774
G2	Core	13.37	0.44	0.4778	0.0097	0.2928	2.092926	0.042489	0.1984	0.0061	0.29592
G2	Core	10.88	0.32	0.4427	0.0075	0.4109	2.258866	0.038269	0.177	0.0049	0.17198
G2	Core	11.68	0.32	0.4548	0.0085	0.7059	2.198769	0.041094	0.1831	0.0038	-0.03867
G2	Core	12.68	0.47	0.471	0.0095	0.34669	2.123142	0.042823	0.1919	0.0064	0.19714
G2	Core	15.03	0.66	0.508	0.014	0.40401	1.968504	0.05425	0.2138	0.0092	0.28506

Sample		Final 207_235	± (2σ)	Final 206_238	± (2σ)	Rho	Final 238_206	± (2σ)	Final 207_206	± (2σ)	Rho
G2	Core	11.62	0.36	0.4582	0.0095	0.53824	2.182453	0.045249	0.1829	0.0049	0.13583
G2	Core	13.99	0.51	0.494	0.011	0.30314	2.024291	0.045075	0.203	0.0074	0.31854
G2	Core	12.08	0.31	0.4689	0.007	0.45066	2.132651	0.031837	0.1861	0.0041	0.15153
G2	Core	13.19	0.45	0.484	0.01	0.40856	2.066116	0.042688	0.1941	0.0061	0.24733
G2	Core	12.17	0.27	0.4679	0.0076	0.68156	2.137209	0.034714	0.1841	0.003	0.047803
G2	Core	13.65	0.79	0.504	0.018	0.31841	1.984127	0.070862	0.203	0.012	0.31141
G2	Core	12.58	0.64	0.481	0.013	0.40255	2.079002	0.056189	0.1895	0.0092	0.22166
G2	Core	14.52	0.48	0.509	0.01	0.28293	1.964637	0.038598	0.2045	0.0069	0.36108
G2	Core	13.62	0.47	0.497	0.01	0.34083	2.012072	0.040484	0.1975	0.0068	0.23261
G2	Core	16.34	0.53	0.536	0.012	0.3765	1.865672	0.041769	0.2197	0.0067	0.26984
G2	Core	12.64	0.27	0.4831	0.007	0.45136	2.069965	0.029993	0.1878	0.0037	0.20999
G2	Core	12.09	0.57	0.475	0.012	0.33852	2.105263	0.053186	0.1834	0.0082	0.1941
G2	Core	16.41	0.72	0.539	0.014	0.32798	1.855288	0.048189	0.2192	0.0091	0.29322
G2	Core	13.58	0.57	0.501	0.012	0.32132	1.996008	0.047809	0.1968	0.0083	0.24791
G2	Core	11.92	0.51	0.474	0.013	0.34395	2.109705	0.057861	0.1816	0.0077	0.27226
G2	Core	14.19	0.3	0.5092	0.0072	0.44047	1.963865	0.027769	0.1997	0.0036	0.259
G2	Core	13.32	0.5	0.499	0.011	0.4794	2.004008	0.044177	0.1934	0.0066	0.14406
G2	Core	12.66	0.44	0.486	0.012	0.64319	2.057613	0.050805	0.1861	0.0048	0.066617
G2	Core	13.06	0.29	0.4923	0.0073	0.54038	2.031282	0.030121	0.1893	0.0036	0.21285
G2	Core	15.3	0.59	0.529	0.012	0.3787	1.890359	0.042881	0.2081	0.0078	0.25277
G2	Core	15.05	0.64	0.529	0.012	0.29222	1.890359	0.042881	0.2081	0.0089	0.31256
G2	Core	12.59	0.6	0.49	0.015	0.31106	2.040816	0.062474	0.1866	0.0088	0.28163
G2	Core	14.13	0.47	0.5136	0.0097	0.51108	1.94704	0.036772	0.1989	0.0059	0.10175
G2	Core	12.9	0.37	0.4927	0.0087	0.38653	2.029633	0.035839	0.1871	0.0048	0.22715
G2	Core	15.99	0.74	0.544	0.016	0.45446	1.838235	0.054066	0.2139	0.0095	0.35147
G2	Core	15.12	0.72	0.532	0.013	0.25862	1.879699	0.045933	0.2067	0.0099	0.24033
G2	Core	17.59	0.58	0.564	0.012	0.44561	1.77305	0.037724	0.2238	0.0071	0.3053
G2	Core	15.22	0.64	0.536	0.014	0.29307	1.865672	0.04873	0.2071	0.0086	0.3079
G2	Core	15.45	0.74	0.537	0.016	0.39395	1.862197	0.055484	0.2068	0.0093	0.32553
G2	Core	15.37	0.68	0.538	0.015	0.39317	1.858736	0.051824	0.2073	0.0086	0.25624
G2	Core	15.09	0.75	0.534	0.017	0.30602	1.872659	0.059616	0.205	0.01	0.2888
G2	Core	15.05	0.47	0.535	0.011	0.45208	1.869159	0.038431	0.2047	0.006	0.26038
G2	Core	14.61	0.42	0.5257	0.0098	0.33224	1.902226	0.035461	0.1996	0.0059	0.35735
G2	Core	12.99	0.32	0.5001	0.0086	0.33826	1.9996	0.034386	0.1861	0.0046	0.33346
G2	Core	14.55	0.74	0.532	0.018	0.3544	1.879699	0.063599	0.2	0.011	0.3815
G2	Core	14.58	0.61	0.534	0.015	0.30998	1.872659	0.052603	0.2004	0.0085	0.41156
G2	Core	14.46	0.71	0.528	0.015	0.29452	1.893939	0.053805	0.197	0.0092	0.34729
G2	Core	16.18	0.81	0.556	0.016	0.33734	1.798561	0.051757	0.212	0.01	0.31775

Sample		Final 207_235	± (2σ)	Final 206_238	± (2σ)	Rho	Final 238_206	± (2σ)	Final 207_206	± (2σ)	Rho
G2	Core	14.9	0.53	0.537	0.013	0.43224	1.862197	0.045081	0.2015	0.007	0.32648
G2	Core	13.64	0.41	0.52	0.01	0.33089	1.923077	0.036982	0.1881	0.0057	0.34681
G2	Core	14.23	0.46	0.532	0.012	0.45869	1.879699	0.042399	0.1939	0.0059	0.32125
G2	Core	14.76	0.6	0.539	0.014	0.29104	1.855288	0.048189	0.1974	0.0081	0.41564
G2	Core	13.55	0.39	0.524	0.01	0.28438	1.908397	0.03642	0.1862	0.0056	0.3796
G2	Core	10.5	0.3	0.4694	0.0087	0.57547	2.130379	0.039485	0.1614	0.0039	0.043235
G2	Core	15.25	0.58	0.554	0.013	0.2902	1.805054	0.042357	0.1999	0.0079	0.31331
G2	Core	14.22	0.56	0.536	0.012	0.398	1.865672	0.041769	0.1901	0.007	0.25486
G2	Core	17.45	0.42	0.5833	0.0093	0.4905	1.714384	0.027334	0.2122	0.0044	0.2434
G2	Core	16.31	0.66	0.573	0.014	0.35727	1.745201	0.04264	0.2064	0.0084	0.26484
G2	Core	13.07	0.69	0.525	0.018	0.41688	1.904762	0.065306	0.1827	0.0093	0.33138
G2	Core	16.51	0.71	0.576	0.015	0.43079	1.736111	0.045211	0.2053	0.008	0.2591
G2	Core	16.06	0.8	0.573	0.015	0.5035	1.745201	0.045686	0.1987	0.0085	0.057232
G2	Core	17.28	0.37	0.5938	0.009	0.63176	1.684069	0.025525	0.2063	0.0033	0.14659
G2	Core	18.2	3.5	0.768	0.098	0.25532	1.302083	0.166151	0.2	0.037	-0.17321
G2	Core	3.5	1.1	0.108	0.017	-0.02449	9.259259	1.457476	-0.29	0.39	0.38963
G2	Rim	2.11	0.55	0.0825	0.0086	0.040971	12.12121	1.263545	0.2	0.13	0.33819
G2	Rim	4.09	0.82	0.094	0.012	-0.06656	10.6383	1.358081	0.24	0.19	0.5171
G2	Rim	0.813	0.078	0.0972	0.0027	0.061211	10.28807	0.28578	0.0634	0.0061	0.37534
G2	Rim	1.28	0.1	0.1243	0.0048	0.38364	8.045052	0.31067	0.0751	0.0054	0.022649
G2	Rim	1.92	0.48	0.1259	0.0094	0.46043	7.942812	0.59303	0.109	0.022	-0.4711
G2	Rim	1.279	0.077	0.1331	0.0027	0.14356	7.513148	0.152408	0.0693	0.0042	0.18345
G2	Rim	6.1	2.1	0.14	0.029	0.20231	7.142857	1.479592	-0.06	0.34	0.37271
G2	Rim	1.337	0.082	0.1464	0.003	0.077169	6.830601	0.139971	0.0662	0.0042	0.20621
G2	Rim	1.604	0.084	0.1494	0.0032	0.30385	6.69344	0.143367	0.0769	0.004	0.09356
G2	Rim	2.58	0.12	0.191	0.0053	0.63401	5.235602	0.145281	0.0965	0.0036	-0.04014
G2	Rim	3	0.25	0.195	0.0085	0.75759	5.128205	0.223537	0.1065	0.0059	-0.41885
G2	Rim	2.88	0.17	0.2211	0.0058	0.36343	4.52284	0.118645	0.0941	0.0054	0.055851
G2	Rim	3.12	0.1	0.2335	0.0037	0.16473	4.282655	0.067862	0.0948	0.0032	0.29176
G2	Rim	4.65	0.31	0.241	0.0071	0.27992	4.149378	0.122243	0.1362	0.0082	0.26346
G2	Rim	3.77	0.26	0.247	0.01	0.75396	4.048583	0.16391	0.1044	0.0044	-0.35673
G2	Rim	3.54	0.23	0.255	0.012	0.85699	3.921569	0.184544	0.0959	0.0033	-0.32256
G2	Rim	3.85	0.22	0.2685	0.0092	0.71791	3.724395	0.127614	0.0998	0.0036	-0.23539
G2	Rim	3.98	0.18	0.2694	0.0094	0.78109	3.711952	0.129519	0.1028	0.0027	0.14769
G2	Rim	4.03	0.15	0.271	0.0048	0.43031	3.690037	0.065359	0.1055	0.0034	0.091123
G2	Rim	3.9	0.19	0.279	0.0092	0.68813	3.584229	0.11819	0.1002	0.0034	-0.04096
G2	Rim	4.79	0.3	0.281	0.011	0.72852	3.558719	0.139309	0.1172	0.0048	-0.21465

Sample		Final 207_235	± (2σ)	Final 206_238	± (2σ)	Rho	Final 238_206	± (2σ)	Final 207_206	± (2σ)	Rho
G2	Rim	4.67	0.16	0.296	0.0062	0.61773	3.378378	0.070763	0.1125	0.003	0.01233
G2	Rim	4.18	0.16	0.2966	0.0057	0.23019	3.371544	0.064794	0.1013	0.0039	0.25672
G2	Rim	4.51	0.14	0.2994	0.0045	0.26803	3.340013	0.050201	0.1064	0.0032	0.1957
G2	Rim	4.437	0.087	0.3038	0.0046	0.62505	3.291639	0.04984	0.1047	0.0016	0.10849
G2	Rim	4.64	0.13	0.3047	0.0053	0.41145	3.281917	0.057086	0.1089	0.0029	0.16846
G2	Rim	5.58	0.33	0.313	0.011	0.66942	3.194888	0.11228	0.1265	0.005	-0.15267
G2	Rim	4.3	0.2	0.3154	0.009	0.46587	3.170577	0.090473	0.098	0.0035	0.16642
G2	Rim	4.97	0.18	0.3177	0.0068	0.31049	3.147624	0.067371	0.1136	0.0041	0.2631
G2	Rim	5.42	0.21	0.3219	0.0057	0.61004	3.106555	0.055009	0.1204	0.0038	-0.15205
G2	Rim	4.81	0.24	0.3244	0.0084	0.36536	3.082614	0.079821	0.1048	0.0047	0.14734
G2	Rim	6.15	0.38	0.327	0.014	0.49445	3.058104	0.130928	0.1368	0.0079	0.19128
G2	Rim	6.19	0.36	0.33	0.014	0.88456	3.030303	0.128558	0.1299	0.0043	-0.40644
G2	Rim	7.13	0.3	0.3331	0.0078	0.44386	3.002101	0.070298	0.1548	0.0062	0.066617
G2	Rim	7.4	0.24	0.3353	0.0076	0.75894	2.982404	0.0676	0.155	0.0031	-0.06324
G2	Rim	6.53	0.26	0.3366	0.0073	0.64666	2.970885	0.064431	0.1376	0.0041	-0.13086
G2	Rim	7.09	0.25	0.3409	0.0068	0.54736	2.933412	0.058513	0.1477	0.0042	0.043977
G2	Rim	8.21	0.51	0.342	0.011	0.23528	2.923977	0.094046	0.176	0.011	0.26557
G2	Rim	6.65	0.3	0.3524	0.0097	0.77962	2.837684	0.078109	0.1335	0.0042	-0.24276
G2	Rim	7.55	0.51	0.353	0.015	0.76063	2.832861	0.120377	0.1458	0.007	-0.40209
G2	Rim	8.39	0.42	0.364	0.01	0.31559	2.747253	0.075474	0.1643	0.008	0.26691
G2	Rim	9.04	0.37	0.3761	0.0083	0.27216	2.658867	0.058677	0.1727	0.0065	0.18412
G2	Rim	7.96	0.38	0.3775	0.0095	0.45645	2.649007	0.066664	0.1478	0.0059	0.096014
G2	Rim	8.82	0.45	0.3895	0.0094	0.66936	2.567394	0.06196	0.1564	0.0058	-0.24693
G2	Rim	9.71	0.3	0.3952	0.0089	0.50427	2.530364	0.056984	0.1747	0.0048	0.16415
G2	Rim	8.7	0.2	0.4073	0.0064	0.57445	2.455193	0.038579	0.1525	0.0031	0.092881
G2	Rim	9.03	0.41	0.413	0.01	0.71392	2.421308	0.058627	0.1519	0.0049	-0.23388
G2	Rim	8.98	0.23	0.4146	0.008	0.67533	2.411963	0.046541	0.1555	0.0028	0.051367
G2	Rim	9.69	0.44	0.4159	0.0098	0.79212	2.404424	0.056656	0.1625	0.0048	-0.39527
G2	Rim	10.38	0.27	0.4197	0.0083	0.58945	2.382654	0.047119	0.1771	0.0038	0.21357
G2	Rim	7.91	0.31	0.436	0.011	0.64785	2.293578	0.057866	0.1285	0.0038	-0.03307
G2	Rim	11.06	0.23	0.4424	0.0075	0.56891	2.260398	0.03832	0.1798	0.0032	0.21926
G2	Rim	10.36	0.54	0.446	0.014	0.52053	2.242152	0.070381	0.1677	0.008	-0.03637
G2	Rim	10.21	0.46	0.448	0.012	0.33771	2.232143	0.05979	0.1633	0.0073	0.21933
G2	Rim	10.87	0.28	0.4487	0.0082	0.6072	2.228661	0.040729	0.1706	0.0034	0.080782
G2	Rim	11.93	0.38	0.449	0.01	0.52212	2.227171	0.049603	0.1881	0.0053	0.11262
G2	Rim	11.29	0.4	0.4498	0.0091	0.51751	2.22321	0.044978	0.1769	0.005	0.11404
G2	Rim	10.15	0.34	0.4525	0.0099	0.42803	2.209945	0.04835	0.1588	0.005	0.26827
G2	Rim	10.78	0.6	0.462	0.014	0.72062	2.164502	0.065591	0.162	0.0059	-0.29579

Sample		Final 207_235	± (2σ)	Final 206_238	± (2σ)	Rho	Final 238_206	± (2σ)	Final 207_206	± (2σ)	Rho
G2	Rim	11.76	0.27	0.4709	0.0071	0.43461	2.123593	0.032019	0.1805	0.0039	0.18241
G2	Rim	12.05	0.3	0.4788	0.0092	0.54084	2.088555	0.040131	0.182	0.0041	0.24935
G2	Rim	12.45	0.44	0.483	0.012	0.57534	2.070393	0.051438	0.1855	0.0056	0.18775
G2	Rim	12.45	0.48	0.487	0.012	0.43085	2.053388	0.050597	0.182	0.0063	0.23654
G2	Rim	12.37	0.3	0.4901	0.0089	0.56468	2.0404	0.037053	0.1799	0.0038	0.16054
G2	Rim	12.08	0.67	0.496	0.015	0.3689	2.016129	0.060972	0.1771	0.0095	0.22512
G2	Rim	12.42	0.46	0.496	0.012	0.50952	2.016129	0.048777	0.179	0.006	0.23555
G2	Rim	12.66	0.52	0.497	0.011	0.51507	2.012072	0.044533	0.18	0.0068	0.01634
G2	Rim	13.5	0.56	0.497	0.013	0.44587	2.012072	0.05263	0.1937	0.0074	0.19364
G2	Rim	12.61	0.64	0.498	0.014	0.42636	2.008032	0.056451	0.1829	0.0078	0.12406
G2	Rim	12.2	1	0.499	0.024	0.42826	2.004008	0.096385	0.188	0.023	0.98481
G2	Rim	12.48	0.44	0.501	0.011	0.2783	1.996008	0.043825	0.1817	0.0067	0.37127
G2	Rim	12.68	0.4	0.502	0.011	0.67238	1.992032	0.04365	0.1813	0.0043	-0.02317
G2	Rim	12.28	0.41	0.503	0.012	0.60431	1.988072	0.047429	0.1753	0.0046	0.094831
G2	Rim	12.28	0.45	0.504	0.013	0.30104	1.984127	0.051178	0.1764	0.0069	0.4191
G2	Rim	12.8	0.29	0.5071	0.0077	0.51356	1.971998	0.029944	0.1804	0.0036	0.21198
G2	Rim	12.97	0.39	0.5089	0.009	0.49743	1.965023	0.034752	0.1829	0.0045	0.22169
G2	Rim	12.54	0.5	0.51	0.012	0.27322	1.960784	0.046136	0.1748	0.0069	0.34569
G2	Rim	13.22	0.38	0.5116	0.008	0.32015	1.954652	0.030565	0.1841	0.0052	0.26536
G2	Rim	13.93	0.33	0.5121	0.0088	0.54757	1.952744	0.033556	0.1931	0.0038	0.22851
G2	Rim	13.95	0.55	0.513	0.012	0.29374	1.949318	0.045598	0.1901	0.0074	0.37174
G2	Rim	13.15	0.45	0.517	0.012	0.4454	1.934236	0.044895	0.1816	0.0058	0.30078
G2	Rim	14.37	0.36	0.5176	0.0088	0.32854	1.931994	0.032847	0.1968	0.005	0.37576
G2	Rim	13.64	0.45	0.519	0.01	0.29406	1.926782	0.037125	0.184	0.0056	0.3139
G2	Rim	13.65	0.57	0.52	0.013	0.33294	1.923077	0.048077	0.1881	0.008	0.35289
G2	Rim	14.26	0.3	0.5295	0.0081	0.57043	1.888574	0.02889	0.1931	0.0032	0.075153
G2	Rim	15.37	0.71	0.54	0.013	0.037209	1.851852	0.044582	0.2033	0.0098	-0.01359
G2	Rim	14.68	0.39	0.5406	0.0097	0.40813	1.849797	0.033191	0.1958	0.005	0.2554
G2	Rim	14.67	0.51	0.543	0.013	0.27438	1.841621	0.04409	0.1936	0.0072	0.43874
G2	Rim	14.81	0.72	0.543	0.014	0.40935	1.841621	0.047482	0.1973	0.0086	0.23794
G2	Rim	15.85	0.76	0.555	0.017	0.40003	1.801802	0.05519	0.209	0.0096	0.31283
G2	Rim	16.6	0.98	0.603	0.024	0.58116	1.658375	0.066005	0.201	0.012	0.43741

Sample	Final 207_235	± (2σ)	Final 206_238	± (2σ)	Rho	Final 238_206	± (2σ)	Final 207_206	± (2σ)	Rho
Plesovice	0.399	0.032	0.0534	0.0011	0.009032	18.72659	0.385754	0.0542	0.0044	0.22296
Plesovice_1	0.421	0.031	0.05402	0.00097	-0.0055	18.51166	0.332401	0.0548	0.0041	0.21512
Plesovice_2	0.415	0.035	0.0544	0.0011	-0.07046	18.38235	0.371702	0.0549	0.0048	0.36824
Plesovice_3	0.381	0.033	0.0535	0.0011	0.090797	18.69159	0.384313	0.0507	0.0044	0.11962

Sample		Final 207_235	± (2σ)	Final 206_238	± (2σ)	Rho	Final 238_206	± (2σ)	Final 207_206	± (2σ)	Rho
Plesovice_5	0.407	0.036	0.0541	0.0012	0.15376	18.48429	0.410003	0.0548	0.0049	0.075823	
Plesovice_6	0.374	0.025	0.0533	0.0011	-0.01684	18.76173	0.387203	0.0507	0.0035	0.29384	
Plesovice_7	0.395	0.026	0.0539	0.0011	0.041988	18.55288	0.37863	0.0533	0.0037	0.23749	
Plesovice_8	0.359	0.025	0.054	0.0011	0.15718	18.51852	0.377229	0.0492	0.0037	0.12048	
Plesovice_9	0.384	0.029	0.0524	0.0012	0.010339	19.08397	0.437038	0.0537	0.0042	0.24882	
Plesovice_10	0.379	0.026	0.0535	0.001	0.14481	18.69159	0.349376	0.0516	0.0036	0.073641	
Plesovice_11	0.396	0.035	0.0545	0.0012	0.091894	18.34862	0.404006	0.0537	0.0049	0.37013	
Plesovice_12	0.382	0.034	0.0536	0.0012	0.059489	18.65672	0.417688	0.053	0.0047	0.1513	
Plesovice_13	0.415	0.03	0.0525	0.001	0.035733	19.04762	0.362812	0.0573	0.0043	0.16431	
Plesovice_14	0.375	0.034	0.0527	0.0012	-0.01975	18.97533	0.432076	0.0499	0.0045	0.29588	
Plesovice_15	0.367	0.029	0.0541	0.0012	-0.0261	18.48429	0.410003	0.0494	0.004	0.29227	
Plesovice_16	0.373	0.028	0.0538	0.0013	-0.02232	18.58736	0.449137	0.0507	0.004	0.30382	
Plesovice_17	0.551	0.041	0.0526	0.0011	0.31905	19.01141	0.397577	0.073	0.0052	-0.08057	
Plesovice_18	0.455	0.03	0.0574	0.0012	0.26387	17.4216	0.364215	0.0559	0.0036	0.082809	
Plesovice_19	0.366	0.023	0.0528	0.0011	0.029592	18.93939	0.394571	0.0494	0.0032	0.29575	
91500	1.94	0.21	0.197	0.007	0.095971	5.076142	0.180371	0.0751	0.0086	0.28793	
91500_1	7.5	1.6	0.204	0.013	0.66086	4.901961	0.31238	0.193	0.032	-0.09391	
91500_2	2.86	0.29	0.1849	0.0076	0.0118	5.408329	0.2223	0.119	0.013	0.31762	
91500_3	1.88	0.23	0.1798	0.0062	0.064957	5.561735	0.191784	0.075	0.0096	0.26649	
91500_4	2.01	0.21	0.1732	0.0067	0.042124	5.773672	0.223346	0.0897	0.0099	0.21475	
91500_5	1.93	0.25	0.1816	0.0073	-0.01376	5.506608	0.221356	0.084	0.012	0.41071	
91500_6	1.86	0.22	0.1889	0.0071	0.028718	5.293806	0.198973	0.0743	0.0092	0.33631	
91500_7	2.17	0.22	0.1778	0.0059	0.07627	5.624297	0.186633	0.0922	0.0096	0.241	
91500_8	1.82	0.21	0.1883	0.0069	0.19974	5.310674	0.194603	0.0685	0.0078	0.17313	
91500_9	1.97	0.23	0.1834	0.0067	0.049567	5.452563	0.199194	0.0808	0.0099	0.21305	
91500_10	1.97	0.23	0.1812	0.006	0.018158	5.518764	0.182741	0.0813	0.0097	0.35553	
91500_11	1.84	0.21	0.1862	0.0069	0.085002	5.370569	0.199017	0.0743	0.0092	0.38075	
91500_12	88	30	0.81	0.22	0.95315	1.234568	0.335315	0.214	0.04	-0.72738	
91500_13	1.95	0.23	0.1905	0.0076	0.28253	5.249344	0.209423	0.0737	0.0084	0.094488	
91500_14	1.83	0.23	0.1815	0.007	0.038714	5.509642	0.212493	0.0769	0.0099	0.25961	
91500_15	1.97	0.22	0.1884	0.0064	0.025248	5.307856	0.180309	0.0754	0.0086	0.17588	
91500_16	2.03	0.22	0.1805	0.0066	0.068788	5.540166	0.202577	0.0821	0.0093	0.29045	
91500_17	1.8	0.2	0.1778	0.0073	-0.05672	5.624297	0.230919	0.0796	0.0099	0.33369	
91500_18	2.11	0.28	0.183	0.0084	0.055652	5.464481	0.250829	0.089	0.011	0.27593	
91500_19	2.02	0.23	0.1782	0.0062	0.30725	5.611672	0.195243	0.0807	0.0092	0.22479	

Sample		Final 207_235	± (2σ)	Final 206_238	± (2σ)	Rho	Final 238_206	± (2σ)	Final 207_206	± (2σ)	Rho
G3	**core**	4.64	0.28	0.241	0.011	0.92519	4.149378	0.189391	0.1264	0.0038	-0.60806
G3	**core**	6.25	0.36	0.3446	0.0083	0.19272	2.901915	0.069895	0.1188	0.0065	0.27762
G3	**core**	14	1.3	0.476	0.027	0.045378	2.10084	0.119165	0.191	0.02	0.55628
G3	**core**	15.29	0.43	0.519	0.011	0.41665	1.926782	0.040837	0.1942	0.0054	0.22212
G3	**core**	12.54	0.59	0.384	0.012	0.083915	2.604167	0.08138	0.204	0.011	0.46476
G3	**core**	7.85	0.72	0.309	0.024	0.94002	3.236246	0.251359	0.1573	0.0059	-0.49627
G3	**core**	14.7	1.4	0.459	0.02	0.70934	2.178649	0.09493	0.202	0.014	-0.25879
G3	**core**	12.15	0.76	0.422	0.014	0.2393	2.369668	0.078615	0.187	0.012	0.30816
G3	**core**	5.42	0.32	0.3152	0.0073	0.70014	3.172589	0.073477	0.1103	0.0039	-0.24781
G3	**core**	15.35	0.53	0.527	0.012	0.69422	1.897533	0.043208	0.1929	0.0044	0.17501
G3	**core**	11.41	0.93	0.413	0.02	0.93956	2.421308	0.117255	0.1698	0.0069	-0.74902
G3	**core**	17.8	0.54	0.554	0.012	0.36307	1.805054	0.039099	0.2074	0.0062	0.38959
G3	**core**	15.01	0.51	0.5045	0.009	0.806	1.982161	0.035361	0.1882	0.003	-0.20904
G3	**core**	6.22	0.27	0.3436	0.0047	-0.17415	2.910361	0.03981	0.1196	0.005	0.42266
G3	**core**	7.06	0.86	0.331	0.023	0.87964	3.021148	0.209929	0.1282	0.0077	-0.47235
G3	**rim**	13.2	0.38	0.4564	0.0064	0.51521	2.19106	0.030725	0.1892	0.0043	0.14544
G3	**rim**	13.79	0.68	0.492	0.013	0.46796	2.03252	0.053705	0.1782	0.0072	0.16191
G3	**rim**	15.92	0.33	0.5231	0.0049	0.37638	1.91168	0.017907	0.1938	0.0027	0.19215
G3	**rim**	15.1	0.75	0.473	0.014	0.622	2.114165	0.062576	0.2014	0.0077	0.10412
G3	**rim**	1.278	0.082	0.1259	0.0032	0.43579	7.942812	0.201882	0.0651	0.0035	0.00813
G3	**rim**	10.82	0.91	0.421	0.023	-0.15078	2.375297	0.129767	0.158	0.016	0.60028
G3	**rim**	3.78	0.22	0.1929	0.0067	0.55474	5.184033	0.180057	0.1236	0.0061	0.20783
G3	**rim**	15.4	2.6	0.491	0.051	0.40343	2.03666	0.211547	0.204	0.033	0.37943
G3	**rim**	3.38	0.27	0.1916	0.0068	0.68118	5.219207	0.185233	0.1104	0.0068	-0.20778
G3	**rim**	4.64	0.24	0.2455	0.0057	0.23131	4.07332	0.094574	0.1228	0.0056	0.165
G3	**rim**	14.79	0.31	0.4924	0.007	0.29244	2.030869	0.028871	0.1878	0.0037	0.37602
G3	**rim**	3.33	0.25	0.22	0.012	0.70165	4.545455	0.247934	0.0937	0.0053	0.25789
Z_Plesovice_1	**Plesovice**	0.406	0.022	0.05359	0.00094	0.092165	18.6602	0.327311	0.0549	0.0031	0.19822
Z_Plesovice_2	**Plesovice_1**	0.419	0.021	0.05333	0.00091	0.01853	18.75117	0.319962	0.0563	0.0029	0.24825
Z_Plesovice_3	**Plesovice_2**	0.395	0.024	0.05256	0.00086	0.080472	19.02588	0.311306	0.0545	0.0034	0.17624
Z_Plesovice_4	**Plesovice_3**	0.385	0.023	0.05322	0.00092	0.1734	18.78993	0.324817	0.052	0.0031	0.090949
Z_Plesovice_5	**Plesovice_4**	0.403	0.025	0.05348	0.00084	0.080709	18.69858	0.293695	0.0536	0.0033	0.12584
Z_Plesovice_6	**Plesovice_5**	0.402	0.023	0.05342	0.00088	0.11019	18.71958	0.308372	0.0546	0.0031	0.18235
Z_Plesovice_7	**Plesovice_6**	0.404	0.025	0.0526	0.00089	0.19832	19.01141	0.321676	0.0555	0.0036	0.20703
Z_Plesovice_8	**Plesovice_7**	0.389	0.025	0.05342	0.00096	0.065617	18.71958	0.336406	0.0528	0.0034	0.1898
Z_Plesovice_9	**Plesovice_8**	0.412	0.026	0.05474	0.00093	-0.01037	18.26818	0.310365	0.0546	0.0035	0.30789
Z_Plesovice_10	**Plesovice_9**	0.391	0.022	0.05249	0.00087	0.13695	19.05125	0.315767	0.0551	0.0033	0.15928
Z_Plesovice_11	**Plesovice_10**	0.405	0.025	0.05273	0.00085	0.14587	18.96454	0.305706	0.0555	0.0035	0.12626

Sample		Final 207_235	± (2σ)	Final 206_238	± (2σ)	Rho	Final 238_206	± (2σ)	Final 207_206	± (2σ)	Rho
Z_Plesovice_12	**Plesovice_11**	0.371	0.025	0.05459	0.00092	0.11269	18.31837	0.308718	0.0489	0.0033	0.063145
Z_Plesovice_13	**Plesovice_12**	0.404	0.022	0.05433	0.00096	0.040767	18.40604	0.325231	0.0549	0.0031	0.25809
Z_Plesovice_14	**Plesovice_13**	0.412	0.025	0.05401	0.00082	0.079651	18.51509	0.281103	0.0567	0.0036	0.18156
Z_Plesovice_15	**Plesovice_14**	0.398	0.023	0.05479	0.00094	0.048887	18.25151	0.31313	0.0533	0.0032	0.2492
Z_Plesovice_16	**Plesovice_15**	0.404	0.026	0.05395	0.00088	0.12574	18.53568	0.302343	0.0542	0.0035	0.17905
Z_91500_1	**91500**	1.97	0.16	0.1822	0.0043	0.11429	5.488474	0.12953	0.077	0.0063	0.16508
Z_91500_2	**91500_1**	1.87	0.13	0.1791	0.0047	0.010831	5.583473	0.146523	0.0774	0.0059	0.31446
Z_91500_3	**91500_2**	1.77	0.14	0.1803	0.0048	0.066772	5.546312	0.147656	0.0717	0.0061	0.44139
Z_91500_4	**91500_3**	1.78	0.14	0.1743	0.0044	0.11248	5.737235	0.14483	0.0738	0.0059	0.2778
Z_91500_5	**91500_4**	2.02	0.15	0.1805	0.0043	0.17788	5.540166	0.131982	0.0815	0.0063	0.23642
Z_91500_6	**91500_5**	1.78	0.14	0.1807	0.0045	0.13594	5.534034	0.137815	0.0702	0.0054	0.12771
Z_91500_7	**91500_6**	1.9	0.14	0.1804	0.0045	0.17897	5.543237	0.138274	0.0749	0.0054	0.11302
Z_91500_8	**91500_7**	1.72	0.14	0.1741	0.0042	-0.00267	5.743825	0.138564	0.0736	0.0062	0.28998
Z_91500_9	**91500_8**	1.79	0.15	0.1785	0.0045	0.01199	5.602241	0.141233	0.0738	0.0065	0.21118
Z_91500_10	**91500_9**	1.77	0.13	0.1778	0.0046	0.22022	5.624297	0.145511	0.0718	0.0054	0.18554
Z_91500_11	**91500_10**	1.88	0.14	0.1807	0.0047	0.12547	5.534034	0.14394	0.0767	0.0057	0.19945
Z_91500_12	**91500_11**	1.9	0.15	0.1775	0.0042	0.19308	5.633803	0.133307	0.0773	0.0062	0.10238
Z_91500_13	**91500_12**	1.79	0.13	0.1838	0.0043	-0.01253	5.440696	0.127285	0.0708	0.0055	0.28551
Z_91500_14	**91500_13**	1.8	0.14	0.1824	0.0045	0.11184	5.482456	0.135258	0.0718	0.0057	0.19611
Z_91500_15	**91500_14**	1.95	0.15	0.1757	0.0046	0.13955	5.69152	0.14901	0.0807	0.0063	0.252
Z_91500_16	**91500_15**	1.96	0.14	0.1791	0.0042	0.10948	5.583473	0.130936	0.0783	0.0056	0.15934
G_NIST612_1	**612**	33.5	2.3	0.221	0.016	0.26892	4.524887	0.327594	1.041	0.088	0.75735
G_NIST612_2	**612_1**	34.1	2.5	0.255	0.018	0.24278	3.921569	0.276817	0.932	0.081	0.74329
G_NIST612_3	**612_2**	32.7	2.3	0.244	0.017	0.26739	4.098361	0.285542	0.965	0.086	0.82593
G_NIST612_4	**612_3**	30.1	2.4	0.24	0.015	0.14695	4.166667	0.260417	0.855	0.076	0.64721
G_NIST612_5	**612_4**	34.5	2.9	0.216	0.015	0.41122	4.62963	0.321502	1.092	0.092	0.64752
G_NIST612_6	**612_5**	31.3	2.4	0.232	0.018	0.42946	4.310345	0.334423	0.983	0.099	0.8775
G_NIST612_7	**612_6**	31.4	2.1	0.243	0.018	0.33658	4.115226	0.304832	0.947	0.087	0.87308
G_NIST612_8	**612_7**	31.2	2.3	0.219	0.016	0.50326	4.56621	0.333604	0.994	0.074	0.62755
G_NIST612_9	**612_8**	32.3	2.6	0.23	0.019	0.3371	4.347826	0.359168	1.02	0.12	0.66123
G_NIST612_10	**612_9**	32.9	2.8	0.24	0.017	0.43574	4.166667	0.295139	0.944	0.087	0.57063
G_NIST612_11	**612_10**	33.7	2.8	0.243	0.016	0.48914	4.115226	0.270961	0.925	0.083	0.7348
G_NIST612_12	**612_11**	34.6	2.3	0.239	0.019	0.4754	4.1841	0.332627	1.1	0.1	0.73508
G_NIST612_13	**612_12**	34.5	2.5	0.249	0.015	0.44914	4.016064	0.241932	0.901	0.057	0.39001
G_NIST612_14	**612_13**	34.4	2.8	0.252	0.017	0.44542	3.968254	0.2677	0.946	0.086	0.61148
G_NIST612_15	**612_14**	32.8	2.5	0.243	0.015	0.39823	4.115226	0.254026	0.901	0.068	0.42587
G_NIST612_16	**612_15**	33.4	2.6	0.239	0.018	0.24157	4.1841	0.315121	0.965	0.085	0.8458

Sample		Final 207_235	± (2σ)	Final 206_238	± (2σ)	Rho	Final 238_206	± (2σ)	Final 207_206	± (2σ)	Rho
SCAR 2A	**Core**	~~115~~	~~44~~	~~1.62~~	~~0.54~~	~~0.5352~~	~~0.617284~~	~~0.205761~~	~~0.64~~	~~0.31~~	~~0.67213~~
SCAR 2A	**Core**	18.8	1.5	0.611	0.03	0.93253	1.636661	0.08036	0.2015	0.0066	-0.61701
SCAR 2A	**Core**	16.36	0.84	0.586	0.019	0.8385	1.706485	0.05533	0.1938	0.0056	-0.25994
SCAR 2A	**Core**	17.85	0.71	0.608	0.016	0.81405	1.644737	0.043283	0.2041	0.0037	-0.14485
SCAR 2A	**Core**	19.01	0.61	0.628	0.012	0.40952	1.592357	0.030427	0.2168	0.0062	0.29405
SCAR 2A	**Core**	14.6	1.4	0.542	0.035	0.6031	1.845018	0.119143	0.186	0.013	0.17247
SCAR 2A	**Core**	11.78	0.43	0.4964	0.0092	0.51991	2.014504	0.037336	0.1666	0.0049	0.24073
SCAR 2A	**Core**	12.99	0.8	0.523	0.017	0.53587	1.912046	0.062151	0.1789	0.0099	-0.1025
SCAR 2A	**Core**	12.45	0.39	0.5053	0.0087	0.2709	1.979022	0.034074	0.173	0.0049	0.37584
SCAR 2A	**Core**	12.57	0.61	0.505	0.015	0.86062	1.980198	0.058818	0.175	0.0057	-0.45675
SCAR 2A	**Core**	16.23	0.28	0.5635	0.0052	0.60363	1.774623	0.016376	0.2033	0.0021	0.22059
SCAR 2A	**Core**	4.61	0.42	0.319	0.015	0.60937	3.134796	0.147404	0.1083	0.0094	0.21557
SCAR 2A	**Core**	11.51	0.78	0.482	0.022	0.82355	2.074689	0.094695	0.1668	0.0065	-0.41706
SCAR 2A	**Core**	4.45	0.15	0.3031	0.0042	0.17973	3.299241	0.045717	0.1044	0.0034	0.23368
SCAR 2A	**Core**	12.85	0.31	0.5049	0.0072	0.42011	1.98059	0.028244	0.1811	0.0041	0.20825
SCAR 2A	**Core**	12.73	0.31	0.503	0.0069	0.30288	1.988072	0.027272	0.1804	0.004	0.24737
SCAR 2A	**Core**	14.07	0.52	0.529	0.011	0.35889	1.890359	0.039308	0.1933	0.0062	0.30708
SCAR 2A	**Core**	14.15	0.55	0.529	0.011	0.59092	1.890359	0.039308	0.1939	0.0055	0.16891
SCAR 2A	**Core**	12.48	0.58	0.495	0.013	0.43943	2.020202	0.053056	0.1789	0.0074	0.22059
SCAR 2A	**Core**	12.82	0.34	0.5011	0.0093	0.27222	1.99561	0.037037	0.1833	0.0051	0.39415
SCAR 2A	**Core**	13.97	0.24	0.5178	0.0055	0.30845	1.931248	0.020513	0.1921	0.0029	0.33137
SCAR 2A	**Core**	15.49	0.45	0.5389	0.0076	0.51273	1.855632	0.02617	0.2053	0.0042	0.23632
SCAR 2A	**Core**	12.38	0.35	0.4894	0.0075	0.53965	2.043318	0.031314	0.1801	0.0039	0.17987
SCAR 2A	**Core**	12.55	0.43	0.4932	0.0089	0.39725	2.027575	0.036588	0.1824	0.006	0.25528
SCAR 2A	**Core**	12.35	0.98	0.49	0.022	0.5504	2.040816	0.091628	0.181	0.013	0.10208
SCAR 2A	**Core**	10.82	0.26	0.4601	0.0062	0.48866	2.173441	0.029288	0.167	0.003	0.20771
SCAR 2A	**Core**	12.84	0.35	0.5007	0.006	0.40374	1.997204	0.023933	0.1867	0.0042	0.22357
SCAR 2A	**Core**	5.65	0.19	0.339	0.0049	0.29424	2.949853	0.042638	0.1201	0.0042	0.041362
SCAR 2A	**Core**	12.2	0.27	0.4845	0.0062	0.27382	2.063983	0.026412	0.1806	0.0038	0.25596
SCAR 2A	**Core**	11.76	0.43	0.479	0.0089	0.51795	2.087683	0.03879	0.1785	0.0057	0.024125
SCAR 2A	**Core**	11.62	0.46	0.4781	0.0092	0.59051	2.091613	0.040249	0.1794	0.0055	-0.03959
SCAR 2A	**Core**	4.29	0.59	0.29	0.018	0.59332	3.448276	0.214031	0.1058	0.0096	0.60157
SCAR 2A	**Core**	4.26	0.1	0.2882	0.0035	0.60199	3.469813	0.042139	0.1056	0.0021	0.060724
SCAR 2A	**Core**	9.44	0.4	0.4256	0.0082	0.55742	2.349624	0.04527	0.1571	0.0046	0.02473
SCAR 2A	**Core**	12.11	0.25	0.4736	0.0049	0.43441	2.111486	0.021846	0.1804	0.003	0.23594
SCAR 2A	**Core**	8.07	0.65	0.408	0.018	0.068364	2.45098	0.108132	0.15	0.012	0.37715
SCAR 2A	**Core**	12.67	0.63	0.482	0.012	0.4038	2.074689	0.051652	0.185	0.0083	0.21985
SCAR 2A	**Core**	10.95	0.5	0.454	0.013	0.41339	2.202643	0.063071	0.1717	0.0079	-0.0128

Sample		Final 207_235	± (2σ)	Final 206_238	± (2σ)	Rho	Final 238_206	± (2σ)	Final 207_206	± (2σ)	Rho
SCAR 2A	**Core**	8.03	0.38	0.3931	0.0095	0.62825	2.543882	0.061478	0.1451	0.0049	-0.06755
SCAR 2A	**Core**	8.3	0.5	0.404	0.015	0.5179	2.475248	0.091903	0.1515	0.0079	0.049586
SCAR 2A	**Core**	9.12	0.3	0.4145	0.0074	0.22699	2.412545	0.043071	0.1567	0.0051	0.3898
SCAR 2A	**Core**	11.27	0.23	0.4544	0.0059	0.45654	2.200704	0.028574	0.1765	0.0029	0.25727
SCAR 2A	**Core**	10.97	0.28	0.4473	0.0056	0.40591	2.235636	0.027989	0.1735	0.0037	0.10239
SCAR 2A	**Core**	5.99	0.38	0.345	0.012	0.49865	2.898551	0.100819	0.1287	0.0069	0.15844
SCAR 2A	**Core**	11.08	0.39	0.4511	0.0087	0.36985	2.216803	0.042754	0.1766	0.0059	0.22679
SCAR 2A	**Core**	12.94	0.35	0.4773	0.0078	0.69606	2.095118	0.034238	0.1918	0.0032	0.056068
SCAR 2A	**Core**	12.45	0.52	0.4708	0.0082	0.49327	2.124044	0.036995	0.189	0.0059	0.24227
SCAR 2A	**Core**	8.98	0.32	0.4022	0.0079	0.59548	2.486325	0.048836	0.1558	0.0045	-0.26144
SCAR 2A	**Core**	10.23	0.58	0.426	0.013	0.82793	2.347418	0.071635	0.1677	0.0057	-0.45741
SCAR 2A	**Core**	10.31	0.33	0.4267	0.0073	0.55078	2.343567	0.040094	0.1695	0.0041	0.15516
SCAR 2A	**Core**	11.05	0.23	0.449	0.0049	0.33615	2.227171	0.024305	0.1818	0.0026	0.2797
SCAR 2A	**Core**	10.82	0.45	0.434	0.011	0.8447	2.304147	0.0584	0.174	0.0035	-0.19681
SCAR 2A	**Core**	9.45	0.22	0.408	0.0045	0.72079	2.45098	0.027033	0.1615	0.002	0.019078
SCAR 2A	**Core**	10.17	0.27	0.4209	0.0051	0.79879	2.375861	0.028788	0.1686	0.0019	-0.27828
SCAR 2A	**Core**	12.36	0.37	0.4651	0.0069	0.44798	2.150075	0.031897	0.1934	0.0043	0.13845
SCAR 2A	**Core**	12.24	0.53	0.463	0.012	0.48252	2.159827	0.055978	0.1926	0.0073	0.27374
SCAR 2A	**Core**	10.54	0.3	0.4286	0.0066	0.47121	2.333178	0.035929	0.1737	0.0039	0.18801
SCAR 2A	**Core**	9.5	0.37	0.4096	0.0091	0.41595	2.441406	0.05424	0.1641	0.0055	0.24441
SCAR 2A	**Core**	12.23	0.52	0.4525	0.0096	0.67336	2.209945	0.046885	0.1873	0.0049	-0.05533
SCAR 2A	**Core**	5.72	0.31	0.3216	0.0086	0.64396	3.109453	0.083151	0.1253	0.0059	-0.21594
SCAR 2A	**Core**	10.08	0.72	0.419	0.017	0.74769	2.386635	0.096832	0.1698	0.008	-0.04504
SCAR 2A	**Core**	8.46	0.27	0.3895	0.0079	0.35384	2.567394	0.052073	0.1551	0.0049	0.22027
SCAR 2A	**Core**	3.9	0.58	0.282	0.01	0.13764	3.546099	0.125748	0.111	0.016	0.59532
SCAR 2A	**Core**	8.24	0.36	0.3832	0.0084	0.34051	2.609603	0.057204	0.1559	0.0068	0.25708
SCAR 2A	**Core**	11.48	0.41	0.4356	0.0081	0.44598	2.295684	0.042688	0.1842	0.005	0.11938
SCAR 2A	**Core**	10.03	0.31	0.4089	0.0066	0.49096	2.445586	0.039474	0.1724	0.0042	0.19834
SCAR 2A	**Core**	8.16	0.41	0.377	0.011	0.44455	2.65252	0.077394	0.1564	0.0076	-0.00178
SCAR 2A	**Core**	7.23	0.32	0.3518	0.0066	0.45798	2.842524	0.053328	0.1448	0.005	0.10824
SCAR 2A	**Core**	8.68	0.77	0.381	0.018	0.608	2.624672	0.124	0.16	0.01	-0.06198
SCAR 2A	**Core**	8.97	0.34	0.3879	0.0075	0.30853	2.577984	0.049845	0.1647	0.0062	0.21476
SCAR 2A	**Core**	9.97	0.23	0.4052	0.0056	0.31634	2.467917	0.034107	0.175	0.0039	0.23033
SCAR 2A	**Core**	5.61	0.42	0.302	0.017	0.88228	3.311258	0.186395	0.1253	0.0046	-0.08535
SCAR 2A	**Core**	7.82	0.22	0.3604	0.0061	0.74723	2.774695	0.046963	0.1523	0.0025	-0.1753
SCAR 2A	**Core**	8.32	0.34	0.3759	0.0087	0.84022	2.660282	0.061571	0.1607	0.0039	-0.56606
SCAR 2A	**Core**	9.85	0.29	0.4026	0.0064	0.2323	2.483855	0.039485	0.1766	0.005	0.36639
SCAR 2A	**Core**	9.51	0.41	0.397	0.01	0.46534	2.518892	0.063448	0.1749	0.006	0.19855

Sample		Final 207_235	± (2σ)	Final 206_238	± (2σ)	Rho	Final 238_206	± (2σ)	Final 207_206	± (2σ)	Rho
SCAR 2A	**Core?**	4.05	0.33	0.2605	0.0091	0.30295	3.838772	0.134099	0.1104	0.0088	0.22281
SCAR 2A	**Core**	9.67	0.29	0.3954	0.007	0.43104	2.529084	0.044774	0.1744	0.0048	0.19768
SCAR 2A	**Core**	7.79	0.35	0.3603	0.0087	0.36426	2.775465	0.067018	0.1575	0.006	0.080486
SCAR 2A	**Core**	1.6	0.16	0.1571	0.0048	0.089141	6.365372	0.194486	0.0784	0.0076	0.327
SCAR 2A	**Core**	5.52	0.47	0.298	0.013	0.56349	3.355705	0.14639	0.129	0.0091	0.002775
SCAR 2A	**Core**	8.36	0.32	0.3678	0.0088	0.51336	2.718869	0.065052	0.1651	0.0055	0.25991
SCAR 2A	**Core**	9.32	0.24	0.3812	0.0066	0.15763	2.623295	0.045419	0.174	0.0042	0.31048
SCAR 2A	**Core**	10.97	0.59	0.41	0.012	0.89806	2.439024	0.071386	0.1924	0.0034	-0.37279
SCAR 2A	**Core**	4.99	0.41	0.289	0.011	0.35178	3.460208	0.131703	0.1262	0.0086	0.275
SCAR 2A	**Core**	1.673	0.067	0.151	0.002	0.53694	6.622517	0.087715	0.0775	0.0026	-0.1552
SCAR 2A	**Core**	6.89	0.33	0.3347	0.0067	0.22785	2.98775	0.059809	0.1492	0.0064	0.22535
SCAR 2A	**Core**	5.79	0.24	0.3012	0.0068	0.92399	3.320053	0.074955	0.1328	0.002	-0.56956
SCAR 2A	**Core**	9.42	0.32	0.3787	0.0071	0.55616	2.640613	0.049507	0.1764	0.0041	-0.06854
SCAR 2A	**Core**	10.13	0.42	0.3919	0.0081	0.50759	2.551671	0.052739	0.1852	0.0054	0.10649
SCAR 2A	**Core**	1.309	0.09	0.1325	0.0029	0.14845	7.54717	0.165183	0.0732	0.005	0.23155
SCAR 2A	**Core**	8.76	0.29	0.3736	0.0084	0.72268	2.67666	0.060182	0.1746	0.0036	0.012158
SCAR 2A	**Core**	8.87	0.33	0.3689	0.0084	0.63154	2.710762	0.061725	0.1717	0.0045	0.076001
SCAR 2A	**Core**	5.1	0.24	0.2814	0.0064	0.44011	3.55366	0.080822	0.1288	0.0052	0.079509
SCAR 2A	**Core**	7.74	0.38	0.341	0.01	0.79913	2.932551	0.085999	0.1616	0.0048	-0.42132
SCAR 2A	**Core**	7.88	0.24	0.3425	0.0057	0.3557	2.919708	0.048591	0.1631	0.0044	0.27771
SCAR 2A	**Core**	7.99	0.25	0.3492	0.0055	0.45312	2.863688	0.045104	0.1673	0.0041	0.17565
SCAR 2A	**Core**	7.51	0.39	0.3297	0.0094	0.75806	3.03306	0.086475	0.1574	0.0046	-0.02334
SCAR 2A	**Core**	6.01	0.43	0.305	0.011	0.38381	3.278689	0.118248	0.144	0.0094	0.29624
SCAR 2A	**Core**	8.18	0.4	0.3481	0.0097	0.43953	2.872738	0.08005	0.172	0.007	0.096513
SCAR 2A	**Core**	2.61	0.3	0.1981	0.0073	0.32555	5.047956	0.186018	0.097	0.01	0.13137
SCAR 2A	**Core**	7.18	0.34	0.3173	0.0087	0.9264	3.151592	0.086413	0.1551	0.0028	-0.54628
SCAR 2A	**Core**	3.5	0.43	0.239	0.014	0.31349	4.1841	0.245094	0.115	0.013	0.13777
SCAR 2A	**Core**	6.66	0.47	0.306	0.011	0.63059	3.267974	0.117476	0.1503	0.0077	-0.06771
SCAR 2A	**Core**	5.24	0.37	0.278	0.0088	0.33905	3.597122	0.113866	0.1351	0.0091	0.13869
SCAR 2A	**Core**	7.28	0.28	0.3248	0.0069	0.23805	3.078818	0.065406	0.1633	0.0061	0.34897
SCAR 2A	**Core**	6.38	0.31	0.3037	0.0082	0.53793	3.292723	0.088905	0.1504	0.0063	0.028197
SCAR 2A	**Core**	7.29	0.34	0.3209	0.007	0.49116	3.116236	0.067976	0.1642	0.0063	0.16287
SCAR 2A	**Core**	4.73	0.37	0.2643	0.0084	0.3542	3.783579	0.12025	0.1307	0.0097	0.1838
SCAR 2A	**Core**	4.93	0.15	0.2667	0.0042	0.34575	3.749531	0.059048	0.1325	0.0036	-0.01126
SCAR 2A	**Core**	5.66	0.16	0.2845	0.0042	0.28027	3.514938	0.05189	0.1426	0.0039	0.17224
SCAR 2A	**Core**	5.2	0.54	0.269	0.012	0.39272	3.717472	0.165835	0.137	0.012	0.22584
SCAR 2A	**Core**	3.88	0.28	0.2363	0.0066	0.17114	4.231909	0.1182	0.1197	0.0085	0.10167
SCAR 2A	**Core**	1.005	0.083	0.1071	0.0027	0.38602	9.337068	0.235388	0.0705	0.0054	-0.02796

Sample		Final 207_235	± (2σ)	Final 206_238	± (2σ)	Rho	Final 238_206	± (2σ)	Final 207_206	± (2σ)	Rho
SCAR 2A	**Core**	7.17	0.39	0.3049	0.0091	0.72298	3.279764	0.097887	0.1657	0.0061	-0.24599
SCAR 2A	**Core**	5.21	0.19	0.2642	0.0048	0.39092	3.785011	0.068766	0.1398	0.0045	0.38888
SCAR 2A	**Core**	1.91	0.13	0.1579	0.0033	0.10058	6.333122	0.132358	0.0887	0.0058	0.25301
SCAR 2A	**Core**	1.7	0.17	0.1489	0.0049	0.24805	6.715917	0.221007	0.0858	0.0079	0.19648
SCAR 2A	**Core**	3.98	0.15	0.2295	0.0039	0.28664	4.357298	0.074046	0.1241	0.0045	0.047744
SCAR 2A	**Core**	6.69	0.26	0.2944	0.0056	0.30611	3.396739	0.064612	0.1675	0.0056	0.30554
SCAR 2A	**Core**	5.9	0.32	0.2703	0.0084	0.68133	3.699593	0.114971	0.1507	0.0053	-0.03888
SCAR 2A	**Core**	6.33	0.55	0.283	0.012	0.49838	3.533569	0.149833	0.16	0.012	0.20718
SCAR 2A	**Core**	5.2	0.69	0.233	0.018	0.92247	4.291845	0.331559	0.128	0.009	-0.65454
SCAR 2A	**Core**	4.44	0.38	0.2423	0.0089	0.14454	4.127115	0.151594	0.134	0.011	0.33159
SCAR 2A	**Core**	5.18	0.34	0.2539	0.0075	0.50136	3.938558	0.116342	0.144	0.0078	-0.04925
SCAR 2A	**Core**	2.97	0.19	0.1941	0.0057	0.48045	5.151984	0.151295	0.1094	0.006	0.003998
SCAR 2A	**Core**	9.1	1.2	0.331	0.023	0.48424	3.021148	0.209929	0.208	0.032	0.15479
SCAR 2A	**Core**	3.65	0.25	0.2162	0.007	0.49375	4.625347	0.149757	0.1231	0.0069	-0.00854
SCAR 2A	**Core**	4.35	0.94	0.219	0.014	0.89625	4.56621	0.291904	0.125	0.014	0.027617
SCAR 2A	**Core**	5.24	0.21	0.2552	0.0047	0.74237	3.918495	0.072167	0.1492	0.0034	-0.13674
SCAR 2A	**Core**	3.42	0.28	0.2056	0.0064	0.49723	4.863813	0.151403	0.1182	0.0075	0.0967
SCAR 2A	**Core**	3.55	0.17	0.2043	0.0036	0.37669	4.894763	0.086251	0.1199	0.004	0.10146
SCAR 2A	**Core**	2.79	0.27	0.1807	0.0081	0.53394	5.534034	0.248067	0.1073	0.0087	-0.0322
SCAR 2A	**Core?**	3.6	0.44	0.217	0.01	0.090236	4.608295	0.212364	0.129	0.016	0.26108
SCAR 2A	**Core**	2.61	0.2	0.1747	0.0047	0.24383	5.724098	0.153997	0.1084	0.0079	0.23526
SCAR 2A	**Core**	2.46	0.17	0.168	0.0041	0.21613	5.952381	0.145266	0.1057	0.0072	0.13367
SCAR 2A	**Core**	2.71	0.16	0.1752	0.0043	0.33846	5.707763	0.140088	0.1118	0.0061	0.012948
SCAR 2A	**Core**	3.19	0.24	0.1891	0.0052	0.30338	5.288207	0.145419	0.123	0.0079	0.053688
SCAR 2A	**Core**	2.63	0.48	0.172	0.011	0.059062	5.813953	0.371823	0.156	0.031	0.29556
SCAR 2A	**Rim**	3.3	8.3	0.18	0.1	0.05312	5.555556	3.08642	-0.2	0.35	0.46044
SCAR 2A	**Rim**	6.38	0.83	0.458	0.058	0.59819	2.183406	0.276501	0.1089	0.0035	0.26789
SCAR 2A	**Rim**	12.6	1.6	0.562	0.051	0.85347	1.779359	0.161472	0.172	0.016	0.051419
SCAR 2A	**Rim**	18.24	0.93	0.635	0.021	0.79611	1.574803	0.05208	0.2093	0.006	-0.3158
SCAR 2A	**Rim**	4.78	0.94	0.367	0.029	0.046384	2.724796	0.215311	0.117	0.037	0.32894
SCAR 2A	**Rim**	10.3	1.2	0.476	0.041	0.11359	2.10084	0.180955	0.159	0.014	-0.48497
SCAR 2A	**Rim**	14.67	0.48	0.549	0.01	0.51571	1.821494	0.033178	0.1923	0.0055	0.22074
SCAR 2A	**Rim**	13.15	0.48	0.521	0.011	0.50446	1.919386	0.040524	0.1803	0.0051	0.14454
SCAR 2A	**Rim**	13.29	0.46	0.5294	0.0095	0.59352	1.888931	0.033897	0.1868	0.0043	0.096219
SCAR 2A	**Rim**	4.3	0.14	0.2978	0.0039	0.29892	3.357958	0.043976	0.1033	0.0029	0.15765
SCAR 2A	**Rim**	13.75	0.37	0.5161	0.0074	0.5734	1.937609	0.027782	0.1886	0.0039	0.166
SCAR 2A	**Rim**	14.65	0.7	0.524	0.014	0.80033	1.908397	0.050988	0.1938	0.0053	-0.25657
SCAR 2A	**Rim**	12.1	0.56	0.485	0.01	0.58687	2.061856	0.042512	0.1749	0.006	0.020928

Sample		Final 207_235	± (2σ)	Final 206_238	± (2σ)	Rho	Final 238_206	± (2σ)	Final 207_206	± (2σ)	Rho
SCAR 2A	**Rim**	4.193	0.099	0.2912	0.0032	0.2171	3.434066	0.037737	0.1033	0.0023	0.25747
SCAR 2A	**Rim**	8.58	0.28	0.4206	0.0076	0.24344	2.377556	0.042961	0.1482	0.0049	0.29423
SCAR 2A	**Rim**	7.99	0.21	0.4014	0.0045	0.45834	2.491281	0.027929	0.1409	0.0028	0.012635
SCAR 2A	**Rim**	9.42	0.75	0.42	0.016	0.78874	2.380952	0.090703	0.1495	0.0069	-0.30685
SCAR 2A	**Rim**	9.53	0.42	0.434	0.01	0.46515	2.304147	0.053091	0.1556	0.0059	0.20851
SCAR 2A	**Rim**	9.51	0.34	0.4322	0.0089	0.41895	2.313744	0.047645	0.1575	0.0051	0.30186
SCAR 2A	**Rim**	4.25	0.48	0.287	0.019	0.86111	3.484321	0.230669	0.1049	0.0054	0.008149
SCAR 2A	**Rim**	7.97	0.33	0.4009	0.0077	0.43769	2.494388	0.047909	0.1465	0.0053	-0.04961
SCAR 2A	**Rim**	5.6	0.36	0.338	0.012	0.68864	2.95858	0.105038	0.1227	0.0056	0.059364
SCAR 2A	**Rim**	11.31	0.38	0.4602	0.0085	0.42638	2.172968	0.040135	0.1746	0.0045	0.2074
SCAR 2A	**Rim**	11.9	0.42	0.4663	0.0089	0.41803	2.144542	0.040932	0.1802	0.0053	0.13266
SCAR 2A	**Rim**	11.57	0.5	0.458	0.013	0.81331	2.183406	0.061974	0.1788	0.0042	-0.22291
SCAR 2A	**Rim**	8.44	0.17	0.3998	0.0051	0.34157	2.501251	0.031907	0.151	0.0031	0.17513
SCAR 2A	**Rim**	8.13	0.33	0.391	0.0076	0.48885	2.557545	0.049712	0.1472	0.0049	0.12783
SCAR 2A	**Rim**	9.46	0.28	0.4191	0.0074	0.2443	2.386065	0.04213	0.1613	0.0048	0.32873
SCAR 2A	**Rim**	10.5	0.48	0.433	0.012	0.80655	2.309469	0.064004	0.1687	0.004	-0.08868
SCAR 2A	**Rim**	11.9	0.18	0.4687	0.005	0.26947	2.133561	0.02276	0.1875	0.0017	0.11695
SCAR 2A	**Rim**	9.35	0.31	0.4149	0.0073	0.6906	2.410219	0.042407	0.1602	0.0036	0.043473
SCAR 2A	**Rim**	10.39	0.18	0.4344	0.0046	0.39765	2.302026	0.024377	0.1711	0.0029	0.2717
SCAR 2A	**Rim**	11.31	0.48	0.45	0.01	0.3045	2.222222	0.049383	0.1796	0.0072	0.29793
SCAR 2A	**Rim**	11	0.34	0.4442	0.0087	0.41937	2.251238	0.044092	0.1771	0.005	0.056328
SCAR 2A	**Rim**	4.32	0.55	0.283	0.014	0.31502	3.533569	0.174806	0.109	0.011	0.20215
SCAR 2A	**Rim**	10.56	0.33	0.4323	0.0068	0.49714	2.313208	0.036386	0.1721	0.0043	0.16681
SCAR 2A	**Rim**	9.93	0.46	0.416	0.011	0.87587	2.403846	0.063563	0.166	0.0037	-0.20248
SCAR 2A	**Rim**	3.55	0.18	0.256	0.0056	0.23109	3.90625	0.085449	0.1016	0.0051	0.18747
SCAR 2A	**Rim**	11.54	0.31	0.4512	0.0065	0.37809	2.216312	0.031928	0.1873	0.0039	0.15757
SCAR 2A	**Rim**	8.09	0.39	0.3843	0.0095	0.31585	2.602134	0.064325	0.1528	0.007	0.24502
SCAR 2A	**Rim**	8.44	0.27	0.3854	0.0062	0.63198	2.594707	0.041742	0.1543	0.0034	-0.07858
SCAR 2A	**Rim**	6.63	0.21	0.3454	0.0059	0.43051	2.895194	0.049455	0.1364	0.0037	0.15921
SCAR 2A	**Rim**	3.64	0.14	0.2537	0.0046	0.40552	3.941663	0.071469	0.1025	0.0038	0.034036
SCAR 2A	**Rim**	4.69	0.39	0.281	0.014	0.20381	3.558719	0.177303	0.113	0.026	0.313
SCAR 2A	**Rim**	8.73	0.42	0.385	0.011	0.80569	2.597403	0.074212	0.1577	0.0041	-0.22713
SCAR 2A	**Rim**	7.9	0.28	0.3699	0.0079	0.74168	2.703433	0.057738	0.1507	0.0037	-0.19074
SCAR 2A	**Rim**	7.89	0.44	0.371	0.01	0.16414	2.695418	0.072653	0.1514	0.0085	0.32267
SCAR 2A	**Rim**	9.7	0.58	0.405	0.012	0.62939	2.469136	0.07316	0.1719	0.007	-0.11037
SCAR 2A	**Rim**	5.96	0.35	0.321	0.01	0.71406	3.115265	0.097049	0.1311	0.0054	0.12599
SCAR 2A	**Rim**	8.36	0.38	0.3707	0.0078	0.75597	2.697599	0.056761	0.1562	0.0044	-0.26533
SCAR 2A	**Rim**	4.15	0.12	0.2666	0.0042	0.41941	3.750938	0.059092	0.1111	0.003	-0.01594

Sample		Final 207_235	± (2σ)	Final 206_238	± (2σ)	Rho	Final 238_206	± (2σ)	Final 207_206	± (2σ)	Rho
SCAR 2A	**Rim**	9.27	0.26	0.3954	0.0067	0.84812	2.529084	0.042855	0.1713	0.0015	-0.13013
SCAR 2A	**Rim**	4.81	0.47	0.294	0.016	0.097822	3.401361	0.185108	0.1222	0.0099	0.32779
SCAR 2A	**Rim**	4.19	0.43	0.279	0.015	0.62076	3.584229	0.192701	0.117	0.011	0.27463
SCAR 2A	**Rim**	7.98	0.33	0.3662	0.007	0.5585	2.730748	0.052199	0.1575	0.0046	0.033216
SCAR 2A	**Rim**	5.93	0.97	0.294	0.016	0.65879	3.401361	0.185108	0.124	0.009	-0.23853
SCAR 2A	**Rim**	6.75	0.38	0.3386	0.0098	0.53975	2.953337	0.085478	0.145	0.0053	0.05169
SCAR 2A	**Rim**	6.41	0.42	0.3172	0.0085	0.69913	3.152585	0.08448	0.1357	0.0047	-0.46096
SCAR 2A	**Rim**	1.51	0.23	0.1521	0.0066	0.14399	6.574622	0.285289	0.077	0.012	0.033911
SCAR 2A	**Rim**	6.68	0.34	0.3266	0.0073	0.68042	3.061849	0.068437	0.1421	0.0049	-0.1167
SCAR 2A	**Rim**	5.93	0.45	0.321	0.011	0.23942	3.115265	0.106754	0.142	0.011	0.29265
SCAR 2A	**Rim**	8.03	0.22	0.3615	0.0066	0.70517	2.766252	0.050504	0.1643	0.0025	0.12322
SCAR 2A	**Rim**	3.07	0.27	0.231	0.012	0.50955	4.329004	0.224883	0.1044	0.0057	0.29131
SCAR 2A	**Rim**	2.95	0.46	0.218	0.011	0.32055	4.587156	0.231462	0.1	0.017	0.11428
SCAR 2A	**Rim**	7.38	0.47	0.339	0.012	0.52139	2.949853	0.10442	0.1568	0.0071	-0.04595
SCAR 2A	**Rim**	8.68	0.3	0.3657	0.0073	0.41692	2.734482	0.054585	0.1729	0.0053	0.20482
SCAR 2A	**Rim**	6.11	0.33	0.3033	0.0072	0.6657	3.297066	0.078269	0.1391	0.0056	-0.26106
SCAR 2A	**Rim**	6.01	0.41	0.3072	0.0098	0.5754	3.255208	0.103845	0.1416	0.0075	-0.05912
SCAR 2A	**Rim**	5.56	0.18	0.2942	0.0053	0.28678	3.399048	0.061234	0.1355	0.0043	0.16667
SCAR 2A	**Rim**	3.42	0.16	0.2295	0.0053	0.24151	4.357298	0.100626	0.1073	0.005	0.22598
SCAR 2A	**Rim**	6.93	0.38	0.3293	0.0083	0.26971	3.036745	0.076541	0.158	0.0071	0.12938
SCAR 2A	**Rim**	2.71	0.19	0.2048	0.0053	0.03513	4.882812	0.126362	0.0984	0.0054	-0.01627
SCAR 2A	**Rim**	2	0.31	0.168	0.0069	0.058389	5.952381	0.244473	0.086	0.014	-0.3818
SCAR 2A	**Rim**	1.321	0.044	0.1278	0.0019	0.15004	7.824726	0.11633	0.0739	0.0025	0.16918
SCAR 2A	**Rim**	3.64	0.46	0.235	0.013	-0.07748	4.255319	0.235401	0.112	0.014	0.25844
SCAR 2A	**Rim**	4.77	0.47	0.267	0.013	0.44688	3.745318	0.182356	0.127	0.01	0.052095
SCAR 2A	**Rim**	4.87	0.29	0.2696	0.0079	0.62597	3.709199	0.108689	0.1288	0.0052	0.013642
SCAR 2A	**Rim**	5.52	0.22	0.2852	0.0044	0.41911	3.506311	0.054095	0.137	0.0044	0.036902
SCAR 2A	**Rim**	7.51	0.21	0.3335	0.0051	0.89535	2.998501	0.045854	0.1658	0.0019	-0.14942
SCAR 2A	**Rim**	1.76	0.1	0.1569	0.0043	0.42549	6.373486	0.174672	0.0835	0.0037	0.095518
SCAR 2A	**Rim**	7.73	0.16	0.3359	0.0063	0.6512	2.977077	0.055837	0.1699	0.0018	0.031539
SCAR 2A	**Rim**	3.76	0.27	0.2349	0.0074	0.37644	4.257131	0.134111	0.1147	0.0069	0.16071
SCAR 2A	**Rim**	5.16	0.42	0.272	0.011	0.46651	3.676471	0.148681	0.1334	0.0094	0.064906
SCAR 2A	**Rim**	3.54	0.3	0.2272	0.0085	0.3882	4.401408	0.164665	0.1125	0.0085	0.089111
SCAR 2A	**Rim**	9.42	0.35	0.3555	0.0069	0.29171	2.81294	0.054597	0.1914	0.0069	0.12837
SCAR 2A	**Rim**	2.59	0.14	0.1857	0.0045	0.37576	5.38503	0.130493	0.0986	0.0049	0.09179
SCAR 2A	**Rim**	7.3	0.39	0.3084	0.0088	0.64118	3.242542	0.092524	0.167	0.0059	0.11022
SCAR 2A	**Rim**	4.88	0.27	0.258	0.0068	0.29087	3.875969	0.102157	0.1348	0.0072	0.22095
SCAR 2A	**Rim**	3.27	0.41	0.2179	0.0096	0.22491	4.589261	0.202189	0.114	0.014	0.30631

Sample		Final 207_235	± (2σ)	Final 206_238	± (2σ)	Rho	Final 238_206	± (2σ)	Final 207_206	± (2σ)	Rho
SCAR 2A	**Rim**	~~31~~	~~14~~	~~0.89~~	~~0.22~~	~~0.66942~~	~~1.123596~~	~~0.277743~~	~~1.9~~	~~2.3~~	~~0.44401~~
SCAR 2A	**Rim**	17.8	9.6	0.313	0.043	0.97613	3.194888	0.438914	0.178	0.014	-0.3829
SCAR 2A	**Rim**	3.31	0.26	0.2143	0.0065	0.12428	4.666356	0.141537	0.1152	0.009	0.3199
SCAR 2A	**Rim**	3.6	0.59	0.212	0.015	0.2248	4.716981	0.333749	0.118	0.031	0.41269
SCAR 2A	**Rim**	4.15	0.17	0.2257	0.0052	0.71103	4.43066	0.10208	0.1342	0.0032	-0.11783
SCAR 2A	**Rim**	4.7	0.13	0.24	0.0034	0.4155	4.166667	0.059028	0.1444	0.0035	0.1494
SCAR 2A	**Rim**	3.11	0.34	0.2004	0.0089	0.20513	4.99002	0.221613	0.119	0.013	0.29247
SCAR 2A	**Rim**	3.69	0.25	0.2109	0.0064	0.29318	4.741584	0.143889	0.126	0.0075	0.13434
SCAR 2A	**Rim**	2.71	0.1	0.1765	0.0029	0.28967	5.665722	0.093091	0.1097	0.004	0.02443
SCAR 2A	**Rim**	6.4	1.9	0.243	0.034	-0.41238	4.115226	0.575793	0.169	0.038	0.20277
Z_Plesovice_1		0.376	0.024	0.05195	0.00083	-0.06692	19.24928	0.307544	0.0524	0.0035	0.27616
Z_Plesovice_2		0.39	0.028	0.05532	0.00091	0.099916	18.07664	0.297356	0.0509	0.0037	0.13884
Z_Plesovice_3		0.348	0.023	0.05321	0.00086	0.061213	18.79346	0.303747	0.0478	0.0032	0.17776
Z_Plesovice_4		0.395	0.025	0.05304	0.0009	-0.14782	18.8537	0.319916	0.0535	0.0035	0.3783
Z_Plesovice_5		0.384	0.027	0.05327	0.00084	0.16537	18.77229	0.296015	0.051	0.0034	0.1174
Z_Plesovice_6		0.386	0.024	0.05357	0.00081	0.18896	18.66716	0.282255	0.0521	0.0032	0.070087
Z_Plesovice_7		0.394	0.025	0.05318	0.00082	0.15528	18.80406	0.289946	0.0526	0.0033	0.10172
Z_Plesovice_8		0.357	0.022	0.05359	0.00093	0.066656	18.6602	0.323829	0.0474	0.003	0.2382
Z_Plesovice_9		0.365	0.021	0.05324	0.00088	-0.05758	18.78287	0.310461	0.0497	0.003	0.34854
Z_Plesovice_10		0.383	0.021	0.05257	0.00073	0.067601	19.02226	0.264148	0.0517	0.0028	0.21462
Z_Plesovice_11		0.402	0.021	0.05544	0.00076	0.12261	18.03752	0.247268	0.0521	0.0026	0.1778
Z_Plesovice_12		0.413	0.016	0.05424	0.00052	0.2505	18.43658	0.176752	0.0544	0.002	-0.00578
Z_Plesovice_13		0.413	0.017	0.05531	0.00067	0.1761	18.07991	0.219012	0.0531	0.002	0.24902
Z_Plesovice_14		0.378	0.021	0.05404	0.00089	0.13068	18.50481	0.304761	0.0504	0.0029	0.24411
Z_Plesovice_15		0.397	0.024	0.05375	0.00081	-0.01079	18.60465	0.280368	0.0523	0.003	0.2874
Z_Plesovice_16		0.388	0.022	0.05337	0.00084	-0.04905	18.73712	0.294907	0.0524	0.0031	0.32421
Z_Plesovice_17		0.406	0.022	0.05544	0.00087	0.21409	18.03752	0.283056	0.0522	0.0027	0.18237
Z_Plesovice_18		0.399	0.016	0.05382	0.00057	0.25909	18.58045	0.196783	0.0521	0.0019	0.095529
Z_Plesovice_19		0.39	0.017	0.05458	0.00066	0.13345	18.32173	0.221553	0.0518	0.0022	0.16072
Z_Plesovice_20		0.388	0.016	0.05398	0.00061	0.06672	18.52538	0.209346	0.0515	0.0021	0.19282
Z_91500_1		1.83	0.13	0.1773	0.0038	0.13666	5.640158	0.120883	0.0764	0.0057	0.21498
Z_91500_2		1.82	0.14	0.1788	0.0042	0.2251	5.592841	0.131376	0.0741	0.0058	0.14656
Z_91500_3		1.81	0.13	0.1809	0.0041	0.047463	5.527916	0.125287	0.0732	0.0052	0.24654
Z_91500_4		1.85	0.14	0.18	0.0035	0.33112	5.555556	0.108025	0.0739	0.0056	-0.08853
Z_91500_5		1.86	0.13	0.1807	0.004	0.14336	5.534034	0.122502	0.0742	0.005	0.18238
Z_91500_6		1.86	0.15	0.176	0.0043	0.024607	5.681818	0.138817	0.0771	0.0064	0.084756
Z_91500_7		1.86	0.14	0.1811	0.0039	0.08983	5.521811	0.118913	0.0717	0.0052	0.24509
Z_91500_8		1.88	0.14	0.1804	0.0042	0.11372	5.543237	0.129055	0.075	0.0055	0.28349

Sample	Final 207_235	± (2σ)	Final 206_238	± (2σ)	Rho	Final 238_206	± (2σ)	Final 207_206	± (2σ)	Rho
Z_91500_9	1.97	0.13	0.1797	0.0043	0.036075	5.56483	0.13316	0.0789	0.0054	0.27292
Z_91500_10	1.76	0.13	0.1782	0.0038	0.079208	5.611672	0.119665	0.0727	0.0054	0.20157
Z_91500_11	1.93	0.14	0.1776	0.0041	0.076495	5.630631	0.129986	0.0783	0.0057	0.29296
Z_91500_12	1.8	0.13	0.1762	0.004	-0.03701	5.675369	0.128839	0.0745	0.0055	0.37231
Z_91500_13	1.81	0.13	0.1809	0.0041	0.11737	5.527916	0.125287	0.0735	0.0053	0.32145
Z_91500_14	1.94	0.14	0.1815	0.0046	0.032079	5.509642	0.139638	0.0781	0.0056	0.29555
Z_91500_15	2.02	0.15	0.1775	0.0043	0.2311	5.633803	0.136481	0.081	0.0059	0.10596
Z_91500_16	1.8	0.12	0.1796	0.0042	0.18142	5.567929	0.130208	0.0723	0.0048	0.1233
Z_91500_17	1.92	0.14	0.1806	0.0037	0.14081	5.537099	0.11344	0.0764	0.0054	0.1485
Z_91500_18	1.79	0.12	0.1771	0.0042	-0.03026	5.646527	0.13391	0.0736	0.0054	0.37334
Z_91500_19	1.72	0.13	0.1784	0.004	0.072884	5.605381	0.125681	0.0702	0.0055	0.24767
Z_91500_20	1.88	0.13	0.1806	0.0041	0.15624	5.537099	0.125704	0.0758	0.0054	0.23226
G_NIST612_1	14.19	0.55	0.1166	0.0048	0.23179	8.576329	0.353056	0.908	0.049	0.65888
G_NIST612_2	14.32	0.62	0.1171	0.0047	0.13611	8.53971	0.342755	0.92	0.051	0.70223
G_NIST612_3	14.75	0.64	0.1219	0.0054	0.043803	8.203445	0.363401	0.899	0.052	0.78764
G_NIST612_4	15.84	0.67	0.1304	0.0046	0.14827	7.668712	0.270522	0.914	0.053	0.7373
G_NIST612_5	21.46	0.91	0.1778	0.0079	0.24713	5.624297	0.249899	0.934	0.057	0.88416
G_NIST612_6	28.1	1.3	0.226	0.01	0.30483	4.424779	0.195787	0.96	0.057	0.80983
G_NIST612_7	28.1	1.1	0.223	0.01	0.21293	4.484305	0.20109	0.956	0.055	0.82475
G_NIST612_8	28	1.2	0.225	0.01	0.34244	4.444444	0.197531	0.938	0.05	0.6786
G_NIST612_9	29	1.3	0.2326	0.0096	0.25358	4.299226	0.17744	0.934	0.048	0.55541
G_NIST612_10	27.8	1.2	0.219	0.01	0.29965	4.56621	0.208503	0.958	0.052	0.48247
G_NIST612_11	27.4	1.2	0.225	0.01	0.36091	4.444444	0.197531	0.916	0.049	0.68478
G_NIST612_12	28.7	1.4	0.234	0.011	0.43204	4.273504	0.200891	0.908	0.048	0.56712
G_NIST612_13	26.1	1.2	0.2153	0.0098	0.45824	4.644682	0.211416	0.919	0.05	0.75997
G_NIST612_14	27.5	1.2	0.2251	0.0093	0.39886	4.44247	0.183541	0.915	0.046	0.58785
G_NIST612_15	28.7	1.2	0.2297	0.0096	0.33658	4.353505	0.181949	0.942	0.047	0.63722
G_NIST612_16	27.8	1.2	0.231	0.011	0.44587	4.329004	0.206143	0.924	0.05	0.93069
G_NIST612_17	28.4	1.2	0.23	0.01	0.39405	4.347826	0.189036	0.929	0.044	0.52218
G_NIST612_18	27.8	1.2	0.2265	0.0099	0.27082	4.415011	0.192974	0.934	0.051	0.62796
G_NIST612_19	15.34	0.63	0.1257	0.0052	0.17999	7.955449	0.329104	0.926	0.049	0.60689
G_NIST612_20	22.43	0.97	0.1828	0.0081	0.38308	5.47046	0.2424	0.922	0.047	0.7115
Z_Plesovice_1	0.403	0.019	0.05369	0.00071	0.053104	18.62544	0.246304	0.0545	0.0025	0.28501
Z_Plesovice_2	0.405	0.019	0.05367	0.00056	0.12291	18.63238	0.194413	0.0548	0.0025	0.20613
Z_Plesovice_3	0.384	0.018	0.05372	0.00066	0.12063	18.61504	0.228703	0.0524	0.0023	0.14443
Z_Plesovice_4	0.39	0.019	0.05363	0.00059	0.12039	18.64628	0.205133	0.054	0.0026	0.097508
Z_Plesovice_5	0.382	0.017	0.05373	0.00063	0.05705	18.61158	0.218226	0.0511	0.0022	0.20169
Z_Plesovice_6	0.396	0.019	0.05364	0.00064	0.08931	18.6428	0.222435	0.0528	0.0023	0.18433

Sample	Final 207_235	± (2σ)	Final 206_238	± (2σ)	Rho	Final 238_206	± (2σ)	Final 207_206	± (2σ)	Rho
Z_Plesovice_7	0.397	0.019	0.0537	0.00061	0.025854	18.62197	0.211535	0.0529	0.0025	0.21505
Z_Plesovice_8	0.402	0.02	0.05373	0.00062	0.11322	18.61158	0.214762	0.0544	0.0025	0.22054
Z_Plesovice_9	0.392	0.019	0.05352	0.00065	-0.0074	18.6846	0.226924	0.0531	0.0023	0.30838
Z_Plesovice_10	0.407	0.018	0.05388	0.00068	0.11979	18.55976	0.234236	0.0536	0.0023	0.28385
Z_Plesovice_11	0.395	0.019	0.05362	0.00065	0.12278	18.64976	0.226079	0.0529	0.0025	0.14724
Z_Plesovice_12	0.376	0.018	0.05364	0.00065	0.029758	18.6428	0.22591	0.052	0.0025	0.25983
Z_Plesovice_13	0.403	0.02	0.05374	0.00061	0.011097	18.60811	0.21122	0.055	0.0027	0.27618
Z_Plesovice_14	0.386	0.02	0.0536	0.0007	0.075592	18.65672	0.243651	0.0528	0.0026	0.20899
Z_Plesovice_15	0.399	0.019	0.0537	0.00066	0.12464	18.62197	0.228873	0.054	0.0024	0.25493
Z_Plesovice_16	0.376	0.019	0.05372	0.00064	0.15762	18.61504	0.221773	0.0505	0.0024	0.10319
Z_Plesovice_17	0.386	0.019	0.05366	0.00061	0.24266	18.63586	0.21185	0.0526	0.0024	0.031959
Z_Plesovice_18	0.397	0.021	0.05363	0.00067	0.095379	18.64628	0.232948	0.0547	0.0027	0.24023
Z_Plesovice_19	0.401	0.022	0.05369	0.00068	0.1539	18.62544	0.235897	0.0538	0.0027	0.14466
Z_Plesovice_20	0.414	0.022	0.0537	0.00066	0.28192	18.62197	0.228873	0.0545	0.0025	0.057495
Z_91500_1	1.83	0.13	0.1732	0.0039	0.16166	5.773672	0.130008	0.076	0.0052	0.15821
Z_91500_2	1.74	0.14	0.1784	0.0043	0.33616	5.605381	0.135107	0.0716	0.0052	-0.01264
Z_91500_3	1.88	0.15	0.1841	0.0042	0.11961	5.431831	0.12392	0.0755	0.0057	0.30318
Z_91500_4	1.83	0.13	0.1788	0.0041	0.095414	5.592841	0.128248	0.0774	0.0055	0.22105
Z_91500_5	1.82	0.13	0.1792	0.0042	0.031646	5.580357	0.13079	0.0768	0.0058	0.35816
Z_91500_6	1.89	0.15	0.1802	0.0041	0.064585	5.54939	0.126263	0.076	0.0054	0.25318
Z_91500_7	2.02	0.17	0.1793	0.0041	0.074288	5.577245	0.127533	0.0813	0.0066	0.25513
Z_91500_8	1.95	0.16	0.1788	0.0044	0.19436	5.592841	0.137631	0.0792	0.0064	0.22305
Z_91500_9	1.86	0.16	0.184	0.0044	0.086109	5.434783	0.129962	0.0764	0.0062	0.15896
Z_91500_10	1.75	0.14	0.1693	0.0036	0.14037	5.906675	0.1256	0.0725	0.0055	0.14699
Z_91500_11	1.95	0.14	0.1738	0.0042	0.13417	5.75374	0.139043	0.0788	0.0055	0.25127
Z_91500_12	1.91	0.16	0.1768	0.0042	0.13022	5.656109	0.134365	0.0781	0.0062	0.1257
Z_91500_13	1.81	0.16	0.1758	0.0042	0.074402	5.688282	0.135898	0.0735	0.0063	0.29954
Z_91500_14	1.86	0.14	0.1804	0.0041	0.016651	5.543237	0.125983	0.0757	0.0058	0.2774
Z_91500_15	1.8	0.14	0.1766	0.0041	0.17692	5.662514	0.131463	0.0739	0.0056	0.1193
Z_91500_16	1.91	0.14	0.1765	0.0038	0.11089	5.665722	0.121982	0.078	0.0059	0.20413
Z_91500_17	1.77	0.14	0.1796	0.0041	0.056728	5.567929	0.127108	0.0745	0.0058	0.31715
Z_91500_18	1.9	0.15	0.1815	0.0044	0.13408	5.509642	0.133567	0.0795	0.0063	0.1105
Z_91500_19	2	0.14	0.1824	0.0042	0.037085	5.482456	0.126241	0.0825	0.0062	0.34524
Z_91500_20	1.69	0.15	0.1801	0.0042	0.01875	5.552471	0.129486	0.0692	0.006	0.20531
G_NIST612_1	26.5	1.4	0.211	0.01	0.58413	4.739336	0.224613	0.979	0.053	0.80385
G_NIST612_2	28.9	1.7	0.234	0.012	0.80972	4.273504	0.219154	0.929	0.044	0.66033
G_NIST612_3	27.7	1.6	0.222	0.011	0.691	4.504505	0.223196	0.95	0.048	0.6211
G_NIST612_4	27.5	1.5	0.2199	0.0098	0.42016	4.547522	0.202664	0.956	0.051	0.66571

Sample	Final 207_235	± (2σ)	Final 206_238	± (2σ)	Rho	Final 238_206	± (2σ)	Final 207_206	± (2σ)	Rho
G_NIST612_5	27.8	1.5	0.223	0.012	0.66184	4.484305	0.241308	0.966	0.05	0.63012
G_NIST612_6	27.8	1.7	0.224	0.011	0.7003	4.464286	0.219228	0.946	0.053	0.71115
G_NIST612_7	28.3	1.6	0.228	0.011	0.70963	4.385965	0.211604	0.944	0.05	0.60384
G_NIST612_8	28	1.7	0.224	0.012	0.63658	4.464286	0.239158	0.992	0.06	0.64709
G_NIST612_9	28.2	1.6	0.237	0.012	0.59605	4.219409	0.213641	0.929	0.055	0.82792
G_NIST612_10	28.2	1.5	0.216	0.011	0.49739	4.62963	0.235768	0.996	0.058	0.63993
G_NIST612_11	27.6	1.6	0.218	0.011	0.57444	4.587156	0.231462	0.946	0.049	0.56654
G_NIST612_12	28.3	1.8	0.231	0.01	0.47416	4.329004	0.187403	0.943	0.058	0.79756
G_NIST612_13	28.9	1.8	0.232	0.014	0.62502	4.310345	0.260107	0.982	0.056	0.44887
G_NIST612_14	29.9	2.2	0.226	0.011	0.46364	4.424779	0.215365	0.983	0.055	0.42748
G_NIST612_15	28.9	2.1	0.228	0.012	0.5407	4.385965	0.23084	0.971	0.055	0.44616
G_NIST612_16	28.6	1.6	0.224	0.011	0.68306	4.464286	0.219228	0.972	0.052	0.74648
G_NIST612_17	28.7	1.6	0.231	0.011	0.56621	4.329004	0.206143	0.976	0.054	0.61065
G_NIST612_18	29.1	1.8	0.219	0.011	0.38448	4.56621	0.229353	1.07	0.078	0.88513
G_NIST612_19	28.6	1.7	0.235	0.012	0.65571	4.255319	0.217293	0.964	0.053	0.66285
G_NIST612_20	29.4	2.5	0.225	0.013	0.68416	4.444444	0.25679	0.95	0.051	0.74666

	La		Ce		Pr		Nd		Sm		Eu		Gd	
	ppm	*RSD%*	ppm	RSD%	ppm	*RSD%*	ppm	*RSD%*	ppm	*RSD%*	ppm	*RSD%*	ppm	*RSD%*
Samples names														
SCAR 2	1.41	*1.31*	3.68	1.12	0.61	*1.71*	3.28	*2.24*	1.26	*1.51*	0.55	*1.97*	1.82	*1.48*
SCAR 3	3.05	*1.21*	9.99	1.50	1.63	*1.34*	7.81	*2.43*	1.99	*3.04*	0.30	*2.13*	1.82	*2.43*
SCAR 4	1.97	*1.07*	6.39	1.01	1.06	*1.82*	5.41	*2.14*	1.51	*1.17*	0.24	*4.88*	1.43	*4.15*
SCAR 5	0.44	*1.65*	1.44	2.38	0.23	*1.40*	1.07	*4.96*	0.25	*3.80*	0.02	*3.20*	0.23	*4.49*
SCAR 6	8.16	*0.58*	25.04	0.63	4.15	*1.07*	21.36	*0.49*	6.58	*1.05*	2.08	*1.17*	7.58	*1.04*
	Tb		**Dy**		**Ho**		**Er**		**Tm**		**Yb**		**Lu**	
	ppm	*RSD%*	ppm	*RSD%*	ppm	*RSD%*	ppm	*RSD%*	ppm	*RSD%*	ppm	*RSD%*	ppm	*RSD%*
SCAR 2	0.39	*1.64*	2.83	*0.92*	0.62	*1.22*	1.91	*1.58*	0.31	*1.39*	1.92	*1.41*	0.30	*1.60*
SCAR 3	0.28	*2.04*	1.56	*2.58*	0.28	*1.03*	0.76	*4.02*	0.11	*5.64*	0.63	*3.50*	0.09	*3.07*
SCAR 4	0.23	*0.93*	1.30	*2.01*	0.24	*3.54*	0.62	*2.73*	0.09	*6.02*	0.53	*5.24*	0.07	*4.92*
SCAR 5	0.04	*2.89*	0.21	*2.51*	0.04	*6.67*	0.12	*3.18*	0.02	*8.81*	0.12	*7.77*	0.02	*5.40*
SCAR 6	1.36	*0.87*	8.80	*0.69*	1.80	*1.00*	5.17	*1.27*	0.79	*1.47*	4.77	*0.76*	0.71	*2.17*
	Hf		**Ta**		**Pb**		**Th**		**U**		**K**			
	ppm	*RSD%*	ppm	*RSD%*	ppm	*RSD%*	ppm	*RSD%*	ppm	*RSD%*	ppm	*RSD%*		
SCAR 2	0.54	*1.66*	0.07	*1.60*	1.93	*1.45*	0.14	*2.02*	0.12	*1.04*	3439	*0.924415*		
SCAR 3	0.23	*5.54*	0.12	*1.41*	0.59	*4.29*	0.34	*1.56*	0.10	*3.63*	290	*14.87996*		
SCAR 4	0.20	*8.14*	0.11	*2.11*	0.30	*5.38*	0.36	*1.23*	0.12	*1.80*	269	*14.79981*		
SCAR 5	0.02	*64.98*	0.19	*2.78*	0.20	*7.89*	0.29	*2.58*	0.04	*6.13*	96	*18.22975*		
SCAR 6	1.10	*7.10*	0.22	*2.48*	2.92	*1.04*	0.43	*1.94*	0.31	*1.05*	3864	*0.551777*		
	Sc		**Rb**		**Y**		**Zr**		**Nb**		**Ba**			
	ppm	*RSD%*	ppm	*RSD%*	ppm	*RSD%*	ppm	*RSD%*	ppm	*RSD%*	ppm	*RSD%*		
SCAR 2	46.93	*0.52*	6.00	*1.13*	8.44	*2.18*	8.59	*1.94*	1.18	*1.02*	31	*0.341418*		
SCAR 3	9.76	*0.70*	0.61	*2.00*	2.33	*2.17*	2.40	*3.99*	1.84	*1.02*	2	*2.402967*		
SCAR 4	10.40	*0.84*	0.71	*2.54*	2.35	*5.35*	2.39	*5.48*	1.88	*2.31*	2	*0.553073*		
SCAR 5	5.60	*1.51*	0.13	*4.15*	1.31	*3.39*	1.33	*10.54*	3.81	*1.72*	2	*1.685593*		
SCAR 6	39.21	*0.79*	6.04	*0.47*	20.47	*2.04*	20.79	*1.67*	4.49	*1.02*	74	*0.617067*		
	Zn		**Co**		**Cr**		**Cu**		**Ni**		**V**		**Sr**	
	ppm	*RSD%*	ppm	RSD%	ppm	*RSD%*	ppm	*RSD%*	ppm	*RSD%*	ppm	*RSD%*	ppm	*RSD%*
SCAR 2	50.92	*0.49*	51.47	0.33	283.05	*0.53*	24.40	*3.20*	109.32	*0.72*	300.88	*4.31*	99.9405	0.793341
SCAR 3	56.86	*0.47*	128.12	1.19	5811.72	*0.43*	13.56	*4.19*	1641.28	*0.42*	38.33	*0.58*	8.151864	0.56412
SCAR 4	54.47	*0.40*	127.59	0.32	4081.19	*0.54*	21.86	*3.03*	1515.63	*0.30*	108.70	*1.66*	21.65533	0.179373
SCAR 5	115.14	*0.24*	115.21	0.82	6018.31	*0.49*	21.21	*4.91*	1867.97	*0.10*	49.29	*1.14*	4.556418	0.374324
SCAR 6	96.34	*1.21*	61.39	0.87	177.93	*0.07*	24.63	*1.66*	48.48	*2.26*	551.50	*3.92*	310.8455	0.472408

	SiO2 (%)	Al2O3 (%)	Fe2O3 (%)	MgO (%)	CaO (%)	Na2O (%)	K2O (%)	TiO2 (%)	MnO (%)	P2O5 (%)	LOI (%)	Total (%)	Alkalis
SCAR 2	47.55	13.21	12.93	8.89	12.34	1.76	0.399	0.629	0.201	0.033	1.45	99.64	2.15479
SCAR 3	39.79	3.02	14.75	29.83	2.81	n.d.	0.009	0.482	0.178	0.049	8.87	99.68	0.00900
SCAR 4	40.18	3.44	15.56	29.00	2.90	n.d.	0.007	0.516	0.165	0.077	8.02	99.48	0.00700
SCAR 5	45.25	3.50	12.69	29.26	0.34	n.d.	n.d.	0.598	0.137	0.029	7.99	99.78	0.00000
SCAR 6	45.56	14.61	14.44	6.71	10.63	2.87	0.465	2.904	0.221	0.332	1.04	99.74	3.33500

SCAR2 garnet amphibolite Hill	GR	224590, 856875
SCAR3 ultramafic	GR	224400, 856902
SCAR4 ultramafic	GR	224400, 856902
SCAR5 ultramafic east	GR	226281, 856405
SCAR6 garnet amphibolite Loch	GR	222451, 851980

SCAR 2	Collected by Emma Waters. Think this *may* be the more silicic part of a larger dismembered layered body whose ultramafic layers are represented by SCAR3 and 4 found a wee bit further down the hill.
SCAR 3	Collected by Emma Waters. Think *may* be the ultramafic part of a layered intrusion.
SCAR 4	Collected by Emma Waters. Think *may* be the ultramafic part of a layered intrusion.
SCAR 5	Collected as an attempt to get at the most NE exposure of ultramafic rock.
SCAR 6	Collected as an example of the garnet amphibolite rocks which are common as small bodies within the gneisses and are often seen as distinctive boulders. George Strachan thinks may be retrogressed eclogite, but proof not clear (plag-gnt relations/corona textures maybe important if could be seen?)

OMAC Laboratories Limited

IDA Business Park
Dublin Road
Loughrea, Co. Galway
Phone: +353 (0)91 841 741 Fax: +353 (0)91 842 146
www.alsglobal.com/geochemistry

An INAB accredited testing laboratory Reg. No. 173T. Accredited methods are listed in the Scope of Accreditation available on request.

To: **GREENORE GOLD PLC**
2 ORD DISTILLERY
MUIR OF ORD HIL IV6 7UJ
UNITED KINGDOM

Page: 1
Total # Pages: 3 (A - C)
Plus Appendix Pages
Finalized Date: 18-NOV-2019
This copy reported on 19-NOV-2019
Account: GROGOP

QC CERTIFICATE LR19281447

Project: Scotland

P.O. No.: G003

This report is for 24 Rock samples submitted to our lab in Loughrea, Ireland on 6-NOV-2019.

The following have access to data associated with this certificate:

GAVIN BERKENHEGER

SAMPLE PREPARATION

ALS CODE	DESCRIPTION
WEI-21	Received Sample Weight
PUL-QC	Pulverizing QC Test
CRU-QC	Crushing QC Test
BAG-01	Bulk Master for Storage
LOG-21	Sample logging - ClientBarCode
CRU-31	Fine crushing - 70% <2mm
SPL-21	Split sample - riffle splitter
PUL-32	Pulverize 1000g to 85% < 75 um

ANALYTICAL PROCEDURES

ALS CODE	DESCRIPTION	INSTRUMENT
Au-AA25	Ore Grade Au 30g FA AA finish	AAS
ME-ICP61a	High Grade Four Acid ICP-AES	ICP-AES

This is the Final Report and supersedes any preliminary report with this certificate number. Results apply to samples as submitted. All pages of this report have been checked and approved for release.

***** See Appendix Page for comments regarding this certificate *****

Signature:

Andrey Tairov, Technical Manager, Ireland

OMAC Laboratories Limited

IDA Business Park
Dublin Road
Loughrea, Co. Galway
Phone: +353 (0)91 841 741 Fax: +353 (0)91 842 146
www.alsglobal.com/geochemistry

An INAB accredited testing laboratory Reg. No. 173T. Accredited methods are listed in the Scope of Accreditation available on request.

To: **GREENORE GOLD PLC**
2 ORD DISTILLERY
MUIR OF ORD HIL IV6 7UJ
UNITED KINGDOM

Page: 2 - A
Total # Pages: 3 (A - C)
Plus Appendix Pages
Finalized Date: 18-NOV-2019
Account: GROGOP

Project: Scotland

QC CERTIFICATE OF ANALYSIS LR19281447

Sample Description	Method	Au-AA25	ME-ICP61a	ME-ICP61a	ME-ICP61a	ME-ICP61a	ME-ICP61a	ME-ICP61a	ME-ICP61a	ME-ICP61a	ME-ICP61a	ME-ICP61a	ME-ICP61a	ME-ICP61a	ME-ICP61a	ME-ICP61a
	Analyte	Au	Ag	Al	As	Ba	Be	Bi	Ca	Cd	Co	Cr	Cu	Fe	Ga	K
	Units	ppm	ppm	%	ppm	ppm	ppm	ppm	%	ppm	ppm	ppm	ppm	%	ppm	%
	LOD	0.01	1	0.05	50	50	10	20	0.05	10	10	10	10	0.05	50	0.1
STANDARDS																
G914-10		10.10														
G914-10		10.55														
Target Range - Lower Bound		9.63														
Upper Bound		10.90														
MP-1b			51	0.66	22900	<50	<10	980	2.59	560	<10	<10	30600	8.27	110	0.2
Target Range - Lower Bound			45	0.50	21300	<50	<10	860	2.25	480	<10	<10	29200	7.56	<50	<0.1
Upper Bound			53	0.76	24700	100	20	1040	2.69	570	20	20	32200	8.82	210	0.4
OGGeo08			21	3.46	140	920	<10	20	2.13	20	100	100	8370	5.13	<50	2.5
Target Range - Lower Bound			17	5.21	<50	780	<10	<20	2.00	<10	70	70	7960	4.86	<50	2.3
Upper Bound			22	6.47	220	1020	20	50	2.41	40	120	110	8820	5.70	120	2.8
PMP-18		0.31														
PMP-18		0.30														
Target Range - Lower Bound		0.28														
Upper Bound		0.34														
BLANKS																
BLANK		<0.01														
BLANK		<0.01														
Target Range - Lower Bound		<0.01														
Upper Bound		0.02														
BLANK			<1	<0.05	<50	<50	<10	<20	<0.05	<10	<10	<10	<10	<0.05	<50	<0.1
Target Range - Lower Bound			<1	<0.05	<50	<50	<10	<20	<0.05	<10	<10	<10	<10	<0.05	<50	<0.1
Upper Bound			2	0.10	100	100	20	40	0.10	20	20	20	20	0.10	100	0.2
DUPLICATES																
ORIGINAL		3.18														
DUP		3.25														
Target Range - Lower Bound		3.04														
Upper Bound		3.39														

***** See Appendix Page for comments regarding this certificate *****

OMAC Laboratories Limited

IDA Business Park
Dublin Road
Loughrea, Co. Galway
Phone: +353 (0)91 841 741 Fax: +353 (0)91 842 146
www.alsglobal.com/geochemistry

An INAB accredited testing laboratory Reg. No. 173T. Accredited methods are listed in the Scope of Accreditation available on request.

To: **GREENORE GOLD PLC**
2 ORD DISTILLERY
MUIR OF ORD HIL IV6 7UJ
UNITED KINGDOM

Page: 2 - B
Total # Pages: 3 (A - C)
Plus Appendix Pages
Finalized Date: 18-NOV-2019
Account: GROGOP

Project: Scotland

QC CERTIFICATE OF ANALYSIS LR19281447

Sample Description	Method	ME-ICP61a	ME-ICP61a	ME-ICP61a	ME-ICP61a	ME-ICP61a	ME-ICP61a	ME-ICP61a	ME-ICP61a	ME-ICP61a	ME-ICP61a	ME-ICP61a	ME-ICP61a	ME-ICP61a	ME-ICP61a	ME-ICP61a
	Analyte	La	Mg	Mn	Mo	Na	Ni	P	Pb	S	Sb	Sc	Sr	Th	Ti	Tl
	Units	ppm	%	ppm	ppm	%	ppm	ppm	ppm	%	ppm	ppm	ppm	ppm	%	ppm
	LOD	50	0.05	10	10	0.05	10	50	20	0.05	50	10	10	50	0.05	50
STANDARDS																
G914-10																
G914-10																
Target Range - Lower Bound																
Upper Bound																
MP-1b		<50	<0.05	540	300	<0.05	<10	180	21100	>10.0	<50	<10	10	<50	<0.05	<50
Target Range - Lower Bound		<50	<0.05	450	260	<0.05	<10	100	19400	11.70	<50	<10	<10	<50	<0.05	<50
Upper Bound		150	0.12	550	320	0.13	20	300	22400	10.00	150	20	20	100	0.14	100
OGGeo08		<50	1.11	520	940	1.87	8700	840	7280	2.82	<50	<10	210	<50	0.40	<50
Target Range - Lower Bound		<50	1.11	470	860	1.63	8040	730	6710	2.55	<50	<10	200	<50	0.29	<50
Upper Bound		120	1.38	560	1010	1.99	9290	970	7770	3.05	130	30	250	110	0.51	100
PMP-18																
PMP-18																
Target Range - Lower Bound																
Upper Bound																
BLANKS																
BLANK																
BLANK																
Target Range - Lower Bound																
Upper Bound																
BLANK		<50	<0.05	<10	<10	<0.05	<10	<50	<20	<0.05	<50	<10	<10	<50	<0.05	<50
Target Range - Lower Bound		<50	<0.05	<10	<10	<0.05	<10	<50	<20	<0.05	<50	<10	<10	<50	<0.05	<50
Upper Bound		100	0.10	20	20	0.10	20	100	40	0.10	100	20	20	100	0.10	100
DUPLICATES																
ORIGINAL																
DUP																
Target Range - Lower Bound																
Upper Bound																

***** See Appendix Page for comments regarding this certificate *****

OMAC Laboratories Limited

IDA Business Park
Dublin Road
Loughrea, Co. Galway
Phone: +353 (0)91 841 741 Fax: +353 (0)91 842 146
www.alsglobal.com/geochemistry

An INAB accredited testing laboratory Reg. No. 173T. Accredited methods are listed in the Scope of Accreditation available on request.

To: **GREENORE GOLD PLC**
2 ORD DISTILLERY
MUIR OF ORD HIL IV6 7UJ
UNITED KINGDOM

Project: Scotland

QC CERTIFICATE OF ANALYSIS LR19281447

Sample Description	Method	ME-ICP61a	ME-ICP61a	ME-ICP61a	ME-ICP61a
	Analyte	U	V	W	Zn
	Units	ppm	ppm	ppm	ppm
	LOD	50	10	50	20
STANDARDS					
G914-10					
G914-10					
Target Range - Lower Bound					
Upper Bound					
MP-1b		<50	<10	1060	>100000
Target Range - Lower Bound		<50	<10	910	154500
Upper Bound		120	20	1150	>100000
OGGeo08		<50	90	<50	7080
Target Range - Lower Bound		<50	70	<50	6570
Upper Bound		110	110	100	7610
PMP-18					
PMP-18					
Target Range - Lower Bound					
Upper Bound					
BLANKS					
BLANK					
BLANK					
Target Range - Lower Bound					
Upper Bound					
BLANK		<50	<10	<50	<20
Target Range - Lower Bound		<50	<10	<50	<20
Upper Bound		100	20	100	40
DUPLICATES					
ORIGINAL					
DUP					
Target Range - Lower Bound					
Upper Bound					

***** See Appendix Page for comments regarding this certificate *****

OMAC Laboratories Limited

IDA Business Park
Dublin Road
Loughrea, Co. Galway
Phone: +353 (0)91 841 741 Fax: +353 (0)91 842 146
www.alsglobal.com/geochemistry

An INAB accredited testing laboratory Reg. No. 173T. Accredited methods are listed in the Scope of Accreditation available on request.

To: **GREENORE GOLD PLC**
2 ORD DISTILLERY
MUIR OF ORD HIL IV6 7UJ
UNITED KINGDOM

Finalized Date: 18-NOV-2019
Account: GROGOP

Project: Scotland

QC CERTIFICATE OF ANALYSIS LR19281447

Sample Description / Method / Analyte / Units / LOD	Au-AA25 Au ppm 0.01	ME-ICP61a Ag ppm 1	ME-ICP61a Al % 0.05	ME-ICP61a As ppm 50	ME-ICP61a Ba ppm 50	ME-ICP61a Be ppm 10	ME-ICP61a Bi ppm 20	ME-ICP61a Ca % 0.05	ME-ICP61a Cd ppm 10	ME-ICP61a Co ppm 10	ME-ICP61a Cr ppm 10	ME-ICP61a Cu ppm 10	ME-ICP61a Fe % 0.05	ME-ICP61a Ga ppm 50	ME-ICP61a K % 0.1
DUPLICATES															
K25260		<1	6.33	<50	100	<10	<20	3.16	<10	40	10	110	9.94	<50	0.5
DUP		<1	6.19	<50	100	<10	<20	3.09	<10	40	10	110	9.69	<50	0.5
Target Range - Lower Bound		<1	5.90	<50	<50	<10	<20	2.96	<10	30	<10	100	9.42	<50	0.4
Upper Bound		2	6.62	100	150	20	40	3.29	20	50	20	120	10.20	100	0.6
K25262	<0.01														
DUP	<0.01														
Target Range - Lower Bound	<0.01														
Upper Bound	0.02														
K25274	<0.01	<1	6.77	<50	<50	<10	<20	6.27	<10	80	990	240	8.42	<50	0.1
DUP	<0.01	<1	7.09	<50	<50	<10	<20	6.32	<10	80	980	240	8.50	<50	0.1
Target Range - Lower Bound	<0.01	<1	6.53	<50	<50	<10	<20	6.02	<10	70	940	220	8.11	<50	<0.1
Upper Bound	0.02	2	7.33	100	100	20	40	6.57	20	90	1030	260	8.81	100	0.2
ORIGINAL	0.05														
DUP	0.06														
Target Range - Lower Bound	0.04														
Upper Bound	0.07														
ORIGINAL	0.09														
DUP	0.11														
Target Range - Lower Bound	0.09														
Upper Bound	0.12														
ORIGINAL	0.15														
DUP	0.14														
Target Range - Lower Bound	0.13														
Upper Bound	0.16														

***** See Appendix Page for comments regarding this certificate *****

OMAC Laboratories Limited
IDA Business Park
Dublin Road
Loughrea, Co. Galway
Phone: +353 (0)91 841 741 Fax: +353 (0)91 842 146
www.alsglobal.com/geochemistry

An INAB accredited testing laboratory Reg. No. 173T. Accredited methods are listed in the Scope of Accreditation available on request.

To: **GREENORE GOLD PLC**
2 ORD DISTILLERY
MUIR OF ORD HIL IV6 7UJ
UNITED KINGDOM

Finalized Date: 18-NOV-2019
Account: GROGOP

Project: Scotland

QC CERTIFICATE OF ANALYSIS LR19281447

Sample Description / Method	ME-ICP61a	ME-ICP61a	ME-ICP61a	ME-ICP61a	ME-ICP61a	ME-ICP61a	ME-ICP61a	ME-ICP61a	ME-ICP61a	ME-ICP61a	ME-ICP61a	ME-ICP61a	ME-ICP61a	ME-ICP61a	ME-ICP61a
Analyte	La	Mg	Mn	Mo	Na	Ni	P	Pb	S	Sb	Sc	Sr	Th	Ti	Tl
Units	ppm	%	ppm	ppm	%	ppm	ppm	ppm	%	ppm	ppm	ppm	ppm	%	ppm
LOD	50	0.05	10	10	0.05	10	50	20	0.05	50	10	10	50	0.05	50
DUPLICATES															
K25260	<50	3.42	620	<10	3.06	40	540	<20	<0.05	<50	10	140	<50	0.59	<50
DUP	<50	3.36	600	<10	3.02	40	500	<20	<0.05	<50	10	130	<50	0.58	<50
Target Range - Lower Bound	<50	3.22	580	<10	2.88	30	450	<20	<0.05	<50	<10	120	<50	0.51	<50
Upper Bound	100	3.56	640	20	3.20	50	590	40	0.10	100	20	150	100	0.66	100
K25262															
DUP															
Target Range - Lower Bound															
Upper Bound															
K25274	<50	3.77	1150	10	1.23	480	380	<20	1.56	<50	40	110	<50	0.27	<50
DUP	<50	3.88	1160	10	1.25	480	370	<20	1.52	<50	40	120	<50	0.27	<50
Target Range - Lower Bound	<50	3.64	1100	<10	1.15	450	310	<20	1.44	<50	30	100	<50	0.21	<50
Upper Bound	100	4.01	1210	20	1.33	510	440	40	1.64	100	50	130	100	0.33	100
ORIGINAL															
DUP															
Target Range - Lower Bound															
Upper Bound															
ORIGINAL															
DUP															
Target Range - Lower Bound															
Upper Bound															
ORIGINAL															
DUP															
Target Range - Lower Bound															
Upper Bound															

***** See Appendix Page for comments regarding this certificate *****

OMAC Laboratories Limited

IDA Business Park
Dublin Road
Loughrea, Co. Galway
Phone: +353 (0)91 841 741 Fax: +353 (0)91 842 146
www.alsglobal.com/geochemistry

An INAB accredited testing laboratory Reg. No. 173T. Accredited methods are listed in the Scope of Accreditation available on request.

To: **GREENORE GOLD PLC**
2 ORD DISTILLERY
MUIR OF ORD HIL IV6 7UJ
UNITED KINGDOM

Project: Scotland

QC CERTIFICATE OF ANALYSIS LR19281447

Sample Description	Method / Analyte / Units / LOD	ME-ICP61a U ppm 50	ME-ICP61a V ppm 10	ME-ICP61a W ppm 50	ME-ICP61a Zn ppm 20
		DUPLICATES			
K25260		<50	290	<50	50
DUP		<50	280	<50	50
Target Range - Lower Bound		<50	260	<50	30
Upper Bound		100	310	100	70
K25262					
DUP					
Target Range - Lower Bound					
Upper Bound					
K25274		<50	320	<50	130
DUP		<50	310	<50	130
Target Range - Lower Bound		<50	290	<50	110
Upper Bound		100	340	100	150
ORIGINAL					
DUP					
Target Range - Lower Bound					
Upper Bound					
ORIGINAL					
DUP					
Target Range - Lower Bound					
Upper Bound					
ORIGINAL					
DUP					
Target Range - Lower Bound					
Upper Bound					

***** See Appendix Page for comments regarding this certificate *****

OMAC Laboratories Limited
IDA Business Park
Dublin Road
Loughrea, Co. Galway
Phone: +353 (0)91 841 741 Fax: +353 (0)91 842 146
www.alsglobal.com/geochemistry

An INAB accredited testing laboratory Reg. No. 173T. Accredited methods are listed in the Scope of Accreditation available on request.

To: **GREENORE GOLD PLC**
2 ORD DISTILLERY
MUIR OF ORD HIL IV6 7UJ
UNITED KINGDOM

Page: Appendix 1
Total # Appendix Pages: 1
Finalized Date: 18-NOV-2019
Account: GROGOP

Project: Scotland

QC CERTIFICATE OF ANALYSIS LR19281447

CERTIFICATE COMMENTS

ACCREDITATION COMMENTS

Applies to Method: The methods immediately below this line are ISO 17025:2005 Accredited. INAB Registration No: 173T
Au-AA25

LABORATORY ADDRESSES

Applies to Method: Processed at ALS Loughrea located at Dublin Road, Loughrea, Co. Galway, Ireland.

Au-AA25	BAG-01	CRU-31	CRU-QC
LOG-21	ME-ICP61a	PUL-32	PUL-QC
SPL-21	WEI-21		